QUANTUM LIQUIDS AND QUANTUM CRYSTALS

Coherently precessing spatially inhomogeneous structures of half magnetization in the *B* phase of superfluid ^{3}He

S. Mikeladze and N. Suramlishvili*

E. Andronikashvili Institute of Physics, Academy of Sciences of Georgia, ul. Tamarashvili 6, 380077 Tbilisi, Georgia

(Submitted March 14, 2002; revised December 9, 2002)
Fiz. Nizk. Temp. **29**, 727–732 (July 2003)

Spatially inhomogeneous coherently precessing structures of half magnetization in superfluid ^{3}He-*B* are investigated in the presence of small nonuniformities of a high external magnetic field. It is shown that, depending on the degree of nonuniformity of the field, both two-domain and three-domain coherently precessing structures can exist. © *2003 American Institute of Physics.* [DOI: 10.1063/1.1596574]

1. The superfluidity of liquid ^{3}He is due to Cooper pairing in a state with spin and orbital moments equal to unity. The presence of spin on the Cooper pair and the complexity of the order parameter lead to a diversity of dynamic magnetic properties of the superfluid phases of liquid ^{3}He. The dynamics of the magnetization in the superfluid phases is determined by the interrelationship of the magnetic moment **M** and the order parameter of the triplet condensate.

In the absence of magnetic field the magnetization and the averaged orbital moment of the superfluid *B* phase of liquid ^{3}He are equal to zero. In an external magnetic field a magnetic moment **M** is induced in the system and, as a result of the spin–orbit coherence, an orbital moment **L** is formed. If the magnetization deviates from the magnetic field direction it begins to precess around the field direction. In that case a state in which the spins of the Cooper pairs precess coherently is formed in the bulk of the superfluid liquid. Such a state is characterized by anomalous stability even in the presence of nonuniformities of the external magnetic field. The reasons for this are the stiffness of the order parameter of ^{3}He-*B* with respect to spatial inhomogeneities and the presence in the system of a spin–orbit interaction, which derives from the dipole–dipole interaction between the nuclear moments of the ^{3}He atoms.

The dipole shift of the precession frequency of the magnetization from the Larmor frequency is due to the presence of the dipole–dipole energy. The values of the energy and the frequency shift depend on the spin–orbit configuration of the precessing system.

The stiffness of the order parameter is manifested as spatial stiffness of the magnetization precession angle α_S, which generates nondissipative spin currents that restore the uniform distribution of the phase of the precession over the entire volume. These currents effect a redistribution of the longitudinal component of the magnetization and orbital moment. The local frequency shift that arises compensates the spatial difference of the Larmor precession frequency. In ^{3}He-*B* placed in a nonuniform external magnetic field a coherently precessing two-domain spin structure can exist.[1,2] In such a system the modulus of the magnetization M is equal to the equilibrium value $M_0=\chi_B H_0$ (here H_0 is the static magnetic field applied to the system, and χ_B is the magnetic susceptibility of the superfluid *B* phase of liquid ^{3}He). In one of the domains the magnetization is directed along the field, while in the other it deviates by approximately 104° from the field direction; the axis of the orbital anisotropy is parallel to the field direction throughout the entire volume. This spatial pattern is due to the spin–orbit structure of the dipole–dipole interaction potential in the case of precession with $M=M_0$.

In the superfluid *B* phase of liquid ^{3}He, according to the results of Ref. 3, it is possible to have coherent precession of half magnetization ($M=M_0/2$) and double magnetization ($M=2M_0$). The existence of coherently precessing states of half magnetization has been confirmed experimentally.[4,5] The dipole–dipole interaction potential for $M=M_0/2$ has a more complex spin–orbit structure. Since in a nonuniform external magnetic field coherent precession of half magnetization should be characterized by an inhomogeneous distribution of both the spin and orbital degrees of freedom. The study of this question is the subject of this paper.

2. In the presence of a high external magnetic field the dipole–dipole interaction energy is much less than the Zeeman energy, and it can be treated as a perturbation. In the zeroth approximation it can be neglected. In that case the solutions for the precessing states can be obtained with the aid of the Larmor theorem, which states that in a spin space rotating with the Larmor frequency $\omega_L=gH$ (g is the gyromagnetic ratio of the ^{3}He nuclei) the magnetic field has no influence whatsoever on the nuclear spins of the ^{3}He atoms, and the symmetry with respect to three-dimensional spin rotations is restored. Thus the total symmetry group of the precessing states, $\hat{G}=SO_3^{\tilde{S}}\times SO_3^L$, includes the three-dimensional spin rotation group $SO_3^{\tilde{S}}$ in the rotating reference frame and the three-dimensional orbital rotation group SO_3^L in the laboratory frame.[6] By applying the operations of

the group $\hat{G}$ to some initial state, one can obtain all the degenerate coherently precessing states.

As the initial state we take one of the solutions of the system of Leggett equations describing the interrelationship between the magnetization $\mathbf{M}$ and the spin part of the order parameter $\hat{A}$:[7]

$$\mathbf{M}=g\mathbf{M}\times\mathbf{H}+\mathbf{R}_D, \tag{1}$$

$$\hat{\mathbf{A}}_i=\mathbf{A}_i\times g\left(\mathbf{H}-\frac{\mathbf{M}}{\chi_B}\right). \tag{2}$$

Here $\mathbf{R}_D$ is the dipole moment, the external magnetic field $\mathbf{H}\|\mathbf{z}$, and $(\mathbf{A}_i)_\mu=A_{\mu i}$ $(\mu=x,y,z)$. The simplest solution of this system in the case of half magnetization is of the form

$$\mathbf{M}^0=\frac{\chi_B\mathbf{H}}{2},\quad \hat{A}^0=\hat{O}\left(\mathbf{z},-\omega_L\frac{t}{2}\right), \tag{3}$$

where $\hat{O}(\mathbf{z},-\omega_L t/2)$ describes a rotation around the $\mathbf{z}$ axis by an angle $-\omega_L t/2$. The operation of an element of the group $\hat{G}$ on state (3) gives a general solution for the Larmor precession of the half magnetization:

$$\begin{aligned}\hat{A}&=\hat{O}(\mathbf{z},-\omega_L t)\hat{R}^{(\tilde{S})}\hat{O}(\mathbf{z},\omega_L t)\hat{A}^0\hat{R}^{(L)^{-1}}\\&=\hat{O}(\mathbf{z},-\omega_L t)\hat{R}^{(\tilde{S})}\hat{O}(\mathbf{z},\omega_L,t/2)\hat{R}^{(L)^{-1}},\end{aligned} \tag{4}$$

$$\mathbf{M}(t)=\hat{O}(\mathbf{z},-\omega_L t)\hat{R}^{(\tilde{S})}\mathbf{M}^0=\hat{O}(\mathbf{z},-\omega_L t)\hat{R}^{(\tilde{S})}\frac{\chi_B\mathbf{H}}{2}, \tag{5}$$

where $\hat{R}^L$ is the time-independent matrix of the orbital rotations SO_3^L in the laboratory reference frame, and $\hat{R}^{(\tilde{S})}$ is the time-independent matrix of spin rotations $SO_3^{\tilde{S}}$ in the precessing reference frame. The rotation matrix $\hat{O}(\mathbf{z},\omega_L t)$ describes the transition from the laboratory frame to a frame rotating with frequency ω_L.

The physical meaning of these matrices is as follows. $\hat{R}^{(\tilde{S})}$ describes the orientation of the magnetization in the precessing frame, $\mathbf{s}=\tilde{\mathbf{M}}/M^0=\hat{R}^{(\tilde{S})}\mathbf{z}$ ($\tilde{\mathbf{M}}$ is the magnetization vector in the precessing frame), and $\hat{R}^{(L)}$ is the orientation of the orbital moment of the Cooper pair in the laboratory reference frame $\mathbf{l}=\mathbf{L}/M^0=\hat{R}^{(L)}\mathbf{z}$. Parametrizing $\hat{R}^{(\tilde{S})}$ and $\hat{R}^{(L)}$ by the Euler angles and writing them in the form

$$\begin{aligned}\hat{R}^{(\tilde{S})}&=\hat{R}_Z(\alpha_S^0)\hat{R}_Y(\beta_S)\hat{R}_Z(\gamma_S^0),\\\hat{R}^{(L)}&=\hat{R}_Z(\alpha_L)\hat{R}_Y(\beta_L)\hat{R}_Z(\gamma_L),\end{aligned} \tag{6}$$

where $(\alpha_S^0,\beta_S,\gamma_S^0)$ and $(\alpha_L,\beta_L,\gamma_L)$ are the corresponding Euler angles, we obtain for the order parameter (4)

$$\hat{A}=\hat{R}^{(S)}(\alpha_S,\beta_S,\gamma_S)\hat{R}^{(L)^{-1}}(\alpha_L,\beta_L,\gamma_L). \tag{7}$$

Here $\alpha_S=\alpha_S^0=\omega_L t$ and $\gamma_S=\gamma_S^0-\omega_L t/2$. In this notation α_S and β_S are the azimuthal and polar angles of the precessing magnetization $\mathbf{M}(t)$, and α_L and β_L are the azimuthal and polar angles of the orbital moment of the Cooper pairs. The angles γ_S and γ_L in the order parameter, as can easily be seen, are present only in the combination $\gamma=\gamma_S-\gamma_L$. These five variables, i.e., $\mathbf{s}(\alpha_S,\beta_S)$, $\mathbf{l}(\alpha_L,\beta_L)$, and the angle γ, completely describe the physical state of the system, and the space of degeneracy of the coherent Larmor precession of the magnetization in ^{3}He-B is five-dimensional.

3. Owing to the small dipole–dipole interaction, the potential of which is given by the expression

$$F_D=\frac{2}{15}\chi_B\left(\frac{\Omega_B}{g}\right)^2\left(\mathrm{Tr}\hat{A}-\frac{1}{2}\right)^2, \tag{8}$$

the degree of degeneracy is lowered (Ω_B is the NMR frequency, which characterizes the intensity of the dipole–dipole interaction). At high magnetic field, when $\omega_L\gg\Omega_B$, the state of the system is described by fast and slow variables, and one can average the dipole energy over the fast variables. The averaged potentials of the dipole interaction differ substantially for the equilibrium value M_0 of the magnetization modulus and for half magnetization. This is because the combinations of fast variables making up the slow variable are different. For the case of half magnetization this variable is $\Phi_{12}\equiv\alpha_S-\alpha_L+2(\gamma_S-\gamma_L)$, and the averaged energy of the dipole–dipole interaction has the form[3,8]

$$\begin{aligned}F_D=\chi_B\left(\frac{\Omega_B}{g}\right)^2 f_D=\frac{1}{10}\chi_B\left(\frac{\Omega_B}{g}\right)^2\Big[1+(1-s_Z^2)(1-l_Z^2)\\+2s_Z^2l_Z^2+\frac{2}{3}(1+s_Z)(1+l_Z)\sqrt{1-s_Z^2}\sqrt{1-l_Z^2}\cos\Phi_{12}\Big].\end{aligned} \tag{9}$$

Here $s_Z=\cos\beta_S$ and $l_Z=\cos\beta_L$ are the orientations of the magnetization and orbital moment relative to the direction of the applied magnetic field. The potential (9) has two degenerate absolute minima at $\Phi_{12}\equiv\pi$, which correspond to the following spin–orbit configurations:

$$s_Z=0.75,\quad l_Z=0.3, \tag{10}$$

$$s_Z=0.3,\quad l_Z=0.75. \tag{11}$$

They determine the stable precessing states of half magnetization. In addition, two more, metastable degenerate states can exist, with the spin–orbit configurations:[9]

$$s_Z=-1,\quad l_Z=0, \tag{12}$$

$$s_Z=0,\quad l_Z=-1. \tag{13}$$

The characteristic degeneracy of the dipole energy (9) is lifted by the so-called spectroscopic energy. It is manifested when the frequency ω_p of the coherent precession of the magnetization differs from the Larmor frequency ω_L. Then the Zeeman energy $-\boldsymbol{\omega}_p\cdot\mathbf{M}/g$ is incompletely compensated by the Larmor energy $\boldsymbol{\omega}_L\cdot\mathbf{M}/g$. The difference, which is the Zeeman energy in the frame rotating with frequency ω_p, is equal to the spectroscopic energy:

$$F_\omega=\frac{1}{g}(\omega_p-\omega_L)\mathbf{M}=\frac{\chi_B}{2g^2}(\omega_p-\omega_L)\omega_L s_Z. \tag{14}$$

In this situation the spin–orbit configurations of the stably precessing states can be determined by minimizing the free energy of the system, which is the sum of the dipole and spectroscopic energies:

$$F=F_D+\frac{\chi_B}{2g^2}(\omega_p-\omega_L)\omega_L s_Z. \tag{15}$$

Here each minimum of the free energy (15) is obtained by displacement of a definite state of the spin–orbit configuration from (10) and (11).[9] At a negative spectroscopic energy the stable precessing states correspond to spin–orbit configurations obtained by displacement of state (10). In this case, depending on the value of F_ω, one has $0.75<s_Z<1$ and $0<l_Z<0.3$. In the case of a positive spectral energy the stable states correspond to spin–orbit configurations obtained by displacement of state (11). However, with increasing F_ω, after it exceeds a certain critical value, state (12), with the opposite magnetization direction, will be the stable state.

4. Let us discuss the features of the precession of the half magnetization in a nonuniform external magnetic field. We shall assume that the spatial nonuniformity is manifested along the direction of the external magnetic field $\mathbf{H}=H\mathbf{z}$, and we write the Larmor frequency in the form

$$\omega_L(z)=\omega_L(z_0)+(z-z_0)\nabla\omega_L=\omega_p+(z-z_0)\nabla\omega_L. \quad (16)$$

In this case the spectroscopic energy of the system will also depend on the coordinate z, and that dependence will lead to a nonuniform spatial distribution of s_Z and l_Z, while the free energy of the system will be the sum of the dipole, spectroscopic, and gradient energies:

$$F=F_D+F_\omega+F_\nabla, \quad (17)$$

where F_∇ has the following form:[6]

$$F_\nabla=\frac{1}{4}\frac{\chi_B}{g^2}c_\parallel^2(\nabla_j R_{\alpha k})^2+\frac{1}{2}\frac{\chi_B}{g^2}(c_\perp^2-c_\parallel^2)(\nabla_i R_{\alpha i})^2. \quad (18)$$

Here $c_\parallel$ and $c_\perp$ are the spin-wave velocities parallel to and perpendicular to the external magnetic field. In the case of precession of half magnetization the gradient energy averaged over the fast variables is given by the expression

$$\begin{aligned}F_\nabla=&\frac{1}{2}\frac{\chi_B}{g^2}c_\parallel^2\Bigg[\left(\frac{5}{4}-s_Z\right)(\partial_Z\alpha_S)^2+\left(\frac{5}{4}-l_Z\right)(\partial_Z\alpha_L)^2\\&+\frac{1}{4}(\partial_Z\Phi_{12})^2+\frac{1}{1-s_Z^2}(\partial_Z s_Z)^2+\frac{1}{1-l_Z^2}(\partial_Z l_Z)^2\\&-2\left(\frac{1}{2}-s_Z\right)\left(\frac{1}{2}-l_Z\right)\partial_Z\alpha_S\partial_Z\alpha_L-\left(\frac{1}{2}-s_Z\right)\\&\times\partial_Z\alpha_S\partial_Z\Phi_{12}+\left(\frac{1}{2}-l_Z\right)\partial_Z\alpha_L\partial_Z\Phi_{12}\Bigg]\\&+\frac{1}{2}\frac{\chi_B}{g^2}(c_\perp^2-c_\parallel^2)\Bigg\{\frac{1}{2}\Bigg[2(1+s_Z^2l_Z^2)+(1-s_Z^2)\\&\times(1-l_Z^2)+2\left(\frac{1}{4}-s_Z\right)(1+l_Z^2)\Bigg](\partial_Z\alpha_S)^2+\frac{1}{4}(1+l_Z^2)\\&\times[(\partial_Z\alpha_L)^2+(\partial_Z\Phi_{12})^2]+\frac{3-l_Z^2}{2(1-s_Z^2)}(\partial_Z s_Z)^2\\&+\frac{1}{1-l_Z^2}(\partial_Z l_Z)^2-\left(\frac{1}{2}-s_Z\right)(1+l_Z^2)(\partial_Z\alpha_S\partial_Z\alpha_L\\&+\partial_Z\alpha_S\partial_Z\Phi_{12})+\frac{1}{2}(1+l_Z^2)\partial_Z\alpha_L\partial_Z\Phi_{12}\Bigg\}. \quad (19)\end{aligned}$$

It follows from Eqs. (9), (14), and (19) that in the free energy (17) of the system, only the dipole energy potential depends explicitly on the angle Φ. In the experiments the nonuniformity of the external magnetic field, which determines the scale of the spatial inhomogeneity of the precessing state of the system, is small not only in comparison with the field itself but also in comparison with the dipole energy. It follows from what we have said that $F_\nabla \ll F_D$. This makes it possible to assume that $\Phi=\Phi_{st}=\pi$ and $\partial_Z\Phi_{12}=0$ even in the inhomogeneous case.

The free energy (17) does not depend explicitly on the angles α_S and α_L—they enter only in the form of the gradients $\partial_Z\alpha_S$ and $\partial_Z\alpha_L$. A study of the free energy of the precessing system at the minimum with respect to these gradients leads to a homogeneous system of equations for $\delta_Z\alpha_S$ and $\partial_Z\alpha_L$:

$$\begin{aligned}\frac{\partial F_\nabla}{\partial(\partial_Z\alpha_S)}=&\Bigg\{2c_\parallel^2\left(\frac{5}{4}-s_Z\right)+(c_\perp^2-c_\parallel^2)\Bigg[2(1+s_Z^2l_Z^2)\\&+(1-s_Z^2)(1-l_Z^2)+2\left(\frac{1}{4}-s_Z\right)(1+l_Z^2)\Bigg]\Bigg\}\partial_Z\alpha_S\\&-\Bigg[2c_\parallel^2\left(\frac{1}{2}-s_Z\right)\left(\frac{1}{2}-l_Z\right)+(c_\perp^2-c_\parallel^2)\left(\frac{1}{2}-s_Z\right)\\&\times(1+l_Z^2)\Bigg]\partial_Z\alpha_L=0, \quad (20)\end{aligned}$$

$$\begin{aligned}\frac{\partial F_\nabla}{\partial(\partial_Z\alpha_L)}=&-\Bigg[2c_\parallel^2\left(\frac{1}{2}-s_Z\right)\left(\frac{1}{2}-l_Z\right)+(c_\perp^2-c_\parallel^2)\\&\times\left(\frac{1}{2}-s_Z\right)(1+l_Z^2)\Bigg]\partial_Z\alpha_S+\Bigg[c_\parallel^2\left(\frac{5}{4}-l_Z\right)\\&+\frac{1}{4}(c_\perp^2-c_\parallel^2)(1+l_Z^2)\Bigg]\partial_Z\alpha_L=0. \quad (21)\end{aligned}$$

The determinant of this system is nonzero for any values of s_Z and l_Z, and the system has a zero solution $\partial_Z\alpha_S=\partial_Z\alpha_L=0$. We note that the following inequality is also satisfied:

$$\frac{\partial^2F_\nabla}{\partial(\partial_Z\alpha_S)^2}\frac{\partial^2F_\nabla}{\partial(\partial_Z\alpha_L)^2}-\left(\frac{\partial^2F_\nabla}{\partial(\partial_Z\alpha_S)\partial(\partial_Z\alpha_L)}\right)^2>0.$$

It follows from this that the minimum value of the free energy corresponds to a homogeneous distribution of the precession phase α_S and of the azimuthal angle α_L of the orbital moment of the Cooper pair.

The expression for the spectroscopic energy with Eq. (16) taken into account becomes:

$$F_\omega=-\frac{\chi_B}{2g^2}(z-z_0)\omega_p\nabla\omega_L s_Z. \quad (22)$$

In the case of continuous NMR the frequency ω_p is determined by the frequency of the external transverse rf field. At the point z_0 the local Larmor frequency of the external static magnetic field coincides with the frequency of the coherent precession, and at the lower and upper boundaries of the system $|(z-z_0)\nabla\omega_L|\ll\omega_p$.

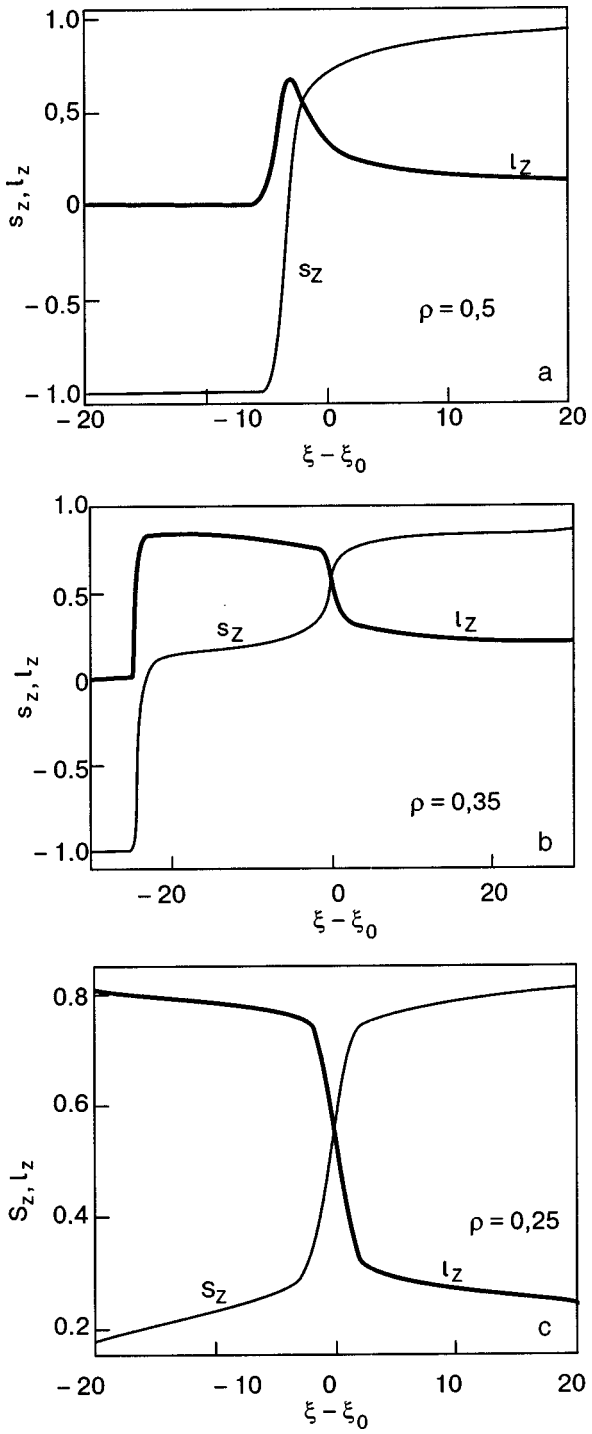

FIG. 1. Dependence of s_Z and l_Z on the coordinate ξ for several different values of ρ.

It follows from what we have said that the free energy of a steadily precessing spin system of superfluid ^{3}He-B in the presence of a nonuniform external magnetic field takes the following form:

$$\overline{F}=\frac{g^2}{\chi_B c_\parallel^2}F=\frac{1}{2}\left\{\left[1+\frac{1}{2}\left(\frac{c_\perp^2}{c_\parallel^2}-1\right)(3-l_z^2)\right]\frac{(\partial_Z s_Z)^2}{1-s_Z^2}+\frac{c_\perp^2}{c_\parallel^2}\frac{(\partial_Z l_Z)^2}{1-l_Z^2}\right\}-\frac{1}{2}\frac{\omega_p\nabla\omega_L}{c_\parallel^2}(z-z_0)s_Z+\frac{\Omega_B^2}{c_\parallel^2}f_D. \tag{23}$$

In contrast to the precession at the equilibrium value of the magnetization modulus,[1,2] in this case two spatial parameters enter the problem: one characterizing the intensity of the dipole–dipole interaction, and one characterizing the nonuniformity of the magnetic field:

$$\lambda_D=\frac{c_\parallel}{\Omega_B},\quad \lambda_\nabla=\left(\frac{c_\parallel^2}{\omega_p\nabla\omega_L}\right)^{1/3}. \tag{24}$$

Measuring the coordinate in units of the dipole length ($\xi=z/\lambda_D$) and introducing the parameter

$$\rho=\frac{\lambda_D}{\lambda_\nabla}, \tag{25}$$

which characterizes the degree of nonuniformity of the external magnetic field relative to the intensity of the dipole interaction, we obtain from expression (23)

$$\overline{F}=\frac{1}{2}\left\{\left[1+\frac{1}{2}\left(\frac{c_\perp^2}{c_\parallel^2}-1\right)(3-l_Z^2)\right]\frac{1}{1-s_Z^2}\left(\frac{ds_Z}{d\xi}\right)+\frac{c_\perp^2}{c_\parallel^2}\frac{1}{1-l_Z^2}\left(\frac{dl_Z}{d\xi}\right)\right\}-\frac{1}{2}\rho(\xi-\xi_0)s_Z+f_D. \tag{26}$$

The spatial structure of the coherently precessing spin system depends on the value of the parameter ρ and the ratio $c_\perp^2/c_\parallel^2$. Larger values of the parameter γ correspond to larger nonuniformity of the magnetic field.

A numerical analysis of the Euler–Lagrange equations obtained in minimizing the free energy (26) shows that for a value $\rho>0.38$ a two-dimensional structure forms (Fig. 1a) in which $s_Z\to 1$ and $l_Z\to 0$ with increasing field, while with decreasing field a domain with $s_Z=-1$ and $l_Z=0$ is realized. In this case the transition region (domain wall) is shifted relative to the point ξ_0 (z_0) into the region $\xi<\xi_0$ ($z<z_0$).

When $0.29<\rho<0.38$, the inhomogeneous coherently precessing system has a rather complex spatial structure (Fig. 1b). With increasing field a domain forms in which $s_Z\to 1$, $l_Z\to 0$. With decreasing field there is initially a transition to an intermediate domain in which $0.1\leqslant s_Z\leqslant 0.3$ and $0.75\leqslant l_Z\leqslant 0.83$. The transition region between these domains

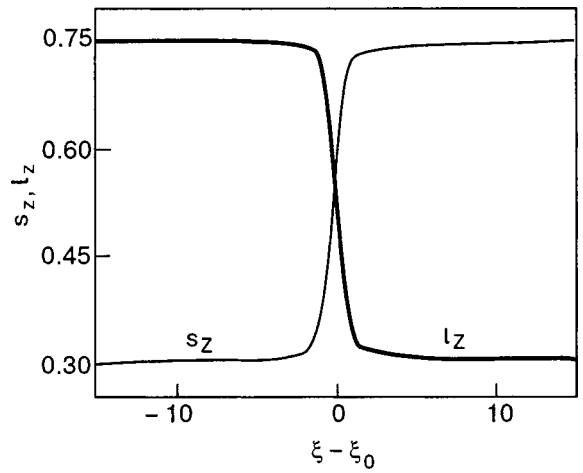

FIG. 2. Dependence of s_Z and l_Z on the coordinate ξ in the limit of a uniform magnetic field, $\rho\to 0$.

is located at $\xi \approx \xi_0$ ($z \approx z_0$). Then, in the region $\xi < \xi_0$ ($z < z_0$) one observes a sharp transition to a state with $s_Z = -1$ and $l_Z = 0$.

When $\rho < 0.29$ the two-domain structure is restored. Now with increasing field one has $s_Z \to 1$ and $l_Z \to 0$, and with decreasing field $s_Z \to 0$ and $l_Z \to 1$ (Fig. 1c). In this case the domain wall is located at $\xi \approx \xi_0$ ($z \approx z_0$).

In the limit of a uniform field $\rho \to 0$. Then the spin–orbit configuration of the precessing states should correspond to absolute minima of the dipole energy, and in the region $\xi > \xi_0$ ($z > z_0$) the state that is realized is a precessing state with the spin–orbit configuration $s_Z = 0.75$ and $l_Z = 0.3$, while in the region $\xi < \xi_0$ ($z < z_0$) it will be a state with $s_Z = 0.3$ and $l_Z = 0.75$ (Fig. 2).

The authors express their deep gratitude to G. A. Kharadze for steadfast interest and numerous discussions.

This study was supported in part by Grant No. 2.16 of the Academy of Sciences of Georgia.

*E-mail: nugzars@iph.hepi.edu.ge

[1] A. S. Borovik-Romanov, Yu. M. Bun'kov, V. V. Dmitriev, Yu. M. Mukharskiĭ, K. Flachbart, Zh. Éksp. Teor. Fiz. **88**, 2025 (1985) [Sov. Phys. JETP **61**, 1199 (1985)]; A. S. Borovik-Romanov, Yu. M. Bun'kov, V. V. Dmitriev, Yu. M. Mukharskiĭ, E. V. Podd'yakova, and O. D. Timofeevskaya, ZhETF **96**, 956 (1989) [Sov. Phys. JETP **69**, 542 (1989)].
[2] I. A. Fomin, Zh. Éksp. Teor. Fiz. **88**, 2039 (1985) [Sov. Phys. JETP **61**, 1207 (1985)].
[3] G. Kharadze and G. Vachnadze, JETP Lett. **56**, 458 (1992).
[4] V. V. Dmitriev, I. V. Kosarev, M. Krusius, D. V. Ponarin, V. M. H. Ruutu, and G. E. Volovik, Phys. Rev. Lett. **78**, 86 (1997).
[5] V. B. Elstov, V. V. Dmitriev, M. Krusius, J. J. Ruohio, and G. E. Volovik, J. Low Temp. Phys. **113**, 645 (1998).
[6] T. Sh. Misirpashaev and G. E. Volovik, Zh. Éksp. Teor. Fiz. **102**, 1197 (1992) [JETP **75**, 650 (1992)].
[7] A. J. Leggett, Rev. Mod. Phys. **47**, 331 (1975).
[8] G. Kharadze, N. Suramlishvili, and G. Vachnadze, J. Low Temp. Phys. **110**, 851 (1998).
[9] G. E. Vachnadze and N. G. Suramlishvili, Fiz. Nizk. Temp. **22**, 711 (1996) [Low Temp. Phys. **22**, 545 (1996)].

Translated by Steve Torstveit

SUPERCONDUCTIVITY, INCLUDING HIGH-TEMPERATURE SUPERCONDUCTIVITY

Influence of electron–electron interactions on supercurrent in SNS structures

K. Engström,* J. Kinaret, and R. I. Shekhter

Department of Applied Physics, Chalmers University of Technology, and Göteborg University, SE-412 96 Göteborg, Sweden

M. Puska and H. Saarikoski

Laboratory of Physics, Helsinki University of Technology, P.O. Box 1100, FIN-02015 HUT, Finland
(Submitted August 22, 2002; revised November 1, 2002)
Fiz. Nizk. Temp. **29**, 733–739 (2003)

A superconductor–normal quantum dot–superconductor structure where the number of electrons in the dot can be controlled by a gate voltage is considered. The effect of electron–electron interactions on the supercurrent between the two superconductors is studied. Using an analytic model and numerical density functional calculations it is found that Coulomb interactions can make the system quantum-mechanically more ''rigid,'' i.e. increase its sensitivity to phase gradients, thereby *enhancing* the supercurrent through the structure, especially for small phase differences. Accordingly, it is found that the supercurrent in this structure can be controlled by the gate voltage. © *2003 American Institute of Physics.* [DOI: 10.1063/1.1596575]

1. INTRODUCTION

The impact of quantum mechanical coherence on macroscopic quantities, such as electric currents, is interesting for basic research and for potential applications. In view of the latter an ability to control the supercurrent in hybrid normal/superconducting systems—preferably electrically—is desirable. Examples of structures with a controlled supercurrent are the Josephson field-effect transistor (JOFET),[1] the injected-current SNS transistor,[2] and devices which effectuate Cooper-pair transport via tunable resonant states.[3,4]

The novel effects described in these works were essentially of single-particle origin. The effects of Coulomb interactions on Copper-pair transport through confined regions have been investigated using different formulations of the tunneling-Hamiltonian formalism, where a (repulsive) on-site Hubbard term modeled the interactions. It was established that a single impurity level in general suppresses the current,[5,6] except in the presence of spin-flip processes, where it may in fact be enhanced by the Kondo effect.[5] Strictly one-dimensional approaches, where a Luttinger liquid description of the system was employed, likewise gave significant suppression of the Josephson current with increasing interaction strength,[7,8] except for perfectly transmitting NS interfaces where interactions were found to have virtually no impact on the supercurrent.[8] Recently, Rozhkov *et al.*[9] considered Josephson tunneling through an interacting gated quantum dot and showed that the system is a π-junction in certain ranges of the gate voltage and for sufficiently strong interactions, i.e. the energy of the system is minimized at a phase difference π between the order parameters of the two superconducting leads.

In the works cited above the interaction Hamiltonian describes a situation where the interacting charge is allowed to fluctuate, so that the electrostatic potential is constant throughout the system. In the present paper we shall consider the opposite boundary condition where the interacting charge is *fixed*, and we shall discuss its consequences in terms of a simple qualitative model and a more rigorous density functional formulation.

In the present paper we study a superconductor–quantum dot–superconductor structure and show that Coulomb interactions in the dot can be used to control the supercurrent electrostatically. The fundamental question we address is the nature of the interplay between the electrostatic ''rigidity'' (reluctance towards change in the charge configuration) and the superconducting ''rigidity,'' i.e. the macroscopic quantum coherence described by the phase of the superconducting order parameter. Ordinarily, electrostatic interactions cause fluctuations of the phase by fixing the number of charges, in accordance with the well-known particle number–phase uncertainty relation $\Delta N \Delta \varphi \gtrsim 1$, thereby destroying global phase coherence. In the present case, however, we have a unique situation where electrostatic rigidity *reinforces* phase rigidity. This possibility arises due to the accumulation of nonquantized electronic charge, *controlled by the phase difference*, in the *nonsuperconducting* part of the device, where the charge–phase uncertainty relation is inapplicable. This charge, associated with the formation of an Andreev state[10] confined to the vicinity of the junction, introduces additional electrostatic rigidity into the quantum mechanical coherent coupling across the junction. As a result, the supercurrent (which is related to the coupling strength) increases. This is a consequence of the constraint that the charge confined in the normal region is fixed, in part by the superconducting pair potential (Andreev contribution) and in part by the gate potential (normal contribution). Thus the novel operating principle of the present device greatly enhances the maximum supercurrent.

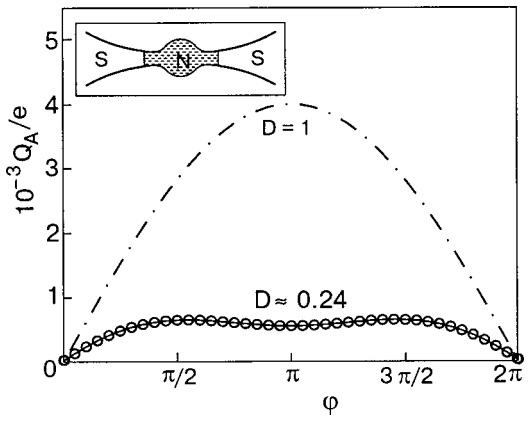

FIG. 1. Charge Q_A as a function of the phase difference φ across the junction. The circles (○) correspond to numerical DFT results. The top curve corresponds to $D\approx 1$, for which a simple analytic expression can be obtained (dot–dash curve); the bottom curve is for the more realistic case of small D. Inset: Top view of the SNS setup. The letters S denote superconducting leads and N denotes the normal interacting dot. A positively charged gate electrode lies beneath the N region.

2. SYSTEM

We consider a structure of the type depicted in the inset in Fig. 1. The electronic states in the normal region can be divided into confined states, which reside in the potential well (quantum dot) created by the gate electrode, and states which couple two superconductors. The latter consist of discrete Andreev states,[10] whose energies lie in the superconducting gap and depend on the superconducting phase difference across the junction, and continuum states lying outside the gap.

In general, states of both types contribute to the phase-dependent supercurrent flowing through the structure. In noninteracting short junctions the contribution due to the continuum states has been shown to be negligible,[11,12] especially for states far outside the gap; however, in more general situations the two contributions tend to have opposite signs.[11–14] The most dramatic manifestation of the charge accumulation effect occurs when the continuous and discrete parts of the spectrum are discriminated with respect to their contribution to the supercurrent. Such discrimination might originate from an energy dependence of the transmission amplitude through the structure. For example, if the interfaces between the dot and the leads form adiabatic microconstrictions,[15] such discrimination occurs with only one transverse mode contributing to the transmission. The contribution of the corresponding continuous spectrum of such a mode (with longitudinal energy $\mu+\epsilon<\mu-|\Delta|$) is suppressed with respect to the contribution of the Andreev states by the factor

$$D^{(1)}(E)\simeq \frac{1}{1+\mathrm{e}^{-\kappa(E-V_{\mathrm{th}}^{(1)})}},\quad \kappa\approx \pi^2\sqrt{\frac{R}{d_0}}\frac{1}{\mu},$$

where E is the energy, $V_{\mathrm{th}}^{(1)}$ is the threshold energy of the lowest transverse mode, d_0 is the minimum width of the neck, and R is the radius of curvature at the neck. Then the discrimination is determined by the parameter $\kappa|\Delta|$ and is substantial even for constriction length $l=\sqrt{d_0R/2}\sim\xi_0/5$, implying that significant discrimination can be obtained for a wide range of structure lengths.

We shall be concerned with the contribution due to discrete states. To reduce the contribution due to the continuum states to a minimum we choose a lead–dot–lead geometry such that (i) only the lowest transverse mode contributes to charge transport and (ii) the transmission amplitude $D(\epsilon)$ for this mode is very small below the bottom gap edge and increases sharply for $\epsilon\gtrsim\Delta$. Indeed, the scenario most vividly illustrating the new effect is the extreme limit $D\sim\Theta(\epsilon+|\Delta|)$. In what follows we shall take this to be the case. A more comprehensive investigation including other states will be made elsewhere. In addition, to simplify the problem we shall neglect possible transmission resonances due to normal reflection.

First we present an analytic model that accounts for the qualitative deviations from the no-interaction problem. Then we give a more general density functional theory (DFT) formulation of the problem.

3. ANALYTICS

The equilibrium zero-temperature current I can be obtained from the total energy E of the system as $I=(2e/\hbar)\partial E/\partial\varphi$,[16] where φ is the phase difference across the junction. In the spirit of the constant-interaction (CI) model[17] we approximate the total energy of the system as[1)]

$$E(V_g,\varphi)=\frac{[Q_c-\overline{Q}]^2}{2C_\Sigma}+\frac{1}{C_A}Q_cQ_A(\varphi)+\sum_j\ \epsilon_{c,j}+\epsilon_A(\varphi),\tag{1}$$

where $Q_c=N_ce$ is the confined normal charge, $\overline{Q}$ is a linear function of V_g, C_Σ is the total dot capacitance, and C_A is an effective capacitance of the order of C_Σ. Here Q_A is the amount of charge that is present inside the normal region and is associated with the formation of an Andreev level. We impose the important boundary condition that Q_c is fixed (at a value determined by V_g). The last two terms represent the eigenenergies of confined and Andreev electronic states, respectively. Since the screening is efficient, we neglect the Coulomb interactions inside the superconductors. Apart from the last term, which is responsible for the conventional Josephson supercurrent, the second term gives an additional contribution which we shall now investigate.

We shall confine our attention to ballistic, short, weak links with adiabatic leads so that only one Andreev level is relevant. For simplicity, we shall consider a quasi-1D system although the essential features of the problem are independent of dimension. Furthermore, we shall assume ideal junctions, i.e. normal reflection and no Schottky barriers, in order to emphasize the role of Andreev reflection as a significant scattering mechanism.

First we consider the limiting case of perfect normal transmission $D(\epsilon)=1$ in the interval $-|\Delta|<\epsilon<|\Delta|$ centered on the chemical potential and a stepwise constant gap parameter $\Delta(x)$.[12,18–20] By matching the bulk solutions $(u(x);v(x))$ of the Bogoliubov–de Gennes equation[22] at the NS interfaces and employing the Andreev approximation,[10,19] we find the Andreev bound state to the

lowest order in L/ξ_0, where L is the dot size and ξ_0 is the superconducting coherence length. The single-particle energy $\epsilon_A(\varphi)$ can be obtained from an asymptotic analysis[11,21] and is given by $\epsilon_A^2=|\Delta|^2(1-D\sin^2(\varphi/2))$. The charge in the normal region ($-L/2<x<L/2$) associated with the coupling between the superconductors is obtained from[22,23]

$$Q_A=2e\int_{-L/2}^{L/2}[|v|^2+f(\epsilon_A)(|u|^2-|v|^2)]dx,$$

where $f(\epsilon)$ is the Fermi–Dirac distribution. For $D(\epsilon>-|\Delta|)=1$ we find $Q_A=eL/\xi_0|\sin(\varphi/2)|$ to leading order in L/ξ_0 at zero temperature (Fig. 1). The current can now be calculated. For $\varphi\in[-\pi,\pi]$ and assuming the superconductors to be coupled[2)] the result is

$$I\approx I_{c,0}\sin\left(\frac{\varphi}{2}\right)+I_{c,0}N_c\frac{E_c}{|\Delta|}\frac{L}{\xi_0}\cos\left(\frac{\varphi}{2}\right)\mathrm{sgn}(\varphi). \qquad (2)$$

Here $I_{c,0}\equiv e|\Delta|/\hbar$, N_c is the (quantized) number of confined electrons in a dot, and $E_c=e^2/2C_A$. This suggests that the current is radically different from the ordinary Josephson effect: (i) the magnitude of the current depends on the gate voltage and (ii) the phase–current relationship does not have the familiar sinusoidal form at zero temperature. The first term of Eq. (2) gives the usual phase–current relationship of the Andreev level alone. The second term originates from the fact that the midgap Andreev states penetrate the leads to a distance that depends on the energy of the states and hence on the phase difference between the superconductors. Consequently, in the normal region the charge associated with these states is also phase-dependent, which results in a phase-dependent electrostatic interaction with the confined charge in the quantum dot. This situation is unique in the sense that the customary phase-dependent Josephson energy is accompanied by a phase-dependent electrostatic energy. Ordinarily, the uncertainty relation $\Delta N\Delta\varphi\lesssim 1$ precludes such an effect, but here the charge relevant to the electrostatics resides in the normal part of the device and is not subject to the uncertainty relation—charges on the superconducting edges are free to fluctuate as required to establish a well-defined phase difference φ.

Since N_c and E_c can be varied over a wide range by varying the depth and width of the confining potential, the current contribution from the last term can dominate the Andreev term.

Although the case of perfect normal transmission is instructive as a limiting behavior, it is not very realistic. Whereas ϵ_A is independent of the details of the scattering potential in the short-junction limit, this is not true for the charge Q_A. However, since the quantity $\sqrt{|\Delta|^2-\epsilon_A^2}$, which determines the reciprocal of the decay length of the wave function inside the leads, is reduced by the factor $\sqrt{D}$ in the presence of normal reflection, the charge Q_A is typically reduced by very roughly the same factor. Therefore normal reflection has a less severe effect on the interaction term than on the ordinary Josephson term ($\sim D$), especially for small D. A quantitative determination of the charge Q_A in the presence of normal reflection will be obtained from numerical DFT calculations.

In the absence of electron–electron interactions the coupling between two superconductors through the formation of an Andreev level always reduces the total energy. In contrast, in the present configuration Coulomb interactions in the dot destroy the Josephson coupling if the phase differences are large. However, there still exists a phase difference interval $[-\varphi_A,\varphi_A]$—henceforth termed the "Andreev window" (AW)—where the formation of an Andreev state is energetically favorable. Remarkably, the supercurrent is greatly enhanced in these regions, and to a good approximation (especially for $D\approx 1$) it is constant throughout the interval.

The criterion for the formation of an Andreev level at zero temperature (i.e. stability with respect to fluctuations of the superconducting phase, corresponding to negative Josephson coupling energy) demands for $|\varphi|\lesssim\varphi_A$ $D=1$, where $\varphi_A=(1/N_c)(\xi_0/L)|\Delta|/E_c\propto(I^{\max})^{-1}$, the latter quantity being the maximum supercurrent flowing through the link. By tuning the gate voltage we can change the number N_c by discrete amounts, which in turn changes φ_A and $I^{\max}$ in a stepwise manner. For $D<1$ the width of the Andreev window increases as a consequence of the diminished charge Q_A. Since the phase difference φ_A corresponds to interaction energy equal to $|\Delta|$, it also represents the limit of validity of Eq. (1). Consequently, the transition from finite to zero supercurrent will be continuous rather than abrupt as implied by Eq. (2).

4. NUMERICAL ANALYSIS

In this section we present a numerical analysis which supports the qualitative analysis given above. Density functional theory[24] has proven to be very successful in the study of small quantum mechanical systems, and it is particularly well suited to equilibrium situations such as the one at hand. Oliveira *et al.*[25] have shown that DFT can be extended to describe systems with general mixed normal and superconducting elements. The Bogoliubov–de Gennes–Kohn–Sham (BdGKS) equations[25,26] take the form

$$\begin{pmatrix}\mathcal{H}(\mathbf{r}) & \Delta(\mathbf{r})\\ \Delta^*(\mathbf{r}) & -\mathcal{H}(\mathbf{r})\end{pmatrix}\begin{pmatrix}u_\kappa(\mathbf{r})\\ v_\kappa(\mathbf{r})\end{pmatrix}=\epsilon_\kappa\begin{pmatrix}u_\kappa(\mathbf{r})\\ v_\kappa(\mathbf{r})\end{pmatrix}, \qquad (3)$$

where u_κ and v_κ are the two components of the κth solutions, ϵ_κ is the energy measured from the chemical potential, $\mathcal{H}$ is the appropriate effective Hamiltonian, and Δ is the self-consistent pair potential. For long weak links ($L\gtrsim\xi_0$) a self-consistent determination of the pair potential is crucial.[27] For short and narrow junctions ($\xi_0\ll L$), however, the exact shape of Δ inside the link is unimportant,[11] and we shall approximate Δ by a piecewise constant $\Delta(x)=|\Delta|\exp(i\varphi/2\mathrm{sign}(x))\Theta(|x|-L/2)$. In this approximation the BdGKS equations simplify significantly in the normal region, coupling the u and v components only through a boundary condition at the interfaces.

The problem separates naturally into a two-component formulation[28,29] where the total energy functional is

$$E[\rho_c,\rho_A]=E_{\mathrm{kin}}[\rho_c]+E_{\mathrm{kin}}[\rho_A]+E_{\mathrm{ext}}[\rho_{\mathrm{tot}}]+E_H[\rho_{\mathrm{tot}}]+E_{xc}[\rho_{\mathrm{tot}}]-E_H[\rho_A]-E_{xc}[\rho_A]. \qquad (4)$$

Here ρ_c and ρ_A are the charge density of the confined and Andreev levels, respectively, and $\rho_{\mathrm{tot}}=\rho_c+\rho_A$. The terms E_{kin}, E_{ext}, E_H, and E_{xc} are to this order the kinetic energy, the interaction with an external potential, the Hartree energy,

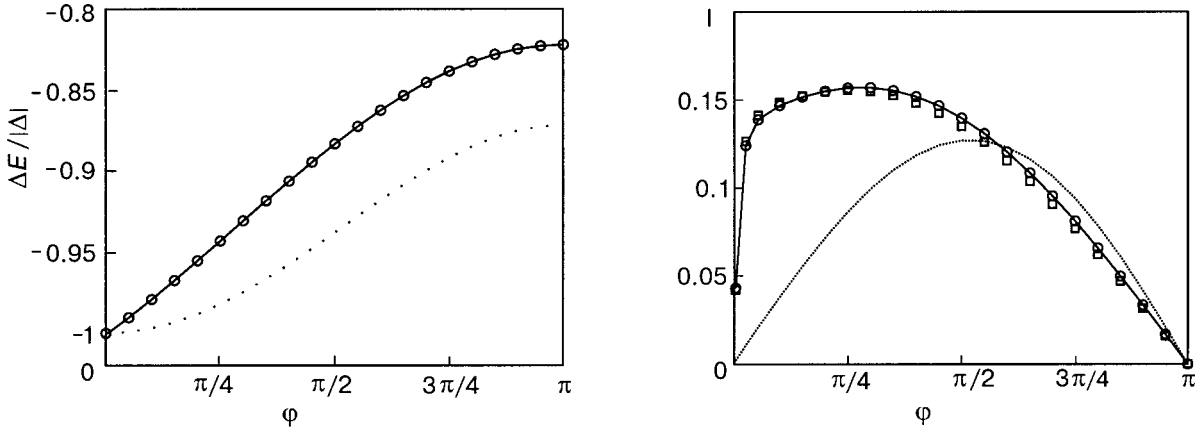

FIG. 2. *Left-hand panel*: Circles: Total energy change due to the formation of an Andreev level (the solid line is drawn as a visual aid). Dotted line: Single-particle energy ϵ_A of the Andreev level. For the parameter values the formation of an Andreev level is energetically favorable throughout the entire phase interval $[0,2\pi]$. *Right-hand panel*: Circles: Supercurrent in the presence of an Andreev level. Dotted line: Supercurrent in the absence of interactions [first term in Eq. (2)]. Squares: Current as predicted by the CI model [Eq. (1)] with the numerically obtained values of Q_A and ϵ_A. The currents are given in units of $e|\Delta|/\hbar$; E and I are, respectively, even and odd with respect to $\varphi=0$.

and the many-body exchange-correlation energy. The last two terms subtract the self-interaction of the Andreev state charge with itself (note that continuum states are not included in the DFT treatment). Provided that the potential is sufficiently deep, the confined states decay to a negligible value close to the interfaces and are unaffected by the superconducting leads. We assume that the screening is perfect everywhere in the leads so that their (infinite) energies are not included in the energy functional of Eq. (4). A local density approximation for a 2D electron gas[30] was used for the exchange-correlation energy E_{xc}. Since the Hartree term typically exceeds the XC term by several orders of magnitude, the choice of E_{xc} does not significantly affect our results. Minimizing the total energy in Eq. (4) with respect to ρ_c and ρ_A gives the generalized Kohn–Sham equations that must be solved self-consistently.

We performed the numerical calculations on a 1D grid containing the entire normal region (in the case of the BdGKS equations the grid extends slightly into the leads in order to manage the boundary conditions). In practice a narrow Gaussian charge distribution of width $W \lesssim k_F^{-1}$ is assumed in the transverse direction; this makes it easier to calculate the Coulomb interactions and justify the use of the 2D XC functionals.

We now discretize the BdGKS equations. This reduces the problem of finding the Andreev state to solving a generalized eigenvalue problem $\hat{K}(\epsilon_A)\Psi=\epsilon_A\Psi$, where $\hat{K}$ is the matrix corresponding to the BdGKS Hamiltonian and Ψ is the vector (u,v). The ϵ_A dependence of the $\hat{K}$ matrix originates from the boundary conditions. We used Arnoldi's iterative method to extract with the required accuracy the eigenvalues near the middle of the spectrum.[31] This method performed very satisfactorily. The localized normal states in the quantum dot are obtained on a 1D grid using an efficient Rayleigh quotient multigrid method.[32]

The channel length was chosen to be $L \simeq 50$ nm and the values of the material parameters were chosen so that $|\Delta| = 0.2$ MeV $\ll \mu = 1$ eV and the effective mass $m^* = 0.024$, which is typical for InAs, so that $\xi_0 \approx 13$ μm. The gate potential was represented by a smooth well which was chosen to accommodate approximately b10 electrons. The charging energy corresponding to our choice of the confining potential is $e^2/2C_A \approx 0.9$ meV.

5. RESULTS

To excellent accuracy we found the expected short-junction result[11] $\epsilon_A^2 = |\Delta|^2(1 - D\sin^2(\varphi/2))$ with the effective normal transmission coefficient $D \approx 0.24$. Figure 2 displays our main results. For our parameter values the interaction term clearly dominates the total energy. As a result of the small effective mass of InAs, the Andreev window is very wide, $\varphi_A > \pi$, and the supercurrent is nonzero for all values of the phase difference. The magnitude of the supercurrent at small phase differences is greatly enhanced and exceeds the noninteracting contribution by as much as an order of magnitude. Normal reflection is responsible for the suppression of the supercurrent for small phase values.

6. DISCUSSION

The electron–electron interactions have two main effects: (i) coupling of the superconductors through the formation of an Andreev level is energetically favorable only for sufficiently small phase differences $\varphi < \varphi_A$ and (ii) the supercurrent is greatly enhanced for small φ and its magnitude is roughly quantized. This suggests two ways to switch the supercurrent: 1) tuning φ into or out of the AW with fixed gate voltage and 2) increasing the depth of the potential well by increasing V_g increases the number N_c of confined charges, which in turn reduces φ_A in a roughly stepwise manner. Therefore for a fixed value of φ inside the initial AW the supercurrent increases in steps (for $D \approx 1$) of height $I_{c,0}(E_c/|\Delta|)(L/\xi_0)$ until $\varphi_A < \varphi$ at which point the supercurrent vanishes. Phase-biasing can be realized by integrating the SNS junction into a SQUID geometry and applying a weak magnetic field.

The interaction effects also change the voltage response of the system. In the presence of a small bias voltage[33] the phase difference changes in time according to the Josephson

relation $d\varphi/dt=2eV/\hbar$. This brings the system periodically into the AW, $|\varphi-2n\pi|<\varphi_A$, and results in a sequence of current pulses of alternating sign.

To summarize, we have considered a SNS device in the short-junction limit and investigated the consequences of the Coulomb interaction between charges confined in the normal region and the charge associated with the coupling of the superconductors. We have presented a model which accurately describes the total energy of the system, and we have derived analytic results for a limiting case which enables us to understand qualitatively the phase dependence of the energy and the stability of the system, specifically, the existence of an Andreev window and the essentially step-like magnitude of the maximum supercurrent inside this region. The numerical results obtained using the DFT support these analytical results. We found that the Coulomb interactions made the dominant contribution to the total energy, resulting in a supercurrent contribution that can greatly exceed the current in a noninteracting system. We discussed the practical consequences and suggested a way to operate a switchable weak link.

The quantitative results in this work were obtained for a relatively high value of the dielectric constant. Therefore the interaction effects in real structures can be even more pronounced than we have indicated above.

We wish to acknowledge fruitful discussions with Leonid Gorelik, Jason Hogan-O'Neill, Göran Johansson, Axel Ruhe, and Vitaly Shumeiko. Financial support was provided by the Swedish Foundation for Strategic Research (SSF) program ''Quantum Devices and Nanoscience,'' by the Swedish Natural Science Research Council, and by the Academy of Finland through its Center of Excellence Program (2000–2005).

*E-mail: klase@fy.chalmers.se

[1)]The separation of the total energy into interacting and noninteracting parts as in Eq. (1) is valid provided that the interaction energy is small compared to $|\Delta|$. In this limit the wave functions of both Andreev and confined states are largely unperturbed.

[2)]Corrections to the Andreev appproximation are required only for φ very close to $n\pi$. At these phase values the corrections ensure that $\partial Q_A/\partial\varphi \rightarrow 0$.

[1] H. Takayanagi and T. Kawakami, Phys. Rev. Lett. **54**, 2449 (1985).
[2] F.K. Wilhelm, G. Schön, and A.D. Zaikin, Phys. Rev. Lett. **81**, 1682 (1998).
[3] H. van Houten, Appl. Phys. Lett. **58**, 1326 (1991).
[4] C.W.J. Beenakker and H. van Houten, in *Single-Electron Tunneling and Mesoscopic Devices*, H. Koch and H. Lübbig (Eds.), Springer, Berlin (1992), p. 175.
[5] L.I. Glazman and K.A. Matveev, JETP Lett. **49**, 659 (1989).
[6] A.A. Clerk and V. Ambegaokar, Phys. Rev. B **61**, 9109 (2000).
[7] R. Fazio, F.W.J. Hekking, and A.A. Odintsov, Phys. Rev. Lett. **74**, 1843 (1995).
[8] D.L. Maslov, M. Stone, P.M. Goldbart, and D. Loss, Phys. Rev. B **53**, 1548 (1996).
[9] A.V. Rozhkov, D.P. Arovas, and F. Guinea, Phys. Rev. B **64**, 233301 (2001).
[10] A.F. Andreev, Zh. Éksp. Teor. Fiz. **46**, 1823 (1964) [Sov. Phys. JETP **19**, 1228 (1964)].
[11] C.W.J. Beenakker and H. van Houten, Phys. Rev. Lett. **66**, 3056 (1991).
[12] P.F. Bagwell, Phys. Rev. B **46**, 12573 (1992).
[13] I.O. Kulik, Zh. Éksp. Teor. Fiz. **57**, 1745 (1970) [Sov. Phys. JETP **30**, 944 (1970)].
[14] A.V. Svidzinsky, T.N. Antsygina, and E.N. Bratus, Sov. J. Low Temp. Phys. **10**, 131 (1973).
[15] L.I. Glazman, G.B. Lesovik, D.E. Khmel'nitskii, and R.I. Shekhter, JETP **48**, 238 (1988).
[16] P.W. Anderson, in *Lectures on the Many-Body Problem*, edited by E. R. Caianello, Academic Press, New York (1964), Vol. 2.
[17] C.W.J. Beenakker, H. van Houten, and A.A.M. Staring, Phys. Rev. B **44**, 1657 (1991).
[18] G.E. Blonder, M. Tinkham, and T.M. Klapwijk, Phys. Rev. B **25**, 4515 (1982).
[19] J. Demers and A. Griffin, Can. J. Phys. **49**, 285 (1971).
[20] A. Griffin and J. Demers, Phys. Rev. B **4**, 2202 (1971).
[21] C.W.J. Beenakker, Phys. Rev. Lett. **67**, 3836 (1991).
[22] P.-G. de Gennes, *Superconductivity of Metals and Alloys, Frontiers in Physics*, Perseus Books, Reading, Massachusetts (1999).
[23] A.A. Abrikosov, *Fundamentals of the Theory of Metals*, North-Holland, Amsterdam (1988).
[24] W. Kohn, Rev. Mod. Phys. **71**, 1253 (1998).
[25] L.N. Oliveira, E.K.U. Gross, and W. Kohn, Phys. Rev. Lett. **60**, 2430 (1988).
[26] S. Kurth, M. Marques, M. Lüders, and E.K.U. Gross, Phys. Rev. Lett. **83**, 2628 (1999).
[27] A. Levy Yeyati, A. Martin-Rodero, and F.J. Garcia-Vidal, Phys. Rev. B **51**, 3743 (1995).
[28] W. Kohn and P. Vashista, in *Theory of the Inhomogeneous Electron Gas*, edited by S. Lundqvist and N. H. March, Plenum, New York (1983), p. 79.
[29] E. Boronski and R.M. Nieminen, Phys. Rev. B **34**, 3820 (1986).
[30] B. Tanatar and D.M. Ceperley, Phys. Rev. B **39**, 5005 (1989).
[31] ARPACK numerical-routine package, available from Netlib (http://www.netlib.org).
[32] M. Heiskanen, T. Torsti, M.J. Puska, and R.M. Nieminen, Phys. Rev. B **63**, 245106 (2001).
[33] H. Kroemer, Superlattices Microstruct. **25**, 877 (1999).

The article was published in English in the original Russian journal. Reproduced here with stylistic changes by AIP.

Nuclear irradiation-induced superconductivity in the binary semiconductor InAs

A. Ya. Karpenko, P. G. Litovchenko, O. N. Shevtsova,* V. I. Sugakov, and G. A. Vikhlii

Institute for Nuclear Research, Pr. Nauki, 47. Kiev 03680, Ukraine
(Submitted September 27, 2002; revised December 23, 2002)
Fiz. Nizk. Temp. **29**, 740–743 (July 2003)

A jumplike increase of the resistance as a function of magnetic field is observed in indium arsenide samples irradiated by α particles with an energy of 80 MeV. The effect is detected at $T<5$ K. The observed effect is explained by the appearance in the crystal of superconducting areas created by nuclear irradiation. The magnetoresistance is caused by suppression of the superconductivity in the inclusions as the magnetic field is increased. The observed effect is considered in terms of a theory of the magnetoresistance of a medium with superconducting inclusions, proposed earlier. The proposed theory explains qualitatively the experimentally measured dependence of the resistance on magnetic field, namely: the jump of the resistance at a certain value of magnetic field; the shift of the curves towards higher magnetic fields with decrease of temperature; at lower values of the temperature the jump takes place in a wider range of magnetic fields (i.e., the curves became flatter). [DOI: 10.1063/1.1596577]

1. INTRODUCTION

In this paper we present experimental and theoretical results which show that areas of superconductivity can be created in a semiconductor crystal as a result of nuclear irradiation.

The appearance of metallic regions in such crystals may be caused by different technological processes, and in particular, as a result of solid-solution decomposition in multicomponent systems.[1] If one of the components exhibits superconducting properties at the corresponding temperatures, then its precipitation gives rise to superconducting regions in the crystal. Peculiarities of the conductivity and magnetic properties which could be interpreted as a phase transition to the superconducting state have been observed in the binary semiconductor PbTe.[2–4] The appearance of superconductivity in semiconductors with departures from the nominal stoichiometry has been observed in GaAs[5] and in other binar semiconductors[6] as well. Another way of creating metal areas embedded in a material is the injection of molten metal into porous glass.[7,8]

The aim of this work is to explain the peculiarities of the magnetoresistance observed in an InAs crystal irradiated by α particles at low temperature.[9] It is well known that irradiation of crystals by high-energy particles leads to generation of different types of radiation defects, for example, to the creation of macroscopic areas with properties differing significantly from those in bulk samples. In multicomponent systems the segregation effect and the creation of microscopic inclusions of the other phase and, in particular, precipitation of a metallic phase were reviewed in Ref. 10. In some systems the metal regions created exist in the superconducting state. In this work it has been shown that the presence of such superconducting regions can explain the peculiarities of the magnetoresistance of irradiated InAs.

2. EXPERIMENT

We present the results of investigations of the radiation-induced abnormal conductivity of single crystals of indium arsenide with *n*- and *p*-type conductivity at temperatures in the range 2–6 K and in the magnetic fields up to 2 T.

The samples, in the form of parallelepipeds ($1\times3\times8$ mm), before irradiation had *n*- and *p*-type conductivity, with concentrations of free carriers at a temperature of 78 K equal to 3.76×10^{16} and $3\times10^{16}\,\mathrm{cm}^{-3}$, respectively. Before irradiation the curves of the temperature and magnetic-field dependence of the conductivity of the samples in the given range of low temperatures had a form typical for InAs crystals, well described in the literature,[11] and had no peculiarities.

These two samples were irradiated by 80-MeV α particles at room temperature in the U-240 cyclotron of the Institute for Nuclear Research, Kiev. The average beam current was 1 μA, and the summary fluence, $4.8\times10^{16}\,\mathrm{cm}^{-2}$. As a result of irradiation of the samples, the electronic type of conductivity was formed, with concentrations of free carriers equal to 1.0×10^{18} and $7\times10^{17}\,\mathrm{cm}^{-3}$ at 4.2 K.

The results of measurements of the irradiated samples after one-week storage at room temperature are adduced. Peculiarities in a form of a jumplike change of the resistance by 10–20% were revealed ($T<5$ K) at certain values of the magnetic fields, temperatures, and currents through a sample. The dependence of the resistance on magnetic field at different values of the temperature is presented in Fig. 1 (dotted curves). An increase of the current through a sample leads to a decrease of the critical magnetic field H_c. An increase of the current from 10 to 1000 mA at a temperature of 4.22 K leads to a decrease of H_c from 0.6 to 0.3 T.

A jump in the temperature dependence of the resistance was observed as well.[9]

The observed peculiarities can be explained as a phase transition from the superconducting state to the normal state on the assumption that irradiation of InAs by α particles

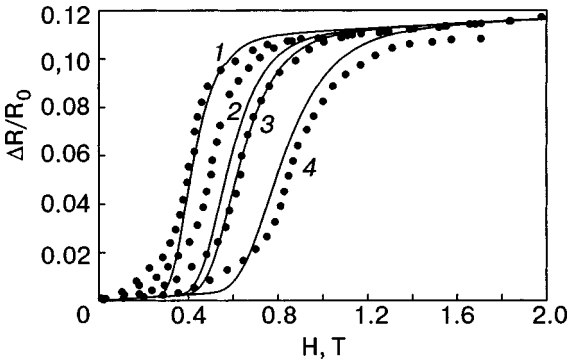

FIG. 1. Resistance of irradiated InAs sample as a function of magnetic field at different temperatures T, K: 4.22 (*1*); 3.49 (*2*); 3.23 (*3*); 2.02 (*4*). The solid lines correspond to the theoretical results, the dotted lines to the experimentally measured results. The fitting parameters are as follows: $r_0=0.52$; $s=0.2$; $P=0.07$; $\sigma_2/\sigma_3=5$.

leads to the formation of the superconducting phase in the volume of the sample.

Other peculiarities in the properties of the samples were as follows:

- After the removal of surface layers up to 50 μm (1st sample), the sample was still in the superconducting state; that allows us to affirm that the superconducting areas are located in the volume of the crystal.

- The residual resistance $(3\cdot 10^{-3}\,\Omega)$ (in the *n*- and *p*-type materials (1st and 2nd samples, respectively) indicates that the volume of the superconducting areas is a small part of the whole volume of the crystal.

- The peculiarities in the conductivity of the irradiated sample disappeared upon room-temperature annealing. In the *p*-InAs sample the conductivity jumps disappeared irreversibly after 2 months storage at room temperature. In the *n*-type sample the peculiarities of the conductivity persisted over a longer period of time (about one year). As is well known, radiation defects in crystals can disappear as a result of room-temperature annealing. Therefore it is possible to consider the disappearance of peculiarities in the conductivity as another confirmation that the conductivity jump is caused by irradiation.

3. THE MODEL OF THE SYSTEM. COMPARISON OF THE THEORY AND EXPERIMENT

We assume that the above-mentioned peculiarities of the magnetoresistance can be caused by the creation of superconducting areas in the crystals.

To explain the peculiarities of the conductivity of the irradiated crystal we apply the theory of the magnetic resistance of a crystal with superconducting inclusions, presented in Refs. 12 and 13. According to this theory the crystal under consideration consists of a matrix and metallic inclusions, which can be either in the superconducting or in the normal state, depending on their radius. The critical magnetic field quenching the superconductivity of the inclusions increases with decreasing radius of the inclusion. Thus, if the magnetic field increases, the number of the inclusions in the superconducting state is reduced.

To calculate the conductivity of a system containing superconducting inclusions we assume that the total volume occupied by the inclusions is less than the volume necessary for percolation to occur. Thus there is no superconducting current through the whole sample. So, in the calculation of the conductivity it was supposed that, depending on the temperature, magnetic field, and radius, a spherical inclusion can exist in two states: in a superconducting state with infinite conductivity, or in a normal state, with resistance corresponding to the material of the inclusion at the given temperature. Thus the irradiated crystal can be considered as a two-component system consisting of a nonsuperconducting matrix and the inclusions. According to the formula for the conductivity in multicomponent systems (see, for example, Ref. 14) we have:

$$\frac{\sigma_1-\sigma}{\sigma_1+2\sigma}P_s+\frac{\sigma_2-\sigma}{\sigma_2+2\sigma}P_n+\frac{\sigma_3-\sigma}{\sigma_3+2\sigma}P_3=0, \tag{1}$$

where σ_1 is the conductivity of an inclusion in the superconducting state ($\sigma_1=\infty$), σ_2 is the conductivity of an inclusion in the nonsuperconducting state, σ_3 is the conductivity of the matrix ($\sigma_2>\sigma_3$), and P_s and P_n are the relative volumes of the superconducting and normal inclusions, respectively,

$$P_s=P\frac{\int_0^{r_c(T,H)}r^3W(r)dr}{\int_0^{\infty}r^3W(r)dr},\quad P_n=P-P_s,\quad P_3=1-P, \tag{2}$$

where P is the relative volume of inclusions in the sample, and $W(r)$ is the distribution function of the spherical inclusion with respect to radius r. The numerical calculations were done for inclusions with a normalized Gaussian distribution over radius with a variance s^2 and center r_0:

$$W(R)=Zr^3\exp\left[-\frac{(r-r_0)^2}{2s^2}\right]. \tag{3}$$

The critical radius at given T and H is determined by the formula $r_c(T,H)=\sqrt{5}(2\kappa/H)\sqrt{1-T/T_{c0}}$ (Ref. 15). Thus the relative volume of inclusions in the superconducting state depends on the magnetic field. The criterion of applicability of this consideration and the results of calculations of the magnetoresistance at different parameters of the system $(r_0,s,\sigma_2,\sigma_3,\kappa)$ are presented in Refs. 12 and 13.

The theory describes the jumplike change of the resistance on changing temperature and magnetic field which is observed experimentally in irradiated InAs crystals. The values and location of these jumps depend on the radii of the inclusions, the radius variance, and other parameters. It should be noted that in the case considered, the dependence of the conductivity on magnetic field (magnetoresistance) is caused by suppression of the superconductivity by the magnetic field. As the magnetic field is increased, superconductivity is suppressed in the inclusions of the larger sizes and then in the inclusions of the smaller sizes.

From a comparison of the theoretical and experimental dependences of the resistance on the magnetic field, one can conclude that the curves have qualitatively similar behavior: 1) a jump of the resistance at a certain value of magnetic field is observed; 2) a shift of the curves towards larger mag-

netic fields with the decrease of temperature is observed as well; 3) at the lower values of the temperature the jump takes place in a wider range of magnetic fields (i.e., the curves became flatter).

To find the parameters of the system the following experimental facts were used:

1. The critical temperature of the regions arising as result of the irradiation is equal to $T_{c0} \approx 5$ K.

2. From Eq. (2) one can determine the interrelation between the parameters being measured. Thus by the use of the solution of Eq. (1) for the two limiting cases a) $H=0$ ($P_s=P$, $P_n=0$) and b) $H \gg H_0$ ($P_s=0$, $P_n=P$) we obtain the formula for the conductivity jump η of the irradiated material: $\eta=(\sigma_0-\sigma_\infty)/\sigma_3$. Here σ_0 is the value of the conductivity at zero magnetic field, and σ_∞ is the conductivity at a magnetic field value which exceeds the value of the critical field, and

$$\frac{\sigma_2}{\sigma_3}=\frac{-9P+2\eta+9P^2+3\eta P-18\eta^2P^2+12\eta^2P+27\eta P^3-36\eta P^2-2\eta^2}{\eta(-27P^2+27P^3+9P-1)}. \tag{4}$$

At the known η (according to the experimental data the value of the jump is approximately $\eta=0.12$) formula (4) sets up a correspondence between the volume of the inclusions P and the ratio σ_2/σ_3.

3. The inflection point of the curve $\Delta R/R_0(H)$

$$\left(\partial^2\frac{\Delta R}{R_0}(H,T)/\partial H^2=0\,\middle|_{T=(T_1,H_1)}\right)$$

and the slope of the curve at the same point

$$\partial\frac{\Delta R}{R_0}(H,T)/\partial H=\gamma_1|_{T=(T_1,H_1)}$$

were taken from experiment. Here H_1 and γ_1 are the magnetic field and the slope at the inflection point for the curve observed at the temperature T_1.

To determine the parameters of a system we used the data (plateau, inflection, and slope) of only curve *1* from Fig. 1. The other curves *2–4* were obtained without introducing new fitting parameters. One can see that there is a satisfactory coincidence of the experimental and the theoretical curves (see Fig. 1; the solid lines correspond to the theoretical curves; the dotted lines denote the experimentally measured curves). From the calculations the value $\kappa H_{c0}=0.2$ T was estimated. The other parameters are given in the figure caption.

It is seen that the curves coincide well enough except at low values of magnetic field. The disagreement of the theoretical and experimental results at low magnetic fields H may be explained by the fact that at the low fields the resistance is caused by inclusions of large sizes (the critical field of an inclusion is inversely proportional to r). Meanwhile, the proposed theory is correct for $r \leqslant 1$, and it cannot describe this magnetic-field range.

The proposed theoretical explanation of the observed effect is a phenomenological one. It confirms the appearance of the superconducting areas. To obtain experimental verification of the appearance of such areas, to estimate their sizes, and to determine their mutual arrangement, it will be necessary to carry out structural investigations.

The microscopic mechanisms responsible for creation of the metal areas may be the followings:

1) The appearance of the superconducting inclusions can be caused by the generation of metal-enriched regions due to instability of the binary crystals with respect to generation of the antisite defects during irradiation by high-energy particles.[16,17] These defects are formed by the abnormal substitution of the lattice sites by the atoms (i.e., the In atom is situated on the lattice site of the As and *vice versa*). Irradiation facilitates the accumulation of such types of defects. The metal-enriched region may have a high conductivity or be in the superconducting state. It should be noted that the appearance of superconducting properties in the binary semiconductor GaAs with departures from the nominal stoichiometry was explained in Ref. 17 by a large concentration of antisite defects.

2) The appearance of regions of high pressure near dislocations created by irradiation is possible as well. Such areas are centers of origination of strain-induced localized superconductivity.[18]

CONCLUSION

Thus, the experimental magnetic-field dependence of the resistance of InAs irradiated by α particles can be explained by the presence of superconducting inclusions. The appearance of the superconducting regions may be caused by the generation of metal-enriched areas under irradiation. The presence of inclusions which are in the superconducting phase leads to an increase of the conductivity of a crystal at low temperatures. Also, at low temperatures a strong dependence of the conductivity on magnetic field takes place. The dependence is caused by phase transitions of the inclusions from the superconducting to the nonsuper-conducting state upon increase of the magnetic field. All the effects listed depend strongly on the radius of the inclusions and the radius variance.

This research work was partially supported by the Ukrainian Ministry of Education and Sciences, Project No. 02.07/00147.

*E-mail: shevtsova@naverex.kiev.ua, shevtsova@kinr.kiev.ua

[1] M. G. Milvidskii and V. B. Osvenskii, *Structure Defects in Semiconductor Single Crystals*, Metallurgia, Moscow (1984).
[2] T. T. Dedegkaev, V. A. Moshnikov, D. B. Chesnokova, and D. A. Jaskov,

Pis'ma Zh. Tekh. Fiz. **6**, 1030 (1980) [Sov. Tech. Phys. Lett. **6**, 443 (1980)].
[3] S. D. Darchuk, L. A. Korovina, F. F. Sizov, T. Dietl, S. Kolesnik, and M. Savitskii, Fiz. Tekh. Poluprovodn. **32**, 786 (1998) [Semiconductors **32**, 700 (1998)].
[4] S. Takaoka, T. Sugita, and K. Murase, Jpn. J. Appl. Phys. **26**, 1345 (1987).
[5] J. M. Baranowski, Z. Liliental-Weber, W.-F. Yau, and E. R. Weber, Phys. Rev. Lett. **66**, 3079 (1991).
[6] R. A. Smith, *Semiconductors*, 2nd ed., Cambridge University Press, Cambridge—New York (1978), Mir, Moscow (1982).
[7] M. J. Graf, T. E. Huber, and C. A. Huber, Phys. Rev. B **45**, 3133 (1992).
[8] E. V. Charnaya, C. Tien, K. J. Lin, and C. S. Wur, Phys. Rev. B **58**, 468 (1998).
[9] G. A. Vikhlii, A. Ya. Karpenko, and P. G. Litovchenko, Ukr. Fiz. Zh. (Russ. Ed.) **43, 11**, 103 (1998).
[10] K. C. Russel, Prog. Mater. Sci. **28**, 229 (1984).
[11] C. Hilsum and A. C. Rose-Innes, *Semiconducting III–V Compounds*, Pergamon Press, New York (1961), Inostr. Lit., Moscow (1963).
[12] V. I. Sugakov and O. N. Shevtsova, Fiz. Nizk. Temp. **27**, 121 (2001) [Low Temp. Phys. **27**, 88 (2001)].
[13] V. I. Sugakov and O. N. Shevtsova, Supercond. Sci. Technol. **13**, 1409 (2000).
[14] B. E. Springett, Phys. Rev. Lett. **31**, 1483 (1973).
[15] V. L. Ginzburg, Zh. Éksp. Teor. Fiz. **34**, 113 (1958) [Sov. Phys. JETP **7**, 78 (1958)].
[16] V. V. Mykhaylovskyy, K. C. Russell, and V. I. Sugakov, *Microstructural Processes in Irradiated Materials*, Materials Research Society Symposium Proceedings, Vol. 540, S. J. Zinkle, G. E. Lucas, R. C. Ewing, and J. S. Williams (eds.), Materials Research Society, Warrendale, PA (1999), p. 667.
[17] V. V. Mikhaĭlovskiĭ, K. C. Russell, and V. I. Sugakov, Fiz. Tverd. Tela (St. Petersburg) **42**, 471 (2000) [Phys. Solid State **42**, 481 (2000)].
[18] A. Gurevich and E. A. Pashitskii, Phys. Rev. B **56**, 6213 (1997).

This article was published in English in the original Russian journal. Reproduced here with stylistic changes by AIP.

LOW-TEMPERATURE MAGNETISM

Phase states of a non-Heisenberg ferromagnet with complex single-ion anisotropy

Ya. A. Fridman,* O. A. Kosmachev, and B. L. Eingorn

V. I. Vernadskiĭ Tavricheskiĭ National University, ul. Yaltinskaya 4, 95007 Simferopol, Ukraine
(Submitted September 24, 2002; revised December 10, 2002)
Fiz. Nizk. Temp. **29**, 744–753 (July 2003)

The phase states and spectra of coupled magnetoelastic waves of a non-Heisenberg ferromagnet with complex single-ion anisotropy are investigated. The influence of inclined anisotropy on the phase states and spectra of the system is determined. The phase diagrams of the system are constructed for different relationships among the material constants. © *2003 American Institute of Physics.* [DOI: 10.1063/1.1596578]

INTRODUCTION

In compounds of rare-earth elements with low magnetic ordering temperatures a significant role in the formation of the thermodynamic and spectral properties of the magnet is played by crystal-field effects.[1–3] The effect of the crystalline field on the $4f$ electrons is weakened because of the screening by the outer electron shell, and that prevents freezing of the orbital moment of the magnetic ion. Because of the unfrozen orbital moment and strong spin–orbit coupling, the direction of the magnetic moment of the ion is influenced by the highly anisotropic crystalline field, and this leads to a large single-ion magnetic anisotropy.

It follows from the Jahn–Teller theorem[2–4] that in the case of integer spin a lowering of the symmmetry of the crystalline field should occur, leading to lifting of the degeneracy of the ground state of the magnetic ion. And because the spin Hamiltonian should have the same symmetry as the crystalline field, this can lead to a complex form of the single-ion anisotropy (SA) operator. For example, it was noted in Ref. 5 that in the crystallization of salts of rare-earth elements with the general formaula RBO_4, where R is a rare-earth ion and B=P, V, or As, as the temperature is lowered one observes a crystallographic distortion with a lowering of the lattice symmetry to monoclinic, and, accordingly, off-diagonal components of the anisotropy tensor, B_2^{xy}, B_2^{yz}, or B_2^{zx}, appear in the SA Hamiltonian.

The influence of inclined anisotropy on the phase states and spectra of coupled magnetoelastic (ME) waves of a Heisenberg ferromagnet was studied in Ref. 4. Further analysis showed that this model requires more careful study of the influence of single-ion anisotropy of monoclinic symmetry on the formation of phases and of the behavioral features of the spectra of quantum excitations.

It has been noted repeatedly[3,6–12] that the inclusion of non-Heisenberg terms in the exchange Hamiltonian can enhance the SA effects. Here quadrupolar ordering will be realized even when the SA constants are smaller than the Heisenberg exchange constants. For this reason it is of interest to study the system with the biquadratic exchange interaction taken into account for different relationships among the exchange interaction constants.

In this paper we study the influence of complex single-ion anisotropy on the phase states of a non-Heisenberg magnet with allowance for the ME interaction and investigate the behavior of the spectra near lines of phase transitions for different relationships among the exchange interaction constants.

MODEL

The Hamiltonian of a ferromagnet with a complex SA and a biquadratic exchange interaction is written in the form

$$H=-\frac{1}{2}\sum_{n\neq n'}\{I(n-n')\mathbf{S}_n\cdot\mathbf{S}_{n'}+K(n-n')(\mathbf{S}_n\cdot\mathbf{S}_{n'})^2\}$$
$$-B_2^0\sum_n O_{2n}^0-B_2^2\sum_n O_{2n}^2-B_2^{zx}\sum_n O_{2n}^{zx}$$
$$+\nu\sum_n u_{ij}(n)S_n^iS_n^j+\int dr\left\{\frac{\lambda+\eta}{2}\sum_i u_{ii}^2+\eta\sum_{i\neq j}u_{ij}^2\right.$$
$$\left.+\lambda\sum_{i\neq j}u_{ii}u_{jj}\right\}; \qquad (1)$$

the operators O_{2n}^p $(p=0, 2, zx)$ are related to the spin operators as follows: $O_{2n}^0=3(S_n^z)^2-2$, $O_{2n}^2=1/2[(S_n^+)^2+\frac{1}{2}]$, and $O_{2n}^{ij}=S_n^iS_n^j+S_n^jS_n^i$, where S_j^i are the spin operators at site n; $I(n-n')>0$ is the Heisenberg exchange constant; $K(n-n')>0$ is the biquadratic exchange constant; B_2^0, B_2^2, and B_2^{zx} are the SA constants; ν is the ME interaction constant; $u_{ij}(n)$ are the components of the elastic strain tensor; λ and η are elastic moduli. We shall further assume that the magnetic ion has spin $S=1$, since the quantum properties of the system are most clearly manifested in that case.[2]

We assume that the magnetic moment of the system lies in the ZOX plane and makes an angle θ with the OZ axis. Such a state of the system will be called the FM_{zx} phase. Let us investigate the FM_{zx} phase in the mean field approximation. We rotate the coordinate system around S^y so as to make the direction of the magnetic moment coincide with the S^z direction:

$$\mathcal{H}(\theta)=\mathrm{U}H\ \mathrm{U}^{+},\ \ \mathrm{U}(\theta)=\prod_{n}\ \exp[i\theta S_n^y].$$

After the self-consistent field $\langle S^z\rangle$ due to the ordering of the magnetic moment and the additional fields q_2^p ($p=0, 2, zx$) due to the quadrupole moments are separated out in the exchange part of the Hamiltonian (1), we obtain the following Hamiltonian of the system:

$$\begin{aligned}H(\theta)=&-\frac{1}{2}\sum_{n\neq n'}\left(I_{nn'}-\frac{1}{2}K_{nn'}\right)[S_n^+S_{n'}^-+(S_n^z-\langle S^z\rangle)\\&\times(S_{n'}^z-\langle S^z\rangle)]-\frac{K_0}{2}\sum_n\left(\frac{1}{3}q_2^0O_{2n}^0+\sum_t\ q_2^tO_{2n}^t\right)\\&-\frac{1}{2}\sum_{n\neq n'}\ K_{nn'}\left[\frac{1}{3}(O_{2n}^0-q_2^0)(O_{2n'}^0-q_2^0)\right.\\&\left.+\sum_{\substack{t=2,xy,\\xz,yz}}(O_{2n}^t-q_2^t)(O_{2n'}^0-q_2^t)\right]+\frac{N\nu s(s+1)}{3}\\&\times(u_{xx}+u_{yy}+u_{zz})-\sum_n\left(I_0-\frac{K_0}{2}\right)\langle S^z\rangle S_n^z+\frac{1}{2}N\\&\times\left[\left(I_0-\frac{K_0}{2}\right)\langle S^z\rangle^2+\frac{K_0}{2}\left(\frac{1}{3}(q_2^0)^2+\sum_t\ (q_2^t)^2\right)\right]\\&-\frac{K_0}{6}Ns^2(s+1)^2-\sum_n\ [B_2^0(\theta)O_{2n}^0+B_2^2(\theta)O_{2n}^2\\&+B_2^{zx}(\theta)O_{2n}^{zx}]+\nu\sum_n\ [u_{xy}(O_{2n}^{xy}\cos\theta+O_{2n}^{zy}\sin\theta)\\&+u_{yz}(O_{2n}^{zy}\cos\theta-O_{2n}^{xy}\sin\theta)].\end{aligned}\tag{2}$$

Here we have introduced the notation

$$B_2^0(\theta)=\frac{1}{2}\sin 2\theta(B_2^{zx}-\nu u_{zx})+A-B\cos 2\theta;$$

$$B_2^2(\theta)=-\frac{1}{2}\sin 2\theta(B_2^{zx}-\nu u_{zx})+3A+B\cos 2\theta;$$

$$B_2^{zx}(\theta)=(B_2^{zx}-\nu u_{zx})\cos 2\theta+2B\sin 2\theta;$$

$$A=\frac{1}{4}[B_2^2+B_2^0+\nu(b+b_0)];$$

$$B=\frac{1}{4}[B_2^2-3B_2^0+\nu(b-3b_0)];$$

$$b=\frac{1}{2}(u_{yy}-u_{xx});\quad b_0=\frac{1}{6}(u_{yy}+u_{xx}-2u_{zz});$$

$$q_2^p=\langle O_{2n}^p\rangle;\ \ I_0=\sum_{n'}\ I(n-n');\ \ K_0=\sum_{n'}\ K(n-n').$$

From Hamiltonian (2) we we separate out the one-site Hamiltonian

$$\begin{aligned}H_0(n)=&\varepsilon_0-\overline{H}S_n^z-\tilde{B}_2^0O_{2n}^0-\tilde{B}_2^2O_{2n}^2-\tilde{B}_2^{zx}O_{2n}^{zx}\\&+\nu S_n^iS_n^ju_{ij},\end{aligned}\tag{3}$$

where

$$\begin{aligned}\varepsilon_0=&\frac{2}{3}\nu(u_{xx}+u_{yy}+u_{zz})-\frac{2}{3}K_0+\frac{1}{2}\left(I_0-\frac{K_0}{2}\right)\langle S^z\rangle^2\\&+\frac{K_0}{4}\left(\frac{1}{3}(q_2^0)^2+(q_2^2)^2+(q_2^{zx})^2\right);\end{aligned}$$

$$\overline{H}=\left(I_0-\frac{K_0}{2}\right)\langle S^z\rangle;\ \ \tilde{B}_2^0=B_2^0(\theta)+\frac{1}{6}K_0q_2^0;$$

$$\tilde{B}_2^2=B_2^2(\theta)+\frac{1}{2}K_0q_2^2;\ \ \tilde{B}_2^{zx}=B_2^{zx}(\theta)+\frac{1}{2}K_0q_2^{zx}.$$

Solving the one-site problem with Hamiltonian (3), we obtain the eigenfunctions of the one-site Hamiltonian:

$$\begin{aligned}&|\Psi_1\rangle=\cos\varphi|1\rangle+\sin\varphi|-1\rangle;\ \ |\Psi_0\rangle=|0\rangle;\\&|\Psi^{-1}\rangle=-\sin\varphi|1\rangle+\cos\varphi|-1\rangle,\end{aligned}\tag{4}$$

and the energy levels of the magnetic ion:

$$E_{1,-1}=-\tilde{B}_2^0\mp\rho;\ \ E_0=2\tilde{B}_2^0,\tag{5}$$

where $\rho^2=\overline{H}^2+(\tilde{B}_2^2)^2$; the parameter φ is related to the material constants as

$$\tan 2\varphi=\tilde{B}_2^2/\overline{H}.$$

The spontaneous strains are determined from the minimum of the free energy. In the low-temperature limit ($T\ll T_C$, where T_C is the Curie temperature), to which we restrict discussion, E_1 is the lowest energy level of the magnetic ion. In that case we obtain the following expressions for the spontaneous strains:

$$u_{xx}^{(0)}+u_{zz}^{(0)}=-\frac{\nu}{2\eta}\sin 2\varphi-\frac{\nu(3\eta+\lambda)}{2\eta(\eta+3\lambda)};$$

$$u_{xx}^{(0)}-u_{zz}^{(0)}=\frac{\nu}{2\eta}(1-\sin 2\varphi)\cos 2\theta;$$

$$u_{yy}^{(0)}=\frac{\nu}{2\eta}\sin 2\varphi-\frac{\nu(\eta-\lambda)}{2\eta(\eta+3\lambda)};$$

$$u_{zx}^{(0)}=-\frac{\nu}{4\eta}(1-\sin 2\varphi)\sin 2\theta.$$

The equilibrium angle θ is also determined from the minimum free energy density:

$$\tan 2\theta=\frac{2(B_2^{zx}-\nu u_{zx})}{3B_2^0-B_2^2+\nu(u_{xx}-u_{zz})}.$$

Using a basis of the wave functions (4) we construct the Hubbard operators $X_n^{MM'}=|\Psi_n(M)\rangle\langle\Psi_n(M')|$, which describe the transition of the magnetic ion from the state $\Psi_n(M')$ to the state $\Psi_n(M)$.[13] These operators are related to the spin operators as follows:

$$\begin{aligned}&S^z=(X^{11}-X^{-1-1})\cos 2\varphi-(X^{1-1}+X^{-11})\sin 2\varphi;\\&S^-=(S^+)^+;\\&S^+=\sqrt{2}(X^{10}+X^{0-1})\cos\varphi+\sqrt{2}(X^{01}-X^{-10})\sin\varphi.\end{aligned}\tag{6}$$

Using expression (6), we determine the order parameters characterizing the FM_{zx} phase at low temperatures:

$$q_2^0=1;\quad q_2^2=\sin 2\varphi;\quad \langle S^z\rangle=\cos 2\varphi,$$

the parameters φ and θ taking the form:

$$\tan 2\theta=\frac{2B_2^{zx}}{3B_2^0-B_2^2};\quad \sin 2\varphi=\frac{\frac{3}{2}(B_2^0+B_2^2)-\chi}{2(I_0-K_0-a_0)},$$

where $a_0=\nu^2/2\eta$ is the ME coupling parameter, and

$$\chi^2=(B_2^{zx})^2+\left(\frac{3B_2^0-B_2^2}{2}\right)^2.$$

We write the components of the strain tensor in the form $u_{ij}=u_{ij}^{(0)}+u_{ij}^{(1)}$ is the dynamic part of the strain tensor, which describes vibrations of the sites of the crystal lattice. Separating out the terms proportional to $u_{ij}^{(1)}$ in the Hamiltonian (3) and quantizing them in the standard way,[14] we obtain a Hamiltonian describing processes of interconversion of magnons and phonons:

$$H_{TR}=\sum_n\left[\sum_M P_M H_n^M+\sum_\alpha P_\alpha X_n^\alpha\right],$$

where

$$P_{M(\alpha)}=\frac{1}{\sqrt{N}}\sum_{k,\lambda}(b_{k,\lambda}+b_{k,\lambda}^+)T_n^{M(\alpha)}(k,\lambda);\quad b_{k,\lambda}^+(b_{k,\lambda})$$

are the creation (annihilation) operators for phonons with polarization λ, N is the number of sites in the crystal lattice, $T_n^{M(\alpha)}(k,\lambda)$ are the conversion amplitudes of λ-polarized phonons and in this case have the form

$$\begin{aligned}T^{10}(k,\lambda)=&\frac{\nu}{2}A(k,\lambda)[(e_\lambda^y k_x+e_\lambda^x k_y)\sin\tilde\varphi\sin\theta\\&+(e_\lambda^y k_z+e_\lambda^z k_y)\sin\tilde\varphi\cos\theta\\&+i(e_\lambda^x k_x-e_\lambda^z k_z)\cos\tilde\varphi\sin 2\theta\\&+i(e_\lambda^x k_z+e_\lambda^z k_x)\cos\tilde\varphi\cos 2\theta],\end{aligned}$$

$$\begin{aligned}T^{1-1}(k,\lambda)=&\frac{\nu}{2}A(k,\lambda)\Big[-(e_\lambda^y k_x+e_\lambda^x k_y)\cos\theta\\&+i(e_\lambda^x k_x\cos^2\theta+e_\lambda^z k_z\sin^2\theta-e_\lambda^y k_y)\\&\times\sin 2\tilde\varphi-\frac{i}{2}(e_\lambda^x k_z+e_\lambda^z k_x)\sin 2\tilde\varphi\sin 2\theta\\&+(e_\lambda^y k_z+e_\lambda^z k_y)\sin\theta\Big],\end{aligned}$$

$$\begin{aligned}T^{-10}(k,\lambda)=&\frac{\nu}{2}A(k,\lambda)[(e_\lambda^y k_x+e_\lambda^x k_y)\cos\tilde\varphi\sin\theta\\&+(e_\lambda^y k_z+e_\lambda^z k_y)\cos\tilde\varphi\cos\theta\\&-i(e_\lambda^x k_x-e_\lambda^z k_z)\sin\tilde\varphi\sin 2\theta\\&-i(e_\lambda^x k_z+e_\lambda^z k_x)\sin\tilde\varphi\cos 2\theta],\end{aligned}$$

$$T^{\alpha(p,q)}(k,\lambda)=-(T^{\alpha(q,p)}(k,\lambda))^*,$$

$$A(k,\lambda)=\frac{\exp(\mathbf{ik\cdot n})}{\sqrt{2m\omega_\lambda(k)}};$$

$\tilde\varphi=\varphi+\pi/4$, m is the mass of the magnetic ion, and $\omega_\lambda(k)=c_\lambda k$ is the spectrum of noninteracting λ-polarized phonons.

The spectra of elementary excitations are found from the poles of the Green's function:[15]

$$G^{\alpha\alpha'}(n,\tau,n',\tau')=-\langle\hat T\tilde X_n^\alpha(\tau)\tilde X_{n'}^{\alpha'}(\tau')\rangle,$$

where $\hat T$ is the Wick operator, $\tilde X_n^\alpha(\tau)=\exp(H\tau)X_n^\alpha\times\exp(-H\tau)$ is the Hubbard operator in the Heisenberg representation, and $H=H_0+H_{TR}+H_{\rm int}$.

Further calculations will be done in the mean field approximation, and we shall therefore need only the "transverse" part of the exchange Hamiltonian $H_{\rm int}$, which has the following form in terms of the Hubbard operators:

$$H_{\rm int}=-\frac{1}{2}\sum_{n,n',\alpha,\beta}\{\mathbf{c}(\alpha),\quad\hat A_{nn'}\mathbf{c}(\beta)\}X_n^\alpha X_{n'}^\beta.$$

The eight-dimensional vector $\mathbf{c}(\alpha)$ has the following components:

$$\begin{aligned}\mathbf{c}(\alpha)=&\{\gamma_1^\parallel(\alpha),\gamma_1^\perp(\alpha),\gamma_1^\perp{}^*(-\alpha),\\&\gamma_2^\parallel(\alpha),\ \gamma_2^\perp(\alpha),\gamma_2^\perp{}^*(-\alpha),\ \gamma_3^\perp(\alpha),\ \gamma_3^\perp{}^*(-\alpha)\},\end{aligned}$$

while the 8×8 matrix $\hat A_{nn'}$ decomposes into the direct sum of two matrices: $\hat A_{nn'}=\hat A_{nn'}^{(3)}\oplus\hat A_{nn'}^{(5)}$ (see, e.g., Ref. 12).

The functions $\gamma_i^{\parallel(\perp)}(\alpha)$ are determined from the relation (6) between the spin operators and the Hubbard operators; α are root vectors which are determined by the algebra of the Hubbard operators.[13,16]

The Larkin equation for the Green's function of our system has the form[9,11]

$$\begin{aligned}G^{\alpha\alpha'}(k,\omega_n)=&\Sigma^{\alpha\alpha'}(k,\omega_n)-\frac{1}{2}\Sigma^{\alpha\alpha_1}(k,\omega_n)\\&\times\{\mathbf{c}(-\alpha_1),\ \hat A(k)\mathbf{c}(\alpha_2)\}G^{\alpha_2\alpha'}(k,\omega_n)\\&+\Sigma^{\alpha\alpha_1}(k,\omega_n)\\&\times T^{-\alpha_1}(k,\lambda)D_\lambda(k,\omega_n)T^{\alpha_2}\\&(-k,\lambda')G^{\alpha_2\alpha'}(k,\omega_n),\end{aligned}$$

where

$$D_\lambda(k,\omega_n)=\frac{2\omega_\lambda(k)}{\omega_n^2-\omega_\lambda^2(k)}$$

is the Green's function of a free λ-polarized phonon. This equation can be solved because of the separable dependence on the index α. In the mean field approximation the Larkin-irreducible part has the form $\Sigma^{\alpha\alpha'}=\delta_{\alpha\alpha'}b(\alpha)G_0^\alpha(\omega_n)$, where $b(\alpha)=\langle\boldsymbol{\alpha}\cdot\mathbf{H}\rangle_0$, and $G_0^\alpha(\omega_n)=[i\omega_n+\boldsymbol{\alpha}\cdot\mathbf{E}]^{-1}$ is the zeroth Green's function; the components of the vector $\mathbf{E}$ are the energy levels of the magnetic ion, and the components of the vector $\mathbf{H}$ are the diagonal Hubbard operators. In this approximation the dispersion relation of coupled ME waves has the form

$$\det\|\delta_{ij}+X_{ij}\|=0;\quad i,j=1,\ldots,8,\qquad(7)$$

where

$$X_{ij}=G_0^{\alpha}(\omega_n)b(\alpha)c_{ij}(\alpha)$$
$$+B^0(k,\lambda,\lambda')T^{-\alpha}(k,\lambda)G_0^{\alpha}(\omega_n)b(\alpha)T^{\beta}$$
$$(-k,\lambda')G_0^{\beta}(\omega_n)b(\beta)c_{ij}(\alpha,\beta);$$

$$B^0(k,\lambda,\lambda')=\frac{D_{\lambda}(k,\omega_n)}{1-Q_{\lambda\lambda'}D_{\lambda}(k,\omega_n)};$$

$$Q_{\lambda\lambda'}=T^{\alpha}(k,\lambda)G_0^{\alpha}(\omega_n)b(\alpha)T^{-\alpha}(k,\lambda');$$

$$c_{ij}(\alpha,\beta)=a_{ik}(\alpha,\beta)A_{kj};\quad a_{ik}(\alpha,\beta)=c_i(\alpha)c_k(-\beta).$$

It should be noted that all of the single-ion correlations have been taken into account exactly, and Eq. (7) is therefore valid for arbitrary values of the SA constants, arbitrary relationships among the exchange interaction constants, and arbitrary temperatures. For this reason one can write out its solution in the most general form, assuming that the wave vector **k** is directed along the $0Y$ axis. Then the components of the polarization unit vector of the acoustic waves are e_t^x, e_l^y, and e_{τ}^z.

The spectra of quasiphonon excitations [two transversely polarized branches (t and τ) and one longitudinally polarized (l) branch] have the form:

$$\omega_1^2(k)=\omega_t^2(k)\left(1+\frac{2a_0}{E_{1-1}+K(k)}\right), \tag{8}$$

$$\omega_2^2(k)=\omega_{\tau}^2(k)$$
$$\times\left[1+2a_0\frac{E_{10}+I(k)+(I(k)-K(k))\sin^2 2\varphi}{(E_{10}+I(k))^2-(I(k)-K(k))^2\sin^2 2\varphi}\right],$$

$$\omega_0^2(k)=\omega_l^2(k)$$
$$\times\left[1+\frac{c_0\cos^2 2\varphi}{E_{10}+K(k)+2(I(k)-K(k))\sin^2 2\varphi}\right], \tag{9}$$

and the quasimagnon spectra are

$$\varepsilon_1^2(k)=(E_{1-1}+K(k))[E_{1-1}+K(k)+2(I(k)$$
$$-K(k))\sin^2 2\varphi]. \tag{10}$$

$$\varepsilon_2^2(k)=(E_{10}+I(k))^2-(I(k)-K(k))^2\sin^2 2\varphi,$$

$$E_{1-1}=E_1-E_{-1};\quad E_{10}=E_1-E_0;\quad c_0=\frac{\nu^2}{2(\lambda+\eta)}. \tag{11}$$

In addition, it is assumed that the velocities of the t- and τ-polarized phonons are equal, i.e.,

$$\omega_t^2(k)=\omega_t^2(k)=\frac{\eta}{2m}k^2.$$

PHASE DIAGRAMS OF A NON-HEISENBERG FERROMAGNET WITH COMPLEX SINGLE-ION ANISOTROPY

As an analysis of the single-ion problem shows, in the case $I_0-K_0-a_0>0$ there are four phase states that can be realized.

The order parameters of the two phases with nonzero magnetic moment are:

For the FM_{zx} phase:

$$\langle S^z\rangle=\cos 2\varphi\cos\theta;\quad \langle S^x\rangle=\cos 2\varphi\sin 0;$$

$$q_2^{zx}=\frac{\sin 2\theta(1-\sin 2\varphi)}{2};$$

$$q_2^0=\frac{1+3\sin 2\varphi+3\cos 2\theta(1-\sin 2\varphi)}{4};$$

$$q_2^2=\frac{1+3\sin 2\varphi-\cos 2\theta(1-\sin 2\varphi)}{4};$$

$$\tan 2\theta=\frac{2B_2^{zx}}{3B_2^0-B_2^2};\quad \sin 2\varphi=\frac{\frac{3}{2}(B_2^0+B_2^2)-\chi}{2(I_0-K_0-a_0)}.$$

and for the FM_y phase:

$$\langle S^y\rangle=\cos 2\varphi;\quad q_2^0=-\frac{1+3\sin 2\varphi\cos\mu}{2};$$

$$q_2^2=-\frac{1-\sin 2\varphi\cos\mu}{2};\quad q_2^{zx}=\sin 2\varphi\sin\mu;$$

$$\sin 2\varphi\sin\mu=\frac{B_2^{zx}}{I_0-K_0-a_0};$$

$$\sin 2\varphi\cos\mu=\frac{B_2^2-3B_2^0}{2(I_0-K_0-a_0)}.$$

The parameter μ in the FM_y phase arises in the diagonalization of the one-site Hamiltonian obtained from (1) with allowance for the fact that the magnetization is directed along the OY axis. This parameter is related to the angle θ in the FM_{zx} phase by the relation $\mu+2\theta=\pi$, and the magnetization in these phases never reaches saturation, i.e., $\langle S\rangle\neq 1$.

The order parameters of the two phases with zero magnetic moment are:

For the QU_{zx} phase:

$$\langle S\rangle=0;\quad q_2^{zx}=\frac{B_2^{zx}}{I_0-K_0-a_0};$$

$$q_2^0=-\frac{1}{2}\left(1+\frac{3}{2}\frac{B_2^2-3B_2^0}{I_0-K_0-a_0}\right);$$

$$q_2^2=-\frac{1}{2}\left(1-\frac{B_2^2-3B_2^0}{2(I_0-K_0-a_0)}\right);$$

and for the QU_1 phase:

$$\langle S\rangle=0;\quad q_2^{zx}=0;\quad q_2^2=q_2^0=1.$$

The existence regions of the phases are shown on the phase diagram. For clarity the cases $B_2^2>0$ (Fig. 1a) and $B_2^2<0$ (Fig. 1b) are shown separately. Sections through the FM_{zx} phase are shaded with vertical lines, and sections

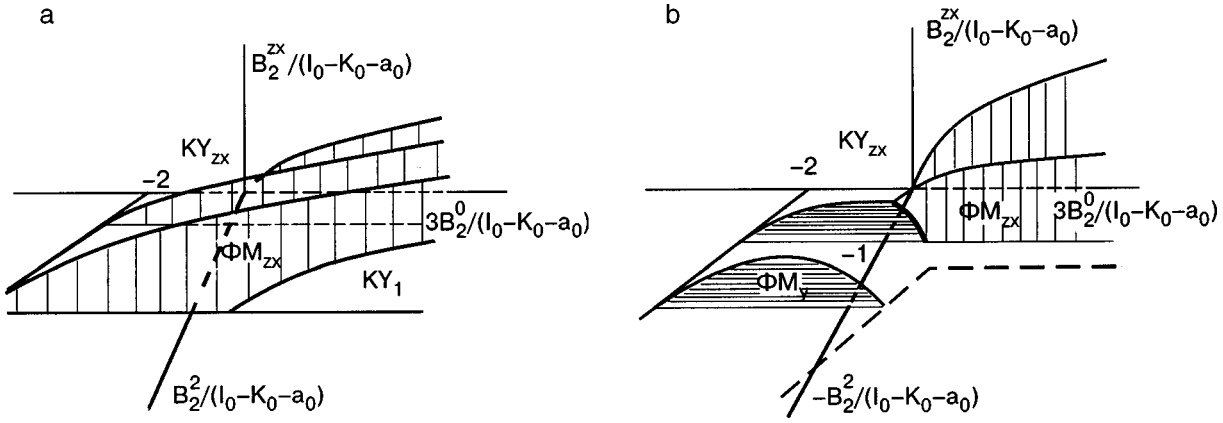

FIG. 1. Phase diagrams of a ferromagnet with inclined single-ion anisotropy when the Heisenberg interaction is predominant, $I_0-K_0-a_0>0$; $B_2^2>0$ (a), $B_2^2<0$ (b).

through the FM_y phase are shaded with horizontal lines. Below the FM phase is the QU_1 phase, and above it is the QU_{zx} phase. The heavy line in Fig. 1b shows the line of the phase transitions between the FM_{zx} and FM_y phases. In the parameter region bounded by the lines $B_2^2=-I_0+K_0+a_0$ and $B_2^2=3B_2^0-2(I_0+K_0+a_0)$ (the dashed lines in Fig. 1b) the ferromagnetic phases become unstable, and the QU_{zx} phase is realized.

Let us turn to an analysis of the expressions obtained for the spectra of coupled magnetoelastic waves. Substituting E_{1-1} and E_{10} into Eqs. (8)–(11), we obtain for the FM_{zx} phase

$$\varepsilon_1^2(k)=(2I_0-K(k)-K_0)[2I_0-K(k)-K_0-2(I(k)-K(k))\sin^2 2\varphi], \tag{12}$$

$$\omega_1^2(k)=\omega_t^2(k)\,\frac{2I_0-K(k)-K_0-2a_0}{2I_0-K(k)-K_0}, \tag{13}$$

$$\varepsilon_2^2(k)=\left(I_0-I(k)+a_0+\frac{3}{2}\chi+\frac{3}{4}(B_2^2+B_2^0)\right)^2-(I(k)-K(k))^2\sin^2 2\varphi, \tag{14}$$

$$\omega_2^2(k)=\omega_\tau^2(k)\,\frac{\left(I_0-I(k)+\frac{3}{2}\chi+\frac{3}{4}(B_2^2+B_2^0)\right)^2-(I(k)-a_0-K(k))^2\sin^2 2\varphi}{\left(I_0-I(k)+a_0+\frac{3}{2}\chi+\frac{3}{4}(B_2^2+B_2^0)\right)^2-(I(k)-K(k))^2\sin^2 2\varphi}. \tag{15}$$

Near the line of phase transitions between the FM_{zx} and FM_y phases a softening of the spectra of the quasiphonons $\omega_2(k)$ occurs, and on the line of phase transitions, which is determined by the relation

$$B_2^{zx}=\sqrt{2B_2^2(B_2^2+3B_2^0)},$$

and in the long-wavelength limit ($a_0\gg ak^2$), the quasiphonon spectrum becomes quadratic in the wave vector:

$$\omega_2^2(k)=\omega_\tau^2(k)\,\alpha k^2\left(a_0\frac{1+\sin 2\varphi_c}{1-\sin 2\varphi_c}\right)^{-1}, \tag{16}$$

and a magnetoelastic gap appears in the quasimagnon spectrum:

$$\varepsilon_2^2(0)=-2a_0(I_0-K_0-a_0)(1-\sin 2\varphi_c)\sin 2\varphi_c, \tag{17}$$

where $\alpha=I_0R_0^2$, where R_0 is the Heisenberg exchange radius, and

$$\sin 2\varphi_c=\frac{B_2^2+B_2^0}{2(I_0-K_0-a_0)}<0.$$

In the neighborhood of the lines of phase transitions $FM_{zx}-QU_1$ or $FM_{zx}-QU_{zx}$ the quasimagnon branch of excitations $\varepsilon_1(k)$ softens, and $\varepsilon_1(0)=0$ on the lines of phase transitions. The quasiphonon spectrum $\omega_1(k)$ remains linear in the wave vector, and the quasielastic wave velocity is slightly renormalized:

$$\tilde{c}_t^2=c_t^2\left(1-\frac{a_0}{I_0-K_0}\right).$$

For the $FM_{zx}-QU_1$ phase transition the line B_2^{zx} is equal to

$$\sqrt{2[B_2^2+(I_0-K_0-a_0)][B_2^2+3B_2^0+2(I_0-K_0-a_0)]}.$$

For the $FM_{zx}-QU_{zx}$ phase transition the line B_2^{zx} is equal

to

$$\sqrt{2[B_2^2-(I_0-K_0-a_0)][B_2^2+3B_2^0-2(I_0-K_0-a_0)]}.$$

On approaching the lines of phase transitions to the QU phases there is a decrease of the magnetization, and the phase transition is accompanied by the vanishing of $\langle S\rangle$.

In the QU_1 phase relations (8)–(11) take the form

$$\varepsilon_1^2(k)=\left[K(k)-K_0-2a_0+\chi-\frac{3}{2}(B_2^2+B_2^0)\right]\times\left[2I(k)-K(k)-K_0-2a_0+\chi-\frac{3}{2}(B_2^2+B_2^0)\right], \tag{18}$$

$$\omega_1^2(k)=\omega_t^2(k)\,\frac{K(k)-K_0+\chi-\frac{3}{2}(B_2^2+B_2^0)}{K(k)-K_0-2a_0+\chi-\frac{3}{2}(B_2^2+B_2^0)}, \tag{19}$$

$$\varepsilon_2^2(k)=\left[K(k)-K_0-2a_0-\chi-\frac{3}{2}(B_2^2+B_2^0)\right]\times\left[2I(k)-K(k)-K_0-2a_0-\chi-\frac{3}{2}(B_2^2+B_2^0)\right], \tag{20}$$

$$\omega_2^2(k)=\omega_\tau^2(k)\,\frac{K(k)-K_0-\chi-\frac{3}{2}(B_2^2+B_2^0)}{K(k)-K_0-2a_0-\chi-\frac{3}{2}(B_2^2+B_2^0)}. \tag{21}$$

As we see from expressions (18)–(21), the spectra of the quasiphonons $\omega_1(k)$ and $\omega_2(k)$ remain linear in the wave vector in the vicinity of the line of phase transitions QU_1–FM_{zx}, and their velocities are slightly renormalized. The quasimagnon branch of excitations $\varepsilon_1(k)$ softens near the QU_1–FM_{zx} phase boundary, and the gap in the quasimagnon spectra vanishes on the phase transition line. The phase transition is accompanied by the appearance of a magnetic moment in the ZOX plane.

In the QU_{zx} phase the spectra of coupled magnetoelastic waves, with the expressions for the order parameters taken into account, become

$$\varepsilon_1^2(k)=\left[K(k)-K_0-2a_0-\chi+\frac{3}{2}(B_2^2+B_2^0)\right]\times\left[2I(k)-K(k)-K_0-2a_0-\chi+\frac{3}{2}(B_2^2+B_2^0)\right], \tag{22}$$

$$\omega_1^2(k)=\omega_t^2(k)\,\frac{K(k)-K_0-\chi+\frac{3}{2}(B_2^2+B_2^0)}{K(k)-K_0-2a_0-\chi+\frac{3}{2}(B_2^2+B_2^0)}; \tag{23}$$

$$\varepsilon_2^2(k)=(K(k)-K_0-2(\chi+a_0))(2I(k)-K(k)-K_0-2(\chi+a_0)). \tag{24}$$

$$\omega_2^2(k)=\omega_\tau^2(k)\,\frac{2\chi+K_0-K(k)}{2(a_0+\chi)+K_0-K(k)}. \tag{25}$$

In the QU_{zx} phase the spectra of the quasiphonons $\omega_1(k)$ and $\omega_2(k)$ are practically insensitive to the influence of the magnetic subsystem and remain linear. In the vicinity of the line of phase transitions QU_{zx}–FM_{zx} a softening of the quasimagnon branch of excitations (22) occurs, and $\varepsilon_1(0)=0$ on the phase transition line. In the vicinity of the line of phase transitions QU_{zx}–FM_y the quasimagnon spectrum (24) softens, and it vanishes on the phase transition line

$$B_2^{zx}=\sqrt{(I_0-K_0-a_0)^2-((B_2^2-3B_2^0)/2)^2}.$$

For $I_0-K_0-a_0<0$ the phase states with nonzero magnetic moment become unstable, and only quadrupolar ordering is realized.

Let us consider the properties of the quadrupolar phases in more detail. If $B_2^{zx}=0$, then, as was shown in Refs. 9 and 11, for certain relationships among the SA constants the phases QU_1, QU_1', and QU_2 are realized. The ground state Ψ_{GS} of the magnetic ion in these phases is described by the following functions: $|\Psi_{GS}\rangle=1/\sqrt{2}\,(|1\rangle+|-1\rangle)$ (the QU_1 phase); $|\Psi_{GS}\rangle=1/\sqrt{2}\,(|1\rangle-|-1\rangle)$ (the QU_1' phase); $|\Psi_{GS}\rangle=|0\rangle$ (the QU_2 phase).

If $B_2^{zx}\neq 0$, then the ground state functions of the magnetic ion take the forms:

for $\varphi=\pi/4$: $|\Psi_{GS}\rangle=1/\sqrt{2}\,(|1\rangle+|-1\rangle)$, which corresponds to the QU_1 phase;

for $\varphi=-\pi/4$: $|\Psi_{GS}\rangle=\cos\theta/\sqrt{2}\,(|1\rangle-|-1\rangle)-\sin\theta|0\rangle$, which corresponds to the QU_{zx} phase.

The ground state function of the magnetic ion in the QU_{zx} phase is a superposition of its ground state functions in the QU_1' and QU_2 phases.

The spectra of coupled ME waves in the case $I_0-K_0-a_0<0$ have the form

$$\varepsilon_1^2(k)=(E_{1-1}+K(k))(E_{1-1}+2I(k)-K(k)), \tag{26}$$

$$\omega_1^2(k)=\omega_t^2(k)\left(1+\frac{2a_0}{E_{1-1}+K(k)}\right); \tag{27}$$

$$\varepsilon_2^2(k)=(E_{10}+K(k))(E_{10}+2I(k)-K(k)), \tag{28}$$

$$\omega_2^2(k)=\omega_\tau^2(k)\left(1+\frac{2a_0}{E_{10}+K(k)}\right). \tag{29}$$

In the QU_1 phase

$$E_{1-1}=-K_0-2a_0+\chi-\frac{3}{2}(B_2^2+B_2^0),$$

$$E_{10}=-K_0-2a_0-\chi-\frac{3}{2}(B_2^2+B_2^0).$$

In the QU_{zx} phase

$$E_{1-1}=-K_0-2a_0-\chi+\frac{3}{2}(B_2^2+B_2^0),$$

$$E_{10}=-K_0-2a_0-\chi.$$

Substituting the values of E_{1-1} and E_{10} into Eqs. (26)–(29), we obtain

$$\varepsilon_1^2(k)=\left(K(k)-K_0-2a_0+\chi-\frac{3}{2}(B_2^2+B_2^0)\right)$$
$$\times\left(2I(k)-K(k)-K_0-2a_0+\chi-\frac{3}{2}(B_2^2+B_2^0)\right),$$

$$\omega_1^2(k)=\omega_t^2(k)\,\frac{K(k)-K_0+\chi-\frac{3}{2}(B_2^2+B_2^0)}{K(k)-K_0-2a_0+\chi-\frac{3}{2}(B_2^2+B_2^0)};$$

$$\varepsilon_2^2(k)=\left(K(k)-K_0-2a_0-\chi-\frac{3}{2}(B_2^2+B_2^0)\right)$$
$$\times\left(2I(k)-K(k)-K_0-2a_0-\chi-\frac{3}{2}(B_2^2+B_2^0)\right),$$

$$\omega_2^2(k)=\omega_\tau^2(k)\,\frac{K(k)-K_0-\chi-\frac{3}{2}(B_2^2+B_2^0)}{K(k)-K_0-2a_0-\chi-\frac{3}{2}(B_2^2+B_2^0)}.$$

In the vicinity of the line of phase transitions QU_1-QU_{zx} the spectrum of the quasiphonons $\omega_1(k)$ softens, and on the phase transition line

$$B_2^{zx}=\sqrt{2B_2^2(B_2^2+3B_2^0)}$$

and in the long-wavelength limit it becomes quadratic:

$$\omega_1^2(k)=\omega_t^2(k)\,\frac{\gamma k^2}{a_0}, \tag{30}$$

and a magnetoelastic gap appears in the quasimagnon spectrum:

$$\varepsilon_1^2(0)=4a_0(K_0-I_0+a_0); \tag{31}$$

here $\gamma=K_0\tilde{R}_0^2$, where $\tilde{R}_0$ is the biquadratic exchange radius.

The features of the behavior of the ME waves attest to the orientational nature of the phase transition. As in the $B_2^{zx}=0$ case considered in Refs. 9 and 11, the reorientation reduces to a rotation of the principal axes of the quadrupole moment tensor.

Analogously, by substituting the values of E_{1-1} and E_{10} for the QU_{zx} phase into Eqs. (26)–(29) we obtain

$$\varepsilon_1^2(k)=\left(K(k)-K_0-2a_0-\chi+\frac{3}{2}(B_2^2+B_2^0)\right)$$
$$\times\left(2I(k)-K(k)-K_0-2a_0-\chi+\frac{3}{2}(B_2^2+B_2^0)\right),$$

$$\omega_1^2(k)=\omega_t^2(k)\,\frac{K(k)-K_0-\chi+\frac{3}{2}(B_2^2+B_2^0)}{K(k)-K_0-2a_0-\chi+\frac{3}{2}(B_2^2+B_2^0)};$$

$$\varepsilon_2^2(k)=(K(k)-K_0-2(\chi+a_0))(2I(k)-K(k)-K_0$$
$$-2(\chi+a_0)).$$

$$\omega_2^2(k)=\omega_\tau^2(k)\,\frac{2\chi+K_0-K(k)}{2(a_0+\chi)+K_0-K(k)}.$$

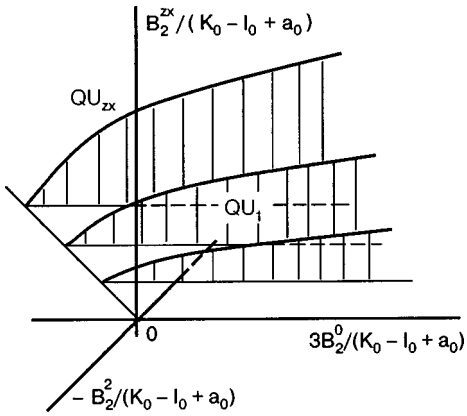

FIG. 2. Phase diagram of a ferromagnet with inclined single-ion anisotropy when the biquadratic interaction is predominant, $I_0-K_0-a_0<0$.

In the vicinity of the line of phase transitions $QU_{zx}-QU_1$ the spectrum of the quasiphonons $\omega_1(k)$ softens, and in the long-wavelength limit it becomes quadratic on the phase transition line, and a magnetoelastic gap appears in the quasimagnon spectrum [the equations are analogous to (30) and (31)].

The spectra of the quasimagnons $\varepsilon_2(k)$ and quasiphonons $\omega_2(k)$ in the vicinity of the line of phase transitions $QU_{zx}-QU_1$ behave as noninteracting excitations of the magnetic and elastic subsystems.

Several sections through the phase diagram of the system under study are presented in Fig. 2. The shaded region corresponds to the QU_1 phase; in the region of parameters satisfying the inequality $(B_2^{zx})^2>2B_2^2(B_2^2+3B_2^0)$ the QU_{zx} phase is realized.

CONCLUSION

These studies have clarified the influence of monoclinic single-ion anisotropy on the formation of phase states and the dynamic properties of non-Heisenberg magnets. A comparison of the results with those of Refs. 9, 11, and 12, in which an analogous system without the inclined anisotropy was studied, shows that the influence of the inclined anisotropy leads to substantial changes in the behavior of the system.

First, the influence of the inclined anisotropy is manifested in a complication of the phase diagram of the system. For example, in the case studied here, unlike the situation investigated in Refs. 9, 11, and 12, taking the inclined anisotropy into account leads to the formation of canted phases. In addition, the $FM_{zx}-FM_y$ phase transition occurs via the quasiphonon branch of elementary excitations; this attests to the reorientational character of this phase transition.[17] The other phase transitions that are realized in the system under study in the case of a large Heisenberg exchange occur via the quasimagnon branch of excitations. Furthermore, taking the inclined anisotropy and the biquadratic interaction into account leads to a narrowing of the existence region of the ferromagnetic phases.

In the case of a large biquadratic interaction only the quadrupolar phases are realized in the system. The structure

of these phases is more complex than in the absence of inclined anisotropy.[9,11,12] For example, a nonzero component q_2^{zx} of the quadrupole moment tensor arises.

It should be noted that the phase transitions between QU phases occur via the quasiphonon branch of excitations and are reorientational. However, the reorientation in the given case reduces to a rotation of the principal axes of the quadrupole moment tensor.

This study was supported by the Ministry of Education and Science of Ukraine (Project No. 235/03).

*E-mail: frid@tnu.crimea.ua

[1] K. P. Belov, *Rare-Earth Magnets and Their Application* [in Russian], Nauka, Moscow (1980).
[2] K. N. R. Taylor and M. I. Darby, *Physics of Rare Earth Compounds*, Chapman and Hall, London (1972), Mir, Moscow (1974).
[3] É. L. Nagaev, *Magnets with Complex Exchange Interactions* [in Russian], Nauka, Moscow (1988).
[4] L. Ya. Arifov, Yu. A. Fridman, V. I. Butrim, and O. A. Kosmachev, Fiz. Nizk. Temp. **27**, 860 (2001) [Low Temp. Phys. **27**, 636 (2001)].
[5] V. V. Val'kov and B. V. Fedoseev, Fiz. Tverd. Tela (Leningrad) **32**, 3522 (1990) [Sov. Phys. Solid State **32**, 2042 (1990)].
[6] V. M. Loktev and V. C. Ostrovskiĭ, Fiz. Nizk. Temp. **20**, 983 (1994) [Low Temp. Phys. **20**, 775 (1994)].
[7] V. V. Val'kov, G. N. Matsuleva, and S. G. Ovchinnikov, Fiz. Tverd. Tela (Leningrad) **31**(6), 60 (1989) [Sov. Phys. Solid State **31**, 948 (1989)].
[8] V. M. Loktev and V. C. Ostrovskiĭ, Ukr. Fiz. Zh. **23**, 1708 (1978).
[9] Yu. A. Fridman and O. A. Kosmachev, J. Magn. Magn. Mater. **236**, 272 (2001).
[10] V. M. Kalita and A. F. Lozenko, Fiz. Nizk. Temp. **24**, 958 (1998) [Low Temp. Phys. **24**, 721 (1998)].
[11] Yu. N. Mitsaĭ, Yu. A. Fridman, O. V. Kozhemyako, and O. A. Kosmachev, Fiz. Nizk. Temp. **25**, 690 (1999) [Low Temp. Phys. **25**, 513 (1999)].
[12] Yu. A. Fridman and O. A. Kosmachev, Fiz. Nizk. Temp. **27**, 642 (2001) [Low Temp. Phys. **27**, 473 (2001)].
[13] R. O. Zaĭtsev, Zh. Éksp. Teor. Fiz. **68**, 207 (1975) [Sov. Phys. JETP **41**, 100 (1975)].
[14] L. D. Landau and E. M. Lifshitz, *Statistical Physics*, Parts 1 and 2, 3rd ed., Pergamon Press, Oxford (1980), Nauka, Moscow (1976).
[15] Yu. A. Izyumov, F. A. Kassan-Ogly, and Yu. N. Skryabin, *Field Methods in the Theory of Magnetism* [in Russian], Nauka, Moscow (1974).
[16] Yu. N. Mitsaĭ and Yu. A. Fridman, Teor. Mat. Fiz. **81**, 263 (1988).
[17] E. A. Turov and V. G. Shavrov, Usp. Fiz. Nauk **140**, 429 (1983) [Sov. Phys. Usp. **26**, 593 (1983)].

Translated by Steve Torstveit

Current-induced change in the character of the conduction in $La_{0.775}Sr_{0.225}MnO_{3-\delta}$ films

A. N. Pogorily, A. I. Tovstolytkin,* I. V. Lezhnenko, A. I. Matviyenko, and V. P. Kravchik

Institute of Magnetism of the National Academy of Sciences of Ukraine, pr. Vernadskogo 36-b, 02142 Kiev, Ukraine

(Submitted October 9, 2002; revised December 24, 2002)
Fiz. Nizk. Temp. **29**, 754–757 (July 2003)

A study is made of the electrical properties of thin films of $La_{0.775}Sr_{0.225}MnO_{3-\delta}$ prepared on single-crystal substrates of $SrTiO_3$ by magnetron sputtering. A substantially nonlinear character of the current–voltage characteristic of the film samples is observed at temperatures below 270 K. It is shown that increasing the current density leads to a transition from a semiconducting to a metallic character of the conduction. An explanation of the results is proposed, based on the hypothesis of phase separation of the samples into conducting and insulating layers, stimulated by the mechanical stresses arising near the film–substrate boundary. © *2003 American Institute of Physics.* [DOI: 10.1063/1.1596580]

For the last decade the substituted manganites $La_{1-x}A_xMnO_3$ (A=Ba, Sr, Ca ...) have been the subject of steady interest from investigators, because of both the unusual nature of their properties[1,2] and the possibility of developing fundamentally new devices based on them.[3,4] It has been shown that the properties of these materials are determined by a complex interaction of the structural, magnetic, electronic, and orbital degrees of freedom.[1,2] While the transition of manganites from a paramagnetic insulating state to a ferromagnetic metallic state can be explained qualitatively by the classical double-exchange model,[5] for a more complete understanding of their properties it is necessary to invoke electron–lattice coupling.[1,6] Theoretical calculations show that uniform compression of the crystal lattice increases the amplitude of the intersite electronic transitions and tends to stabilize the metallic state.[6] However, the biaxial stresses that arise, for example, in epitaxial films with lattice parameters differing from those of the substrate enhance the tendency toward localization of the electrons. Fang *et al.*[7] investigated the stability of the ferromagnetic metallic state theoretically and came to the conclusion that increasing the biaxial stress promotes additional ordering of the orbitals of the manganese ions, which in turn tends to stabilize the antiferromagnetic insulating state.

Experimental studies, which in the majority of cases have been done on epitaxial films of the $La_{1-x}Ca_xMnO_3$ system, agree qualitatively with the theoretical calculations. For example, Zandbergen *et al.*[8] have shown that in ultrathin films (8 nm or less) of $La_{0.73}Ca_{0.27}MnO_3$ on $SrTiO_3$ substrates, the magnetic moment is weakened, the Curie temperature T_C is lowered, and the resistivity is increased in comparison with bulk samples. A comprehensive study of the structural, electrical, magnetic, and resonance properties of $La_{2/3}Ca_{1/3}MnO_3$ epitaxial films grown on $SrTiO_3$ substrates was reported in Ref. 9. The experimental results convincingly demonstrated that films of thickness $t \leqslant 50$ nm are characterized by lower values of T_C, smaller magnetic moments, and increased resistivity. Moreover, a nuclear magnetic resonance study has distinguished phases with different magnetic and electric properties. It was shown that ferromagnetic metallic, ferromagnetic insulator, and nonferromagnetic insulator regions coexist in the films. Recently Klein *et al.*[10] detected anisotropy of the electric properties, nonlinearity of the current–voltage characteristics, weakened ferromagnetism, and signs of antiferromagnetic ordering in biaxially stressed $La_{2/3}Ca_{1/3}MnO_3$ films. Those authors also showed that with increasing current density the system undergoes a transition to a highly conductive state, a fact that is of independent interest for magnetoelectronic devices.

The influence of biaxial stress on the properties of films of the $La_{1-x}Sr_xMnO_3$ system ($x=0.3$, 0.5) was studied in detail in Ref. 11. It was shown that the mechanical stresses created in $La_{0.7}Sr_{0.3}MnO_3$ films by $SrTiO_3$ substrates are insufficient to destroy the ferromagnetic conducting state. However, since the double exchange becomes weaker and the role of the electron–phonon interaction becomes larger as the strontium content decreases,[1,6] one would expect a stronger effect from these substrates[4] in $La_{1-x}Sr_xMnO_3$ films with lower values of x. In this paper it is shown that the conductivity of $La_{0.775}Sr_{0.225}MnO_{3-\delta}$ films deposited on $SrTiO_3$ substrates depends strongly on external factors (electric field), and that increasing the current density leads to a transition from a semiconducting to a metallic character of the conductivity.

$La_{0.775}Sr_{0.225}MnO_{3-\delta}$ (LSMO) films with a thickness of 270 nm were grown by magnetron deposition on single-crystal substrates of $SrTiO_3$ (STO) oriented in the (001) plane. The target for preparation of thin-film samples was synthesized by the standard solid-phase reaction method.[12,13] In this study we investigated films obtained at a substrate temperature of 880 °C in an atmosphere of 40%Ar and 60%O_2. The pressure of the gaseous medium during deposition was 10^{-2} torr. After preparation the film were annealed in air for 6 h at a temperature of 750 °C. X-ray studies were done on a DRON 3M diffractometer (CuK_α radiation). For the electric measurements, films of dimensions 7×15 mm were glued to a sapphire holder and placed in a massive copper cylinder, which was cooled or heated to vary the temperature of the sample. The value of the temperature was monitored by a thermoresistor glued to the

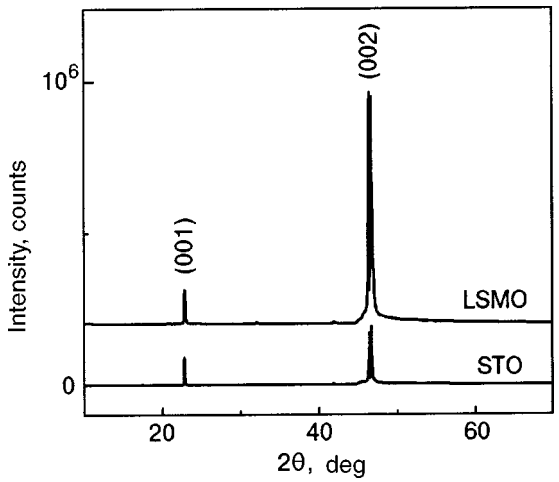

FIG. 1. X-ray diffraction patterns of a $La_{0.775}Sr_{0.225}MnO_{3-\delta}$ film and a $SrTiO_3$ substrate.

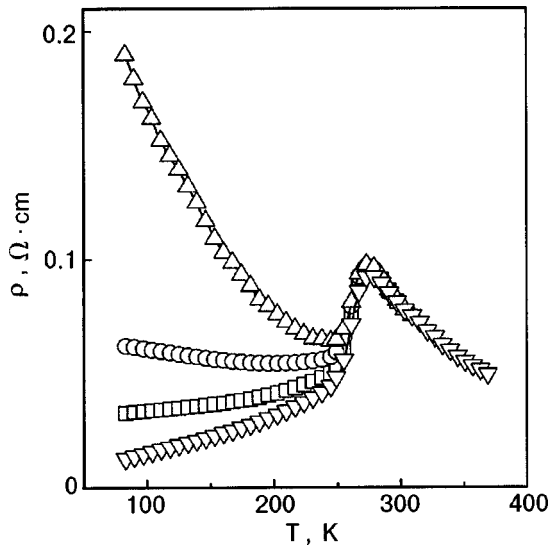

FIG. 2. Dependence of the resistivity of LSMO on the temperature T and the current strength I [mA]: 0.1 (△), 0.5 (○), 1 (□), 5 (▽).

holder a distance 3 mm from the film. Measurements of the resistivity were done in direct current by a four-probe method with the use of a computerized data collection system. The apparatus was capable of measuring the resistivity of a sample at a fixed value of the current in the range from 0.01 to 10 mA. The contacts were formed using silver paste, which was burned in at 350 °C. The temperature dependence of the resistivity was obtained on a slow heating of the samples from 77 to 370 K after a preliminary cooling to liquid helium temperature.

The x-ray diffraction patterns for one of the films studied and for the $SrTiO_3$ substrate (see Fig. 1) attest that the LSMO film is single-phase and that its growth is epitaxial. It is seen that the film has a c-axis texture characterized by high intensity of the $(00l)$ peaks (pseudocubic representation). As in the substrate, the (002) peak is split. The intensity A of the (011) and (111) peaks is not more than 0.8% of $A_{(002)}$. Reflections from phases other than perovskite are not seen on the LSMO diffraction pattern.

The resistivity ρ of the film as a function of temperature T and current strength I is shown in Fig. 2. The form of the $\rho(T)$ curve obtained for $I=5$ mA agrees with the analogous curve for bulk samples of the given composition.[12,14] Near $T_p \cong 270$ K the temperature dependence of the resistivity ($I=5$ mA) has a sharp peak, which is characteristic for a transition from a weakly conductive paramagnetic to a highly conductive ferromagnetic state.[14] In the low-temperature region ($T<T_p$) the temperature coefficient of the resistivity is greater than zero ($d\rho_{5\,\mathrm{mA}}/dT>0$), which may be evidence of complete domination of the ferromagnetic metallic phase. However, in reality the picture is significantly more complicated, as becomes obvious when the current strength is varied. Below T_p the current–voltage characteristics of the film are highly nonlinear, the degree of nonlinearity increasing as the temperature is lowered. Whereas at 250 K decreasing the current from 5 to 1 mA leads to an increase in the resistivity by a factor of 1.1, at $T=77$ K the ratio $\rho_{1\,\mathrm{mA}}/\rho_{5\,\mathrm{mA}}$ reaches 3. Further decrease of the current not only increases the resistivity significantly ($\rho_{0.1\,\mathrm{mA}}/\rho_{5\,\mathrm{mA}} \approx 1.34$ at 250 K and ≈ 16 at 77 K) but also changes the character of the conduction from metallic ($d\rho/dT>0$) to semiconductor ($d\rho/dT<0$).

It was noted above that mechanical stresses generated near the substrate–film boundary not only promote degradation of the ferromagnetic metallic state in manganites but also enhance the tendency toward antiferromagnetic ordering and localization of the charge carriers. Under such conditions the inhomogeneous state characterized by coexisting regions with differing magnetic order and conductivity turns out to be preferable to the homogeneous state,[1,2,9] and that may be the case in the samples studied here. The behavioral features which we observed in the $La_{0.775}Sr_{0.225}MnO_{3-\delta}$ epitaxial films are easily explained by assuming a coexistence of metallic and insulating phases, the relative amounts of which vary as the current density is varied.

The tendency of substituted manganites toward phase separation has been noted in a number of theoretical and experimental papers,[15–18] but only in recent times has there been convincing proof of the stability of the mixed state containing ferromagnetic metallic and nonferromagnetic (antiferromagnetic or paramagnetic) insulating regions.[1,9,19] The appearance of the latter is due in significant measure to the tendency toward mutual ordering of the charges and orbitals of the manganese ions, which in $La_{1-x}A_xMnO_3$ are found in both triply and quadruply ionized states.[1,2] Dubinin *et al.*[20] did an elastic neutron-scattering study of the features of these types of ordering in bulk single crystals of the system $La_{1-x}Sr_xMnO_3$, including samples with $x=0.23$, which are close in composition to the films studied here, and showed that regions with short-range charge/orbital order exist in the single crystal at all temperatures below T_C, i.e., they coexist with the ferromagnetic metallic phase. Since increasing the biaxial stress favors localization of the charge carriers[7,11] and the charge/orbital ordering is highly susceptible to external influences (including an electric field),[1,2] the unusual properties of $La_{0.775}Sr_{0.225}MnO_{3-\delta}$ films are logically explained by the appearance of a two-phase state of this kind.

Thus we have found that at temperatures below 270 K the resistivity of the film samples depends substantially on

the electric current. We have shown that increasing the current strength from 0.1 mA to 5 mA leads to a change in the character of the conduction from semiconductor to metallic. To explain the results we have hypothesized inhomogeneity of the low-temperature state of these films, wherein the ferromagnetic metallic phase which is characteristic for manganites of this composition coexists with another phase having weakened magnetism and conductivity.

The authors thank A. Belous and O. V'yunov (Institute of General and Inorganic Chemistry of the National Academy of Sciences of Ukraine) for providing the targets and for help in performing the x-ray studies. This study was supported in part by the Science and Technology Center in Ukraine, Project No. 1086.

*E-mail: atov@imag.kiev.ua

[1] E. Dagotto, T. Hotta, and A. Moreo, Phys. Rep. **344**, 1 (2001).
[2] V. M. Loktev and Yu. G. Pogorelov, Fiz. Nizk. Temp. **26**, 231 (2000) [Low Temp. Phys. **26**, 171 (2000)].
[3] Y. Xu, V. Dworak, A. Drechsler, and U. Hartmann, Appl. Phys. Lett. **74**, 2513 (1999).
[4] H. Katsu, H. Tanaka, and T. Kawai, Appl. Phys. Lett. **76**, 3245 (2000).
[5] C. Zener, Phys. Rev. **82**, 403 (1951).
[6] A. J. Millis, T. Darling, and A. Migliori, J. Appl. Phys. **83**, 1588 (1998).
[7] Z. Fang, I. V. Solovyev, and K. Terakura, Phys. Rev. Lett. **84**, 3169 (2000).
[8] H. W. Zandbergen, S. Freisem, T. Nojima, and J. Aarts, Phys. Rev. B **60**, 10259 (1999).
[9] M. Bibes, Ll. Balcells, S. Valencia, J. Fontcuberta, M. Wojcik, E. Jedryka, and S. Nadolski, Phys. Rev. Lett. **87**, 067210 (2001).
[10] J. Klein, J. B. Philipp, G. Garbone, A. Vigliante, L. Alff, and R. Gross, Phys. Rev. B **66**, 052414 (2002).
[11] Y. Konishi, Z. Fang, M. Izumi, T. Manako, M. Kasai, H. Kuwahara, M. Kawasaki, K. Terakura, and Y. Tokura, J. Phys. Soc. Jpn. **68**, 3790 (1999).
[12] V. G. Bar'yakhtar, A. N. Pogorily, N. A. Belous, and A. I. Tovstolytkin, J. Magn. Magn. Mater. **207**, 118 (1999).
[13] A. I. Tovstolytkin, A. N. Pogorelyĭ, S. V. Cherepov, G. V. Bondar'kova, and V. I. Silant'ev, Metallofiz. Noveĭshie Tekhnol. **22**, 23 (2000).
[14] A. Urushibara, Y. Moritomo, T. Arima, A. Asamitsu, G. Kido, and Y. Tokura, Phys. Rev. B **51**, 14103 (1995).
[15] V. N. Krivoruchko, Fiz. Nizk. Temp. **22**, 1047 (1996) [Low Temp. Phys. **22**, 798 (1996)].
[16] É. L. Nagaev, Usp. Fiz. Nauk **166**, 833 (1996).
[17] A. I. Tovstolytkin, A. N. Pogorilyi, and S. M. Kovtun, Fiz. Nizk. Temp. **25**, 1282 (1999) [Low Temp. Phys. **25**, 962 (1999)].
[18] M. Fäth, S. Freisem, A. A. Menovsky, Y. Tomioka, J. Aarts, and J. A. Mydosh, Science **285**, 1540 (1999).
[19] F. Rivadulla, M. Freita-Alvite, M. A. Lopez-Quintela, L. E. Hueso, D. R. Miguens, P. Sande, and J. Rivas, J. Appl. Phys. **91**, 785 (2002).
[20] S. F. Dubinin, V. E. Arkhipov, Ya. M. Mukovskiĭ, V. E. Naĭt, V. D. Parkhomenko, and S. G. Teploukhov, Fiz. Met. Metalloved. **93**, 60 (2002).

Translated by Steve Torstveit

Anisotropic magnetoresistive and magnetic properties of $La_{0.5}Sr_{0.5}CoO_{3-\delta}$ film

B. I. Belevtsev,* V. B. Krasovitsky, and A. S. Panfilov

B. Verkin Institute for Low Temperature Physics and Engineering of the National Academy of Science of Ukraine, 47 Lenin Ave., Kharkov 61103, Ukraine

I. N. Chukanova

Institute for Single Crystals of the National Academy of Science of Ukraine 60 Lenin Ave., Kharkov 61001, Ukraine

(Submitted October 14, 2002; revised February 4, 2003)
Fiz. Nizk. Temp. **29**, 758–763 (July 2003)

The magnetic and transport properties of a $La_{0.5}Sr_{0.5}CoO_{3-\delta}$ film grown on a $LaAlO_3$ substrate by pulsed-laser deposition are studied. The properties are found to be influenced by the magnetic anisotropy and inhomogeneity. Magnetoresistance anisotropy is determined by the shape anisotropy of the magnetization and the strain-induced magnetic anisotropy due to the film–substrate lattice interaction. Indications of the temperature-driven spin reorientation transition from an out-of-plane ordered state at low temperatures to an in-plane ordered state at high temperatures as a result of competition between the aforementioned sources of magnetic anisotropy are found. [DOI: 10.1063/1.1596581]

1. INTRODUCTION

Mixed-valence lanthanum cobaltites of the type $La_{1-x}Sr_xCoO_3$ have attracted much attention in recent years due to their unique magnetic and transport properties.[1,2] Study of this system is also important for understanding the nature of colossal magnetoresistance in the related oxides, mixed-valence manganites.[3,4] For technical application, epitaxial films of these compounds are mainly used. In that case the shape anisotropy (due to the demagnetizing effect) and the film-substrate lattice interaction can induce magnetization anisotropy and, therefore, magnetoresistance (MR) anisotropy (bulk samples of these compounds show no marked magnetic or MR anisotropy). This point has been studied rather intensively in manganite films (see Ref. 5 and references therein). Hardly any studies of this type can be found in the literature for cobaltites. In addition, the properties of mixed-valence cobaltites are influenced by their unavoidable magnetic inhomogeneity, which arises due to different extrinsic and intrinsic causes. The extrinsic ones are determined by various technological factors in the sample preparation. They can cause inhomogeneity in chemical composition (for example in oxygen concentration) or in crystal structure (polycrystalline or granular samples). The intrinsic sources of inhomogeneity are believed to arise for thermodynamic reasons and can lead to phase separation into two phases with different concentrations of the charge carriers and, therefore, to significant magnetic inhomogeneity.[1,2,6] In this article we present a study of a $La_{0.5}Sr_{0.5}CoO_{3-\delta}$ film which demonstrates a combined influence of the magnetic anisotropy and inhomogeneity on its transport, magnetoresistive, and magnetic properties. Indications of the temperature-driven spin reorientation transition from an out-of-plane ordered state at low temperatures to an in-plane ordered state at high temperatures as a result of competition between the aforementioned anisotropy sources are found.

2. EXPERIMENTAL

The $La_{0.5}Sr_{0.5}CoO_{3-\delta}$ film (about 220 nm thick) was grown by pulsed-laser deposition (PLD) on a (001) oriented $LaAlO_3$ substrate. The ceramic target used was prepared by a standard solid-state reaction technique. A PLD system with an Nd-YAG laser operating at 1.06 μm was used to ablate the target. The pulse energy was about 0.39 J with a repetition rate of 12 Hz and pulse duration of 10 ns. The film was deposited at a substrate temperature of (880 ± 5)°C in an oxygen atmosphere at a pressure of about 8 Pa. The film was cooled down to room temperature after deposition at an oxygen pressure about 10^5 Pa. The target and film were characterized by an x-ray diffraction (XRD) study.

The film resistance was measured as a function of temperature and magnetic field H (up to 20 kOe) using a standard four-point technique. The field was applied parallel or perpendicular to the film plane. In both cases it was perpendicular to the transport current. The magnetization M was measured in a Faraday-type magnetometer. A rotating electromagnet made it possible to measure the magnetization for different directions of H relative to the plane of the film.

3. RESULTS AND DISCUSSION

We have found a strong anisotropy in magnetic and magnetoresistive properties of the film studied. The anisotropy manifests itself as dramatic differences in those properties for magnetic fields applied parallel and perpendicular to the film plane. Consider at first the anisotropy of the magnetic properties. The magnetization curves for the fields parallel ($H_\parallel$) and perpendicular ($H_\perp$) to the film plane demonstrate a strong anisotropy (Fig. 1). At the maximum field applied (7 kOe), the magnetization seems to be rather close to saturation for the in-plane field orientation, but it is far from it for the out-of-plane one. It is reasonable to suppose that this is determined mainly by the shape anisotropy.

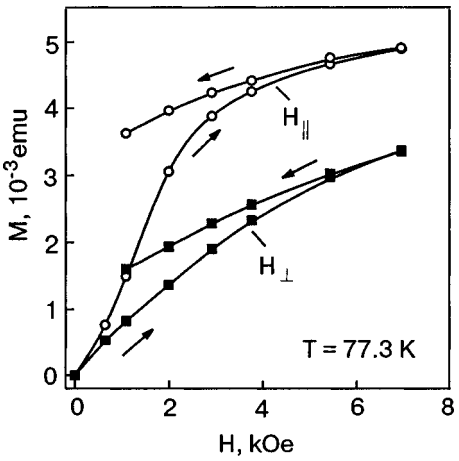

FIG. 1. Magnetization curves of the film studied for fields parallel ($H_{\|}$) and perpendicular ($H_{\perp}$) to the film plane.

The temperature dependence of the film magnetization for the field directions parallel ($M_{\|}$) and perpendicular ($M_{\perp}$) to the film plane is shown in Fig. 2. The Curie temperature T_C is found to be about 250 K. The $M_{\|}(T)$ behavior is quite common for ferromagnetic (FM) metals: it saturates with decreasing temperature. The behavior of $M_{\perp}(T)$ is quite different from that of $M_{\|}(T)$. At the fairly high field used, 2 kOe, the $M_{\perp}(T)$ curve is found to be well below the $M_{\|}(T)$ curve. Besides, in the low-temperature range the $M_{\perp}(T)$ curve is nonmonotonic (Fig. 2).

Figure 2 actually presents the $M(T)$ behavior only for two values of the angle θ between the field and the film plane: θ=0° and θ=90°. It is helpful to consider the whole curves of the angle dependence of the magnetization, presented in Fig. 3a. Here the curves $M_{\rm up}(\theta)$ and $M_{\rm down}(\theta)$ were recorded with the field rotated in steps from 0° to 360° and back to 0°, respectively. It can be seen that the magnetization takes maximum values at $\theta\approx$0°, 180°, and 360°, that

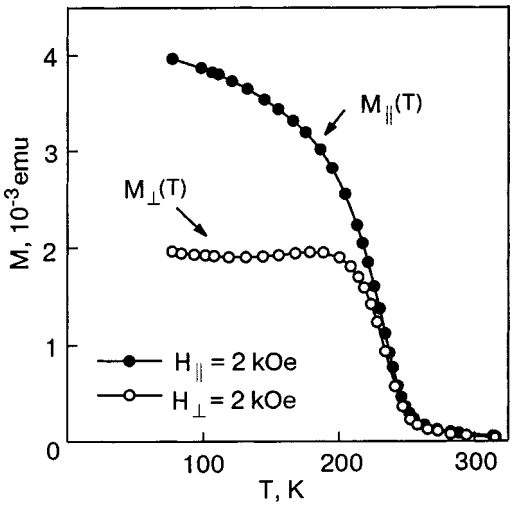

FIG. 2. Temperature dependences of the magnetization of the film studied for the magnetic field (H=2 kOe) applied parallel ($M_{\|}$) and perpendicular ($M_{\perp}$) to the film plane. The thermomagnetic prehistory: the sample was cooled down to liquid nitrogen temperature, $T\approx$77.3 K, in a field close to zero, and then the field was increased to 7 kOe and lowered to 2 kOe (see Fig. 1). After that the dependences were recorded at that field with the temperature increasing.

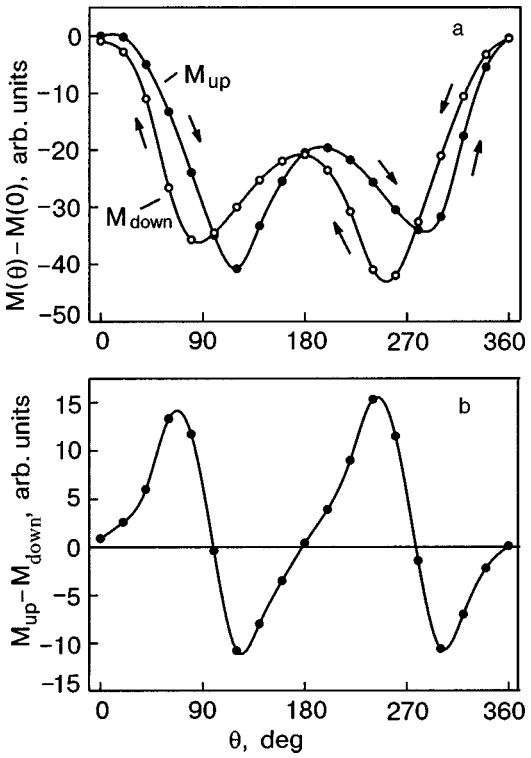

FIG. 3. Panel (a) presents the dependence of the magnetization on the angle θ between the magnetic field and the film plane (at H=2 kOe and T=77.3 K). The thermomagnetic prehistory is described in the caption to Fig. 2. The curves $M_{\rm up}(\theta)$ and $M_{\rm down}(\theta)$ were recorded with a stepwise rotation of the field from 0° to 360° and back to 0°, respectively. A considerable hysteresis effect can be seen. The angular dependence of the difference between $M_{\rm up}(\theta)$ and $M_{\rm down}(\theta)$ in panel (b) reveals this effect more clearly.

is, for the in-plane field orientations. The magnitude of the magnetization at $\theta\approx$180° is less than those at $\theta\approx$0° and 360°. This is determined by the shape of the magnetization loop and by the thermomagnetic prehistory of the sample. The minimum magnetization values are found, as expected, at $\theta\approx$90° and 270°, that is, for the out-of-plane field orientations.

A considerable hysteresis effect in the $M(\theta)$ curves is seen (Fig. 3a). To present the effect more clearly, the angular dependence of the difference between the $M_{\rm up}(\theta)$ and $M_{\rm down}(\theta)$ is shown in Fig. 3b. The function $d(\theta)=M_{\rm up}(\theta)-M_{\rm down}(\theta)$ can be taken as some measure of the angular hysteresis effect. It is seen that the $d(\theta)$ dependence is close to a periodic one with a period equal to 180°. It takes zero value at the angles which are multiples of 90°, corresponding to both the in-plane and out-of-plane directions of magnetic field (Fig. 3b). The extreme values of $d(\theta)$ are situated at some intermediate angles, which are, however, closer to the out-of-plane directions than to the in-plane ones.

As indicated above, the magnetization anisotropy in the film studied should be determined mainly by the shape anisotropy. Closer inspection shows, however, that the $M_{\perp}(T)$ behavior cannot be attributed solely to the shape-anisotropy effect: $M_{\perp}(T)$ and $M_{\|}(T)$ are practically equal in a rather broad temperature range just below T_C, then (going to lower temperature) the $M_{\perp}(T)$ curve rather abruptly goes well below the $M_{\|}(T)$ curve and becomes nonmonotonic, with a pronounced increase in $M_{\perp}(T)$ at low temperatures (Fig. 2). These $M_{\perp}(T)$ features can be caused by the strain-induced

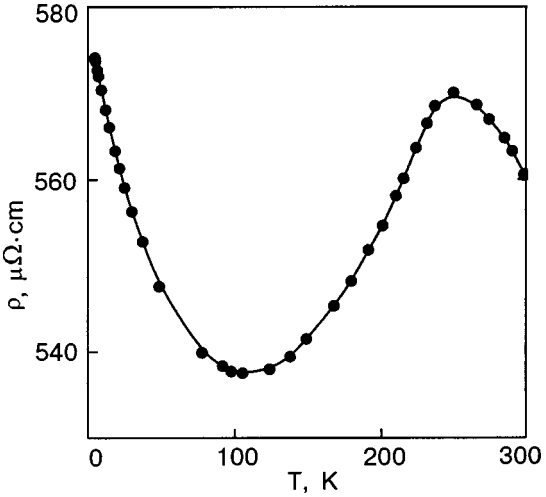

FIG. 4. Temperature dependence of the film resistivity.

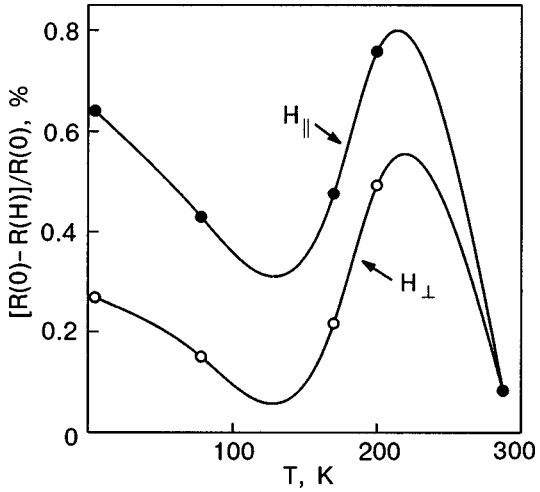

FIG. 5. Temperature dependence of the magnetoresistance at $H=20$ kOe for fields parallel ($H_{\parallel}$) and perpendicular ($H_{\perp}$) to the film plane. In both cases the fields were perpendicular to the transport current. The solid lines present a *B*-spline fitting.

magnetic anisotropy due to lattice mismatch between the film and the substrate. This guess is supported by our XRD study, which has revealed that the film has an out-of-plane tensile strain. For materials with positive magnetostriction this must favor an out-of-plane easy magnetization. Additional corroborations of this suggestion have been found in the MR properties of the film, described below.

Now turn to the transport properties of the film. The temperature dependence of the resistivity, $\rho(T)$, is found to be nonmonotonic with a maximum at $T\approx 250$ K and a minimum at $T\approx 107$ K (Fig. 4). $La_{0.5}Sr_{0.5}CoO_{3-\delta}$ samples with fairly perfect crystalline structure and δ close to zero are known[2] to be metallic ($d\rho/dT>0$) in the whole range below and above T_C. The $\rho(T)$ behavior in Fig. 4 reflects an inhomogeneous structure of the film and some oxygen deficiency. Due to the last factor, the hole concentration is less than the nominal one (at $\delta=0$). This is responsible for a resistance peak at $T=250$ K, which is common[2] for low-doped $La_{1-x}Sr_xCoO_3$ with $0.2\leqslant x\leqslant 0.3$. The low-temperature resistance minimum is typical for systems of FM regions (grains or clusters) with rather weak interconnections. For example, it has been frequently seen in polycrystalline manganites.[7–9] The inhomogeneous structure can be determined by technological factors of sample preparation (causing a polycrystalline structure with rather high tunneling barriers between the grains) or by phase separation into hole-rich and hole-poor phases.[1,2] The conductivity of inhomogeneous systems of this type is determined by the intragrain conductivity and the tunneling of charge carriers through the boundaries between the grains. A competition between these two contributions can lead to a resistance minimum.[8,9] For an extended discussion of the most obvious reasons for the appearance of the resistance minimum in polycrystalline cobaltites see Ref. 6.

The MR in the film studied is found to be anisotropic. The absolute values of negative MR in fields parallel to the film plane are considerably above those in perpendicular fields (Fig. 5). The temperature behavior of the ratio between the in-plane and out-of-plane MRs is shown in Fig. 6. It is seen from Figs. 5 and 6 that this MR anisotropy takes place only in the FM state and disappears for $T>T_C$. Since the conductivity of mixed-valence cobaltites increases with enhancement of the magnetic (spin) order, this behavior just reflects the circumstance that the magnetization increases more easily in a magnetic field parallel to the film plane, as has indeed been found in this study (Figs. 1, 2, and 3).

In polycrystalline samples (beside an intrinsic MR, which depends on magnetic order inside the grains) a significant contribution to the MR comes from grain boundaries, and this contribution increases with decreasing temperature. Discussion of the possible mechanisms for this extrinsic type of MR can be found in Refs. 10–13. The film studied does indeed show a continuous increase in MR with decreasing temperature (for temperatures well below T_C) (Fig. 5). This behavior is expected for polycrystalline FM samples with poor enough intergrain conductivity.[10,11] In contrast, for cobaltite and manganite samples with fairly good crystal perfection and even for polycrystalline samples of these materials but with a good intergrain connectivity, the MR goes nearly to zero with decreasing temperature.[10,14] It should be mentioned that grain boundaries in FM oxides are regions of perturbation of the structural and magnetic orders, and,

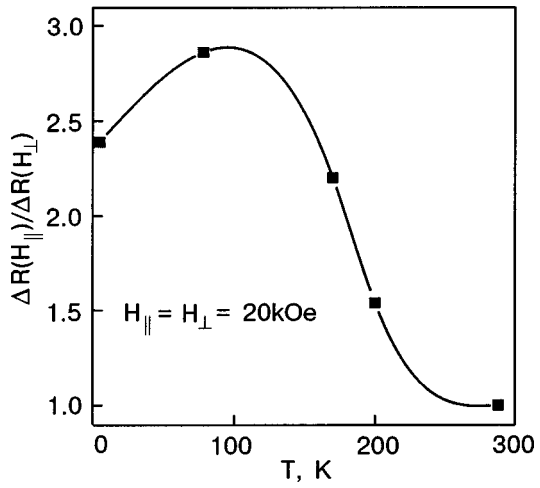

FIG. 6. Temperature dependence of the ratio of magnetoresistances for fields parallel ($H_{\parallel}$) and perpendicular ($H_{\perp}$) to the film plane. The fields were equal to 20 kOe.

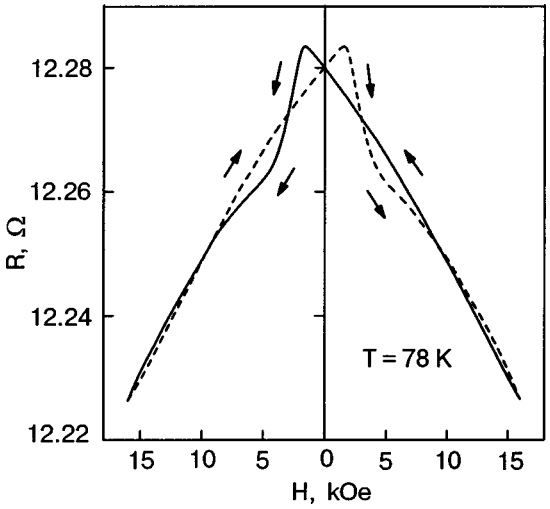

FIG. 7. Magnetoresistive hysteresis at $T=78$ K for fields parallel to the film plane and perpendicular to the transport current.

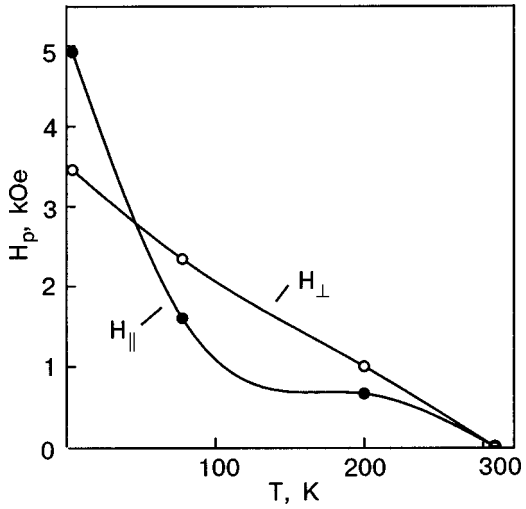

FIG. 8. Temperature dependence of characteristic field, H_p, at which resistance peaks in the magnetoresistive hysteresis curves (Fig. 7), for fields parallel ($H_\parallel$) and perpendicular ($H_\perp$) to the film plane. The field H_p corresponds to the coercive force (H_c) in the magnetization loops.

therefore, induce a magnetic inhomomogeneity as well. These boundaries (and, maybe, other sources of inhomogeneity, e.g., phase separation) can cause the significant angular hysteresis effect found in this study (Fig. 3), since they hinder the motion of FM domains upon rotation of the magnetic field. It is noteworthy, however, that the hysteresis effect is minimal at the angles corresponding to both the in-plane and out-of-plane directions of the magnetic field. In summary, the behavior of the resistivity, MR, and magnetization of the film corresponds to that of a system of weakly connected grains.

The data presented in Fig. 5 correspond to negative MR for fairly high fields. In general, the MR curves are hysteretic and have specific features in the low-field range (Fig. 7). Symmetric hysteresis curves, like that in Fig. 7, were obtained for the film after some number of repeated sweeps between the chosen maximum (positive and negative) field magnitudes. For the first sweeps, the hysteresis curves were some-what asymmetric. Actually, their behavior correlates with that of magnetization loops.[13] In particular, the field $H=H_p$ at which the resistance peaks (Fig. 7) corresponds to the value of the coercive force H_c. The value of H_p decreases with increasing temperature and goes to zero on approaching T_C. The magnitude of positive MR in the low-field range, $\Delta R(H_p)=[R(H_p)-R(0)]/R(0)$, is some measure of the remanent magnetization.

We found that H_p and $\Delta R(H_p)$ depend on the field direction and in this way reflect the magnetization anisotropy. The temperature dependences of H_p for the in-plane and out-of-plane directions of magnetic field are shown in Fig. 8. It is seen that at $T\simeq 4.2$ K the value of H_p in the out-of-plane field is less than that in the in-plane field, but at $T\approx 78$ K and higher temperatures the opposite relation is true. For high enough temperature ($T>T_C$) the H_p values go to zero for both field directions. The $\Delta R(H_p)$ values are found to be higher for the out-of-plane field direction as compared with the in-plane one at $T\simeq 4.2$ K. At $T\approx 78$ K and $T=200$ K, the opposite relation holds true. All this implies that at low temperatures the out-of-plane magnetization is favored, whereas for higher temperatures the in-plane magnetization becomes dominant. The pronounced increase in $M_\perp(T)$ at low temperatures (Fig. 2) and decrease in the ratio between the in-plane and out-of-plane MRs below $T\approx 80$ K (Fig. 6) also support this suggestion. All these are indications of a temperature-driven spin reorientation transition which can be determined by competition between the shape anisotropy and the strain-induced anisotropy. This transition has been studied rather intensively (theoretically and experimentally) for films of common FM metals[15,16] but has never been mentioned for cobaltite films. It should be noted, however, that theoretical models like those of Refs. 15 and 16 are applicable only for ultrathin magnetic films (up to 10 monolayers), whereas the film studied is much thicker and rather disordered. Consequently, the spin reorientation transition in the film studied can have a different nature than those proposed for ultrathin films.

In conclusion, we have revealed and investigated magnetic and magnetoresistance anisotropy in a $La_{0.5}Sr_{0.5}CoO_{3-\delta}$ film. Among other things, we found indications of a temperature-driven spin reorientation transition in the film studied: at low temperature, the magnetization vector tends to be perpendicular to the film plane, but with increasing temperature the magnetization vector goes entirely to the in-plane direction.

*E-mail: belevtsev@ilt.kharkov.ua

[1] M. Itoh, I. Natori, S. Kubota, and K. Motoya, J. Phys. Soc. Jpn. **63**, 1486 (1994).
[2] M. A. Senaris-Rodriguez and J. B. Goodenough, J. Solid State Chem. **118**, 323 (1995).
[3] J. M. D. Coey, M. Viret, and S. von Molnar, Adv. Phys. **48**, 167 (1999).
[4] E. Dagotto, T. Hotta, and A. Moreo, Phys. Rep. **344**, 1 (2001).
[5] B. J. Belevtsev, V. B. Krasovitsky, D. G. Naugle, K. D. D. Rathnayaka, A. Parasiris, S. R. Surthi, R. K. Pandey, and M. A. Rom, Phys. Status Solidi **188**, 1187 (2001).

[6] B. I. Belevtsev, N. T. Cherpak, I. N. Chukanova, A. I. Gubin, V. B. Krasovitsky, and A. A. Lavrinovich, J. Phys.: Condens. Matter **14**, 2591 (2002).
[7] R. Mahendiran, R. Mahesh, A. K. Raychaudhuri, and C. N. R. Rao, Solid State Commun. **99**, 149 (1996).
[8] A. de Andrés, M. Garcia-Hernández, and J. L. Martinez, Phys. Rev. B **60**, 7328 (1999).
[9] M. I. Auslender, E. Rozenberg, A. E. Kar'kin, B. K. Chaudhuri, and G. Gorodetsky, J. Alloys Compd. **326**, 81 (2001).
[10] A. Gupta, in *Colossal Magnetoresistance, Charge Ordering and Related Properties of Manganese Oxides*, C. N. R. Rao and B. Raveau (Eds.), World Scientific, Singapore (1998), p. 189.
[11] H. Y. Hwang, S.-W. Cheong, N. P. Ong, and B. Batlogg, Phys. Rev. Lett. **77**, 2041 (1996).
[12] J. E. Evetts, M. G. Blamire, N. D. Mathur, S. P. Isaac, B.-S. Teo, L. F. Cohen, and J. L. MacManus-Driscoll, Philos. Trans. R. Soc. London, Ser. A **356**, 1593 (1998).
[13] M. Ziese, Rep. Prog. Phys. **65**, 143 (2002).
[14] S. Yamaguchi, H. Taniguchi, H. Takagi, T. Arima, and Y. Tokura, J. Phys. Soc. Jpn. **64**, 1885 (1995).
[15] A. Hucht and K. D. Usadel, J. Magn. Magn. Mater. **203**, 88 (1999).
[16] L. Hu, H. Li, and R. Tao, Appl. Phys. Lett. **74**, 2221 (1999).

This article was published in English in the original Russian journal. Reproduced here with stylistic changes by AIP.

Quantum spin liquid and antiferromagnetism

E. V. Kuz'min*

L. V. Kirenskiĭ Institute of Physics, Siberian Branch of the Russian Academy of Sciences, Akademgorodok, 660036 Krasnoyarsk, Russia; Crimean State Humanitarian University, ul. Sevastopol'skaya 2, 98635 Yalta ARK, Ukraine

(Submitted October 18, 2002)
Fiz. Nizk. Temp. **29**, 764–773 (July 2003)

A spin liquid concept for the Heisenberg Hamiltonian (spin $s=1/2$) with antiferromagnetic exchange interactions between nearest neighbors is developed. The spin liquid is described by the Green's function method in the framework of a second-order theory. Equations are presented for the self-consistent calculation of the parameters of the system and its thermodynamic properties at all temperatures. A description of the spin system in the sc and bcc lattices is proposed wherein it is treated as a spatially homogeneous spin liquid with a condensate and with a singlet ground state. It is shown that the modulus of the ''staggered'' magnetization is expressed uniquely in terms of a condensate at a boundary point of the Brillouin zone and is the long-range order parameter. The existence region in temprature of the ordered state of the spin liquid with a condensate ($T<T_0$) is wider than the existence region of the two-sublattice antiferromagnetism ($T_0<T_N$, where T_N is the Néel temperature), while the energy is lower. For $T>T_0$ the system passes into an ordinary spin liquid state. © *2003 American Institute of Physics.* [DOI: 10.1063/1.1596582]

1. MARSHALL EQUATION AND ANTIFERROMAGNETISM

The rigorous theoretical description of antiferromagnetic (AF) ordering still remains an open problem after more than half a century of history. The intensive discussion of the necessary and sufficient conditions for the onset of long-range AF order in a crystal has been going on for almost 50 years since a description was given in the framework of mean (molecular) field theory and a quantum spin-wave theory of antiferromagnetism was developed. The groundwork for this problem was laid in Ref. 1.

The fundamental questions of the theory of antiferromagnetism are discussed, as a rule, on the basis of the isotropic Heisenberg model ($s=1/2$) with antiferromagnetic exchange interactions between nearest neighbors. The Hamiltonian of the system

$$\mathcal{H}=\frac{1}{2}J\sum_{\mathbf{f}\Delta}\mathbf{s_f}\cdot\mathbf{s_{f+\Delta}},\quad \mathbf{S}=\sum_{\mathbf{f}}\mathbf{s_f} \tag{1}$$

is specified on an ideal lattice of dimensionality $d=1,2,3$ with periodic boundary conditions: N is the number of sites, $\mathbf{f}$ are the coordinates of the sites, $J>0$ are the exchange integrals between nearest neighbors, z is the number of nearest neighbors, Δ are vectors connecting nearest neighbors, $\mathbf{S_f}=(\mathbf{s_f^+},\mathbf{s_f^-},\mathbf{s_f^z})$ is the spin operator at site $\mathbf{f}$, and $\mathbf{S}$ is the total spin operator. One of the main problems is to describe the long-range antiferromagnetic order. The properties of the system depend substantially on its dimensionality and geometry.

According to the Merman–Wegner theorem (see Ref. 2), long-range magnetic order in one- and two-dimensional systems (in the case of short-range exchange interactions) is absent at any finite temperature $T\neq 0$. For a linear chain ($d=1$) there is an exact solution due to Hulthén:[2] the ground state is a nondegenerate singlet ($S=0$) with energy per bond $\varepsilon_0=0.25-\ln 2=-0.4431$ (in units of the exchange). In a square lattice ($d=2$) it is only for $T=0$ that a two-sublattice AF state can be constructed and its energy ε_{AF} calculated in the framework of the spin-wave theory. In a previous paper[3] by the author it was shown on the basis of the spin liquid concept that the ground state of a Hamiltonian spin system on a square lattice is a singlet state with an energy $\varepsilon_0<\varepsilon_{AF}$, viz., $\varepsilon_0=-0.352$.

Discussion of the problem of long-range AF order centers mainly on three-dimensional systems and consists in the following.

On the one hand, there is the traditional approach to the description of antiferromagnetism. In alternant lattices[1)] (sc and bcc and also the square lattice and the linear chain) a ''checkerboard'' arrangement of spins is possible which can be described by the Néel wave vector $|AF\rangle$ (an antiferromagnet with two mirror sublattices A and B). It is known that such a function is an eigenfunction only for the operator S^z with a total spin projection $S^z=S_A^z+S_B^z=0$, but it is not an eigenfunction for the Hamiltonian nor for the operator $\mathbf{S}^2$. This means that the antiferromagnetic state is a state with an indeterminate degeneracy.[4] However, the use of the approximate Néel function $|AF\rangle$, in which the sublattices are fixed and long-range AF order is postulated, has its indisputable advantages, since it permits calculation of the excitation spectrum, the energy of the AF state with allowance for transverse quantum spin fluctuations, the sublattice magnetization $\overline{s}(T)$, and the Néel temperature T_N. The theory is approximate and is valid only in the magnetically ordered phase for $T\leqslant T_N$.

On the other hand, Marshall[5] (see Ref. 1) has stated a theoremic assertion that the ground state of Hamiltonian (1) with AF exchange interactions J between nearest neighbors on alternant lattices is a nondegenerate singlet with $S=0$. It

TABLE I. Main characteristics of a spin system with an antiferromagnetic exchange bond between nearest neighbors.

Lattice type	Singlet (SL and SLC)				AF		
	$\lvert\varepsilon_0\rvert$ Ref. 5	$\lvert\varepsilon_0\rvert$	$\lvert\mathbf{m}_0\rvert$	τ_0	$\lvert\varepsilon_{AF}\rvert$	$\overline{S}(0)$	τ_N
Square	0.328	0.352	∞	–	0.335	0.3	0
sc	0.3007	0.312	0.434	0.213	0.296	0.432	0.163
bcc	0.2892	0.297	0.452	0.224	0.287	0.448	0.181

Note: $\varepsilon=\langle H\rangle/\langle zNJ/2\rangle$ is the energy of the system at zero temperature (in units of the exchange per bond) in the singlet (0) and antiferromagnetic (AF) states; $|\mathbf{m}_0|$ is the modulus of the "staggered" magnetization at $T=0$; $\overline{S}(0)$ is the AF order parameter (sublattice magnetization) at $T=0$; $\tau_0=T_0/zJ$ is the temperature at which $|\mathbf{m}|$ vanishes; $\tau_N=T_N/zJ$ is the Néel temperature.

has been *rigorously* proven only for the one-dimensional chain, while for $d=2$ and 3 dimensions there are enormous mathematical difficulties in constructing an exact singlet function, since the number of partial singlet functions contained in it and comprising the total set of states is factorially large in N. The absence of an exact singlet state makes it impossible to directly verify Marshall's assertion, which has a natural quantum mechanical basis. Indeed, Hamiltonian (1) commutes with any component of the total spin operator $\mathbf{S}$, and its eigenfunctions are therefore eigenfunctions of the operators S^z and $\mathbf{S}^2$, while the eigenvalues $E(S)$ are classified according to the value of the total spin S $(0\leqslant S\leqslant N/2)$. According to Marshall, $\min\{E(S)\}=E(0)$ corresponds to a singlet ground state with $S=0$. Marshall constructed an approximate singlet wave function and used a variational method to calculate the energy ε_0 in alternant lattices (see Table I). A comparison of the energies ε_0 (according to Marshall) and $\varepsilon_{\rm AF}$ shows that these energies are very close, but in the context of the approximations made (which are, generally speaking, different), it is impossible to conclusively decide the type of ground state.

The question arises: Can these two approaches be reconciled theoretically? Below, on the basis of the spin liquid concept developed by the author, a theoretical version of the description of the properties of the spin system in sc and bcc lattices is proposed which is valid at all temperatures. It should be noted that the spin liquid (SL) concept has a rather wide domain of applicability. In addition to two-dimensional systems, in the fcc lattice, because of frustration of the exchange J bonds and the presence of transverse quantum spin fluctuations, the AF state is absent at all temperatures, and the system is a spin liquid with a singlet ground state.[6] In this paper it is shown that in the sc and bcc lattices the ground state is a singlet (in accordance with Marshall), but for $T\leqslant T_0$ the system nevertheless has long-range order, which is described by the modulus of the "staggered magnetization." For $T>T_0$ the system is found in an ordinary SL state.

The results of the spin-wave theory and the main equations of the spin liquid theory are briefly set forth below in the framework of a unified Green's function method.[7]

2. SPIN-WAVE THEORY OF ANTIFERROMAGNETISM

On alternant lattices a "checkerboard" distribution is possible, with spins "up" (sublattice A, sites α) and "down" (sublattice B, sites β); for nearest neighbors $\alpha+\Delta=\beta$, $\beta+\Delta'=\alpha'$. It is convenient to go over to a dimensionless Hamiltonian $h=H/zJ$; then all the energy parameters will be measured in units of zJ, including the temperature $\tau=T/zJ$.

The spin-wave theory is based on linearized first-order equations (the Tyablikov decoupling)

$$i\dot{s}_\alpha^+=\overline{s}\left(s_\alpha^+ +\frac{1}{z}\sum_\Delta s_{\alpha+\Delta}^+\right),\quad i\dot{s}_\beta^+=-\overline{s}\left(s_\beta^+ +\frac{1}{z}\sum_\Delta s_{\beta+\Delta}^+\right), \tag{2}$$

where $\langle s_\alpha^z\rangle=-\langle s_\beta^z\rangle\equiv\overline{s}$. After Fourier transformation with respect to the sublattices in the standard way, we find the Green's functions

$$\langle\langle S_A^+(\mathbf{q})|S_A^-(-\mathbf{q})\rangle\rangle_\omega=\frac{2\overline{s}(\omega+\overline{s})}{D(\mathbf{q},\omega)},$$

$$\langle\langle S_A^+(\mathbf{q})|S_B^-(-\mathbf{q})\rangle\rangle_\omega=\frac{2\overline{s}^2\gamma_\mathbf{q}}{D(\mathbf{q},\omega)}, \tag{3}$$

where

$$D(\mathbf{q},\omega)=\omega^2-\Omega_\mathbf{q}^2,\quad \Omega_\mathbf{q}=\overline{s}\sqrt{1-\gamma_\mathbf{q}^2}\equiv\overline{s}\varepsilon_\mathbf{q},$$

$$\gamma_\mathbf{q}=\frac{1}{z}\sum_\Delta e^{i\mathbf{q}\cdot\Delta}. \tag{4}$$

We calculate the Fourier transforms of the correlation functions $\langle S_A^+(\mathbf{q})S_A^-(-\mathbf{q})\rangle$ and $\langle S_A^+(\mathbf{q})S_B^-(-\mathbf{q})\rangle$ according to the spectral theorem and then, using the sum rule $\langle s_\alpha^+ s_\alpha^-\rangle=(1/2)+\overline{s}$, we obtain an equation for calculating the order parameter:

$$\overline{s}(\tau)=\frac{1/2}{l(\tau)},\quad I(\tau)=\frac{1}{N}\sum_\mathbf{q}\frac{1}{\varepsilon_\mathbf{q}}\coth\left(\frac{\overline{s}(\tau)\varepsilon_\mathbf{q}}{2\tau}\right). \tag{5}$$

It follows from (5) that for $\tau=0$

$$\overline{s}(0)=\frac{1/2}{I_1},\quad I_1=\frac{1}{N}\sum_\mathbf{q}\frac{1}{\varepsilon_\mathbf{q}}, \tag{6}$$

and for $\tau\to\tau_N$, $\overline{s}\to 0$, where $\tau_N=T_N/zJ$ is the Néel temperature, we have

$$\tau_N=\frac{1/4}{I_2},\quad I_2=\frac{1}{N}\sum_\mathbf{q}\frac{1}{\varepsilon_\mathbf{q}^2}. \tag{7}$$

The energy of the antiferromagnet (in units of J per bond) is equal to

$$\varepsilon_{AF}(\tau)=\frac{\langle H\rangle}{(1/2)zN\cdot J}$$

$$\approx-\left(\overline{s}^2(\tau)+\overline{s}(\tau)\frac{1}{N}\sum_\mathbf{q}\frac{\gamma_\mathbf{q}^2}{\varepsilon_\mathbf{q}}\coth\frac{\overline{s}(\tau)\varepsilon_\mathbf{q}}{2\tau}\right). \tag{8}$$

For three-dimensional alternant lattices we obtain the following numerical results (the sums over the first Brillouin zone are replaced by integrals with the densities of states given in the Appendix):

$$\text{sc}\ \ (z=6):\varepsilon_{AF}(0)=-0.297,\ \overline{s}(0)=0.432.$$

$$\tau_N=0.163;$$

$$\text{bcc}\ \ (z=8):\varepsilon_{AF}(0)=-0.287,\ \overline{s}(0)=0.448. \tag{9}$$

$\tau_N = 0.181$.

3. QUANTUM SPIN LIQUID

Let us consider a spin system with the Hamiltonian (1) in a lattice of arbitrary dimensionality and geometry. We define a *spin liquid* as a system which is, on average, spatially uniform, with no breaking of the spin symmetry, and in which the spin correlation functions are isotropic,

$$\frac{1}{N}\sum_{\mathbf{f}} \langle s^x_{\mathbf{f}} s^x_{\mathbf{f}+\mathbf{r}}\rangle = \frac{1}{N}\sum_{\mathbf{f}} \langle s^y_{\mathbf{f}} s^y_{\mathbf{f}+\mathbf{r}}\rangle = \frac{1}{N}\sum_{\mathbf{f}} \langle s^z_{\mathbf{f}} s^z_{\mathbf{f}+\mathbf{r}}\rangle \equiv \frac{1}{4}K_r \tag{10}$$

and depend only on the modulus of the distance $r=|\mathbf{r}|$, with $K_0=1$ (the sum rule); the average values for any component of a site spin and for any component of the total spin operator are equal to zero:

$$\langle s^\alpha_{\mathbf{f}}\rangle = 0, \quad \langle S^\alpha\rangle = 0, \quad \alpha = x,y,z \ \text{ or } \ +,-,z; \tag{11}$$

and the average value of a product of spin operators on an odd number of *different* sites is zero:

$$\langle s^\alpha_{\mathbf{f}} s^\beta_{\mathbf{m}} s^\gamma_{\mathbf{n}}\rangle = 0, \ \mathbf{f}\neq\mathbf{m}\neq\mathbf{n}, \ \ldots . \tag{12}$$

Here and below the symbol $\langle ... \rangle$ denotes a thermodynamic average at a temperature $\tau = T/zJ$ and over the ground state wave function for $\tau = 0$.

The whole set of properties of the spin liquid—the ground state, excitation spectrum, and thermodynamics—must be described on the basis of Hamiltonian (1) and postulates (10)–(12). It should be noted that postulate (12) is newly introduced by the author; its consequences will be demonstrated below. Later it will be shown that the ground state is the singlet state with total spin $S=0$, which is equivalent to $\langle \mathbf{S}^2\rangle_{\tau=0} = 0$.

The properties of the SL state are determined mainly by the spatial and temperature dependence of the spin correlation functions $K_r(\tau)$. The energy of the SL state per bond in units of J is given by

$$\varepsilon = \frac{\langle H\rangle}{(1/2)_Z NJ} = -\frac{3}{4}K_1, \tag{13}$$

where $K_{|\Delta|} = -K_1$ ($K_1 > 0$) is the correlator between nearest neighbors. For description of the SL state we go over to the Fourier transforms of the spin operators and introduce the Fourier transform of the correlation function

$$K(\mathbf{q}) = \sum_{\mathbf{r}} e^{-i\mathbf{q}\mathbf{r}} K_r = 4\langle s^z(\mathbf{q}) s^z(-\mathbf{q})\rangle$$

$$= 2\langle s^+(\mathbf{q}) s^-(-\mathbf{q})\rangle, \ \ K_r = \frac{1}{N}\sum_{\mathbf{q}} e^{i\mathbf{q}\cdot\mathbf{r}} K(\mathbf{q}) \tag{14}$$

with the obvious property $K(\mathbf{q}) = K(-\mathbf{q})$. To calculate $K(\mathbf{q})$ we use the method of two-time temperature Green's functions.[7] Because of the isotropicity of the correlators it is sufficient to calculate the retarded commutator Green's function

$$\langle\langle s^z(\mathbf{q}) | s^2(-\mathbf{q})\rangle\rangle_\omega = G(\mathbf{q},\omega).$$

where ω is a dimensionless spectral variable in terms of which $K(\mathbf{q})$ is found according to the spectral theorem.

Second-order equations and their linearization

The spin liquid theory is based on equations not lower than second order, since $\langle s^\alpha_{\mathbf{r}}\rangle = 0$ and the first-order equations cannot be linearized (as is done in spin-wave theory). The exact equations of motion have the form ($\hbar = 1$)

$$i\dot{s}^+_{\mathbf{f}} = \frac{1}{z}\sum_{\Delta} (s^z_{\mathbf{f}} s^\tau_{\mathbf{f}+\Delta} - s^z_{\mathbf{f}+\Delta} s^+_{\mathbf{f}}),$$

$$i\dot{s}^z_{\mathbf{f}} = \frac{1}{2z}\sum_{\Delta} (s^+_{\mathbf{f}} s^-_{\mathbf{f}+\Delta} - s^+_{\mathbf{f}+\Delta} s^-_{\mathbf{f}}) \equiv M_{\mathbf{f}}, \tag{15}$$

$$i\dot{M}_{\mathbf{f}} = \frac{\partial^2 s^z_{\mathbf{f}}}{\partial t^2} = \frac{1}{2z^2}\sum_{\Delta} (s^z_{\mathbf{f}} - s^z_{\mathbf{f}+\Delta}) + R_{\mathbf{f}}, \tag{16}$$

where

$$R_{\mathbf{f}} = \frac{1}{z^2}\sum_{\Delta\neq\Delta'} [s^z_{\mathbf{f}} s^+_{\mathbf{f}+\Delta} s^-_{\mathbf{f}+\Delta'} + (s^z_{\mathbf{f}+\Delta-\Delta'} - s^z_{\mathbf{f}+\Delta'}) s^+_{\mathbf{f}} s^-_{\mathbf{f}+\Delta}$$

$$- s^z_{\mathbf{f}+\Delta} s^+_{\mathbf{f}} s^-_{\mathbf{f}+\Delta-\Delta'}]. \tag{17}$$

Performing the linearization of the operator $R_{\mathbf{f}}$ according to the scheme

$$s^z_{\mathbf{f}} s^+_{\mathbf{n}} s^-_{\mathbf{m}} \approx s^z_{\mathbf{f}} \alpha_{|\mathbf{n}-\mathbf{m}|} \langle s^+_{\mathbf{n}} s^-_{\mathbf{m}}\rangle = \frac{1}{2}\alpha_{|\mathbf{n}-\mathbf{m}|} K_{|\mathbf{n}-\mathbf{m}|} s^z_{\mathbf{f}},$$

$$\mathbf{f}\neq\mathbf{n}\neq\mathbf{m}, \tag{18}$$

where $\alpha_{|\mathbf{n}-\mathbf{m}|}$ are parameters which correct the decoupling, after Fourier transformation we obtain the Green's function of the linear second-order theory in the form

$$G(\mathbf{q},\omega) = \frac{A_{\mathbf{q}}}{\omega^2 - \Omega^2_{\mathbf{q}}}, \ \ A_{\mathbf{q}} = \frac{K_1}{2}(1-\gamma_{\mathbf{q}}),$$

$$\gamma_{\mathbf{q}} = \frac{1}{z}\sum_{\Delta} e^{i\mathbf{q}\cdot\Delta}. \tag{19}$$

Here

$$\Omega^2_{\mathbf{q}} = \lambda^2(1-\gamma_{\mathbf{q}})(|\varepsilon_{\min}| + \gamma_{\mathbf{q}} + \delta), \ \ \lambda^2 = \frac{\alpha_1 K_1}{2}, \tag{20}$$

where α_1 is a correction factor for the nearest neighbors, $\varepsilon_{\min}$ is the lower boundary of the spectrum γ_q, and the parameter δ is a complicated construction of correlators in the first, second, etc. coordination zones, multiplied by the corresponding correction factors. The parameter δ thereby reflects the effective correlations in the ''expanded'' cluster and will be calculated self-consistently later (its explicit form is unimportant). The spectral intensity of the Green's function (19) is equal to

$$J(\mathbf{q},\omega;\tau) = \frac{e^{\omega/\tau}}{e^{\omega/\tau}-1}\frac{A_{\mathbf{q}}}{2\Omega_{\mathbf{q}}}[\delta(\omega-\Omega_{\mathbf{q}}) - \delta(\omega+\Omega_{\mathbf{q}})],$$

$$\Omega_q \geqslant 0. \tag{21}$$

According to the spectral theorem we obtain for the single-time average

$$\langle s^z(\mathbf{q})s^z(-\mathbf{q})\rangle \equiv \frac{1}{4}K(\mathbf{q}) = \int_{-\infty}^{\infty} J(\mathbf{q},\omega;\tau)\,d\omega$$

$$= \frac{A_{\mathbf{q}}}{2\Omega_{\mathbf{q}}}\coth\left(\frac{\Omega_{\mathbf{q}}}{2\tau}\right)$$

or

$$K(\mathbf{q}) = \frac{K_1}{\lambda}\,\frac{1-\gamma_{\mathbf{q}}}{E_{\mathbf{q}}(\delta)}\coth\left(\frac{\lambda E_{\mathbf{q}}(\delta)}{2\tau}\right),\quad \Omega_q \equiv \lambda E_{\mathbf{q}}(\delta). \tag{22}$$

Expression (22) attests to the fact that the proposed version of the SL theory contains three unknown parameters which are functions of temperature: $K_1(\tau)$—the modulus of the correlator between nearest neighbors, $\lambda(\tau)$—the "stiffness" parameter of the excitation spectrum, and $\delta(\tau)$—the "pseudogap" in the spectrum. They must all be calculated self-consistently in accordance with three equations (see below); here $\delta=\delta(\tau)\geqslant 0$, as is necessary for the condition $\Omega_{\mathbf{q}}\geqslant 0$ or $E_{\mathbf{q}}(\delta)\geqslant 0$.

Self-consistency equations

Three parameters must be calculated self-consistently: K_1, λ, and δ. Using the definition (14) of the spatial correlators K_r, we obtain the system of equations

$$\begin{cases} K_0 = 1 = \dfrac{1}{N}\displaystyle\sum_{\mathbf{q}} K(\mathbf{q}) = \dfrac{K_1}{\lambda} I_0(\delta,\tau), \\ K_1 = \dfrac{1}{N}\displaystyle\sum_{\mathbf{q}} (-\gamma_{\mathbf{q}}) K(\mathbf{q}) = \dfrac{K_1}{\lambda} I_1(\delta,\tau), \\ K_{\mathrm{tot}} = \dfrac{1}{N}\displaystyle\sum_{\mathbf{q}} (\gamma_{\mathbf{q}})^2 K(\mathbf{q}) \\ \quad = \dfrac{1}{z^2}\displaystyle\sum_{\Delta,\Delta'} K_{|\Delta+\Delta'|} = \dfrac{K_1}{\lambda} I_2(\delta,\tau), \end{cases} \tag{23}$$

where

$$I_n(\delta,\tau) = \frac{1}{N}\sum_{\mathbf{q}} (-\gamma_{\mathbf{q}})^n \frac{1-\gamma_{\mathbf{q}}}{E_{\mathbf{q}}(\delta)}\coth\left(\frac{\lambda E_{\mathbf{q}}(\delta)}{2\tau}\right),$$

$$n = 0,1,2. \tag{24}$$

From Eqs. (23) we obtain the formal solution (we omit the arguments of the functions)

$$\lambda = I_1,\quad K_1 = I_1/I_0,\quad K_{\mathrm{tot}} = I_2/I_0,\quad \alpha_1 = 2I_0 I_1. \tag{25}$$

The equation for the parameter δ arises from the requirement of an exact value of the second moment[3,6,10] and has the form

$$M_2 = \frac{1}{8}\left(K_{\mathrm{tot}} + \frac{K_1}{z}\right) = \frac{\lambda K_1}{4} P(\delta),$$

$$P(\delta) \equiv \frac{1}{N}\sum_{\mathbf{q}} (1-\gamma_{\mathbf{q}}) E_{\mathbf{q}} \coth\left(\frac{\Omega_{\mathbf{q}}}{2\tau}\right). \tag{26}$$

Using solution (25), we obtain

$$P(\delta) = \frac{I_2(\delta) + I_1(\delta)/z}{2I_1^2(\delta)},\quad \delta = \delta(\tau). \tag{27}$$

Thus the self-consistent second-order linear theory is based on satisfaction of the sum rule $K_0=1$, the definitions of the correlators K_1 and K_{tot} [Eq. (23)], and the requirement of an exact value of the second moment, which leads to Eq. (27). This equation plays a fundamental role in the SL theory and its further generalizations.

The sums over the Brillouin zone for I_n and P are replaced by integrals with a density of states $D(\varepsilon)$ corresponding to a dispersion relation $\gamma_{\mathbf{q}}=\varepsilon$. An approximation for the density of states $D(\varepsilon)$ is given in the Appendix. Combining Eqs. (25) and (27), we obtain a system of three equations for the self-consistent calculation of the parameters of the SL:

$$\begin{cases} \lambda = I_1 \quad (a), \\ K_1 = I_1/l_0 \quad (b), \\ P = \dfrac{I_2 + l_1/z}{2I_1^2} \quad (c). \end{cases} \tag{28}$$

Here

$$l_n(\delta,t) = \int D(\varepsilon)(-\varepsilon)^n \frac{1-\varepsilon}{E(\varepsilon,\delta)}\coth\left(\frac{E(\varepsilon,\delta)}{2t}\right)d\varepsilon,$$

$$P(\delta,t) = \int D(\varepsilon)(1-\varepsilon)E(\varepsilon,\delta)\coth\left(\frac{E(\varepsilon,\delta)}{2t}\right)d\varepsilon.$$

$$E(\varepsilon,\delta) = \sqrt{(1-\varepsilon)(|\varepsilon_{\min}|+\varepsilon+\delta)}.$$

$$\varepsilon_{\min}\leqslant\varepsilon\leqslant 1,\quad t=\tau/\lambda. \tag{29}$$

We now show that the *ground state is a singlet* (total spin $S=0$). We introduce the function (the average per spin of the square of the total spin of the system)

$$S^2(\tau) \equiv \frac{1}{N}\langle \mathbf{S}^2\rangle = \frac{1}{N}\sum_{\mathbf{fm}} \langle s_{\mathbf{f}} s_{\mathbf{m}}\rangle = \sum_{\mathbf{r}} \frac{1}{N}\sum_{\mathbf{f}} s_{\mathbf{f}} s_{\mathbf{f}+\mathbf{r}}$$

$$= \frac{3}{4}\sum_{\mathbf{r}} K_{\mathbf{r}} = \frac{3}{4}K(0), \tag{30}$$

which is expressed in terms of the Fourier transform of the correlation function (22) for $\mathbf{q}=0$. For $\tau\equiv 0$ it follows from (22) that $K(0)=0$ and $S^2(0)=0$, which proves that the ground state is a singlet. On the other hand, expression (30) can be considered as the limit

$$K(0) = \lim_{\mathbf{q}\to 0} K(\mathbf{q}) = \frac{K_1}{\lambda}\lim_{\mathbf{q}\to 0}\frac{1-\gamma_{\mathbf{q}}}{E_{\mathbf{q}}(\delta)}\coth\left(\frac{\lambda E_{\mathbf{q}}(\delta)}{2\tau}\right)$$

$$= \frac{4\tau}{\alpha_1(|\varepsilon_{\min}|+\gamma_0+\delta)}. \tag{31}$$

Hence for $\tau\to 0$ we obtain $K(0)=0$ (singlet) as before, but for $\tau\equiv 0$ triplet excitations arise in the system, and because of them $S^2(\tau)\neq 0$.

In Refs. 3 and 6 the thermodynamic properties of the SL in the square and fcc lattices were described at all temperatures on the basis of the theory set forth above and the self-consistency equations (28). It was shown there that the spatial correlation functions are sign-varying, with a magnitude that falls off with increasing distance, so that the SL contains short-range order of the antiferromagnetic type.

4. SPIN LIQUID WITH A "CONDENSATE" IN THE sc AND bcc LATTICES

Alternant lattices can be regarded as two interposed sublattices A (sites α) and B (sites β), independently of the existence of real magnetic sublattices. The Brillouin zone of these lattices contains a boundary point $\mathbf{Q}$ at which $\gamma_{\mathbf{Q}}=-1=\varepsilon_{\min}$ and the spectrum $E_{\mathbf{Q}}(\delta)=\sqrt{2\delta}$. These points are $\mathbf{Q}=(\pi,\pi)$, $\mathbf{Q}=(\pi,\pi,\pi)$, and $\mathbf{Q}=(2\pi,2\pi,2\pi)$ for the square, sc, and bcc lattices, respectively. It follows from this that

$$\exp(i\mathbf{Q}\cdot\alpha)=1,\ \ \exp(i\mathbf{Q}\cdot\beta)=-1. \tag{32}$$

The function $S^2(\tau)$ was considered above [see Eq. (30)] and it was shown that $S^2(0)=0$ (the ground state is a singlet) at $\tau=0$; this is equivalent to the equation

$$K(0)=\sum_{\mathbf{r}} K_{\mathbf{r}}=0\ \ (\tau=0). \tag{33}$$

Taking relations (32) into account, we can write $K(\mathbf{Q})$ in the form

$$K(\mathbf{Q})=\sum_{\mathbf{r}} e^{-i\mathbf{Q}\mathbf{r}}K_{\mathbf{r}}=\sum_{\mathbf{r}} |K_{\mathbf{r}}|. \tag{34}$$

Since $K_{\mathbf{r}}$ is sign-varying, in Eq. (33) there is complete compensation of all the terms in the sum, while the value of $K(\mathbf{Q})$ in (34) can be macroscopically large and proportional to the volume of the system ($\propto N$).

"Condensate" in the spin liquid

Under this assumption we write $K_{\mathbf{r}}$ in the form

$$K_{\mathbf{r}}=\frac{1}{N}\sum_{\substack{\mathbf{q}\\(\mathbf{q}\neq\mathbf{Q})}} e^{i\mathbf{q}\cdot\mathbf{r}}K(\mathbf{q})+e^{i\mathbf{Q}\cdot\mathbf{r}}\frac{K(\mathbf{Q})}{N},$$

$$\frac{K(\mathbf{Q})}{N}\equiv\frac{K_1}{\lambda}C. \tag{35}$$

where C is a "condensate" (a function of temperature) which is unknown *a priori*. Then

$$K_0=1=\frac{1}{N}\sum_{\substack{\mathbf{q}\\(\mathbf{q}\neq\mathbf{Q})}} K(\mathbf{q})+\frac{K_1}{\lambda}\mathbf{C},$$

$$K_1=\frac{1}{N}\sum_{\substack{\mathbf{q}\\(\mathbf{q}\neq\mathbf{Q})}} (-\gamma_{\mathbf{q}})K(\mathbf{q})+\frac{K_1}{\lambda}C, \tag{36}$$

$$K_{\mathrm{tot}}=\frac{1}{N}\sum_{\substack{\mathbf{q}\\(\mathbf{q}\neq\mathbf{Q})}} \gamma_{\mathbf{q}}^2K(\mathbf{q})+\frac{K_1}{\lambda}\mathbf{C}.$$

In relations (36) we go from summation to integration with a density of states $D(\varepsilon)$. We take into account the following circumstances. First, the lower limit of integration (because of the restriction $\mathbf{q}\neq\mathbf{Q}$) is equal to $-1+\zeta$, where ζ is an infinitesimal quantity ($\zeta\to+0$). In the sc and bcc lattices the density of states $D(\varepsilon)$ goes to zero in a square-root manner at the boundaries of the spectrum. For this reason the value of ζ can be simply set equal to zero (this is the same situation as in the description of Bose condensation in a three-dimensional gas). Second, in the presence of the "condensate" C we assume $\delta=0$ in the expression for $K(\mathbf{q})$. In that case the spectrum $E(\varepsilon,0)=\sqrt{1-\varepsilon^2}$ becomes symmetric with respect to inversion $\varepsilon\leftrightarrow-\varepsilon$, and the density of states has the same property: $D(\varepsilon)=D(-\varepsilon)$. When these symmetry properties are taken into account, the integrals become

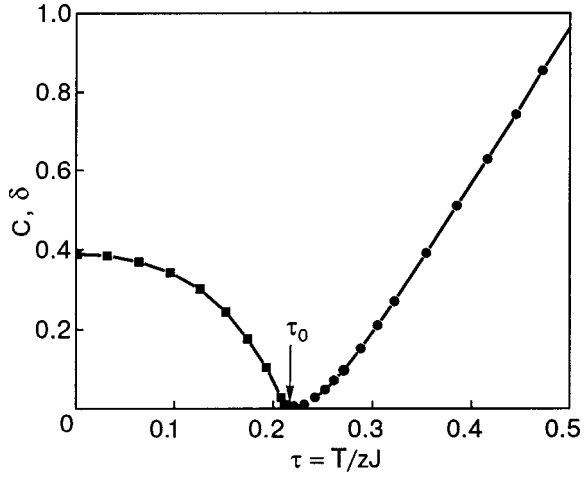

FIG. 1. Temperature behavior of the condensate (■) and the gap parameter (●) in the spin liquid in the sc lattice.

$$I_0(t)=\int_{-1}^{1} D(\varepsilon)\frac{1}{\sqrt{1-\varepsilon^2}}\coth\left(\frac{\sqrt{1-\varepsilon^2}}{2t}\right)d\varepsilon.$$

$$I_1(t)=I_2(t)=\int_{-1}^{1} D(\varepsilon)\frac{\varepsilon^2}{\sqrt{1-\varepsilon^2}}\coth\left(\frac{\sqrt{1-\varepsilon^2}}{2t}\right)d\varepsilon,$$

$$P(t)=\int_{-1}^{1} D(\varepsilon)\sqrt{1-\varepsilon^2}\coth\left(\frac{\sqrt{1-\varepsilon^2}}{2t}\right)d\varepsilon \tag{37}$$

(the function $P(t)$ does not contain a "condensate" term).

Now relations (36) are written in the form

$$1=\frac{K_1}{\lambda}(I_0+C),\ \ K_1=K_{\mathrm{tot}}=\frac{K_1}{\lambda}(I_1+C), \tag{38}$$

and the self-consistency equation (27) assumes the simple form

$$P(I_1+C)=\frac{z+1}{2z}. \tag{39}$$

From the numerical solution of the system of equations (38)–(39) at $\tau=0$ we obtain

$$\lambda=0.645,\ \ K_1=0.416,\ \ \varepsilon_0=-0.312,\ \ C=0.389\ \ (\mathrm{sc}).$$

$$\lambda=0.607,\ \ K_1=0.396,\ \ \varepsilon_0=-0.297,$$

$$C=0.4185\ \ (\mathrm{bcc}). \tag{40}$$

It follows from the results (40) that the energy of the singlet state in the presence of the condensate is lower than the energy of the AF state (see Table I). This proves Marshall's assertion that the ground state of the spin system on alternant lattices is a singlet.

Figure 1 shows the result of a calculation of the temperature behavior of the condensate in the sc lattice. This function goes to zero at a temperature $\tau_0\approx0.213$, which is higher than the Néel temperature $\tau_N=0.163$ of the sc lattice. Thus the temperature region in which the spin liquid with the con-

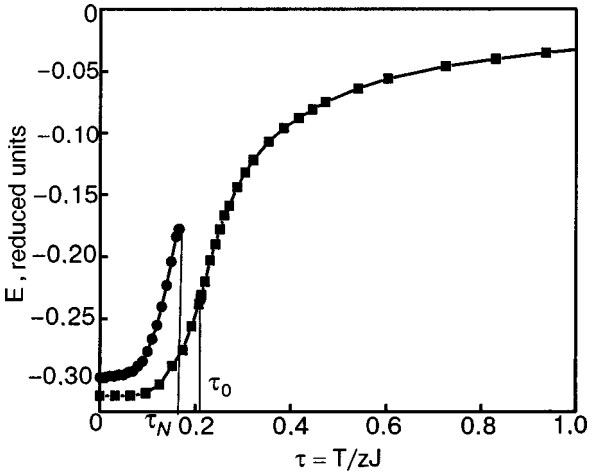

FIG. 2. Energy of the antiferromagnetic state (●) calculated according to spin-wave theory for $\tau \leqslant \tau_N$, and the energy of the spin liquid in the sc lattice (■).

densate exists is wider than the existence region of the AF state, and the energy in this state $\varepsilon_{SLC} < \varepsilon_{AF}$. For $\tau > \tau_0$ a pseudogap δ begins to be "seeded" in the spectrum. To calculate it we use the same universal self-consistency equation (28c). The result is presented in Fig. 1. There is actually a phase transition

$$\mathrm{SLC}(\delta = 0,\ C \neq 0) \Rightarrow \mathrm{SL}(\delta \neq 0,\ C = 0),$$

and the properties of the system can be described at all temperatures. Figures 2 and 3 show the temperature behavior of the main parameters of the system. For comparison, the energy of the AF state (according to spin-wave theory) is shown in Fig. 2; it has a finite value at the Néel point, but above it the spin-wave theory is inapplicable.

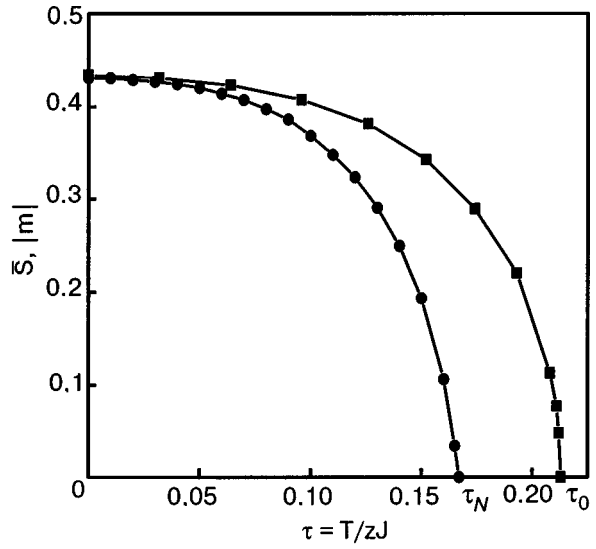

FIG. 3. Order parameters: $\overline{s}(\tau)$ is the relative magnetization of the sublattice in the AF state (●), and $|m(\tau)|$ is the modulus of the "staggered" magnetization in the spin liquid with the condensate (■) in the sc lattice.

"Staggered" magnetization, the "condensate," and long-range order

To explain the physical meaning of the "condensate," let us consider the square of the "staggered" magnetization (SM), which by definition[8] is equal to

$$m^2 = \left\langle \left(\frac{1}{N} \sum_{\mathbf{f}} e^{i\mathbf{Q}\cdot\mathbf{f}} \mathbf{s}_{\mathbf{f}} \right)^2 \right\rangle = \frac{1}{N} \sum_{\mathbf{r}} e^{i\mathbf{Q}\cdot\mathbf{r}} \frac{1}{N} \sum_{\mathbf{f}} \langle \mathbf{s}_{\mathbf{f}} \mathbf{s}_{\mathbf{f}+\mathbf{r}} \rangle$$

$$= \frac{1}{N} \sum_{\mathbf{r}} e^{i\mathbf{Q}\cdot\mathbf{r}} \frac{3}{4} K_{\mathbf{r}} = \frac{3}{4} \frac{K(\mathbf{Q})}{N} = \frac{3}{4} \frac{K_1}{\lambda} C, \tag{41}$$

where we have used the relation $2\mathbf{Q}\cdot\mathbf{f} = 1$ and definition (35). It follows from (41) that the modulus of the SM is equal to

$$|m(\tau)| = \frac{\sqrt{3}}{2} \sqrt{\frac{K_1(\tau)}{\lambda(\tau)} C(\tau)},$$

or, when relations (38) are taken into account,

$$|m(\tau)| = \frac{\sqrt{3}}{2} \sqrt{\frac{C(\tau)}{I_0(\tau) + C(\tau)}}. \tag{42}$$

This function is compared with the order parameter $\overline{s}(\tau)$ in the AF state in Fig. 3; we note that

$$|m(0)| = 0.434,\ \overline{s}(0) = 0.432 \ \text{ in sc},$$

$$|m(0)| = 0.452,\ \overline{s}(0) = 0.448 \ \text{ in bcc}.$$

Thus the modulus of the "staggered" magnetization $|\mathbf{m}|$ is the order parameter in the quantum spin liquid for the sc and bcc lattices.[2)]

Long-range order

The presence of long-range order is detected from the behavior of the spatial correlation functions at $r \to \infty$ (the thermodynamic limit $N \to \infty$, $V \to \infty$, $N/V = \mathrm{const}$ is understood; actually it is necessary to set $r \approx N^{1/d}$ equal to the maximum linear dimension of the system and then take the limit $N \to \infty$). For sign-varying correlation functions the long-range order is defined as a nonzero limit

$$C_\infty = \lim_{r \to \infty} |\langle \mathbf{s}_{\mathbf{f}} \mathbf{s}_{\mathbf{f}+\mathbf{r}} \rangle| = \frac{3}{4} \lim_{r \to \infty} |K_r| = \frac{3}{4} |K_\infty|. \tag{43}$$

Thus it is necessary to calculate K_r according to formula (35) for large values of r. In the sum (integral) over $\mathbf{q}$, as before, the main contribution comes from the vicinity of the point $\mathbf{q} = \mathbf{Q}$ (although the point $\mathbf{Q}$ itself is excluded). We set $\mathbf{q} = \mathbf{Q} + \mathbf{p}$ and perform the expansion $\gamma_{\mathbf{p}+\mathbf{Q}} = -\gamma_{\mathbf{p}} \approx -1 + p^2/z$; in addition, we formally drop the parameter δ in the spectrum. Then

$$K_\tau \approx e^{i\mathbf{Q}\cdot\mathbf{r}} \frac{K_1}{\lambda} \left[\frac{1}{(2\pi)^3} \int d^3\mathbf{p} e^{i\mathbf{p}\cdot\mathbf{r}} \frac{\sqrt{2z}}{\sqrt{p^2 + \kappa^2}} \right.$$

$$\left. \times \coth\left(\sqrt{\frac{2}{z}} \frac{\sqrt{p^2 + \kappa^2}}{2t} \right) + C \right], \tag{44}$$

where $\kappa^2 = z\delta$ and $t = \tau/\lambda$ (we note that the correlation length $\xi = 1/\kappa$). In the approximation $\coth x \approx 1/x$ the integral in (44) reduces to the form

$$2tz\frac{1}{(2\pi)^3}\int d^3\mathbf{p}\frac{e^{i\mathbf{p}\cdot\mathbf{r}}}{p^2+\kappa^2}\approx 2tz\frac{1}{4\pi}\frac{\exp(-\kappa r)}{r}, \qquad (45)$$

which is well known in the Ornstein–Zernike theory. It follows from (45) that this integral goes to zero at large distances (even in the case $\delta=\kappa=0$), so that the long-range order is due to the ''condensate'' term, i.e.,

$$|K_\infty|=\frac{K_1}{\lambda}C \quad \text{or} \quad C_\infty=\frac{3}{4}|K_\infty|=m^2. \qquad (46)$$

Neutron scattering

In the general theory of inelastic neutron scattering (see, e.g., Ref. 7) the expression for the differential cross section for scattering contains the function

$$\Lambda(\mathbf{r},t)=\sum_{\alpha\beta}(\delta_{\alpha\beta}-e_\alpha e_\beta)\langle s^\alpha_{\mathbf{f}}(0)s^\beta_{\mathbf{f}+\mathbf{r}}(t)\rangle, \qquad (47)$$

where $\mathbf{e}=\mathbf{q}/q$, with $\mathbf{q}$ the neutron scattering vector. In a magnetically ordered state (F or AF), using the principle of decay of correlations at large distances, one performs a decoupling of the correlation function:

$$\langle s^\alpha_{\mathbf{f}}s^\beta_{\mathbf{f}+\mathbf{r}}\rangle\approx\langle s^\alpha_{\mathbf{f}}\rangle\langle s^\beta_{\mathbf{f}+\mathbf{r}}\rangle\propto\langle s^z_{\mathbf{f}}\rangle^2=\overline{s}^2,$$

which reduces to the square of the order parameter. In the spin liquid $\langle s^\alpha_{\mathbf{r}}\rangle=0$, and because of the isotropicity of the correlation functions (10), expression (47) assumes the form

$$\Lambda_{SL}(\mathbf{r},t)=\frac{1}{2}K_{\mathbf{r}}(t), \qquad (48)$$

i.e., it is expressed in terms of a time-dependent spatial correlation function.

Thus inelastic neutron scattering experiments measure the correlation function. The interpretation of the experimental data requires a separate and careful analysis.

5. SUMMARY

In this paper a theoretical version of the description of a spin system with an isotropic Heisenberg Hamiltonian (spin $s=1/2$, and an antiferromagnetic exchange only between nearest neighbors) as a spin liquid with a singlet ground state was proposed. It was shown that in three-dimensional alternant lattices (sc and bcc) at the boundary of the Brillouin zone there exists a ''condensate'' of excitations which determines the presence of a long-range order close to antiferromagnetic in the system. The two states (singlet and AF) are very similar (as was noted previously by Anderson[9]).

First, the excitation spectra are identical:

$$(\Omega_{\mathbf{q}})_{AF}=\overline{s}\sqrt{1-\gamma_{\mathbf{q}}^2},\ \ (\Omega_{\mathbf{q}})_{SL}=\lambda\sqrt{1-\gamma_{\mathbf{q}}^2}\ \text{ at }\ \delta=0,$$

where $\overline{s}$ is the order parameter (the relative sublattice magnetization) in the AF state, and $\lambda=\sqrt{\alpha_1K_1/2}$, and K_1 is the modulus of the spin correlator between nearest neighbors in the SL.

Second, the spatial correlation functions of the spins are sign-varying.

Thus in the framework of the proposed version of the theory one is able to confirm Marshall's assertion that the ground state in alternant lattices is a singlet, while preserving the presence of long-range magnetic order of the AF type.

The main results of this paper are as follows:

1. A definition of a spin liquid was given in the form of expressions (10)–(12) for an isotropic Heisenberg Hamiltonian. Postulate (12) was introduced here for the first time; it plays an important role in the construction of the self-consistent and internally closed theory of the SL.

2. The SL is described in the framework of a second-order theory by the Green's function method. In comparison with spin-wave theory (which contains only one order parameter ($\overline{s}(T)$) which is unknown *a priori*), in the SL theory there are three parameters: λ—the ''stiffness'' of the excitation spectrum, K_1—the modulus of the spin correlator in the first coordination zone (between nearest neighbors), and δ—the pseudogap in the spectrum (they are all functions of temperature).

3. A system of equations (37) was proposed for the self-consistent calculation of these parameters. As a result of the solution of this system (numerical and partly analytical) one can describe the thermodynamics of the SL at all temperatures.[3,6,10]

4. It was proved that the ground state of the SL is a singlet state.

5. A theoretical version of the description of a spin system in sc and bcc lattices as a spin liquid with a condensate (SLC) was proposed. The theory leads to the following results:

— the ground state is a singlet (total spin $S=0$, which corresponds to the rigorous quantum mechanical classification of states), the energy of the singlet state is lower than the energy of the AF state calculated according to spin-wave theory;

— the temperature dependence of the condensate was found; it vanishes at a critical temperature τ_0;

— it was shown that the modulus of the ''staggered'' magnetization $|m(\tau)|$ is expressed in terms of the condensate $C(\tau)$ and is the order parameter in the SLC; the existence region of the ordered state of the SL of the condensate is wider than that of the two-sublattice AF state, since $\tau_0>\tau_N$.

Thus the spin system has been described at all temperatures in the framework of the proposed theory.

This study was supported by the Russian Foundation for Basic Research, Grant 00-02-16110.

APPENDIX

Approximation of the density of states for the dispersion relation $\gamma_{\mathbf{q}}=1/z\,\Sigma_\Delta e^{i\mathbf{q}\cdot\Delta}$, where Δ are the vectors connecting the nearest neighbors (the isoenergy surface $x=\gamma_{\mathbf{q}}$; the lattice parameter $a=1$).

Linear chain ($d=1$, $z=2$):

$$D(x)=\frac{1}{\pi}\frac{1}{\sqrt{1-x^2}},\ \ |x|\leqslant 1.$$

The square lattice ($d=2$, $z=4$):

$$\gamma_{\mathbf{q}}=\frac{1}{2}(\cos q_x+\cos q_y),$$

$$D(x)=\frac{1}{\pi}-\left(\frac{1}{2}-\frac{1}{\pi}\right)\ln|x|,\quad |x|\leqslant 1.$$

The sc lattice ($d=3$, $z=6$):

$$\gamma_{\mathbf{q}}=\frac{1}{3}(\cos q_x+\cos q_y+\cos q_z),$$

$$D(x)=\begin{cases}0.876, & |x|\leqslant 0.329,\\ 0.279\dfrac{\sqrt{1-x^2}}{(x^2-0.09)^{0.3}+10^8}, & 0.329\leqslant|x|\leqslant 1.\end{cases}$$

The bcc lattice ($d=3$, $z=8$):

$$\gamma_{\mathbf{q}}=\cos\left(\frac{q_x}{2}\right)\cos\left(\frac{q_y}{2}\right)\cos\left(\frac{q_z}{2}\right),$$

$$D(x)=0.431\frac{(-\ln|x|)}{1+3x^2}+0.186\sqrt{1-x^2},\quad |x|\leqslant 1.$$

The fcc lattice ($d=3$, $z=12$):

$$\gamma_{\mathbf{q}}=\frac{1}{3}(c_xc_y+c_xc_z+c_yc_z),\quad c_j\equiv\cos\left(\frac{q_j}{2}\right),$$

$$D(x)=\begin{cases}A(x), & \text{if}-\dfrac{1}{3}\leqslant x\leqslant 0,\\ B(x), & \text{if}\ \ 0\leqslant x\leqslant 1,\end{cases}$$

$$A(x)=-0.366664\ln\left(0.0671182\left(x+\frac{1}{3}\right)\right)-0.456693x,$$

$$B(x)=0.226573\sqrt{1-x}+\frac{0.202745}{x+0.151142}-0.174703.$$

The density of states for the dispersion relation $\gamma_{\mathbf{q}}$ considered must satisfy the relations

$$\int D(x)dx=1,\quad \int D(x)xdx=0,\quad \int D(x)x^2dx=\frac{1}{z}.$$

*E-mail: evk@iph.krasn.ru; kuzmin@cshi.crimea.edu

[1)]Alternant lattices are those that can be represented in the form of two equivalent sublattices A and B interposed with each other in such a way that the nearest neighbors of sublattice A are sites of sublattice B and *vice versa*.

[2)]In the antiferromagnetic state the "staggered" magnetization itself is the order parameter, $\mathbf{m}_{AF}=\langle 1/N\,\Sigma_{\mathbf{f}}e^{i\mathbf{Q}\cdot\mathbf{f}}\mathbf{S}_{\mathbf{f}}\rangle=\mathbf{e}1/N\,\Sigma_{\mathbf{f}}e^{i\mathbf{Q}\cdot\mathbf{f}}\langle\mathbf{S}_{\mathbf{f}}^z\rangle=\mathbf{e}\overline{s}$ ($\mathbf{e}$ is the unit vector along the quantization axis). In the spin liquid $\mathbf{m}_{SL}=0$, but $m_{SL}^2\neq 0$, and $\sqrt{m_{SL}^2}\equiv|m|$ is the order parameter in the SLC.

[1] S. V. Vonsovskiĭ (ed.), *Antiferromagnetism* [Russian translations], Izd-vo Inostr. Lit., Moscow (1956).
[2] D. Mattis, Teoriya magnetizma, Mir, Moscow (1967).
[3] E. V. Kuz'min, Fiz. Tverd. Tela (St. Petersburg) **44**, 1075 (2002) [Phys. Solid State **44**, 1122 (2002)].
[4] S. V. Vonsovskiĭ and M. S. Svirskiĭ, Zh. Éksp. Teor. Fiz. **57**, 251 (1969) [Sov. Phys. JETP **30**, 141 (1970)].
[5] W. Marshall, Philos. Trans. R. Soc. London, Ser. A **232**, 48 (1955).
[6] E. V. Kuz'min, Zh. Éksp. Teor. Fiz. **123**, 149 (2003) [JETP **96**, 129 (2003)].
[7] S. V. Tyablikov, *Methods in the Quantum Theory of Magnetism*l, 1st ed., Plenum Press, New York (1967), 2nd ed., Nauka, Moscow (1975).
[8] E. Manousakis, Rev. Mod. Phys. **63**, 1 (1991).
[9] P. W. Anderson, Phys. Rev. **86**, 694 (1952).
[10] E. V. Kuz'min, "Quantum spin liquid and antiferromagnetism" [in Russian], Preprint No. 814F, Institute of Physics, Siberian Branch of the Russian Academy of Sciences, Krasnoyarsk (2002)

Translated by Steve Torstveit

Weak ferromagnetism and an intermediate incommensurate antiferromagnetic phase in $LiNiPO_4$

Yu. N. Kharchenko* and N. F. Kharcheno

B. Verkin Institute for Low Temperature Physics and Engineering, National Academy of Sciences of Ukraine, pr. Lenina 47, 61103 Kharkov, Ukraine

M. Baran and R. Szymczak

Institute of Physics, Polish Academy of Sciences, Al. Lotnikow 32/46, PL-02-668 Warsaw, Poland
(Submitted December 28, 2002; revised February 24, 2003)
Fiz. Nizk. Temp. **29**, 774–780 (July 2003)

The temperature dependence of the magnetization of single-crystal $LiNiPO_4$ is measured for magnetic-field orientations along the a, b, and c crystallographic axes. It is found that the value of the magnetization depends on the magnetic prehistory of the sample. The magnetic behavior of the antiferromagnetic sample is explained by the presence of weak ferromagnetism in $LiNiPO_4$. At a temperature of 5 K the value of the spontaneous magnetic moment along the c axis is around 0.005 G. When the sample is heated to 20.8 K the magnetic moment decreases monotonically to zero. All of the magnetic susceptibility curves $M(T)/H$ exhibit two features: a jump and a kink at temperatures T_1 and T_2, respectively. At a magnetic field of 10 kOe these temperatures are close to 20.84 and 21.86 K. The observed features indicate that in the establishment of the main antiferromagnetic order in the $LiNiPO_4$ crystal, an intermediate antiferromagnetic phase is spontaneously formed in the temperature interval from $T_{N1}=20.8(5)$ K to $T_{N2}=21.8(5)$. The sequence of continuous and abrupt transitions at the boundary temperatures of its existence region indicate that the intermediate phase is most likely an incommensurate antiferromagnetic state. © *2003 American Institute of Physics.*
[DOI: 10.1063/1.1596583]

1. INTRODUCTION

Interest in noncentrosymmetric antiferromagnetic crystals has been growing markedly in recent years (see, e.g., Refs. 1–10). One of the reasons for this is that crystals of noncentrosymmetric classes and artificial magnetic systems without a center of inversion can have inhomogeneous magnetic structures form in them on account of the inhomogeneous Dzyaloshinskiĭ interactions describable by Lifshitz invariants.[11] The incommensurate structures resulting from these ''gradient interactions'' differ from the modulated structures that form as a result of a competition between exchange interactions. In particular, they can stabilize magnetic vortex structures[8–10] and lead to the coexistence of spatially modulated antiferromagnetism and weak ferromagnetism.[10] In addition, one group of noncentrosymmetric antiferromagnets—magnetoelectrics—is attracting interest because their symmetry admits the existence of toroidal magnetic structures.[4]

Of particular interest are representatives of the magnetoelectric double phosphate crystals of the olivine crystallographic family.[12–28] These antiferromagnetic crystals have the general chemical formula $LiMPO_4$ (M = Mn, Fe, Co, Ni) and are described by the orthorhombic Fedorov group $Pnma=D_{2h}^{16}$ (Refs. 29–31). Their unit cells contain 4 formula units. The four $3d$ ions occupy all four of the crystallographically equivalent c sites. The magnetic ions are surrounded by six oxygen ions, which form a rather highly distorted octahedron with the symmetry $C_s=\mathbf{m}$. The volume of the unit cell is conserved upon magnetic ordering.[13,20,22] The exchange bonds in the crystals of this family were analyzed in Ref. 12. The most strongly intercoupled ions lie within corrugated layers and are oriented perpendicular to the axis $\mathbf{a}\|\mathbf{X}$. The exchange interaction between ions from neighboring layers is considerably weaker, and the magnetic properties of $LiMPO_4$ can be described using the model of a quasi-2D antiferromagnet.[20,26] The most intensively studied of the antiferromagnetic phosphates are the $LiCoPO_4$ and $LiNiPO_4$ crystals.[15–28] The features of their magnetoelectric, magnetic, and magnetooptic properties have been ascertained, but they have not yet been reconciled among themselves or with the results of neutron diffraction studies.

The physical properties of the $LiNiPO_4$ crystal have been studied in Refs. 15, 19–22, 27, and 28. Its ionic and magnetic structures have been determined numerous times.[13,20,22,29–31] The optical absorption spectrum has been investigated.[15] The temperature dependence of the magnetic susceptibility of powders has been measured.[20] Almost all the frequencies of active vibrational modes of the crystal have been determined by Raman scattering experiments, and two-magnon light scattering has been detected.[28] The behavior of the magnetoelectric effect has been studied over a wide range of magnetic fields and temperatures.[14,21] Upon a cyclic change in the magnetic field the magnetoelectric properties of $LiNiPO_4$ and $LiCoPO_4$ crystals exhibit hysteresis of the ''butterfly'' type, which is characteristic for magnetoelectrics being magnetized in the presence of magnetic and electric

fields. Hysteresis of this type can arise if the crystal has a weak ferromagnetic moment or if the magnetism contains a contribution quadratic in the field. It indicates the absence of anti-inversion among the symmetry operations of the magnetic group of the crystal. However, the symmetry group established in neutron diffraction studies[13,20] corresponds to a completely compensated antiferromagnetic structure symmetric with respect to the anti-inversion operation. In Ref. 27 the magnetic hysteresis of the magnetoelectric effect in $LiNiPO_4$ was attributed to a rearrangement of a weak noncollinear structure of the ''skewed cross'' type, described by the invariant $L_{2x}L_{3x}$. The presence of this invariant in the thermodynamic potential is allowed by the symmetry of the crystal.

In this paper we report a study of the magnetic properties of single-crystal $LiNiPO_4$ in which we have detected an ultraweak ferromagnetic moment, the value of which is not over 0.005 G at a temperature of 5 K, and have found some novel temperature features in the magnetic behavior of the crystal. These features indicate that the transition from the paramagnetic to the antiferromagnetic state occurs in two stages, with the formation of an intermediate magnetic phase.

2. EXPERIMENTAL RESULTS AND DISCUSSION

The $LiNiPO_4$ single crystal for our studies was provided to us by Prof. H. Schmid of Geneva University. The sample cut from the single crystal had a mass of 45.5 mg and was in the form of an irregular truncated pyramid with a base of around 4×4 mm. The experiments were done on a Quantum Design MPMS-5 magnetometer. The error of the temperature stabilization was not over ±0.015 K.

For measurements in the geometry $\mathbf{H}\|\mathbf{c}$ the sample was glued to a quartz rod with an orientation error of 1° or less. Studies in the geometry $\mathbf{H}\perp\mathbf{c}$ were done with the use of a copper turntable, the axis of rotation of which was perpendicular to the magnetic field. The sample was glued to the turntable in such a way that the deviation of the *a* axis from the field direction did not exceed 2°. To aid in orienting the crystallographic axes along **H**, we measured the angular dependence of the magnetization at a field strength of 10 kOe. It was assumed that the magnetic field was parallel to the *a* or *b* axis for those positions of the turntable for which the value of the magnetization reached extremal values as a function of angle. Prior to each measurement of the temperature dependence the sample was heated to a temperature of not less than $3T_N$ and then cooled to 5 K in the presence of a magnetic field H_{FC}. The direction of the field H_{FC} was either parallel to the measuring field (H_{+FC}) or antiparallel to it (H_{-FC}).

1. Figure 1a shows the results of measurements of the temperature dependence of the magnetization of the $LiNiPO_4$ crystal in a magnetic field $H=1$ kOe oriented along the *c* axis. It is seen that at low temperatures the curves $M(T)_{+FC}$ and $M(T)_{-FC}$ do not coincide. The possible measurement errors do not exceed the size of the data points in the figure.

Assuming the presence of a spontaneous magnetization, we can write an expression for the dependence of the magnetization on temperature and magnetic field strength:

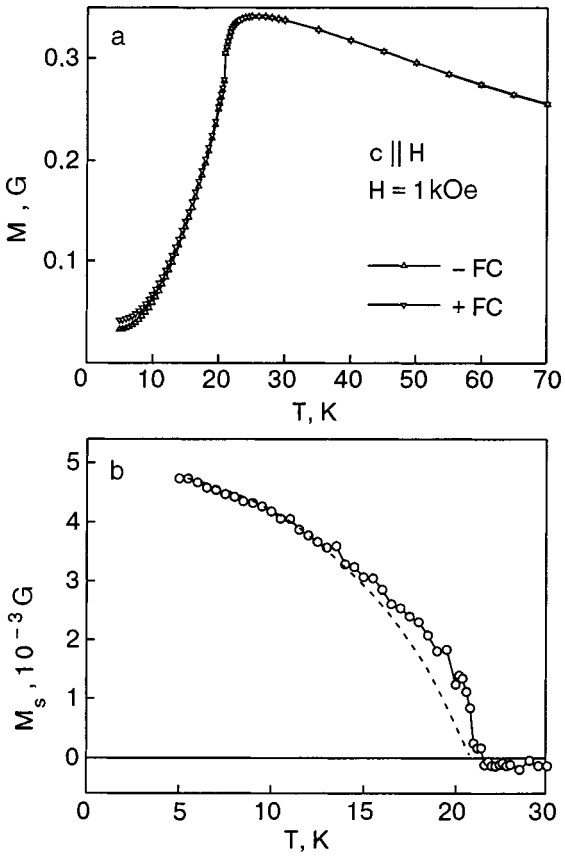

FIG. 1. Temperature dependence of the magnetization of a $LiNiPO_4$ sample cooled in fields $H_{+FC}=+15$ kOe and $H_{-FC}=-15$ kOe (a) and of the spontaneous magnetization $M_s=(M_{+FC}-M_{-FC})/2$ (b). The dashed curve is the temperature dependence of the cube of the antiferromagnetic order parameter, taken from Ref. 20 and normalized to the value of M_s at $T=5$ K.

$$M(T,H)=M_s(T)+\chi(T)H+\chi^{(2)}(T)H^2+\chi^{(3)}(T)H^3.$$

Here $M_s(T)$ and the contribution quadratic in the field, $\chi^{(2)}(T)H^2$, have different signs for antiferromagnetic states with oppositely directed sublattice magnetic moments. From the curves of the magnetization versus magnetic field strength obtained in a field $\mathbf{H}\|\mathbf{c}$ at different temperatures in the field range from $+50$ kOe to -50 kOe we extracted the cubic contribution $\chi^{(3)}(T)H^3$. The largest value of $\chi^{(3)}$ corresponds to about 5×10^{-6} G/kOe^3. The quadratic contribution $\chi^{(2)}(T)H^2$, if it exists at all, is extremely small, the value of $\chi^{(2)}$ being not greater than 10^{-5} G/kOe^2. We note that the usual susceptibility near the Néel temperature is around 0.3 G/kOe. Taking $\chi^{(2)}(T)=0$ and assuming that the coercive force is much larger than the field at which the measurements were made, we can write the temperature dependence of the spontaneous magnetization in the form

$$M_s(T)=[M(T)_{+FC}-M(T)_{-FC}]/2.$$

The $M_s(T)$ curve obtained from the experimental data is shown in Fig. 1b. It is seen that the crystal has a very weak ferromagnetism in the direction of the *c* axis, along which the antiferromagnetic vector is oriented. The spontaneous moment decreases monotonically as the sample is heated, and it vanishes at a temperature near 20.8 K. The absence of steplike changes indicates that the sample remains single-domain throughout the temperature range from 5 K to a tem-

perature almost equal to T_N. Its value at 5 K is 0.0048 G ($\sim$0.2 cgs emu/mole, or $\sim 4\times10^{-5}$ μ_B/mole, where μ_B is the Bohr magneton). Such weak ferromagnetism is appropriately called ultraweak.

If it is assumed that the weak ferromagnetism in $LiNiPO_4$ is a property of the stoichiometric crystal, then it can be described only by invariants not lower than fourth-order, since the usual invariants of the Dzyaloshinskiĭ type are forbidden by the presence in the Fedorov group $Pnma$ of an odd center of inversion with respect to the antiferromagnetic vector of the main mode of ordering, $\mathbf{L}_2=\mathbf{S}_1-\mathbf{S}_2-\mathbf{S}_3+\mathbf{S}_4$. The numbering of the magnetic sites is the same as in Refs. 21, 25, and 27 and differs from the numbering in Ref. 5. Using a table of transformations for the symmetry operations of the magnetic vectors $\mathbf{M}$, $\mathbf{L}_2$, $\mathbf{L}_1=\mathbf{S}_1-\mathbf{S}_2+\mathbf{S}_3-\mathbf{S}_4$, and $\mathbf{L}_3=\mathbf{S}_1+\mathbf{S}_2-\mathbf{S}_3-\mathbf{S}_4$, which is given, e.g., in Refs. 5 and 25, one can determine the invariants that allow the appearance of weak ferromagnetism along the c axis. These are $M_zL_{2z}L_{1y}L_{3y}$ and $M_zL_{2z}L_{1x}L_{3x}$. Since the group $Pnma$ of $LiNiPO_4$ also allows the second-order invariant $L_{2z}L_{3x}$, one expects a preference for the invariant $M_zL_{2z}L_{1x}L_{3x}$. In addition, the thermodynamic potential also admits the magnetoelectric invariants $M_zP_xL_{2z}$ and $L_{2z}L_{1x}P_x$, which couple the parameters of those magnetic vectors with the electric polarization. Therefore, in addition to the spontaneous ferromagnetism in $LiNiPO_4$ there can also exist a spontaneous electric polarization along the a axis, and one of the possible mechanisms for the appearance of such weak ferromagnetism is magnetoelectric.

We write the projections of the vectors L_{1x} and L_{3x} as resulting from small deviations of the spins $\mathbf{S}_1$, $\mathbf{S}_2$, $\mathbf{S}_3$, and $\mathbf{S}_4$ from the orientations described by L_{2z}. The corresponding effective fields giving rise to the antiferromagnetic modes L_{1x} and L_{3x} are perpendicular to the vector of the main antiferromagnetic mode L_{2z}. Their temperature dependence will therefore be largely determined by that of L_{2z}. Consequently, one expects that the temperature dependence of the spontaneous magnetic moment will be determined by that of $L_{2z}^3(T)$. The dashed curve in Fig. 1b shows the normalized temperature dependence of the cube of the antiferromagnetic order parameter as determined in neutron diffraction experiments (see Fig. 8 of Ref. 20). At $T<0.75T_N$ one observes qualitative agreement of the $L_{2z}^3(T)$ curve with the experimentally determined $M_s(T)$ curve.

The appearance of such a small spontaneous magnetic moment might be due to the presence of various kinds of defects and impurities in the sample. The influence of impurities of iron ions on the magnetic properties of $LiNiPO_4$ was investigated in Refs. 19, 20, and 22, and it was found that Fe^{3+} ions have a very strong effect on the magnetic properties of the crystal. Fe^{3+} ions locate between antiferromagnetic layers, replacing Li^+ ions and forming chains of antiferromagnetic clusters having a weak magnetic moment. As a result, the $LiNiPO_4$:Fe^{3+} crystal acquires the properties of a weak ferromagnet. At a concentration of 0.033 Fe^{3+} ions per molecule the magnetic moment is around 4.9 cgs emu/mole.[22] If it is assumed that there are small amounts of uncontrolled Fe^{3+} impurities in the sample and that the weak ferromagnetism is due to clusters of only two iron ions, the concentration of Fe^{3+} impurity ions required to produce the observed moment of 4.8×10^{-3} G$\approx$0.2 cgs emu/mole, as determined by the expression $(x^2/2)\times10^4$ cgs emu/mole, must be not less than $x\sim0.006$ Fe^{3+} ions per molecule. However, such a large concentration of iron ions cannot be present in the nominally pure crystal.

One would also be justified in wondering whether the observed spontaneous moment might be due to topological magnetic inhomogeneities and to frustration of the exchange bonds in imperfect parts of the crystal. The two-dimensional character of the exchange bonds is conducive to the formation of inhomogeneous local structures in the surroundings of various crystal lattice defects. The magnetic structure of $LiNiPO_4$ contains a layer of Ni^{2+} ions with parallel spins. The layers are parallel to the ac plane. On going from layer to layer, the orientation of the spins changes to the opposite. Therefore, the specific contribution of stacking faults forming partial dislocations with Burgers vectors parallel to the b axis could be especially important. Such dislocations are formed when a layer is removed, and, upon the complete breaking of the bonds, will lead to the formation of an uncompensated ferromagnetic layer with a magnetic moment parallel to the c axis. The total area of these idealized ferromagnetic layers which would be needed to produce the observed spontaneous magnetic moment in the sample is at least 0.5 cm^2. This required area may be orders of magnitude larger, since the magnetic moment of the uncompensated layer can be decreased substantially by the formation of new antiferromagnetic exchange bonds in the ''healing'' of the defect. It appears doubtful that the necessary density of partial dislocations (more than 10^3 cm^{-2}) for creating this required total area could be formed during the growth of the crystal.

Another possible cause of weak ferromagnetism is the appearance of inhomogeneous magnetic formations with frustrated exchange bonds in the vicinity of other extended and point stacking faults.[32–34] It is difficult to assess whether such a mechanism is realistic. If it is assumed that one defect site leads to the formation of a magnetic moment of $0.1\mu_{Ni^{2+}}$ in the adjacent region of the crystal, then the required number of such defect sites would be not less than 10^{18} cm^{-3}, which also seems excessively large. On the other hand, if the magnetic moment of the frustrated part were two orders of magnitude larger, then such a mechanism for the appearance of weak ferromagnetism could not be ruled out. We also cannot rule out the possibility that the weak ferromagnetism in $LiNiPO_4$ is an inherent property of its magnetic structure. In any case the observed proportionality $M_s(T)\sim L_{2z}^3(T)$ indicates that the spontaneous magnetic moment is due to the antiferromagnetic ordering in the crystal and is a consequence of interactions of high order in spin. Additional studies will surely be necessary in order to explain the nature of the appearance of the weak ferromagnetic moment.

2. Figures 2 and 3 show the temperature dependence of the magnetic susceptibility $M(T)/H$ and its temperature derivative $\Delta(M(T)/H)/\Delta T$ obtained near the Néel temperature in field orientations $\mathbf{H}\|\mathbf{a}$, $\mathbf{H}\|\mathbf{b}$, and $\mathbf{H}\|\mathbf{c}$. There are two features visible on all three curves: a jump at T_1 and a kink at T_2. The jumplike change in the susceptibility occurs in a temperature interval not greater than 0.06 K. The rate of change of the susceptibility in this interval is 5–9 times

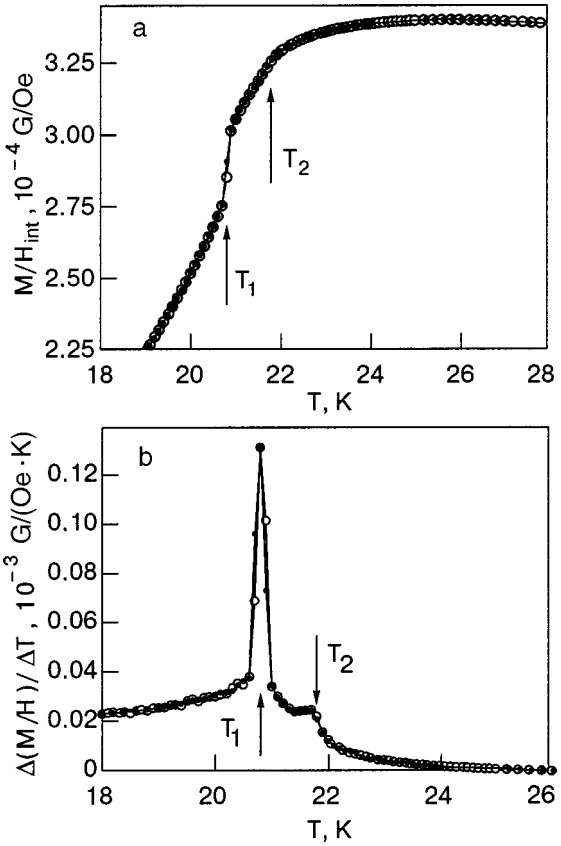

FIG. 2. Temperature dependence of the magnetic susceptibility $M(T)/H$ of the $LiNiPO_4$ crystal (a) and its derivative $\Delta(M/H)/\Delta T$ (b) for **H**‖**c** in the vicinity of the antiferromagnetic ordering temperature on heating (○) and cooling (●) of the sample; $H=20$ kOe, $T_1=20.79$ K, and $T_2=21.77$ K. H_{int} is the value of the internal magnetic field of the sample.

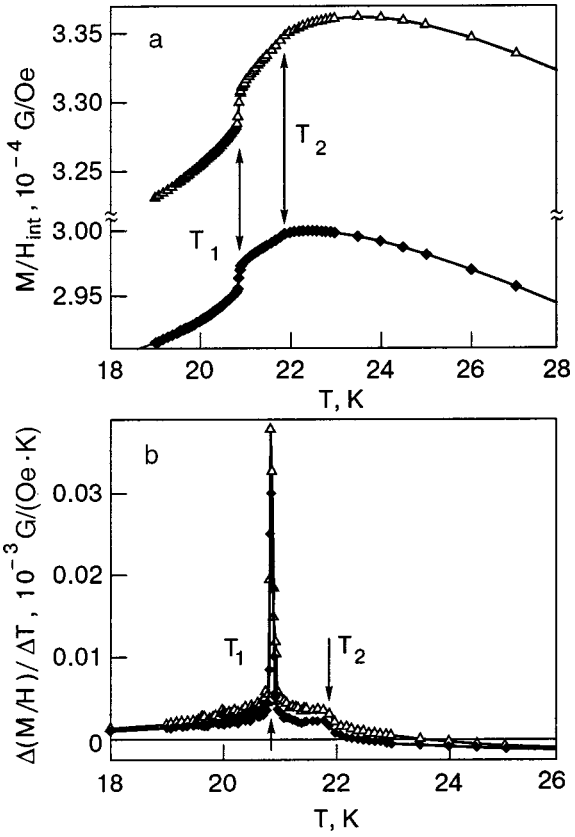

FIG. 3. Temperature dependence of the magnetic susceptibility $M(T)/H$ of the $LiNiPO_4$ crystal (a) and its derivative $\Delta(M/H)/\Delta T$ (b) for **H**‖**a** (△) and **H**‖**b** (♦) in the vicinity of the antiferromagnetic ordering temperature; $H=10$kOe, $T_1=20.84$ K, and $T_2=21.86$ K.

larger than in the regions directly adjacent to it. The maximum of the derivative at a value of the measuring field $H=10$ kOe is reached at a temperature $T_1=20.84$ K. When the field is increased to $H=20$ kOe, the jump is shifted in temperature to 20.79 K. The observed jump cannot be due to the appearance of 180° antiferromagnetic domains on heating and their disappearance on cooling. Such domains can lead to total compensation and the vanishing of the magnetoelectric effect and the spontaneous magnetic moment, but they cannot be manifested in any way on the temperature dependence of the magnetic susceptibility. A jumplike change of the susceptibility $M(T)/H$ can be due solely to a jump in the antiferromagnetic order parameter. Thus a first-order phase transition occurs at the $T=T_1$. We note that a jump in the magnetoelectric effect near T_N was observed in $LiNiPO_4$ in Ref. 21.

The second feature, the kink, is observed for all three directions of the magnetic field. In a field $H=10$ kOe the kink in the temperature dependence is observed at a temperature close to $T_2=21.86$ K, while in a field $H=20$ kOe it occurs near 21.77 K. As we see from Figs. 2b and 3b, the kink corresponds to distinct steps on the temperature dependence of the derivative $\Delta(M(T)/H)/\Delta T$. It is natural to suppose that a second-order phase transition occurs at the temperature T_2, and the magnetic state of the sample in the temperature interval from T_1 to T_2 is a thermodynamically equilibrium intermediate phase. In the absence of magnetic field the temperatures of these transitions are close to $T_{N1}=20.8(5)$ K and $T_{N2}=21.8(5)$ K. One notices that a smooth transition to the intermediate phase occurs on the high-temperature side, while the transition on the low-temperature side is abrupt. Such a sequence of first- and second-order transitions is characteristic for transitions to an incommensurate phase.[35,36] This circumstance suggests that the intermediate phase in $LiNiPO_4$ is an incommensurate antiferromagnetic phase. The thermodynamic potential for antiferromagnetic $LiNiPO_4$ contains invariants that might promote the formation of noncollinear antiferromagnetic modulated structures with a modulation vector directed along the a axis (the invariants $L_{1x}dL_{2z}/dx$ and $L_{2z}dL_{1x}/dx$) or along the b axis (invariants $L_{1y}dL_{2z}/dy$, $L_{2z}dL_{1y}/dy$). Also allowed are inhomogeneous structures with modulated weak ferromagnetism. Their modulation vector may be parallel to either the a axis (invariants M_zdL_{2z}/dx, $L_{2z}dM_z/dx$) or the c axis (invariants M_xdL_{2z}/dz, $L_{2z}dM_x/dz$).

The formation of a modulated phase in $LiNiPO_4$ at temperatures close to T_N may facilitate a weak exchange interaction between the antiferromagnetic layers and a weak magnetic anisotropy in the ac plane at these temperatures. That the single-ion magnetic anisotropy of paramagnetic $LiNiPO_4$ in the ac plane is small is indicated by the closeness of the corresponding temperature dependences of the magnetic susceptibility in the paramagnetic region (see Figs. 2 and 3). Under such conditions the energies of the quasiacoustic and one of the quasiexchange branches of spin waves at small

wave vectors k may be comparable. The resonant interaction between them for $k \neq 0$ may lead to softening of one of the mixed modes. At a structural transformation the formation of an intermediate commensurate phase is an ordinary occurrence, and the resonant interaction of phonon modes is often the operative mechanism.[35,37] At temperatures near T_N one can speak of spin-wave modes only with reservations, and the same is true of the modes of excitation of the fluctuationally ordered regions. These excitations are of a substantially nonlinear character. It is possible that in $LiNiPO_4$ under these conditions a process occurs which is analogous to that considered by Filippov,[38] who examined the possibility of spontaneous formation of a vortical phase in the ferromagnetic ordering of a 2D Heisenberg ferromagnet whose symmetry admits gradient Dzyaloshinskiĭ invariants. Here we are talking about the possible formation of a striped rather than vortical inhomogeneous antiferromagnetic structure.

CONCLUSION

A study of the temperature dependence of the magnetization of single-crystal $LiNiPO_4$ in a magnetic field has revealed a very weak ferromagnetic moment, the value of which along the crystallographic c axis at $T=5$ K amounts to around 0.005 G. The weak ferromagnetic moment in $LiNiPO_4$ varies monotonically with temperature, and for $T < 0.75T_N$ its temperature dependence is close to that of the cube of the antiferromagnetic order parameter. The invariants in the thermodynamic potential which could describe the appearance of the weak ferromagnetic moment in $LiNiPO_4$ must be invariants of not lower than fourth order in the spin.

The temperature dependence of the magnetic susceptibility $M(T)/H$ exhibit anomalies in the form a jump at a temperature $T_{N1} \approx 20.8$ K and a kink at $T_{N2} \approx 21.8$ K, which indicate that the transition of $LiNiPO_4$ from the paramagnetic to the antiferromagnetic state occurs in two stages. The low-temperature antiferromagnetic ordering is preceded by an intermediate phase which exists in a narrow temperature interval with a width of 1 K. The character of the change in susceptibility at the temperature boundaries of its existence region indicates that the intermediate phase is most likely a thermodynamically stable incommensurate antiferromagnetic state.

The results of the magnetic measurements agree in part with the results of as yet unpublished neutron diffraction studies,[39] in which diffraction peaks corresponding to a modulated incommensurate structure with a modulation vector directed along the b axis were observed.

The authors are grateful to Prof. H. Schmid (Geneva University, Switzerland) for providing the $LiNiPO_4$ single crystal and for interest in this study, and to Dr. D. Vaknin (Ames Laboratory, USA) for acquainting them with the unpublished results of neutron diffraction studies of $LiNiPO_4$.

*E-mail: ykharchenko@ilt.kharkov.ua

[1] A. N. Bogdanov and A. A. Schestakov, Fiz. Tverd. Tela (St. Petersburg) **40**, 1350 (1998) [Phys. Solid State **40**, 1350 (1998)].
[2] A. Zheludev, S. Maslov, G. Shirane, I. Tsukuda, T. Masuda, K. Uchinokura, I. Zaliznyak, R. Erwin, and L. P. Regnault, Phys. Rev. B **59**, 11432 (1999).
[3] A. V. Zalessky, A. A. Frolov, T. A. Khimich, A. A. Bush, V. S. Pokatilov, and A. K. Zvezdin, Europhys. Lett. **50**, 547 (2000).
[4] H. Schmid, Ferroelectrics **252**, 41 (2001).
[5] E. A. Turov, A. V. Kolchanov, V. V. Men'shinin, I. F. Mirsaev, and V. V. Nikolaev, *Symmetry and the Physical Properties of Antiferromagnets* [in Russian], Izd-vo Fizmatlit, Moscow (2001).
[6] S. Maruyama, H. Tanaka, Y. Narumi, K. Kindo, H. Nojiri, M. Motokawa, and K. Nagata, J. Phys. Soc. Jpn. **70**, 859 (2001).
[7] B. Roessli, J. Schefer, G. Petrakovskii, B. Oulladiaf, M. Boehm, U. Staub, A. Vorontinov, and L. Bezmaternikh, Phys. Rev. Lett. **86**, 1885 (2001).
[8] A. N. Bogdanov and U. K. Rossler, Phys. Rev. Lett. **87**, 037203 (2001).
[9] J. Chovan, N. Papanocolaou, and S. Komineas, Phys. Rev. B **65**, 064433 (2002).
[10] A. N. Bogdanov, U. K. Rossler, M. Wolf, and K.-H. Muller, Phys. Rev. B **66**, 214410 (2002).
[11] I. E. Dzyaloshinskiĭ, Zh. Éksp. Teor. Fiz. **46**, 1420 (1964); **47**, 992 (1964) [Sov. Phys. JETP **19**, 960 (1964); **20**, 665 (1965)].
[12] J. M. Mays, Phys. Rev. **131**, 38 (1963).
[13] R. P. Santoro, D. J. Segal, and R. E. Newnham, J. Phys. Chem. Solids **27**, 1192 (1966).
[14] M. Mercier, J. Gareyte, and E. F. Bertaut, C. R. Acad. Sci. Paris B **264**, 979 (1967).
[15] A. Belletti, R. Borreomei, R. Cammi, and E. Cavalli, Phys. Status Solidi B **163**, 281 (1991).
[16] J.-P. Rivera, Ferroelectrics **161**, 147 (1994).
[17] J.-P. Rivera, J. Korean Phys. Soc. **32**, 1855 (1998).
[18] I. Kornev, J.-P. Rivera, S. Gentil, S. Gentil, A. G. M. Jansen, M. Bichurin, H. Schmid, and P. Wider, Physica B **270**, 82 (1999).
[19] A. Goñi, L. Lezama, G. E. Barberis, J. L. Pizzarro, M. I. Arriortua, and T. Rojo, J. Magn. Magn. Mater. **164**, 251 (1996).
[20] D. Vaknin, J. L. Zarestky, J. E. Ostenson, B. C. Chacoumakos, A. Goñi, P. Pagliuso, T. Rojo, and G. E. Barberis, Phys. Rev. B **60**, 1100 (1999).
[21] I. Kornev, M. Bichurin, J.-P. Rivera, S. Gentil, H. Schmid, A. G. Jansen, and P. Wyder, Phys. Rev. B **62**, 12247 (2000-II).
[22] A. Goñi, L. Lezama, M. I. Arriortua, G. E. Barberis, and T. Rojo, J. Mater. Chem. **10**, 423 (2000).
[23] M. F. Kharchenko, O. V. Miloslavska, Yu. M. Kharchenko, H. Schmid, and J.-P. Rivera, Ukr. J. Phys. Opt. **1**, 16 (2000).
[24] N. F. Kharchenko, Yu. N. Kharchenko, R. Szymczak, M. Baran, and H. Shmid, Fiz. Nizk. Temp. **27**, 1208 (2001) [Low Temp. Phys. **27**, 895 (2001)].
[25] N. F. Kharchenko, V. A. Desnenko, Yu. N. Kharchenko, R. Szymczak, and M. Baran, Fiz. Nizk. Temp. **28**, 896 (2002) [Low Temp. Phys. **28**, 646 (2002)].
[26] D. Vaknin, J. L. Zarestky, L. L. Miller, J.-P. Rivera, and H. Shmid, Phys. Rev. B **65**, 224414 (2002).
[27] I. E. Chupis, Fiz. Nizk. Temp. **26**, 574 (2000) [Low Temp. Phys. **26**, 419 (2000)].
[28] V. I. Fomin, V. P. Gnezdilov, V. S. Kurnosov, A. V. Peschanskii, and A. V. Eremenko, Fiz. Nizk. Temp. **28**, 288 (2002) [Low Temp. Phys. **28**, 203 (2002)].
[29] S. Geller and J. L. Easson, Acta Crystallogr. **18**, 258 (1960).
[30] I. Abrahams and K. S. Easson, Acta Crystallogr., Sect. C: Cryst. Struct. Commun. **49**, 925 (1993).
[31] F. Kubel, Z. Krystallogr. **209**, 755 (1994).
[32] M. M. Bogdan, A. S. Kovalev, and A. A. Stepanov, Fiz. Nizk. Temp. **18**, 838 (1992) [Low Temp. Phys. **18**, 591 (1992)].
[33] O. K. Dudko and A. S. Kovalev, Fiz. Nizk. Temp. **26**, 821 (2000) [Low Temp. Phys. **26**, 603 (2000)].
[34] E. C. Marino, Phys. Rev. B **65**, 054418 (2002).
[35] H. Z. Cummims, Phys. Rep. **185**, 211 (1990).
[36] P. Bak, Rep. Prog. Phys. **45**, 687 (1982).
[37] J. Mitchell and J. K. Burdett, J. Chem. Phys. **102**, 6762 (1995).
[38] A. E. Filippov, Zh. Éksp. Teor. Fiz. **111**, 1775 (1997) [JETP **84**, 971 (1997)].
[39] D. Vaknin, J. L. Zarestky, J.-P. Rivera, and H. Schmid (to be published).

Translated by Steve Torstveit

ELECTRONIC PROPERTIES OF METALS AND ALLOYS

Static skin effect in organic metals*

O. V. Kirichenko and V. G. Peschansky**

B. Verkin Institute for Low Temperature Physics and Engineering of the National Academy of Science of Ukraine, 47 Lenin Ave., Kharkov 61103, Ukraine

S. N. Savel'eva

A. F. Ioffe Physicotechnical Institute, Russian Academy of Sciences, St. Petersburg, Russia
(Submitted December 19, 2002)
Fiz. Nizk. Temp. **29**, 781–784 (July 2003)

Galvanomagnetic phenomena in layered organic conductors with a multisheet Fermi surface in the form of a weakly corrugated cylinder and weakly corrugated planes are studied. It is shown that in a strong magnetic field **H** unrestricted growth of the resistivity of such conductors with increasing H is accompanied by the current lines being forced out to the surface of the specimen. The main dissipation mechanism of electron current is charge scattering by the boundaries of the sample, even in bulk conductors whose thickness is greater than the free path length l of the conduction electrons. For specular reflection at the surface the resistivity increases linearly with the magnetic field. © *2003 American Institute of Physics.*
[DOI: 10.1063/1.1596584]

Unrestricted growth of the resistivity of a conductor with increasing magnetic field is usually accompanied by the current lines being forced out to the surface of the sample. In a strong magnetic field **H**, when the radius of curvature r of an electron trajectory is much less than the charge-carrier mean free path l, the electric current can be concentrated completely near the conductor surface (static skin effect).[1–6] This occurs in compensated metals, where the number of electrons equals the number of holes, and in metals with an open Fermi surface for magnetic field directions for which the resistivity increases with H. The reason is that the charge carriers colliding with the surface of the sample have a higher mobility than the electrons in the core of the conductor, because the center of an electron orbit undergoes a jump at every collision with the surface. The surface current depends strongly on the specularity of the electron reflections at the boundary of the sample. This allows us to use experimental studies of the H-dependence of the conductor resistivity under static skin-effect conditions as a method for checking the state of the surface without destroying the specimen.[7–12]

In metals the static skin effect is most pronounced when the magnetic field vector is parallel to the surface of the sample and orthogonal to the current density vector ($\mathbf{j}\perp\mathbf{H}$). This occurs when the effective free path length l_{eff} of the electrons which are specularly reflected from perfectly smooth defect-free surfaces is limited by electron collisions in the bulk only, i.e. $l_{\text{eff}}=l$, and the conductivity $\sigma_{\perp}^{\text{skin}}$ of a surface layer of thickness $2r$ is of the same order of magnitude as the conductivity σ_0 in the absence of a magnetic field. In compensated metals the contribution to the transverse conductivity $\sigma_{\perp}^{\text{vol}}$ of the electrons in the interior volume is of the order of $\sigma_0(r/l)^2$ and the electric field is orthogonal to the vector **H**.

As a result, charge carriers that collide with the sample surface make the main contribution to the electric current density

$$j_i=\sigma_{ik}E_k \tag{1}$$

and the resistivity of a sample with thickness $d\ll l^2/r$ increases linearly with H.

In a magnetic field an electron deflected at an angle $\alpha > l/r$ from the surface of the sample goes into the bulk of the conductor after several collisions with the surface. The electron mean free path l_{eff} is much less than l and equals $r/\sin\alpha$. The result is that the transverse resistivity ($\mathbf{j}\perp\mathbf{H}$) of compensated metals increases quadratically with the magnetic field for any ratio of d and l, even if the surface of the sample is perfectly smooth and the energy and momentum projection on a plane tangent to the surface are conserved for specularly reflected electrons.

Investigations of the surface state of layered conductors with a quasi-two-dimensional electron energy spectrum by means of magnetoresistance measurements prove to be effective in magnetic fields inclined away from the surface of the sample.

We shall consider the distribution of the current lines in tetrathiafulvalene-based organic conductors $(\text{BEDT–TTF})_2\text{X}$ (where X is a radical) placed in a strong magnetic field. The organic conductors in this family consist of layered structures with a sharp metal-like anisotropy of the electric conductivity—the conductivity along the layers is much higher than the conductivity across the layers. This is probably due to the sharp anisotropy of the conduction

electron velocity $\mathbf{v}=d\varepsilon(\mathbf{p})/d\mathbf{p}$ at the Fermi surface $\varepsilon(\mathbf{p})=\varepsilon_F$, i.e. the energy of the conduction electrons

$$\varepsilon(\mathbf{p})=\sum_{n=0}^{\infty}\varepsilon_n(p_x,p_y)\cos\left\{\frac{anp_z}{\hbar}+\alpha_n(p_x,p_y)\right\},$$

$$\alpha_n(p_x,p_y)=-\alpha_n(-p_x,-p_y), \tag{2}$$

$$\varepsilon_n(p_x,p_y)=\varepsilon_n(-p_x,-p_y)$$

depends weakly on the momentum projection $p_z=\mathbf{p}\cdot\mathbf{n}$ along the normal $\mathbf{n}$ to the layers.

Here a is the distance between the layers, $\hbar$ is Planck's constant, the functions $\varepsilon_n(p_x,p_y)$ decrease as n increases, so that the maximum value of the function $\varepsilon(\mathbf{p})-\varepsilon_0(p_x,p_y)$, equal to $\hbar\varepsilon_F$ at the Fermi surface, is much less than the Fermi energy ε_F.

The Fermi surface of layered conductors is an open surface which is weakly corrugated along the p_z axis. Experimental observations of the Shubnikov–de Haas quantum oscillations, first in the complexes $(BEDT-TTF)_2IBr_2$ and $(BEDT-TTF)_2I_3$[13,14] and then in all tetrathiafulvalene-based layered conductors,[15,16] in strong magnetic fields $\mathbf{H}=(0,H\sin\theta,H\cos\theta)$ for a wide range of θ prove that at least one Fermi surface sheet is a weakly corrugated cylinder.

In a magnetic field oriented parallel to the layers many electrons with energy equal to the Fermi energy move along open orbits $\varepsilon=\text{const}$, $p_H=\mathbf{p}\cdot\mathbf{H}/H=\text{const}$ in momentum space, and the resistance for the current flowing across the layers increases without bound as H increases.

Let the sample be a plate with thickness d and boundaries $z_s=0,d$ and $y_s=0,L$, where d and L are much greater than l. At $\theta=\pi/2$ the conduction electrons near a saddle point of the Fermi surface make the main contribution to the conductivity σ_{zz} across the layers of the core of the sample.[17] Then the following formulas hold:

$$\sigma_{zz}^{\text{vol}}=\sigma_0\gamma\eta^2,\ \eta^{1/2}\ll\gamma\ll1,$$

$$\sigma_{zz}^{\text{vol}}=\sigma_0\gamma^2\eta^{3/2},\ \gamma\leqslant\eta^{1/2}\ll1, \tag{3}$$

where σ_0 is the conductivity in the absence of a magnetic field.[17,18] Its value is of the order of the conductivity of metals such as copper, gold, and silver. Here and below, $r=ep_F/eH$ is the radius of curvature of an electron orbit at $\theta=0$; $\gamma=r/l$; c is the velocity of light; e is the electron charge; p_F is the characteristic radius of the Fermi surface, which is a weakly corrugated cylinder. If L is not much greater than the free path length l, the contribution of σ_{zz} from charge carriers "slipping" along the boundaries $y_s=0,L$ must be taken into account. These are conduction electrons with closed orbits. Their number relative to the total number of charge carriers is not large (about $\eta^{3/2}$), but their mobility is higher than that of the electrons that do not strike the surface of the sample. For specular reflection of electrons at the boundary of the sample, electron drift along the z axis is limited by volume scattering only. The displacement of an electron along the z axis during the time between two collisions with the surface $y_s=0$ is about $r\eta^{1/2}$. If the probability w of diffuse scattering with partial erasure of the memory of the past history of the electrons is low, then the effective free path of slipping electrons can be estimated as $l_{\text{eff}}=r\eta^{1/2}/(r/l+w)$ and the conductivity of the boundary layer is

$$\sigma_{zz}^{\text{skin}}=\sigma_0\frac{l_{\text{eff}}}{l}=\sigma_0\frac{r\eta^{1/2}/l}{r/l+w}. \tag{4}$$

The fraction of electrons which form the skin layer is about $\eta^{3/2}r/L$ and the conductivity of the entire sample

$$\sigma_{zz}=\sigma_{zz}^{\text{skin}}\eta^{3/2}r/l+\sigma_{zz}^{\text{vol}} \tag{5}$$

essentially depends only on the state of the surface of the bulk specimen ($l\ll L,d$) in very strong and perhaps currently unattainable magnetic fields such that $r/l\ll\eta^2$.

The resistivity for the current flowing along the layers saturates in strong magnetic fields and is of the order of $1/\sigma_0$. When the magnetic field deviates from the direction along the layers all sections of the corrugated cylinder cut by the plane $p_z=\text{const}$ are closed and the resistance for the current flowing across the layers also saturates for $r\ll l$.

Thus the current lines in organic conductors whose Fermi surface is a weakly corrugated cylinder and does not contain any extra sheets are uniformly distributed over the entire cross section normal to the current. For any orientation of a magnetic field the conductivity is determined mainly by charge carriers that do not collide with the boundary.

The distribution of the current lines is substantially different in a conductor whose Fermi surface consists of elements with different topological structure. There are grounds for believing that the Fermi surface in organic complexes $(BEDT-TTF)_2MHg(SCN)_4$ (where M is either a metal from the group (K, Rb, Tl) or NH_3) consists of a weakly corrugated cylinder and weakly corrugated planes.[19] In such conductors open sections of the Fermi surface cut by the plane $p_z=\text{const}$ occur for any orientation of a magnetic field and the resistivity saturates in a strong magnetic field for only selected directions of the current.

When the magnetic field makes an angle $\alpha=(\pi/2-\theta)\gg\eta$ with the layers, the electron trajectories in momentum space are almost indistinguishable. Magnetoresistance investigations of the interaction of charge carriers with the surface of a sample prove to be effective in a wide range of angles α.

Consider the case where the corrugated planes lie in the p_xp_y plane and the electron drift along the p_y axis in momentum space is limited. The equations of motion

$$\frac{\partial p_x}{\partial t}=\frac{eH}{c}(v_y\cos\theta-v_z\sin\theta),$$

$$\frac{\partial p_y}{\partial t}=-\frac{eHv_x}{c}\cos\theta, \tag{6}$$

$$\frac{\partial p_z}{\partial t}=\frac{eHv_x}{c}\sin\theta$$

for charge carriers that do not come into contact with the boundaries of the sample imply

$$\overline{v}_x=\frac{1}{T}\int_0^T dtv_x(t)=0, \tag{7}$$

where $T=2\pi m^*c/eH$ is the period of the electron motion in a magnetic field and m^* is the effective electron cyclotron

mass. If the motion on an open orbit in momentum space is aperiodic, T is a time interval which is long compared to the free path time τ.

Thus the contribution to the conductivity along the x axis by volume electrons for closed and open trajectories in momentum space is inversely proportional to H^2, specifically, $\sigma_{xx}^{\mathrm{vol}} \simeq \sigma_0 (r/l)^2$.

The drift of electrons slipping near the boundaries of the sample is different from zero along the x axis. The contribution of these electrons to the conductivity could predominate. At angles θ different from $\pi/2$ all orbits in the momentum space of the electrons whose states lie on a corrugated cylinder of the Fermi surface are closed. Their drift along the y axis is small. Colliding with the boundary $y_s = 0$ the electrons drift for a long time along the x axis and move slowly with velocity $\overline{v_y} = \overline{v_z} \tan\theta$ into the bulk of the conductor. For θ substantially different from $\pi/2$, i.e. when $\tan\theta$ is of the order of 1, their effective free path is

$$l_{\mathrm{eff}} = \frac{r}{r/l + w + \eta \tan\theta}. \tag{8}$$

Since the quasi-two-dimensionality parameter for the electron energy spectrum in organic layered conductors is of the order of 10^{-2}, in a wide range of angles θ ($\eta \tan\theta \ll 1$) the direct electric current is almost totally concentrated near the surface of the sample if

$$L = \frac{l}{r/l + w + \eta \tan\theta}. \tag{9}$$

Charge carriers that interact with the boundaries $z_s = 0, d$ are also more mobile than electrons that are ''unaware'' of the existence of the sample boundaries. Electron reflection from the boundaries $z_s = 0, d$ is nearly specular because the electrons move slowly along the z axis and approach these boundaries at small angles. Therefore a large fraction of the current is concentrated not only along the boundaries $y_s = 0, L$ but also along the boundaries $z_s = 0, d$. Conduction electrons approaching the boundaries $y_s = 0, L$ at large angles are at most capable of weakening the correlations between the incident and reflected electrons. The possibility of specular reflection of charge carriers at the boundaries $y_s = 0, L$ can be easily determined by studying the resistivity of a layered conductor under static skin effect conditions.

[*] Reported at the 3rd International Workshop on Low Temperature Microgravity Physics (CWS-2002).

[**] E-mail: vpeschansky@ilt.kharkov.ua

[1] M. Ja. Azbel, Zh. Éksp. Teor. Fiz. **44**, 983 (1963) [Sov. Phys. JETP **17**, 1463 (1963)].
[2] M. Ja. Azbel and V. G. Peschansky, Zh. Éksp. Teor. Fiz. **49**, 572 (1965) [Sov. Phys. JETP **22**, 399 (1965)].
[3] M. Ja. Azbel and V. G. Peschansky, Zh. Éksp. Teor. Fiz. **52**, 1003 (1967) [Sov. Phys. JETP **25**, 665 (1967)].
[4] M. Ja. Azbel and V. G. Peschansky, Zh. Éksp. Teor. Fiz. **55**, 1980 (1968) [Sov. Phys. JETP **28**, 1045 (1969)].
[5] G. I. Babkin and V. Ja. Kravchenko, Zh. Éksp. Teor. Fiz. **60**, 695 (1971) [Sov. Phys. JETP **33**, 378 (1971)].
[6] O. V. Kravchenko, V. G. Peschansky, and S. N. Savel'eva, Zh. Éksp. Teor. Fiz. **77**, 2045 (1979) [Sov. Phys. JETP **50**, 976 (1979)].
[7] O. A. Panchenko, A. A. Kharlamov, and Yu. G. Ptushinskii, Zh. Éksp. Teor. Fiz. **67**, 780 (1974) [Sov. Phys. JETP **40**, 386 (1975)].
[8] N. V. Volkenshtein, V. E. Startsev, and V. P. Dyakina, Phys. Status Solidi B **66**, K107 (1974).
[9] Ju. P. Gaydukov, E. M. Galjamina, and N. P. Danilova, JETP Lett. **22**, 107 (1975).
[10] Ju. P. Gaidukov and E. M. Galjamina, Zh. Éksp. Teor. Fiz. **75**, 1426 (1978) [Sov. Phys. JETP **48**, 719 (1978)].
[11] V. G. Peschansky, J. Stat. Phys. **38**, 253 (1985).
[12] V. G. Peschansky, Sov. Sci. Rev. **16**, 1 (1992).
[13] M. V. Kartsonik, V. N. Laukhin, V. N. Nizhankovskii, and A. A. Ignat'ev, JETP Lett. **47**, 363 (1988).
[14] M. V. Kartsovnik, P. A. Kononovich, V. N. Laukhin, and I. F. Shchegolev, JETP Lett. **48**, 541 (1988).
[15] J. Wosnitza, *Fermi Surfaces of Low-Dimensional Organic Metals and Superconductors*, Springer Tracts in Modern Physics (1996), p. 165.
[16] J. Singleton, Rep. Prog. Phys. **116**, (2000).
[17] V. G. Peschansky, Zh. Éksp. Teor. Fiz. **112**, 6183 (1997) [JETP **85**, 337 (1997)].
[18] V. G. Peschansky, Phys. Rep. **288**, 305 (1997).
[19] R. Rossenau, M. L. Doublet, E. Canadell, R. P. Shibaeva, R. P. Rozenberg, N. D. Kushch, and E. B. Jagubskii, J. Phys. (France) **6**, 1527 (1996).

This article was published in English in the original Russian journal. Reproduced here with stylistic changes by AIP.

Resistivity and microscopic characteristics of platinum in different structural states

V. I. Sokolenko,* Ya. D. Starodubov, and V. I. Mirny

National Research "Kharkov Institute of Physics and Technology," ul. Akademicheskaya 1, 61108 Kharkov, Ukraine

A. A. Zavgorodniĭ, B. A. Merisov,** and V. V. Kozinets

V. N. Karazin Kharkov National University, pl. Svobody 4, 61077 Kharkov, Ukraine

(Submitted May 31, 2002; revised December 28, 2002)
Fiz. Nizk. Temp. **29**, 785–792 (July 2003)

The experimental temperature dependence of the resistivity of platinum in different structural states is processed using the two-band Mott–Wilson model of a transition metal. It is found that impurities, deformation defects, and quenching defects have essentially different influences on the Debye temperature, the intensity of electron–electron Coulomb scattering, and the intensity of intra- and interband electron–phonon scattering. A number of effective microscopic characteristics and band parameters are calculated in the Friedel model. The mechanisms by which the different structural factors influence the investigated complex of physical characteristics of platinum are analyzed. © *2003 American Institute of Physics.*
[DOI: 10.1063/1.1596585]

INTRODUCTION

It is known that the temperature dependence of the resistivity of a metal contains important information about the characteristics of the quasiparticle energy spectra and interaction parameters.[1–3] The experimental data for a number of nonferromagnetic transition metals (Nb,[4,5] V,[6,7] Ta,[8] and Pt[7]) of various degrees of purity are described to high accuracy over a wide range of temperatures, from helium to room (the maximum discrepancy between the experimental points and the theoretical curves is not over 2% in all the papers), by the expression[9]

$$\rho(T)=\rho_0+aT^2+b(T/\Theta)^3J_3(\Theta/T)+c(T/\Theta)^5J_5(\Theta/T), \quad (1)$$

where ρ_0 is the residual resistivity, a, b, and c are coefficients characterizing the intensity of the electron–electron Coulomb scattering and the inter- and intraband electron–phonon scattering, Θ is the Debye temperature, and $J_n(\Theta/T)$ are the Debye integrals. Formula (1) corresponds to the two-band Mott–Wilson model of a transition with charge transfer by the s electrons. It was obtained with the use of a number of simplifying assumptions (sphericity of the sheets of the Fermi surface, neglect of umklapp processes, averaging of the values of the matrix elements for intra- and interband electron–phonon scattering, satisfaction of Matthiessen's rule). Each of the temperature-dependent contributions to $\rho(T)$ ($\sim T^2$, $\sim T^3$, $\sim T^5$) has a clear physical meaning.[2] The term proportional to T^5 corresponds to the well-known Bloch–Grüneisen law.

In Refs. 10–12 an approach to the solution of the problem of electronic conduction in transition metals was developed using band-theory calculations of the energy spectrum, experimental data on the phonon spectrum, and the approximation of a rigid MT potential for the electron–phonon matrix elements. That approach amounts to a rather high level of mathematical approximation to the Bloch–Grüneisen theory in regard to the solution of the Boltzmann equation. It has been noted[10,12] that a temperature dependence $\rho(T) \propto T^5$ follows from the character of the frequency dependence of the transport spectral function of the electron–phonon interaction. The model did not include possible contributions to $\rho(T)$ from the electron–electron and electron–paramagnetic scattering, and for this reason the calculated results are lower than the experimental data in the low-temperature region ($T=10-20$ K). In the temperature interval 100–300 K the results of the calculations are higher than the experimental data by $\sim 10\%$. This disagreement was attributed by the authors, first, to the inherent limitations of the model of a rigid MT potential in the electron–phonon interaction, and also to a possible noncorrespondence between the energies characterizing the band structures and the quasiparticle energies in the theory of electron transport and to neglect of the smearing of the Fermi level at the upper boundary of the temperature interval. Although there is no fundamental reason why such an approach cannot be used to study the transport properties of nonideal transition metals, the corresponding calculations for specific types of defects have not been done in view of the obvious difficulties they would entail.

It follows from the data given above that the degree of accuracy in the description of the experimental results in the framework of a simplified Mott–Wilson model of a transition metal is higher than for the description in the refined Bloch–Grüneisen theory. This raises the question of what is the reason for such good agreement of the Mott–Wilson model with experiment. Part of the explanation may lie in the following. The elastic neutron scattering experiments of Ref. 13 showed that for Nb the phonon distribution function at frequencies $\omega \leqslant 0.5\omega_{\max}$ corresponds well to the Debye model of the spectrum, and this provides grounds for using it in calculations of the low-temperature characteristics. It can

be assumed that in other transition metals also an appreciable part of the electron–phonon interaction is realized on account of nearly Debye phonons. Furthermore, it was noted in Ref. 14 that the strong anisotropy and complex structure of individual isoenergy surfaces have only a weak effect on the resistivity. This is because the set of all energy surfaces for each metal can be approximated to a certain degree of accuracy by a sphere. In construction of the Fermi surfaces by the Harrison method the initial spherical surface is divided into separate sheets, and at low values of the pseudopotential the approximation of all the sheets by a sphere is a good approximation.

According to Refs. 15 and 16, the Fermi surface (FS) of platinum consists of three sheets: a closed electronic surface, centered at the Γ point of the Brillouin zone, for which $s-p$ mixing is typical, hole surfaces with d-type symmetry in the form closed ellipsoids of revolution at the X point, and a multiply connected tubular sheet with orientation along [100]. Here the electronic part of the FS surface corresponds to $\sim 18\%$ of the total density of states $N(0)$. This ''architecture'' of the FS admits the possibility of both intrasheet $(s-s)$ and intersheet $(s-d)$ processes of charge carrier scattering by phonons. Calculations of the phononic resistivity of Pd, the FS of which is similar to that of Pt, are in good agreement with intersheet processes in the Mott model, in the opinion of the authors of Ref. 10. In this paper it is shown that the Γ-centered electron sheet of the FS, with an 8% contribution to $N(0)$, carries 80% of the current, and the dominant scattering channel (81%) is the scattering of carriers from the electron sheet of the FS to sheets formed by carriers with a lower velocity.

The brief analysis presented above attests to the possibility of employing formula (1) for approximating the experimental data describing $\rho(T)$ for Pt. Here we have in mind that the microscopic parameters in the coefficients of the different powers of the temperature are some averaged effective values for the corresponding sheets of the isoenergy surfaces. In such an approach the changes of Θ, a, b, c and of the temperature derivative of the resistivity $d\rho/dT|_{T\geqslant\Theta}$ at $T\geqslant\Theta$ upon the introduction of structural defects to the material reflect the changes of the effective parameters of the electron and phonon spectra and the changes of the quasiparticle interaction.

For nonideal superconducting transition metals a number of microscopic characteristics and superconductivity parameters averaged over the FS can be calculated with allowance for effects due to the electron lifetime in scattering on crystal lattice defects and thermal phonons and with the use of data[17] on the conductivity and superconducting transition temperature T_c. For the bcc transition metals Ta and Nb containing various amounts of interstitial impurities and deformation defects, numerical calculations of a number of FS-averaged microscopic characteristics and parameters of the Friedel model[18,19] of a transition metal were carried out in Ref. 5 with the use of experimental data $(\Theta, d\rho/dT|_{T\geqslant\Theta}, T_c)$, and it was found that they change in opposite ways upon the introduction of interstitial impurities and dislocations. The Friedel model gives a simplified description of the electronic structure of transition metals in the form overlapping bands of free s electrons having a quadratic dispersion relation and a band of d electrons characterized by a width W_d, with a ''uniformly smeared'' density of states $N_d(E)=10/W_d$ in it, and an average energy E_d. Taking into account the sphericity of the s band in the Friedel and Mott–Wilson models and the circumstance that the shape of the d band does not play a substantial role for the latter,[2] we can assume that the effective microscopic parameters characterizing the coefficient of the T^5 term, in particular, can also be used for an estimate of the effective parameters of the Friedel model.

The goal of this study was to investigate the influence of impurities, deformation defects, and quenching defects on the temperature dependence of the resistivity of an fcc transition metal (Pt) and to estimate the change of the effective microscopic parameters in the framework of the Friedel model of a two-band transition metal and the change of the FS-averaged characteristics of the energy spectrum (without invoking the characteristics of the superconductivity in the calculations). In addition, we have obtained data on the electron–electron scattering in Pt in different structural states. Since platinum is one of the main thermometric metals, the influence of different kinds of structural defects on $\rho(T)$ is also of applied significance.

SAMPLES AND EXPERIMENTAL TECHNIQUES

We studied Pt samples in various structural states. For the material of purity 99.95 wt. % the total concentration of impurities with lower atomic masses than Pt (Si, Al, Fe, Sn, Sb) amounted to $\sim 1.1\times 10^{-3}$ at. %. The content of the impurities Au, Pb, Ir, Rh, and Pd, with atomic masses comparable to that of Pt, did not exceed $\sim 2.7\times 10^{-4}$ at. %. After annealing at 1800 K for 2 hours, the wire samples, with a diameter of 1.3 mm and an average grain size $\sim 1\ \mu$m, were deformed by twisting at 4.2 K. The degree of deformation and the deformation-related growth of the resistivity were $\gamma=0.082$ and $\Delta\rho_{4.2\ \mathrm{K}}=0.82\ \mathrm{n\Omega\cdot m}$. The structural state of the deformed sample was varied as a result of isochronal ($t=5$ min) annealing at 250 and 450 K. With allowance for the contribution to the resistivity from isolated dislocations ($\sim 9\times 10^{-19}\ \Omega\cdot\mathrm{cm}^3$; Ref. 20), the estimate of the average density of dislocations in the sample after deformation and the 450 K annealing was $3.2\times 10^{10}\ \mathrm{cm}^{-2}$.

Some of the samples of this degree of purity were heated to 1500 K by passage of a current and then quenched in water. According to Ref. 21, the concentration of vacancies in Pt near the melting temperature $T_m\cong 2040$ K is $C_0\approx 3\times 10^{-3}$. Then after quenching from $T_1\cong 1500$ K we have $C_1\approx C_0\exp[E_f(T_m^{-1}-T_1^{-1})]$. With an energy of vacancy formation $E_f\approx 1.4$ eV,[22] this gives $C_1\approx 2.4\times 10^{-4}$.

Data on the treatment regimes, structure factors, and the characteristics of $\rho(T)$ for the samples is given in Table I. Machine processing of the experimental $\rho(T)$ curves for varying values of Θ were done in the temperature interval 4.2–300 K by the least-squares method according to Refs. 4 and 8. The coefficients a, b, c [see Eq. (1)] and $d\rho/dT|_{T\geqslant\Theta}$ correspond to the value of Θ at the minimal rms error σ, which does not exceed 0.5%. Table I also gives the results of an analogous calculation for high-purity (99.998 wt. %) standard thermometric platinum from SST MPTSh-68 with a minimal content of the impurities indicated above.

TABLE I. Characteristics of the treatement, structural state, and parameters of the temperature dependence of $\rho(T)$ for platinum.

Sample	Treatment	Structural state	Θ, K	$\rho_0 \cdot 10^9$, $\Omega \cdot m$	$a_0 \cdot 10^{15}$, $\Omega \cdot m \cdot K^{-2}$	$b \cdot 10^9$, $\Omega \cdot m$	$c \cdot 10^9$, $\Omega \cdot m$	$d\rho/dT\|_{T \geq \Theta} \cdot 10^{11}$, $\Omega \cdot m \cdot K^{-1}$
Pt-1	SST MPTSh -68	99.998 wt.%	235.0	0.01	131	53.1	235	39.6
Pt-2	Annealing at 1800 K, $t = 2$ h	99.95 wt.%	240.0	1.39	117	78.0	190	38.7
Pt-3	Deformation at 4.2 K + annealing at 250 K	99.95 wt.%; dislocations + point defects	225.0	1.94	376	38.5	211	39.1
Pt-4	Deformation at 4,2 K + annealing at 450 K	99.95 wt.%; dislocations	227.5	1.68	348	44.0	204	39.1
Pt-5	Quenching from 1500 K	99.95 wt.%; vacancies	232.5	2.20	306	62.3	198	38.4

As compared to the Pt samples obtained from the fine-grain (2–3 μm) high-purity powder not containing impurities with a large magnetic moment (Fe, Mn), which had a superconducting transition temperature $T_c \approx (0.5-1.5) \times 10^{-3}$ K,[23] for the bulk samples one expects an even lower value of T_c. Experiments in this temperature region require special apparatus. Therefore, in this study the calculations of a number of the microscopic characteristics for all the structural states of platinum were carried out without using data on the superconductivity.

RESULTS AND DISCUSSION

Study of the $\rho(T)$ curves for Pt in different temperature intervals has been the subject of a number of papers.[2,7,24,25] In particular, it was shown in Ref. 24 that in the temperature interval 0.3–4 K for samples characterized by resistance ratios $R_{300\,K}/R_{0\,K} = 6000$ and 5000, the coefficient of T^2 equals $140 \times 10^{-15}\ \Omega \cdot m \cdot K^{-2}$. For platinum with $R_{300\,K}/R_{0\,K} \approx 2000$ the $\rho(T)$ data at temperatures in the helium region are described in Ref. 25 by the formula

$$\rho(T) = \rho_0 + aT^2 + cT^5,$$

where

$$\rho_0 = 5 \times 10^{-9}\ \Omega \cdot m, \quad a = 150 \times 10^{-15}\ \Omega \cdot m \cdot K^{-2},$$

$$c = 130 \times 10^{-18}\ \Omega \cdot m \cdot K^{-5}.$$

The values of the coefficient of T^2 in Refs. 24 and 25 agree with the characteristic of Pt-1 in Table I to an accuracy of $\sim 7-14\%$. In Ref. 7 for Pt with $R_{300\,K}/R_{0\,K} = 7192$ the experimental data obtained in the temperature interval $6\ K < T < 327$ K were processed using formula (1). The differences of the parameters given for that formula in Ref. 7 and those in Table I for Pt-1 are: $\Delta a/a = 7.2\%$, $\Delta b/b = 56\%$, $\Delta c/c = 8.5\%$, and $\Delta\theta/\theta = 16\%$. The value $\Theta = 234 \pm 1$ K obtained from measurement of the heat capacity[26] is practically the same as the characteristic of Pt-1 ($\Theta = 235$ K).

Using the known expressions relating the microscopic parameters characterizing the coefficient of the intensity of $s-s$ scattering,[2] one easily obtains the relation $c\Theta/z_s^{4/3} = \beta = \text{const}$, where z_s is the effective number of s electrons forming the band with a spherical sheet of the Fermi surface. To determine the parameter β in this relation, the values of c and Θ characterizing the sample of 99.998 wt. % purity were substituted in, along with the value of z_s corresponding to band calculations of the energy spectrum of platinum ($z_{s0} = 0.94$; Ref. 20). The values of z_s and $z_d = 10 - z_s$ (z_d is the effective number of d electrons) obtained for all the structural states of platinum in this approximation were used in the calculations of the effective microscopic parameters.

In the framework of the Friedel model of a two-band transition metal[19,20] the s electrons form a band of free electrons with an effective mass m_s^* and a density of states at the Fermi level $N_s(0) = 3n_0 z_s/2E_F$ (E_F is the Fermi energy, n_0 is the atomic concentration). The band of slow d electrons is characterized by a width W_d, an average energy E_d, and an energy-independent density of states $N_d(E) = 10 n_0 z_d / W_d$ in the interval $0.5W_d - (E_F - E_d) < E < 0.5W_d + (E_F - E_d)$. Since $z_s + z_d = 10$ for Pt, the values of E_F, E_d, and z_d will be related by the expression

$$E_F - E_d = 0.1 W_d (z_d - 5). \tag{2}$$

We assume $E_F = \text{const}$ for all the structural states, as is apparently justified by the small ($\sim 10^{-4}$) volume effect realized upon the introduction of the deformation and quenching defects in Pt-2 and by the slight difference of the concentrations of valence electrons of platinum with purities of 99.95 wt. % (Pt-2) and 99.998 wt. % (Pt-1). With the values $z_{d0} = 9.06$, $W_{d0} = 7$ eV, and $E_{d0} = 6.51$ eV,[20] Eq. (2) gives $E_F = 9.35$ eV.

Calculations of the effective microscopic parameters. In the case of small changes, Eq. (2) yields the following rela-

TABLE II. Influence of structural factors on the effective microscopic parameters of platinum.

Sample	z_s	z_d	E_d	W_d	Ω_p	$N_s(0)$	$N_d(E)$	$N(0)$	$\sqrt{\langle v_F^2 \rangle}$, 10^7 cm/s
			eV			states / eV · atom			
Pt-1	0.940	9.060	6.51	7.00	10.09	0.151	1.428	1.579	6.09
Pt-2	0.814	9.186	5.59	8.98	11.38	0.131	1.113	1.244	7.75
Pt-3	0.839	9.161	5.77	8.60	11.18	0.135	1.162	1.297	7.48
Pt-4	0.825	9.176	5.66	8.84	11.29	0.132	1.132	1.264	7.63
Pt-5	0.820	9.180	5.63	8.90	11.33	0.132	1.124	1.256	7.68

tion for the increments δE_d, δW_d, and δz_d to the quantities E_d, W_d, and z_d:

$$\frac{\delta E_d}{\delta z_d} = -(E_F - E_d)\left(\frac{1}{W_d}\frac{\delta W_d}{\delta z_d} + \frac{1}{z_d - 5}\right).$$

For an estimate of $\delta E_d/\delta z_d$ we used the values given above for the parameters E_{d0}, W_{d0}, E_F, and z_{d0} and also the estimate $\delta W_d/\delta z_d \approx 16.3$ eV.[1)] As a result, we have $\delta E_d/\delta z_d \approx -7.3$ eV. Estimates of the values of E_d for the different structural states of platinum are found from the relation $E_d \approx E_{d0} + \frac{\delta E_d}{\delta z_d}(z_d - z_{d0})$, where E_{d0} and z_{d0} characterize Pt-1. The values obtained for E_d are then used in estimating the other parameters of the Friedel model from the relations given above. The results of the calculations are presented in Table II. For the calculations of the FS-averaged values of the charge carrier velocity $\sqrt{\langle v_F^2 \rangle}$ and the plasma frequency Ω_p we used the relations $\Omega_p^2 \overline{\tau}/4\pi\hbar^2 = \rho^{-1}$ (Ref. 27) and $\Omega_p^2 = \frac{4}{3}\pi e^2 \hbar^2 \langle v_F^2 \rangle N(0)$ (Ref. 28). The average electron lifetime here is $\overline{\tau} = l_{\rm tr}/\sqrt{\langle v_F^2 \rangle}$ ($l_{\rm tr}$ is the transport mean free path). Estimates were made for the value $\langle \rho l_{\rm tr} \rangle \cong 2.94 \times 10^{-12}\ \Omega \cdot {\rm cm}^2$, which was obtained with the use of the values of $N(0)$ and Ω_p from Ref. 29. The results of the calculations of $\sqrt{\langle v_f^2 \rangle}$ and Ω_p are also given in Table II.

It follows from the data in Tables I and II that impurities, deformation defects, and quenching defects have a substantial influence on the complex of electrophysical characteristics of platinum. It is seen that they are influenced in the opposite way by impurities as compared to the lattice defects arising in deformation and quenching. Here the effects for all the characteristics (except E_d) are qualitatively similar to those established previously in studies of transition metals with the bcc lattice (Nb, Ta).[5]

Impurities. The main ($\sim$80%) impurities in Pt-2 as compared to Pt-1 are substitutional impurities with a concentration of $\sim 1.4 \times 10^{-3}$ at. % and having mass numbers less than (Sb, Sn) and much less than (Al, Si, Fe) that of platinum. In accordance with the existing ideas (see, e.g., Ref. 30), such impurities cause a deformation of the phonon spectrum which is manifested as an increase in the density of modes in the high-frequency region and also lead to the appearance of split-off discrete frequencies at a rather strong mass difference. Such a change in the vibrational spectrum is reflected in the experimentally registered increase in the Debye temperature of Pt-2, and it is qualitatively similar to effects observed in group V transition metals.[5] Pt-2 also contained impurities of the platinide series (Ir, Rh, Pd), Pb, and Au, with concentrations of $\sim 1.7 \times 10^{-4}$ at. %, $\sim 4.7 \times 10^{-5}$ at. %, and $\sim 5 \times 10^{-5}$ at. %, respectively. The contribution of these impurities to the change in the phonon spectrum is insignificant.

The electronic structures of pure platinum and of the main impurities in Pt-2 are substantially different, and that makes for a local redistribution of the electrons both directly around the substituent atoms in the occupied sites of the fcc lattice and near the neighboring host atoms. We know of no concrete theoretical calculations on this matter. However, by analogy with the results on the electronic structure of group V transition metals containing impurities (Ref. 5 and references cited therein) it can be assumed that the lowering of $N(0)$ and the widening of the d band in Pt-2 in comparison with Pt-1 is due to the transition of a fraction of the electrons from the d and s bands of platinum to hybrid states far from the Fermi level, which are formed with the participation of electrons of the impurity atoms; this is accompanied by enhancement of the lattice stiffness. This redistribution of electrons is especially effective for impurities with which platinum forms intermetallic compounds. Such an effect gives a larger contribution to the change of the parameters of the energy spectrum than does the decrease of the average electron density as a consequence of the lower valence of the main impurity atoms as compared to that of platinum.

Quenching defects. The appearance of quenching vacancies leads to a complex change of the positions of the neighboring atoms, interatomic bonds, local electron density, and electron momentum distribution. It has been shown in the theoretical papers[31–33] that for transition metals with different types of crystal lattices there is characteristically a significant softening of the vibrational spectrum for the nearest neighbors to an unfilled site, and a broad resonance peak appears in the low-frequency region. Here, according to Ref. 31, the form of the spectral function $g_0(\omega)$ has a substantial influence on both the atomic relaxation and the d-band narrowing due to the vacancy. These results correspond qualitatively to the data for Pt-5, which contains quenching vacancies.

Deformation defects. The characteristic defects for Pt-3 are dislocations and defects of the vacancy type in the form of complexes with impurity atoms, formed after a 250 K annealing of a sample deformed at 4.2 K. Annealing at 450 K causes defects of the vacancy type to go to sinks. As a result, the main defects in Pt-4 will be dislocations. A comparison

of the characteristics of Pt-3 and Pt-4 in Table II shows that they are consistent with the above interpretation of the influence of vacancies on the parameters of the electron and phonon spectra.

According to Ref. 5, the change of the transport and microscopic characteristics of Nb containing dislocations is due to the discontinuity of the directional interatomic bonds in the region of the dislocation core and to a change of the characteristic of the overlap of the d-type wave functions of the neighboring atoms. This leads to an increase in the density of states at the Fermi level and to a narrowing of the d band and is accompanied by softening of the phonon spectrum and enhancement of the electron–phonon interaction. A comparison of the results of Ref. 5 and those of the present study shows that the regularities established for the bcc transition metal Nb are qualitatively reflected in the results describing the analogous parameters of platinum—a transition metal with an fcc lattice.

Electron–electron scattering. For transition metals the resistivity contribution quadratic in the temperature is due to scattering of the high-velocity s electrons by the heavier d electrons.[34] Furthermore, for pure transition metals such a dependence can be due to the scattering of electrons on spin fluctuations.[35,36] The results of studies of high-purity single-crystal Pd in Ref. 37, where the presence of a low-temperature component in $\rho(T)$ due to spin fluctuations was not ruled out, indicate that the contribution proportional to T^2 is sharply attenuated for $T>25$ K. According to the results of the studies reported here, for Pt the component $\rho\sim T^2$ is manifested at temperatures ranging from helium to room temperatures. If it is assumed that it is due to the scattering of electrons on spin fluctuations, then such a process presupposes a substantially higher boundary temperature for spin fluctuations in platinum. This is clearly unlikely, since the spin paramagnetism of the d electrons in Pt is considerably weaker than in Pd.[2]

In Ref. 38 an expression for the electron–electron scattering due to the combination of the Coulomb interaction and the exchange of virtual phonons was obtained in the quasiparticle damping rate formalism, and a formula for estimating the coefficient of T^2 was obtained in the form

$$a=\frac{4\pi(1+\lambda)\kappa\alpha}{\Omega_p^2}, \tag{3}$$

where Ω_p is the plasma frequency, λ is the electron–phonon coupling constant, κ is a coefficient which takes into account the fraction of umklapp scattering, and $\alpha=8\pi/3(\lambda/1+\lambda)^2\gamma_{\rm el}$ is the rate coefficient for electron–electron scattering due to phonons. Here $\gamma_{\rm el}=2\pi^2N(0)\times(1+\lambda)k_B^2/3n_0$ is the coefficient of electronic heat capacity. An estimate of $a_{\rm th}\approx 160\kappa\cdot 10^{-15}\ \Omega\cdot{\rm m}\cdot{\rm K}^{-2}$ for Pt-1 according to formula (3) was obtained with the use of the values of $N(0)$ and Ω_p from Table II and the value $\lambda=0.6$ from Ref. 39. If it is assumed that the value of κ for platinum lies in the interval 0.04 to 0.6, which characterize a number of transition metals (Mo, W, Nb, and Re),[38] then one can say that there is qualitative agreement between $a_{\rm exp}=117\times 10^{-15}\ \Omega\cdot{\rm m}\cdot{\rm K}^{-2}$ (Table I) and $a_{\rm th}$ for the minimum value of κ, and $\sim$80% agreement for the maximum value. The substantial (by a factor of $\sim$2.2–1.6) enhancement of the intensity of electron–electron scattering in platinum containing deformation and quenching defects (see Table I) can be linked in the model of Ref. 38 not only to a decrease of Ω_p and growth of $N(0)$ (see Table II) but also to an increase of κ. The latter may reflect, in particular, an enhancement of the anisotropy of the FS and a change in the relation between relaxation times for electron–electron scattering with and without umklapp on account of the regions near the dislocation cores and vacant sites of the crystal lattice.

CONCLUSION

The research reported in this paper combines an experimental study and model calculations of a complex of electrophysical and effective microscopic characteristics of platinum—a group VIII transition metal. The following results were obtained:

1. We investigated how the degree of purity of the platinum and the presence of deformation and quenching defects affect the temperature dependence of the resistivity $\rho(T)$ in the temperature interval 4.2 K$\leqslant T\leqslant$300 K. The experimental data are described to a high degree of accuracy in the framework of the Wilson–Mott model of a two-band transition metal with the electron–electron Coulomb scattering and the inter- and intraband electron–phonon scattering taken into account.

2. For all the structural states of platinum we determined the plasma frequency and charge carrier velocity averaged over the Fermi surface and the band parameters corresponding to the Friedel model of a two-band transition metal (the width and average energy of the d band, the relationship between the numbers of d and s electrons, and the density of states at the Fermi level in each of the bands).

3. The presence of deformation and quenching defects led to qualitatively similar effects: a lowering of the Debye temperature, a weakening of the intraband and enhancement of the intraband electron–phonon scattering, and intensification of the electron–electron Coulomb scattering. In the framework of the Friedel model this corresponds to a narrowing of the d band and an increase of its average energy, a decrease in the number of d electrons, and growth of the density of states in each of the bands. The FS-averaged values of the Fermi velocity and plasma frequency decrease. Substitutional impurities lead to effects of the opposite sign (except for the changes in ρ_0).

4. We have found that the investigated complex of electrophysical and effective microscopic parameters of platinum is influenced in opposite ways by impurities and by lattice defects arising on deformation (dislocations, complexes of point defects) and quenching (vacancies); this result is qualitatively similar to the effects studied previously in transition metals with the bcc lattice (Nb, Ta). Obviously, light impurities with fewer valence electrons than platinum has will cause an effective increase in the density of high-frequency phonon modes and lead to the formation of hybrid bound states lying below the Fermi level, and a portion of the valence electrons of the host crystal will transition into these states. This results in an increase in the lattice stiffness, a widening of the d band, and a decrease in the density of states at the Fermi level. The introduction of linear defects and vacancies in Pt typically causes distension of the lattice

and gives rise to local breaking of the interatomic bonds; this is accompanied by a change in the degree of overlap of the d-type wave functions of neighboring atoms. This causes softening of the phonon spectrum, narrowing of the band, and an increase in the density of states at the Fermi level.

5. The electron–electron Coulomb interaction, which involves the exchange of virtual phonons, is a possible cause of a contribution to $\rho(T)$ which is quadratic in temperature in the different structural states. To refine this idea will require data on the relationship between the normal and umklapp scattering processes.

*E-mail: vsokol@kipt.kharkov.ua
**E-mail: Boris.A.Merisov@univer.kharkov.ua

[1)]This estimate of $\delta W_d/\delta z_d \approx \Delta W_d/\Delta z_d$ was obtained from Ref. 5 and is averaged for Nb and Ta, which represent the $4d$ and $5d$ series of transition metals. The difference between the changes of W_d upon the small changes of z_d corresponding to the introduction of impurities and deformation defects is $\sim 15\%$. This attests to the insignificant changes of $\delta W_d/\delta z_d$ in the $4d$ and $5d$ series in the framework of the Friedel model and makes it possible to use the indicated value of $\delta W_d/\delta z_d$ for estimating the parameters of the energy spectrum of the $5d$ transition metal platinum.

[1] J. M. Ziman, *Electrons and Ions*, Clarendon Press, Oxford (1960), IL, Moscow (1962).
[2] M. L. Cohen, in *Superconductivity*, R. D. Parks (ed.), Dekker, New York (1969), Chapter 12, p. 615; G. Gladston, M. A. Jensen, and J. R. Schrieffer, *ibid.*, Chapter 13, p. 665 [Russian translation: *Superconductivity of Semiconductors and Transistion Metals*, Mir, Moscow (1972)].
[3] P. B. Allen, T. P. Beaulac, F. S. Khan, W. H. Butler, F. J. Pinski, and J. C. Swihard, Phys. Rev. B **34**, 4331 (1986).
[4] P. Haen and J. Teixeira, Rev. Phys. Appl. **9**, 879 (1974).
[5] V. I. Sokolenko, Ya. D. Starodubov, B. A. Merisov, and G. Ya. Khadzhay, Fiz. Nizk. Temp. **27**, 471 (2001) [Low Temp. Phys. **27**, 345 (2001)].
[6] C. L. Tsai, R. L. Fagaly, H. Weinstock, and F. A. Schmidt, Phys. Rev. B **23**, 6430 (1981).
[7] D. B. Poker and C. E. Klabunde, Phys. Rev. B **26**, 7012 (1982).
[8] V. I. Khotkevich, B. A. Merisov, A. M. Ermolaev, and A. V. Krasnokutskii, Fiz. Nizk. Temp. **9**, 1056 (1983) [Sov. J. Low Temp. Phys. **9**, 546 (1983)].
[9] L. Colquitt, J. Appl. Phys. **36**, 2454 (1965).
[10] F. J. Pinski, P. B. Allen, and W. H. Butler, Phys. Rev. Lett. **41**, 431 (1978).
[11] P. B. Allen, Phys. Rev. B **17**, 3725 (1978).
[12] F. J. Pinski, P. B. Allen, and W. H. Butler, Phys. Rev. B **23**, 5080 (1981).
[13] Y. Nakagava, A. D. B. Woods, Phys. Rev. Lett. **11**, 271 (1963).
[14] N. B. Brandt and S. M. Chudinov, *Experimental Methods of Studying Energy Spectra of Electrons and Phonons in Metals* [in Russian], Mir, Moscow (1983).
[15] O. A. Anderson and A. R. Mackintosh, Solid State Commun. **6**, 285 (1968).
[16] V. V. Nemoshkalenko, A. V. Zhalko-Titarenko, and V. N. Antonov, Metallofiz. **5**, 18 (1983).
[17] L. F. Mattheiss and L. R. Testardi, Phys. Rev. B **20**, 2196 (1979).
[18] J. Friedel, in *The Physics of Metals*, J. M. Ziman (ed.), Cambridge University Press (1969), pp. 340–408, Mir, Moscow (1972), p. 375.
[19] W. A. Harrison, *Electronic Strugure and the Physics of Solids: The Physics of the Chemical Bond*, Freeman, San Francisco (1980), Mir, Moscow (1983), Vol. 2.
[20] A. S. Karolik and A. A. Luchvich, J. Phys.: Condens. Matter **6**, 837 (1994).
[21] V. A. Pervakov, Metallofizika (Kiev) **30**, 5 (1970).
[22] J. I. Takamura, ''Point defects,'' in *Physical Metallurgy*, R. W. Cahn (ed.), North-Holland, Amsterdam; Wiley, New York (1965), Mir, Moscow (1968), No. 3, p. 85.
[23] A. Schindler, R. Ktsnig, and T. Herrmannsdtsrfer, Physica B **280**, 247 (2000).
[24] C. Uher, Chi-Wai Lee, and J. Bass, Phys. Rev. Lett. **61A**, 344 (1977).
[25] E. K. Azarbar and G. Williams, Phys. Rev. B **14**, 3301 (1976).
[26] K. A. Gschneidner, ''Physical properties and interrelationships of metallic and semimetallic elements,'' in *Solid State Physics*, Vol. 16, F. Seits and D. Turnbull (eds.), Academic Press, New York and London (1964), p. 276.
[27] B. Chakraborty, W. E. Pickett, and P. B. Allen, Phys. Rev. B **12**, 905 (1975).
[28] M. H. Cohen, Philos. Mag. **3**, 762 (1958).
[29] P. B. Allen, Phys. Rev. B **36**, 2920 (1987).
[30] V. A. Pervakov, *Thermophysical Properties of Metals with Crystal Lattice Defects at Low Temperatures* [in Russian], Osnova, Kharkov (1990).
[31] K. Masuda, in *Proceedings of the Yamada Conference V*, Kyoto, November 16–20, 1981; publ. Tokyo (1982), p. 130.
[32] R. Yamamoto, in *Proceedings of the Yamada Conference V*, Kyoto, November 16–20, 1981; publ. Tokyo (1982), p. 120.
[33] A. Suzuki, R. R. Yamamoto, and M. Doyama, in *Proceedings of the Yamada Conference V, Kyoto, November 16–20, 1981*; publ. Tokyo (1982), p. 126.
[34] F. J. Blatt, *Physics of Electronic Conduction in Solids*, McGraw-Hill, New York (1968), Mir, Moscow (1971).
[35] D. L. Villss and P. Lederer, J. Phys. Chem. Solids **27**, 1805 (1966).
[36] A. I. Shindler and M. J. Rice, Phys. Rev. **164**, 759 (1967).
[37] J. J. Vuillemin and A. Khellaf, J. Appl. Phys. A **69**, 4466 (1991).
[38] K. Schwartzman and W. E. Lawrence, Phys. Rev. B **48**, 14089 (1993).
[39] W. John, in *Ergebnisse in der Elektronentheorie der Metalle*, Vol. 2, P. Ziesche and G. Lehmann, eds., Akademie-Verlag, Berlin (1983), Mir, Moscow (1984).

Translated by Steve Torstveit

Magnetoresistance of tetrathiafulvalene-based organic conductors

H. R. Atalla*

V. N. Karazin Kharkov National University, pl. Svobody 4, 61077 Kharkov, Ukraine
(Submitted February 18, 2003)
Fiz. Nizk. Temp. **29**, 793–796 (July 2003)

It is shown that by studying the angular oscillations of the magnetoresistance of layered conductors, one can determine the character of the falloff of the harmonics as a function of the charge carrier energy from the momentum projection on the normal to the layers. © *2003 American Institute of Physics.* [DOI: 10.1063/1.1596586]

A considerable fraction of charge-transfer complexes of organic origin have a layered structure with a marked anisotropy of the electrical conductivity. Among them is the large family of tetrathiafulvalene salts with a metallic type of electrical conductivity not only along the layers but also across them. In layered conductors the charge carrier energy $\varepsilon = \varepsilon(\mathbf{p})$ depends weakly on the momentum projection $p_z = \mathbf{n}\cdot\mathbf{p}$ onto the normal $\mathbf{n}$ to the layers, so that the maximum value of the velocity v_z of the conduction electrons (equal to ηv_F, where η is the quasi-two-dimensionality parameter) is much less than the Fermi velocity for electron motion in the plane of the layers, v_F.

Because of the quasi-two-dimensional character of the electron energy spectrum in layered conductors, quantum oscillation effects are most clearly manifested in them, since almost all of the charge carriers with the Fermi energy ε_F are involved in their formation. In 1988, Shubnikov–de Haas oscillations of the magnetoresistance were observed[1,2] in the organic conductor $(BEDT–TTF)_2IBr_2$, and subsequently quantum oscillation effects have been observed in practically all tetrathiafulvalene-based organic complexes (see, e.g., the review articles cited as Refs. 3 and 4). The Fermi surface $\varepsilon(\mathbf{p}) = \varepsilon_F$ of layered conductors is open, with a slight corrugation along the p_z axis, and the fact that the Shubnikov–de Haas effect is observed in tetrathiafulvalene salts attests that at least one sheet of the Fermi surface is a slightly corrugated cylinder.

Over the last 15 years there has been active study of another effect in organic charge-transfer complexes of the type $(BEDT–TTF)_2X$ with different radicals X: the resistivity ρ for a current directed perpendicular to the layers has sharp peaks as a function of the angle θ between the normal $\mathbf{n}$ to the layers and the direction of a high magnetic field $\mathbf{H} = (0, H\sin\theta, H\cos\theta)$ strong enough that frequency of gyration Ω of the conduction electrons is much higher than their collision frequency $1/\tau$. This orientation effect, which is specific to quasi-two-dimensional conductors, contains extremely important information about the shape of the Fermi surface—the distance between the sharp peaks of the function $\rho(\theta)$ is directly related to the diameters of a Fermi surface having the form of a slightly corrugated cylinder.[5,6] The amplitude of the Shubnikov–de Haas oscillations, like the part of the magnetoresistance $\rho(\theta)$ which varies monotonically with H, has sharp peaks as a function of θ, but their positions need not coincide write maxima of $\rho(\theta)$. The differences contain information about the relation between the harmonics of the periodic dependence of the energy of the conduction electrons on the quasimomentum projection p_z (Refs. 7 and 8):

$$\varepsilon(\mathbf{p}) = \sum_{n=0}^{\infty} \varepsilon_n(p_x, p_y)\cos\left\{\frac{anp_z}{\hbar} + \alpha_n(p_x, p_y)\right\}, \tag{1}$$

$$\varepsilon_n(-p_x, -p_y) = \varepsilon_n(p_x, p_y),$$

$$\alpha_n(p_x, p_y) = -\alpha_n(-p_x, -p_y).$$

Here a is the distance between layers, $\hbar$ is Planck's constant, and the function $\varepsilon_n(p_x, p_y)$ falls off with increasing index n, so that the maximum value of the function $\{\varepsilon(\mathbf{p}) - \varepsilon_0(p_x, p_y)\}$, which is equal to $\eta\varepsilon_F$ on the Fermi surface, is much smaller than the Fermi energy ε_F.

The results of experimental studies of the dependence of the magnetoresistance on the angle θ are often interpreted using an extremely primitive model for the dispersion relation of the charge carriers:

$$\varepsilon(\mathbf{p}) = (p_x^2 + p_y^2)/2m - (\eta v_F\hbar/a)\cos(ap_z/\hbar). \tag{2}$$

In the case of a Fermi surface in the form of a slightly corrugated cylinder, the conduction electrons do not leave the unit cell in the plane $p_x p_y$, and the explicit form of the functions $\varepsilon_n(p_x, p_y)$ does not play an essential role in the analysis of the experimental results; however, keeping only the first harmonic in the expression for the dependence of the energy on p_z leads to a fundamental disagreement between the theoretical calculations and the experimentally observed angle dependence $\rho(\theta)$. Calculation of the magnetoresistance for a current transverse to the layers with the use of a dispersion relation of the charge carriers in the form (2) leads to a significant growth of the resistance peaks with increasing H for $\eta \ll \eta\Omega\tau \ll 1$. However, the experimentally observed height of the resistance peaks is of the same order of magnitude as the part of the magnetoresistance that varies smoothly with θ.

In the flow of current perpendicular to the layers the electric field in the conductor is almost parallel to the current, and the resistance in the leading approximation in the parameter $\eta \ll 1$ is inversely proportional to the σ_{zz} component of the conductivity tensor. Such a weak manifestation of the Hall effect is due to the slow drift of the charge carriers along the normal to the layers. Using the solution of the kinetic equation for the distribution function of the charge carriers, one can easily obtain an asymptotic expression for σ_{zz} at $\eta \ll 1$ and $\gamma = 1/\Omega\tau \ll 1$:

$$\sigma_{zz}=\frac{ae^2\tau m^*\cos\theta}{\pi\hbar^4}\times\sum_{n=1}^{\infty}\left\{\frac{1}{T}\int_0^T dt\,\varepsilon_n\left|p_x(t),p_y(t)\right|\cos\left(\frac{anp_y(t)\tan\theta}{\hbar}\right)\right\}^2, \tag{3}$$

where e and m^* are the charge and cyclotron effective mass of the conduction electrons, t is the time of motion of the charge in the magnetic fields along an electron orbit $\varepsilon=\text{const}$, $p_H=\mathbf{p}\cdot\mathbf{H}/H$ with a period $T=2\pi m^*c/eH$.

The integrands in formula (3) for $\tan\theta\gg1$ are rapidly oscillating functions, and the integrals in the sum over n are easily calculated by the stationary phase method. If there are only two stationary-phase points, at which v_x vanishes, on the electron orbit, the asymptotic expression for σ_{zz} takes the following form:

$$\sigma_{zz}=\frac{ae^2\tau m^*\cos\theta}{\pi\hbar^4}\sum_{n=1}^{\infty}n^2A_n^2I_n^2(\theta)+\eta^2\sigma_0(\eta^2\varphi_1+\gamma^2\varphi_2), \tag{4}$$

where A_n is the value of the function $\varepsilon_n(p_x,p_y)$ at the stationary-phase points, σ_0 is the conductivity along the layers in the absence of magnetic field, φ_1 and φ_2 are of the order of unity, and the function

$$I_n(\theta)=(\hbar/anD_p\tan\theta)^{1/2}\,2\cos\{(anD_p\tan(\theta/2\hbar))-\pi/4\} \tag{5}$$

has a set of zeros which repeat with period $\Delta(\tan\theta)=2\pi\hbar/naD_p$. Here D_p is the diameter of the Fermi surface along the p_y axis, and with increasing θ the cyclotron effective mass of the charge carriers varies in inverse proportion to $\cos\theta$.

It is natural to assume that the function $\varepsilon_n(p_x,p_y)$ falls off with increasing n, and the number of terms that must be retained in the sum over n in the asymptotic expansion of σ_{zz} in powers of the small parameters η and γ depends on the character of the decay of these functions. Formula (4) contains small corrections to the asymptotics of σ_{zz} for $\eta\ll1$ and $\gamma\ll1$; it is extremely important to take these into account if the functions $I_n(\theta)$ for $n\geqslant2$ have negligibly small values. In such a case at the values $\theta=\theta_c$ where $I_1(\theta)$ vanishes, the resistance to a current along the normal to the layers does not go to saturation in high magnetic fields but increases in proportion to H^2 for $\eta\ll\gamma\ll1$, and saturation of the resistance sets in at higher magnetic fields, when $\gamma\leqslant\eta$. In the case of a slow decay of the functions $\varepsilon_n(p_x,p_y)$ with increasing index n it is sufficient to keep only the sum over n in Eq. (4) in the asymptotic expression for σ_{zz}, since all of the $I_n(\theta)$ cannot vanish simultaneously.

We shall analyze the known experimental results on the θ dependence of the magnetoresistance of tetrathiafulvalene salts, keeping only three terms in the sum over n in the asymptotic expansion of σ_{zz}. If $\varepsilon_0(p_x,p_y)$ is a quadratic function of the momenta, then all of the $I_n(\theta)$ are Bessel functions, and the A_n are functions of $\varepsilon_n\{p_x(t),p_y(t)\}$, which were taken out from under the integral over t in Eq. (3) in the mean-value sense. The presence of the three free parameters A_1, A_2, and A_3, which are to be determined using the experimentally observed dependence $\rho(\theta)$, makes it possible to match the theoretical calculations with experiment and to determine the character of the decay of the functions $\varepsilon_n(p_x,p_y)$.

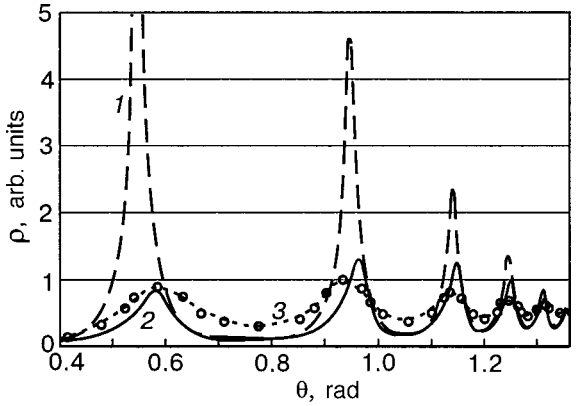

FIG. 1. Position of the maxima of the resistivity as a function of the angle between the normal to the layers and the magnetic field direction for different ratios of the parameters: $A_{n+1}/A_n=0.04$ (*1*), $A_{n+1}/A_n=0.4$ (*2*); the experimental curve *3* is $\rho(\theta)$ for $(\text{BEDT–TTF})_2\text{IBr}_x$ from Ref. 2.

For this purpose in Fig. 1 the experimental data taken from Ref. 2 for the positions of the maxima of the resistivity as functions of the angle θ (curve *3*) for $(\text{BEDT–TTF})_2\text{IBr}_2$ are compared with the theoretical calculations of the function $\rho(\theta)$ for two different ratios of the parameters A_n. As we see from Fig. 1, for curve *1*, where $A_{n+1}/N_n=0.04$, a significant growth of the maxima is observed, unlike the case of curve *2*, for $A_{n+1}/A_n=0.4$, where the height of the maxima is of the same order of magnitude as in the experimental data. In Fig. 2 the calculated curves of the function $\rho(\tan\theta)$ are compared with the experimental data given in Refs. 9 and 10, where the ratios of the parameters are equal to 0.2 for θ-$(\text{BEDT–TTF})_2\text{I}_3$ (Fig. 2a) and 0.1 for $(\text{BEDT–TTF})_2\text{Br(DIA)}$ (DIA is diiodoacetylene) (Fig. 2b). As is seen in the figures, the calculated curves are extremely close to the experimental curves if the ratio of the harmonics A_{n+1}/A_n is large enough. At lower values of this ratio a noticeable disagreement is observed, and it therefore would appear to be incorrect to use an electron dispersion relation of the form (2) for interpreting the experimental data.

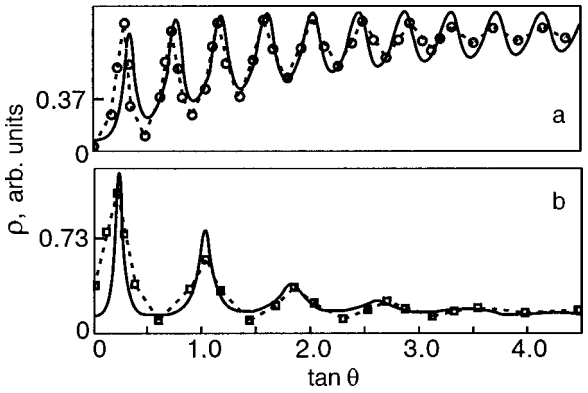

FIG. 2. Position of the resistivity maxima as a function of the tangent of the angle θ between the normal to the layers and the magnetic field direction for different ratios of the parameters: calculation for $A_{n+1}/A_n=0.2$ and the points for θ-$(\text{BEDT–TTF})_2\text{I}_3$ (a); calculation for $A_{n+1}/A_n=0.1$ and points for $(\text{BEDT–TTF})_2\text{Br(DIA)}$ (b). The experimental data are from Refs. 9 and 10.

Thus the experimental study of the angular oscillations of the magnetoresistance of organic layered conductors of the type $(BEDT–TTF)_2X$ indicates that the function $\varepsilon_n(p_x p_y)$ falls off comparatively slowly with increasing n. By analyzing the asymptotic behavior of the magnetoresistance of tetrathiafulvalene-based organic complexes at high magnetic fields for different orientations of the field relative to the layers, one can determine the ratio of the harmonics in the dependence of the energy on the momentum projection on the normal to the layers to a high degree of accuracy.

*E-mail: raed@bigline.kharkov.ua

[1] M. V. Kartsovnik, V. N. Laukhin, V. I. Nizhankovskiĭ, and A. A. Ignat'ev, JETP Lett. **47**, 363 (1988).
[2] M. V. Kartsovnik, P. A. Kononovich, V. N. Laukhin, and I. V. Shchegolev, JETP Lett. **48**, 541 (1988).
[3] J. Wosnitza, in *Fermi Surfaces of Low-Dimensional Organic Metals and Superconductors*, Springer Tracts in Modern Physics (1996), p. 165.
[4] J. Singleton, ''Studies of quasi-two-dimensional organic conductors based on BEDT-TTF using high magnetic fields,'' Rep. Prog. Phys. **63**, 1111–1207 (August 2000), p. 1116.
[5] V. G. Peschansky, J. A. Roldan Lopez, and Toji Gnado Yao, J. Phys. I **1**, 1469 (1991).
[6] V. G. Peschansky, Phys. Rep. **288**, 305 (1997).
[7] V. G. Peschansky and R. Atalla, Fiz. Nizk. Temp. **27**, 945 (2001) [Low Temp. Phys. **27**, 1018 (2001)].
[8] V. G. Peschanskiĭ, Zh. Éksp. Teor. Fiz. **121**, 1205 (2002) [JETP **94**, 1035 (2002)].
[9] T. Terashima, S. Uji, H. Aoki, M. Tamura, M. Kinoshita, and M. Tokumoto, Synth. Met. **70**, 845 (1995).
[10] S. Uji, C. Terakura, T. Terashima, H. Aoki, H. Yamamoto, J. Yamaura, and R. Kato, *Fourth International Symposium on Advances in the Physics of Fields: Quantum Phenomena in Advanced Materials at High Magnetic Fields* (1998), p. 299.

Translated by Steve Torstveit

LOW-DIMENSIONAL AND DISORDERED SYSTEMS

Intrasubband plasmons in a weakly disordered array of quantum wires

Y. V. Bludov*

A. Usikov Institute for Radiophysics and Electronics, of the National Academy of Sciences of Ukraine
12 Acad. Proscura Str., Kharkov 61085, Ukraine
(Submitted August 16, 2002; revised February 4, 2003)
Fiz. Nizk. Temp. **29**, 797–803 (July 2003)

A theoretical investigation is carried out for plasmons in a weakly disordered array of quantum wires, consisting of a finite number of quantum wires arranged at an equal distance from each other. The array of quantum wires is characterized by the fact that the density of electrons of one ''defect'' quantum wire was different from that of the other quantum wires. It is assumed that the defect quantum wire can be arranged at an arbitrary position in the array. The existence of a local plasmon mode, whose properties differ from those of usual modes, is found. It is pointed out that the local plasmon mode spectrum is slightly sensitive to the position of the defect quantum wire in the array. At the same time the spectrum of usual plasmon modes is shown to be very sensitive to the position of the defect quantum wire. © *2003 American Institute of Physics.* [DOI: 10.1063/1.1596592]

1. INTRODUCTION

Quasi-one-dimensional electron systems (1DESs) or quantum wires (QWs) are artificial structures in which the motion of charge carriers is confined in two transverse directions but is essentially free (in the effective-mass sense) in the longitudinal direction.[1–3] Usually QWs are produced by adding an additional one-dimensional confinement to a two-dimensional electron system (2DES). This additional confinement is, in general, weaker than the strong confinement of the original 2DES.[4] One of the motivations for studying QWs is the fact that the charge-carrier mobility is higher than in the 2DESs on which they are built. The reason for this is that the impurity content and distribution around QWs can be selectively controlled, producing enhanced mobility.[5]

Collective charge-density excitations, or plasmons, in QWs are objects of physicists' great interest. Plasmons in QW have been investigated previously both theoretically[5–9] and experimentally.[10–12] In those papers it was shown that plasmons in QWs possess some unusual new dispersion properties. First, the plasmon spectrum depends strongly on the width of the QW. Second, 1D plasmons are free of Landau damping[6,9] in the whole range of wave vectors.

From the point of view of practical application the objects of interest are the so-called weakly disordered arrays of low-dimensional systems. Recently the plasmons in weakly disordered superlattices, formed of a finite number of equally spaced two-dimensional electron systems, have been investigated theoretically.[13–16] The weakly disordered superlattice is characterized by the fact that all 2DESs possess equal electron densities except one (''defect'') 2DES, whose electron density differs from that of the other 2DESs. It was found that the plasmon spectrum of such a superlattice contains a local plasmon mode, whose properties differ from those of other plasmon modes. The existence of a local plasmon mode is completely analogous to the existence of the local phonon mode, first obtained by Lifshitz in 1947 for the problem of the phonon modes in a regular crystal containing a single isotopic impurity.[17] Notice that practically all the electromagnetic energy flux of plasmons corresponding to the local mode is concentrated in the vicinity of the defect 2DES. At the same time, the opportunity of using the peculiarities of the plasmon spectrum to determine the parameters of defects in a superlattice was pointed out in Ref. 16.

This paper deals with the theoretical investigation of plasmons in a finite weakly disordered array of QWs, containing one defect QW whose one-dimensional density of electrons differs from that of the other QWs. We suppose that the defect QW can occupy an arbitrary position in the array. We show that the plasmon spectrum in the weakly disordered array of QWs is characterized by the existence of a local plasmon mode whose electromagnetic field is localized in the region of the defect QW. We find that the position of the defect QW in the array does not affect strongly the spectrum of the local plasmon mode but it exerts a significant influence on the spectrum of other plasmon modes. At the same time, when the defect QW is arranged inside the array, the plasmon spectrum contains modes whose dispersion properties do not depend on the value of the electron density in the defect QW.

This paper is organized as follows. In Sec. 2 we derive the dispersion relation for plasmons in a weakly disordered array of QWs. In Sec. 3 we present the results of a numerical solution of the dispersion relation and discuss the dispersion properties of plasmons in a weakly disordered array of QWs. We conclude the paper with a brief summary of results and possible applications (Sec. 4).

2. DISPERSION RELATION

We consider a weakly disordered array of QWs consisting of a finite number M of QWs, arranged at planes $z=ld$

($l=0,...,M-1$ is the number of QW, d is the distance between adjacent QWs). We suppose that all QWs possess equal 1D electron densities N except one defect QW whose electron density is equal to N_d. So, the density of electrons in the lth QW can be expressed as $N_l=(N_d-N)\delta_{pl}+N$. Here p is the number of the defect QW situated at the plane $z=pd$, and δ_{pl} is the Kronecker delta. The QWs are considered to be placed in a uniform dielectric medium with dielectric constant ε. We use such a simple model (in which the dielectric constants of the media inside and outside the array are equal) to avoid the appearance of a surface plasmon mode. We consider the motion of electrons to be free in the x direction and considerably confined in the directions y and z. At the same time we suppose that the width of all QWs is equal to a in the y direction and equal to zero in the z direction.

In other words, each QW can be represented as a square quantum well with infinite barriers at $y=-a/2$ and $y=a/2$ and a zero thickness in the z direction. Meanwhile we take into account only the lowest subband in each QW. In that case the single-particle wave function for the electron can be written in the form:

$$\psi_{k_x,l}(x,y,z)=|k_x,l\rangle=\exp(ik_x x)\varphi(y)[\delta(z-ld)]^{1/2}, \quad (1)$$

where $\varphi(y)=\sqrt{2/a}\cos\pi y/a$, and k_x is the one-dimensional wave vector describing the motion in the x direction. In that case the single-particle energy can be written as follows:

$$E_{k_x,l}=E_0+\frac{\hbar^2 k_x^2}{2m^*}.$$

Here E_0 is the energy of the subband bottom (for simplicity we may put $E_0=0$), and m^* is the effective mass of the electron.

To obtain the spectrum of collective excitations we start with a standard linear-response theory in a random phase approximation. To obtain the collective excitation spectrum we consider $\delta n(\mathbf{r})$, which is the deviation of the electron density from its equilibrium value. After using the standard linear-response theory and the random phase approximation, $\delta n(\mathbf{r})$ can be related to the perturbation as

$$\delta n(x,y,z)=\sum_{\alpha,\alpha'}\frac{f_{\alpha'}-f_\alpha}{E_{\alpha'}-E_\alpha+\hbar\omega}V_{\alpha\alpha'}\psi^*_{\alpha'}\psi_\alpha, \quad (2)$$

where $\alpha=(k_x,l)$ is a composite index which is defined by (1), f_α is the Fermi distribution function. $V_{\alpha,\alpha'}=\langle\alpha|V|\alpha'\rangle$ are the matrix elements of the perturbing potential $V=V^{\rm ex}+V^H$, and $V^{\rm ex}$ and V^H are the external and Hartree potentials, respectively.

For our system Eq. (2) can be rewritten in the form

$$\delta n(q_x,y,z)=\sum_{l'}\Pi^{l'}V^2_{l'\varphi}(y)\delta(z-l'd), \quad (3)$$

where

$$\Pi^{l'}=\frac{1}{\pi}\int_{-\infty}^{\infty}dk_x\frac{f_{k_x+q_{x,l'}}-f_{k_{x,l'}}}{E_{k_x+q_{x,l'}}-E_{k_{x,l'}}+\hbar\omega}$$

is the noninteracting 1D polarizability (''bare bubble'') function, and $V_{l'}\equiv\langle k_x,l'|V|k_x+q_x,l'\rangle$. At zero temperature the function Π^l can be written as

$$\Pi^l=\frac{m^*}{q_x\pi\hbar^2}\ln\frac{\omega^2-\left(\frac{\hbar q_x k_F^l}{m^*}-\frac{\hbar q_x^2}{2m^*}\right)^2}{\omega^2-\left(\frac{\hbar q_x k_F^l}{m^*}-\frac{\hbar q_x^2}{2m^*}\right)^2}. \quad (4)$$

Here $k_F^l=\pi N_l/2$ is the Fermi wave number in the lth QW. In the long-wavelength limit (where $q_x\to 0$) the function Π^l can be written as $\Pi^l=(N_l/m^*)(q_x^2/\omega^2)$.

Note that the Hartree potential can be expressed in terms of the perturbation[6] as

$$V^H(\mathbf{r})=\int d\mathbf{r}'\frac{e^2}{\varepsilon|\mathbf{r}-\mathbf{r}'|}\delta n(\mathbf{r}'). \quad (5)$$

Using equations (3) and (5), we get the following expression for the matrix element $V_l^H=\langle k_x,l|V^H(x,y,z)|k_x+q_x,l\rangle$:

$$V_l^H=\sum_{l'}\Pi^{l'}V_{l'}U_{l,l'}, \quad (6)$$

where

$$U_{l,l'}=\frac{8e^2}{\varepsilon a^2}\int_{-a/2}^{a/2}dy'\int_{-a/2}^{a/2}dyK_0\{q_x|(y-y')^2+(l-l')^2d^2|^{1/2}\}\cos^2\left(\frac{\pi y}{a}\right)\cos^2\left(\frac{\pi y'}{a}\right),$$

and $K_0(x)$ is the zeroth-order modified Bessel function of the second kind. Collective excitations of the QW array exist when Eq. (6) has a nonzero solution V^H in the case when the external perturbation $V^{\rm ex}=0$. Hence, the intrasubband plasmon dispersion relation takes the form

$$\det|\delta_{l,l'}-\Pi^{l'}U_{l,l'}|=0. \quad (7)$$

It should be noted that for $M=2$ the dispersion relation (7) coincides with the dispersion relation obtained in Ref. 6 for plasmons in a double-layer QW system.

3. NUMERICAL RESULTS

Figure 1 shows the intrasubband plasmon spectrum (solid lines) in a weakly disordered array of QWs in the case $p=0$. The y axis gives the dimensionless frequency ω/ω_0 ($\omega_0^2=2Ne^2/\varepsilon m^* a^2$ is the plasma frequency), and the x axis gives the dimensionless wave vector $q_x a^*$ ($a^*=\varepsilon\hbar^2/m^*e^2$ is the effective Bohr radius). For comparison the dispersion curves for the plasmons in a single QW with electron densities N_d and N are depicted by dashed curves *1* and *2*, respectively. As the model of the QW we use a GaAs heterostructure with an effective mass of the electrons $m^*=0.067\,m_0$ (m_0 is the free electron mass) and a dielectric constant $\varepsilon=12.7$.

As is seen from Fig. 1, the intrasubband plasmon spectrum in the finite array of QWs contains M modes. Thus, the number of modes in the spectrum is equal to the number of QWs in the array.[13] Notice that the plasmon frequency ω increases with increasing wave number q_x. At the same time, the propagation of plasmons in the weakly disordered array of QWs is characterized by the presence of a local plasmon mode (LPM). In the case when the electron density in the defect QW is less than the electron density in the other QWs ($N_d<N$), the LPM lies in a lower-frequency region in

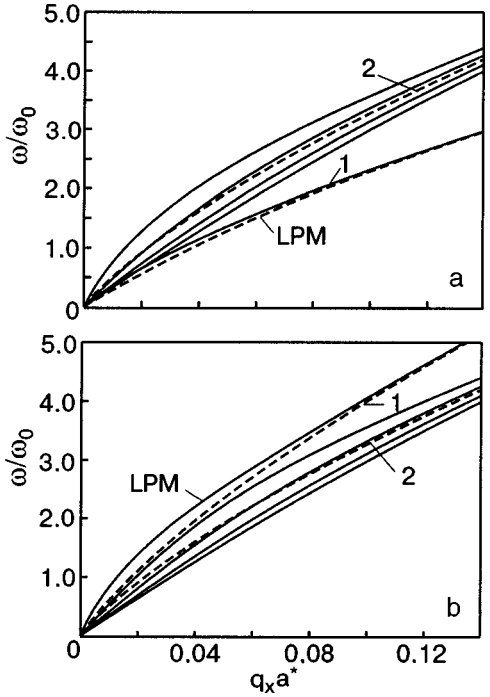

FIG. 1. Dispersion curves of plasmons (solid curves) in a weakly disordered array of QWs with parameters $M=5$, $d=15\,a^*$, $a=20\,a^*$, $p=0$ for two values of the electron density in the defect QW: $N_d/N=0.5$ (a), $N_d/N=1.5$ (b).

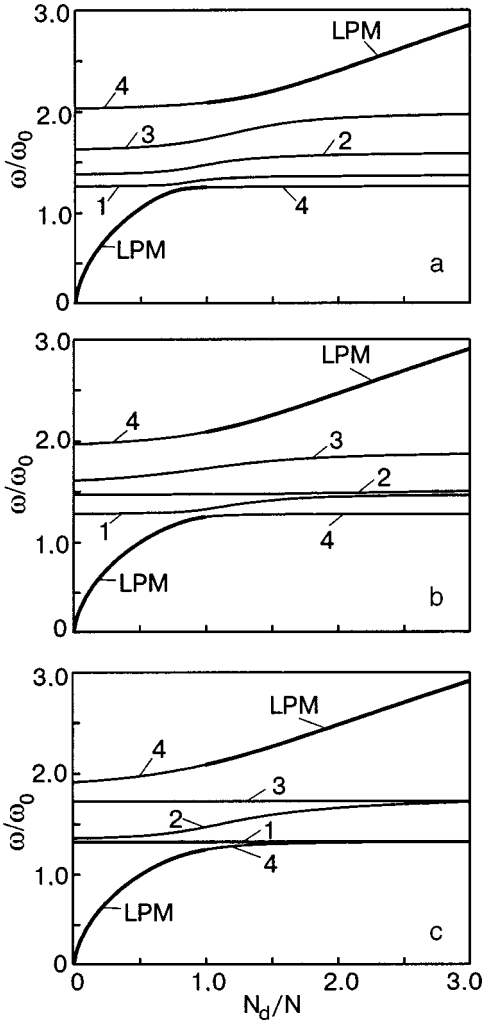

FIG. 2. Dependence of the plasmon frequency upon the ratio N_d/N when $q_xa^*=0.04$, $M=5$, $d=15\,a^*$, $a=20\,a^*$ and for three cases of the defect QW position in the array: $p=0$ (a), $p=1$ (b), $p=2$ (c).

comparison with the usual plasmon modes (Fig. 1a). Accordingly, if $N_d>N$, the LPM lies in a higher-frequen region in comparison with the usual modes (Fig. 1b).[13] It should be emphasized that in the limit $q_xd\to\infty$, when the Coulomb interaction between electrons in adjacent QWs is neglible, the LPM dispersion curve is close to the dispersion curve for the plasmons in a single QW with electron density N_d. In this case the dispersion curves for usual plasmon modes in the limit $q_xd\to\infty$ are gradually drawn together and are close to the dispersion curve for the plasmon in a single QW with electron density N.

Now we consider the dependence of the plasmon spectrum on the value of the 1D electron density in the defect QW. Figure 2 presents the dependence of the plasmon frequency on the ratio N_d/N in the case of a fixed value of the wave vector q_x and for different positions of the defect QW in the array. As is seen from Fig. 2, the frequency of the LPM increases when the value of the ratio N_d/N is increased. At the same time the spectrum of the usual plasmon modes is characterized by the following features. For $p=0$ (Fig. 2a), as the value of the ratio N_d/N is increased, the frequency of all the usual plasmon modes increases as well. In other words, for $N_d<N$ all of the dispersion curves lie in a lower-frequency region as compared with the dispersion curves of plasmons in the QW array with equal electron densities in all the QWs (ordered array of QWs). Correspondingly, in the case $N_d>N$ all the dispersion curves of plasmons in the weakly disordered array of QWs lie in a higher-frequency region in comparison with the plasmons in the ordered array of QWs. However, when $p=1$ (Fig. 2b) the frequency of one of the usual plasmon modes (curve *2*) becomes practically independent of the ratio N_d/N. In the case $p=2$ (Fig. 2c) there are already two plasmon modes (curves *1* and *3*) which possess such a distinctive feature.

Figure 3 presents the dependence of the plasmon frequency ω/ω_0 upon the number p of the defect QW, for different values of M. This dependence is depicted by separate dots. Solid horizontal lines denote the plasmon mode frequencies in the ordered array of QWs. As can be seen from Fig. 3, the LPM spectrum is weakly dependent upon the position of the defect QW in the array. However, the spectrum of usual plasmon modes is more sensitive to the position of the defect QW in the array. Notice that at every value of M, when the defect QW is arranged inside the array of QWs ($1\leqslant p\leqslant M-2$), the usual plasmon mode spectrum contains modes (shown by five-pointed stars), whose frequency does not depend upon the value of the electron density in the defect QW. At the same time, the maximum number of such modes is observed in the case where the defect QW lies at the very center of the array.

To explain the above-mentioned features of the plasmon modes, we consider the spatial distribution of the Hartree potential V^H. Figure 4 shows the dependence of the Hartree potential V^H upon the z coordinate for the LPM (solid curves). This dependence is presented for different positions

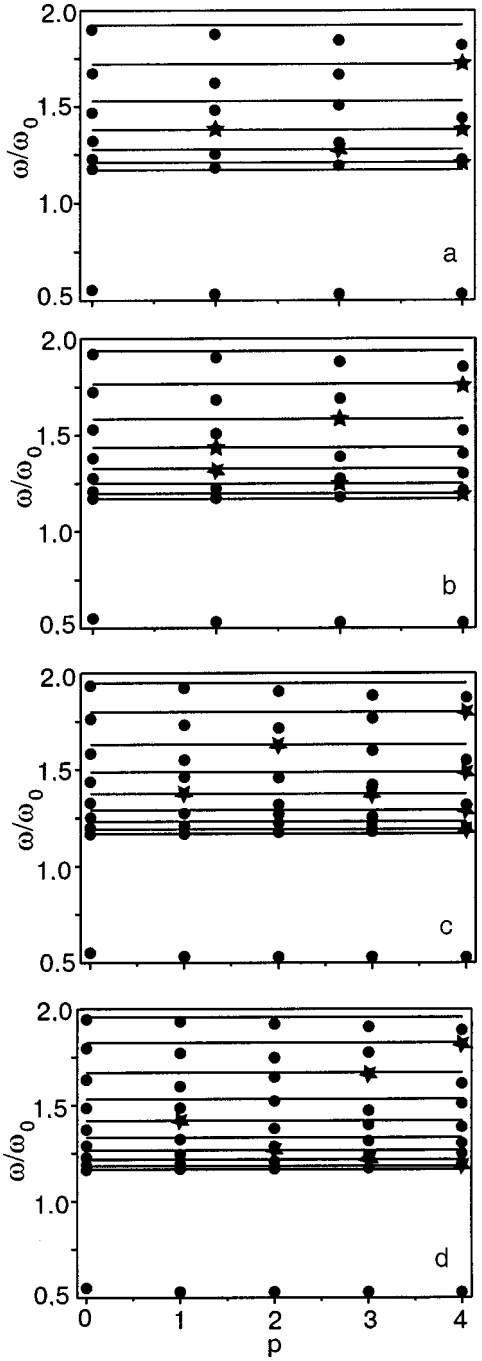

FIG. 3. Dependence of the plasmon frequency upon the position of the "defect" QW in the array p, when $q_x a^* = 0.05$, $N_d/N = 0.15$, $d = 15\,a^*$, $a = 20\,a^*$ and for different values of the amount of QWs in the array: $M = 7$ (a), $M = 8$ (b), $M = 9$ (c), $M = 10$ (d).

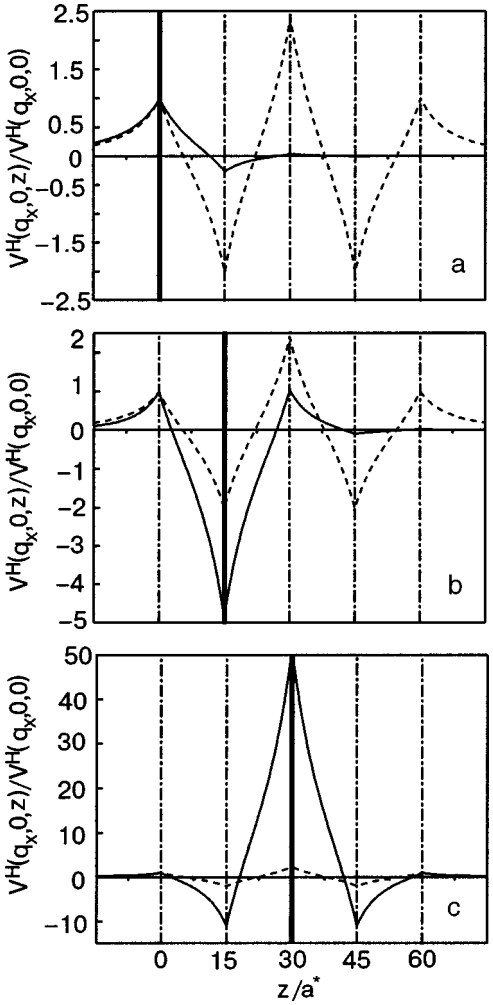

FIG. 4. Spatial distribution of the Hartree potential $V^H(q_x,0,z)$ over the z coordinate for the local plasmon mode in the case when $q_x a^* = 0.05$, $N_d/N = 0.5$, M=5, $d = 15\,a^*$, $a = 20\,a^*$ and for different positions of defect QW in the array: $p = 0$ (a), $p = 1$ (b), $p = 2$ (c).

of the defect QW in the array. The y axis gives the dimensionless Hartree potential $V^H(q_x,0,z)/V^H(q_x,0,0)$, and the x axis gives the dimensionless z coordinate z/a^*. For comparison the spatial distribution of the Hartree potential for the lowest-frequency plasmon mode in the ordered array of QWs is depicted by dashed curves. Vertical dash-and-dot lines denote the positions of QWs in the array. Here the vertical solid bold line corresponds to the position of the defect QW in the array. As is evident from Figs. 4a,b,c the absolute value of the Hartree potential in the vicinity of the defect QW exceeds considerably the absolute values of the Hartree potentials in the vicinity of the other QWs. This implies that practically the whole flux of LPM electromagnetic field energy is concentrated in the vicinity of the defect QW. The weak dependence of the LPM spectrum on the position of the defect QW can be accounted for by that peculiarity.

To explain the fact that usual plasmon mode spectra are sensitive to the position of the defect QW in the array, let us consider, for example, the spatial distribution of the Hartree potential for mode 4 (see Fig. 2). This dependence is represented in Fig. 5 for different positions of the defect QW in the array. The dashed curves present the distribution of the Hartree potential for mode 4 in the case of the ordered array of QWs. As one can see from a comparison of Figs. 5a,b,c, the spatial distribution of the Hartree potential changes when the position of the defect QW in the array is varied. Thus, the changing of the Hartree potential causes the variation of the plasmon frequency.

Figure 6 presents the spatial distribution of the Hartree potential for plasmon modes whose frequencies are slightly sensitive to the value N_d. As is seen from Figs. 6a,b,c, these plasmon modes possess one particular feature. Thus the spatial distribution of the Hartree potential corresponding to the spectra of these modes in a weakly disordered array of QWs either differs insignificantly from that in the ordered array of

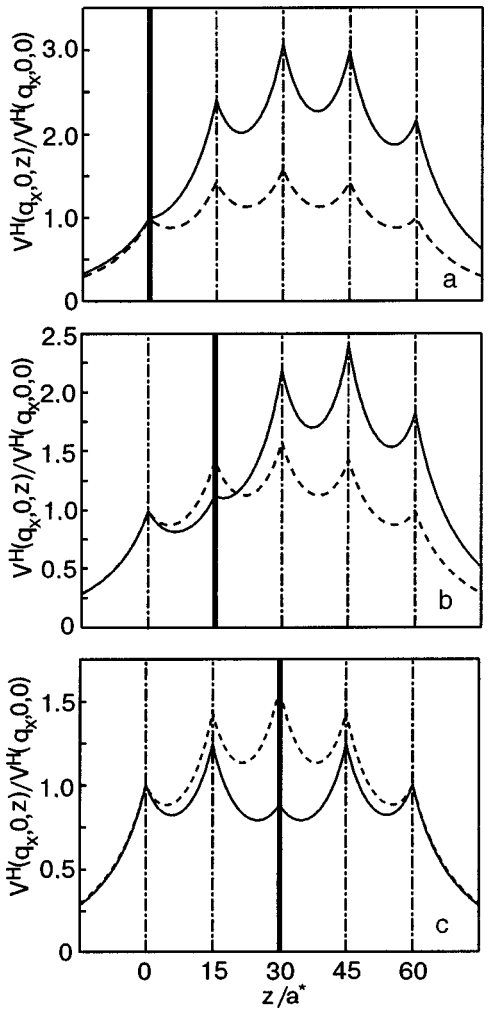

FIG. 5. Spatial distribution of the Hartree potential $V^H(q_x,0,z)$ over the z coordinate for mode 4 (see Fig. 2) in the case when $q_x a^* = 0.05$, $N_d/N = 0.5$, M=5, $d = 15\,a^*$, $a = 20\,a^*$ and for different positions of the defect QW in the array: $p=0$ (a), $p=1$ (b), $p=2$ (c).

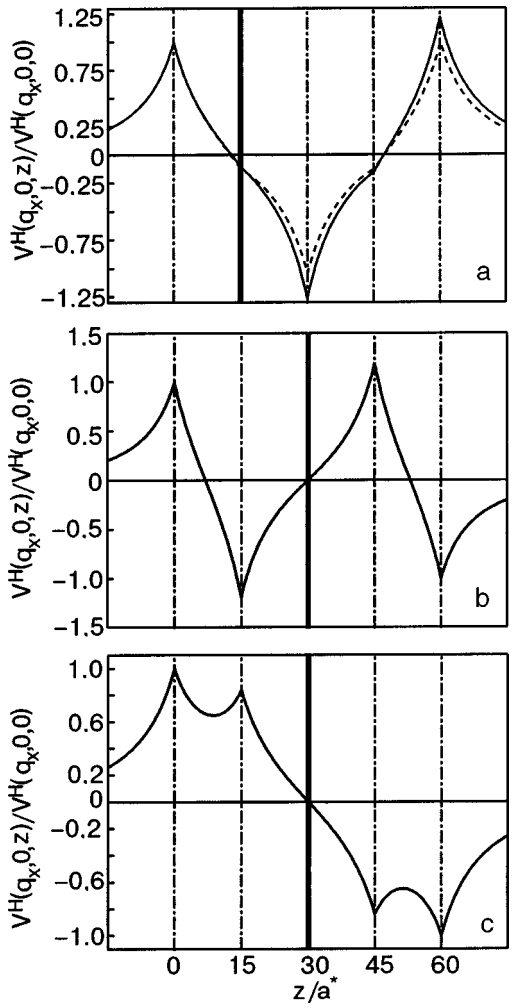

FIG. 6. Spatial distribution of the Hartree potential $V^H(q_x,0,z)$ over z coordinate for the following plasmon modes: $p=1$, mode 2 (see Fig. 2b) (a), $p=2$, mode 1 (see Fig. 2c) (b), $p=2$, mode 3 (see Fig. 2c) (c).

QWs (Fig. 6a) or coincides with it exactly (Figs. 6b,c). At the same time, the absolute value of the Hartree potential in the vicinity of the defect QW is neglible. Thus, in that case the value of the electron density in the defect QW does not exert a substantial effect on the plasmon spectrum.

4. CONCLUSION

In conclusion, we have calculated the plasmon spectrum of a finite, weakly disordered array of QWs which contains one defect QW. It is found that a local plasmon mode whose properties differ from those of other modes exists in the plasmon spectrum. We point out that the LPM spectrum is slightly sensitive to the position of the defect QW in array. That phenomenon can be explained by the fact that practically the whole flux of the LPM electromagnetic energy is localized in the vicinity of the defect QW. At the same time, the position of the defect QW exerts an influence on the spectrum of usual plasmon modes. It is shown that under certain conditions there can exist plasmon modes whose spectrum does not depend upon the density of electrons of the defect QW. The spatial distribution of the Hartree potential for those modes has the feature that the absolute value of the Hartree potential in the vicinity of the defect QW is negligible. Therefore, the defect QW does not exert a significant influence on the dispersion properties of the plasmon modes.

To conclude, it should be emphasized that the abovementioned features of the plasmon spectra can be used for the diagnostics of defects in QW structures. Hence, the LPM properties can be used for determination of the electron density in the defect QW. At the same time, the properties of the usual plasmon modes can be used to determine the position of the defect QW in the array.

*E-mail: bludov@ire.kharkov.ua

[1] M. A. Reed and W. P. Kirk, *Nanostructure Physics and Fabrication*, Academic Press, Boston (1989).
[2] M. A. Reed and W. P. Kirk, *Nanostructures Microscopic System*, Academic Press, Boston (1992).
[3] C. Weisbuch and B. Vinter, *Quantum Semiconductor Structures*, Academic Press, San Diego (1991).
[4] F. A. Reboredo and C. R. Proetto, Phys. Rev. B **50**, 15174 (1994).
[5] S. Das Sarma and Lai Wu-yan, Phys. Rev. B **32**, 1401 (1985).
[6] Q. P. Li and S. Das Sarma, Phys. Rev. B **43**, 11768 (1991).
[7] A. Gold and A. Ghazali, Phys. Rev. B **41**, 7626 (1990).
[8] Q. P. Li, S. Das Sarma, and R. Joynt, Phys. Rev. B **45**, 13713 (1992).
[9] S. Das Sarma and E. H. Hwang, Phys. Rev. B **54**, 1936 (1996).
[10] W. Hansen, M. Horst, J. P. Kotthaus, U. Merkt, Ch. Sikorski, and K. Ploog, Phys. Rev. Lett. **58**, 2586 (1986).

[11] T. Demel, D. Heitmann, P. Grambow, and K. Ploog, Phys. Rev. B **38**, 12732 (1988).
[12] A. R. Goni, A. Pinczuk, J. S. Weiner, J. M. Calleja, B. S. Dennis, L. N. Pfeiffer, and K. W. West, Phys. Rev. Lett. **67**, 3298 (1991).
[13] V. M. Gvozdikov, Fiz. Nizk. Temp. **16**, 1156 (1990) [Sov. J. Low Temp. Phys. **16**, 668 (1990)].
[14] J. K. Jain and S. Das Sarma, Phys. Rev. B **35**, 928 (1987).
[15] H. K. Sy and T. S. Chua, Phys. Status Solidi **176**, 131 (1993).
[16] N. N. Beletskii and Y. V. Bludov, Radiofiz. Élektron. **4**, 93 (1999).
[17] I. M. Litshits, Zh. Eksp. Teor. Fiz. **17**, 1017 (1947).

This article was published in English in the original Russian journal. Reproduced here with stylistic changes by AIP.

Superradiance of *J*-aggregates: correspondence between an infinite disordered chain and a regular finite chain

M. A. Ratner*

Institute for Single Crystals of the National Academy of Sciences of Ukraine, 60 Lenin Ave., Kharkov 61001, Ukraine

(Submitted November 19, 2002)
Fiz. Nizk. Temp. **29**, 804–808 (2003)

The radiative decay of excitons in a slightly disordered molecular chain is studied. The degree of disorder dictates the radius of the excitonic state which determines the enhancement of the decay rate Γ (superradiance). Γ is calculated as a function of the degree of disorder and the temperature and compared with that of a regular chain whose length N determines the excitonic radius. A value of N that gives essentially the same decay rate as a function of the temperature is found for every degree of disorder. © *2003 American Institute of Physics.*
[DOI: 10.1063/1.1596593]

The term *J*-aggregate denotes an almost periodic chain of organic impurity molecules in an organic matrix (*J* aggregates are named after one of their discoverers, E. Jelley (1937)[1]). *J*-aggregates have attracted the attention of researchers in several respects since the 1970s. Of great physical interest is the phenomenon of superradiance—the luminescence decay time of *J*-aggregates is shorter than that of the corresponding monomer. The amount of the decrease (considered below) depends on the degree of chain regularity and can be used for structural diagnostics of the chain and for studying the molecule–matrix interaction responsible for the weak disorder of a chain.[2–11]

The study of *J*-aggregates also holds promise for biological applications. In particular, electronic relaxation processes in a molecular chain are similar to the light energy transformation mechanisms in biological photosynthesis systems.[12,13] In 1991 it was proposed that the excitonic luminescence of some *J*-aggregates be used as a probe of the live state of biological cells.[14] *J*-aggregates are formed on a cell membrane if they are attracted to the membrane potential, which exists only in a live cell and disappears if the cell dies (the luminescence of *J*-aggregates reveals the fact that the aggregates have been formed).

The correspondence between the degree of disorder and the shortening of the luminescence decay time τ, which can be measured experimentally and used for structural diagnostics of *J*-aggregates, is important for all aspects of the study and applications of *J*-aggregates. So far, this correspondence has been established for a model of a regular (strictly periodic) chain of finite length N (the length is expressed in units of the chain period a).[2–9,15,16]

The essence of this model is physically obvious and consists in the following. Consider a one-dimensional excitonic band corresponding to the lowest excited electronic state ψ of a separate molecule. This excitonic state can be represented as a linear combination of the orthonormalized molecular states centered at the chain sites n:

$$\Psi_\alpha = \frac{1}{\sqrt{N}} \sum_{n=1}^{N} c_{n\alpha} \Psi_n \tag{1}$$

(the subscript α enumerates the excitonic states which for a regular chain correspond to the wave vectors k_α). At low temperatures, where only the lowest excitonic state is occupied, the rate Γ of radiative transitions into the ground state is proportional to the squared matrix element of the dipole moment between the excited and ground states. For the lowest excitonic state, since all the coefficients c_n have the same sign and the corresponding matrix element for a separate molecule is independent of n, the matrix element between the state (1) and the ground state is proportional to $N^{1/2}$. Therefore Γ is proportional to the chain length N. The coefficient of proportionality can be found at $N=1$ as the radiative decay rate Γ_0 of a separate excited molecule. Thus the radiative decay rate Γ of the lowest excitonic state is about N times higher than that of a separate molecule:

$$\Gamma \approx N\Gamma_0. \tag{2}$$

The relation (2) is valid only for the lowest excitonic state. For a higher excitonic state the coefficients c_n in Eq. (1) are sign-alternating and Γ is much less than the value (2). It follows that Γ decreases with increasing temperature. The dependence of Γ on N and the temperature are well known for a regular chain. In what follows they shall be used to compare with infinitely long disordered chains.

The model of a regular (periodic) chain of finite length N qualitatively describes the behavior of excitons in an infinitely long slightly disordered chain where the lowest excitonic state is always localized; the localization radius determines the effective value of N. This model is widely used because it is simple and illustrative. However, up to now the model has been qualitative for two reasons. First, no quantitative dependence has been established between N and the degree of disorder of an infinitely long chain (because of the difficulties of modeling an infinitely long disordered chain). Second, it was not known how accurately the model de-

scribes (even with the optimal value of N) the temperature dependence of the superradiance rate of excitons in a disordered chain.

The purpose of the present work is to make the finite-chain model quantitative. For this, first, a quantitative correspondence will be established between the model chain length N and the degree of disorder of a truly infinite chain. Second, the temperature dependence of the superradiance rate of excitons in a disordered chain will be calculated and compared with the case of a regular chain with the best-fit length. It is assumed that superradiance occurs at complete thermodynamic equilibrium.

This work will be based on the general relations for the excitonic states and the superradiance rate of a molecular chain with arbitrary length M and arbitrary degree of disorder. The chain is placed into an inorganic crystalline matrix; the discrepancy between the periods of the chain and the matrix lattice is the origin of the small aperiodicity of the chain potential. The excitonic band is assumed to correspond to the lowest excited electronic state of a separate molecule of the chain (the higher molecular states are ignored). In the absence of disorder $M=N$ this general case becomes a model of a regular chain of finite length N; in the presence of disorder a truly infinitely long, disordered chain obtains for sufficiently large M.

The Hamiltonian of the electronic system of the chain can be written as

$$H=\Sigma H_{0n}-V. \tag{3}$$

Here H_{0n} is the Hamiltonian of a separate molecule including the Hamiltonian of the free molecule and the crystal field acting on the nth molecule in the chain; V describes the interaction between the electronic subsystems of different molecules. Following Eq. (1), the excitonic states Ψ_α, i.e. the eigenfunctions of the Hamiltonian (3), are expanded in the orthonormalized states ψ_n of a chain containing an excited molecule at the nth site ($n=1,\ldots,M$). By definition ψ_n is an eigenfunction of the Hamiltonian H_{0n}, which therefore has no off-diagonal matrix elements, whereas V has no diagonal elements [the diagonal part of V is incorporated into the first term in Eq. (3)]:

$$H_{0n}\Psi_n=\varepsilon_n\Psi_n,\quad H_{0nm}=\varepsilon_n\delta_{nm},\quad V_{nn}=0. \tag{4}$$

The interaction potential V is assumed to be an exchange potential, so that all matrix elements V_{nm} except those between adjacent sites $V_{n,n+1}$ and $V_{n,n-1}$ can be neglected. The latter assume random values centered on an average value V and the site levels ε_n assume random values centered on their average position, which is zero. In the absence of disorder the width of the excitonic band is $W=4V$ and the band extends from $-2V$ to $2V$.

The Schrödinger equation for the Hamiltonian (3) can be written in the site representation in the usual way. Finally, allowing for the relations (1) and (4), we obtain the following system of linear homogeneous equations for the expansion coefficients $c_{n\alpha}$:

$$\varepsilon_n c_{n\alpha}+V_{n,n+1}c_{n+1,\alpha}+V_{n,n-1}c_{n-1,\alpha}=E_\alpha c_{n\alpha} \tag{5}$$

$$(\alpha,n=1,\ldots,M)$$

(the subscript α enumerates excitonic states with energy E_α). The equation (5) must be supplemented with a boundary condition for a linear chain of length M:

$$c_0=0,\quad c_{M+1}=0. \tag{6}$$

The chain can also be closed into a ring of length M with periodic boundary conditions

$$c_{n+M}\equiv c_n, V_{n+M'n+M+1}=V_{n,n+1}. \tag{7}$$

The excitonic energy levels E_α can be found by equating to zero the determinant of the system (5). Then the orthonormalized set of solutions $\{c_{n\alpha}\}$ is obtained from Eq. (5) after substituting for every α the corresponding value of E_α

The rate Γ_α of radiative decay from the αth excited state to the ground state can be expressed in the usual way by solving Eq. (5):

$$\Gamma_\alpha=\Gamma_0\left|\sum_{n=1}^{M} c_{n\alpha}\right|^2. \tag{8}$$

The total decay rate $\overline{\Gamma}$ at thermodynamic equilibrium is

$$\overline{\Gamma}(M,T)=\frac{\Sigma_{\alpha=1}^{M}\Gamma_\alpha\exp(-E_\alpha/T)}{\Sigma_{\alpha=1}^{M}\exp(-E_\alpha/T)} \tag{9}$$

(T is the temperature in energy units). The lowest excited state with $\alpha=1$ makes the dominant contribution to the decay rate (9) because the sign of $c_{n\alpha}$ is constant, whence follows the decreasing temperature dependence of $\overline{\Gamma}$.

For a regular chain ε_n and $V_{n,n+1}=V$ are independent of n. The equation (5) has the simple solution

$$c_{nk}=\frac{\exp(ikan)}{\sqrt{M}}, \tag{10}$$

$$E_k=2V\cos ka,\quad k=2\pi\alpha/Ma,\quad \alpha=1,\ldots,M.$$

Taking account of Eq. (10) the expression (8) becomes

$$\Gamma_k=\frac{4\sin^2[(M+1)ka/2]\sin^2(Mka/2)\operatorname{ctan}(ka/2)}{M\sin(ka)-\cos[(M+1)ka]\sin(Mka)}. \tag{11}$$

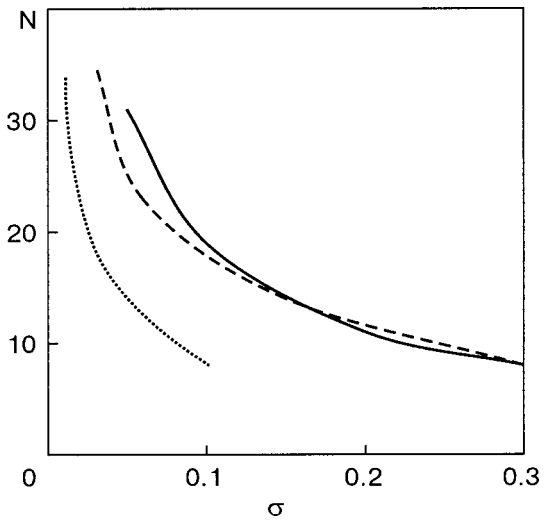

FIG. 1. The equivalent length N of a regular chain versus the degree of disorder σ of an infinitely long chain. Solid curve—$N(\sigma_{\text{dia}})$ with $\sigma_{\text{off}}=0$; dotted curve—$N(\sigma_{\text{off}})$ with $\sigma_{\text{dia}}=0$; the dashed curve represents $N(\sigma_{\text{off}}/3)$ with $\sigma_{\text{dia}}=0$.

Let us now consider an infinitely long, slightly disordered chain. Two possible types of disorder will be considered: (1) diagonal disorder, i.e. random straggling of site levels ε_n near their average value $\langle\varepsilon\rangle=0$, and (2) off-diagonal disorder, i.e. straggling of the interaction matrix elements $V_{n,n+1}$ near their average value $\langle V_{n,n+1}\rangle=V=0.25W$ (W is the bandwidth of a long regular chain). The straggling is described by a Gaussian distribution with standard deviation σ_{dia} in the former case and σ_{off} in the latter case.

The cases of diagonal and off-diagonal disorder were considered separately. For given σ_{dia} or σ_{off}, 1000 realizations of a chain with random sets of ε_n or $V_{n,n+1}$ were constructed. The system (5) was solved numerically for every realization. The boundary condition (7) for a chain closed into a ring was used to avoid edge effects; such a ring of length $M\gg N$ models almost exactly an infinitely long chain (N is the length of the equivalent regular chain). It was verified numerically that a ring with length $M=100$ models almost exactly an infinitely long chain with the equivalent length $N\leqslant 35$.

The standard deviation σ was varied from $0.05W$ to $0.3W$ for diagonal disorder and from $0.01W$ to $0.1W$ for off-diagonal disorder. For every σ_{diag} or σ_{off} there is an equivalent regular chain length $N(\sigma)$ which gives the same decay rate at zero temperature. Figure 1 shows N versus σ_{dia} and σ_{off}. According to Fig. 1, off-diagonal disorder with standard σ_{off} is approximately equivalent to diagonal disorder with standard deviation $3\sigma_{\text{off}}$. For estimation purposes, considering diagonal and off-diagonal disorder as independent random processes, simultaneous diagonal disorder with standard deviation σ_{dia} and off-diagonal disorder with standard deviation σ_{off} can be reduced to diagonal disorder with the standard deviation $(\sigma_{\text{dia}}^2+9\sigma_{\text{off}}^2)^{1/2}$.

It was found that the temperature dependence of the decay rate $\overline{\Gamma}(T)$ for an infinitely long disordered chain can be approximated well by that of a regular chain with the corre-

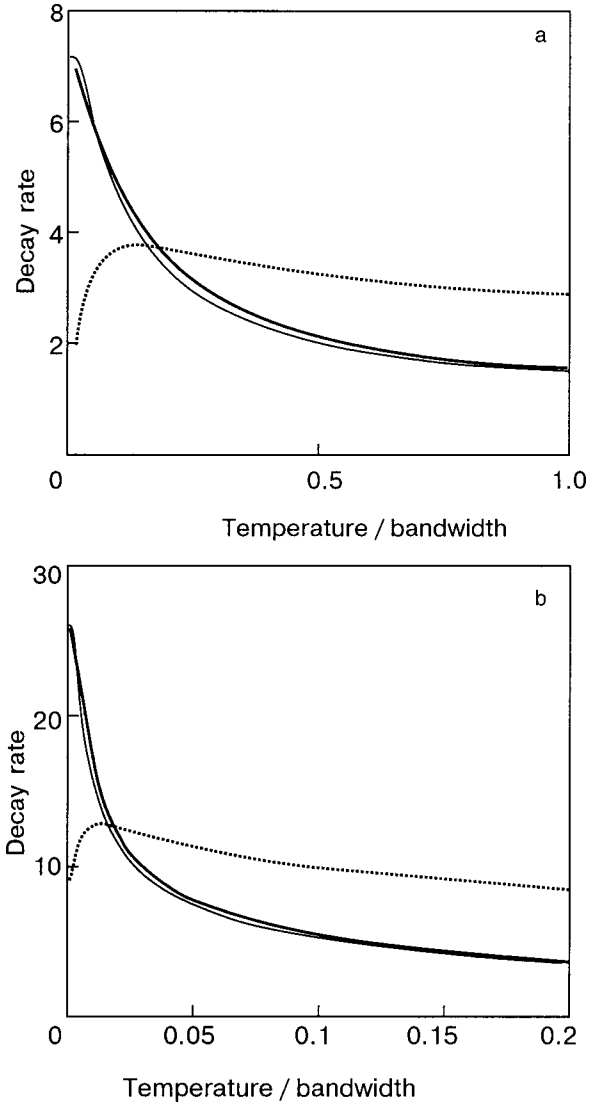

FIG. 2. Temperature dependence of the radiative decay rate $\overline{\Gamma}$ for a chain with diagonal disorder in units of that of the monomer. The thick solid line is for an infinitely long disordered chain with $\sigma_{\text{dia}}=0.3$ (a) and 0.05 (b). The thin solid line is for a regular chain of length $N=8$ (a) and $N=31$ (b) that best simulates a disordered chain. The dotted line shows the standard deviation of $\overline{\Gamma}$ for random realizations of a disordered chain.

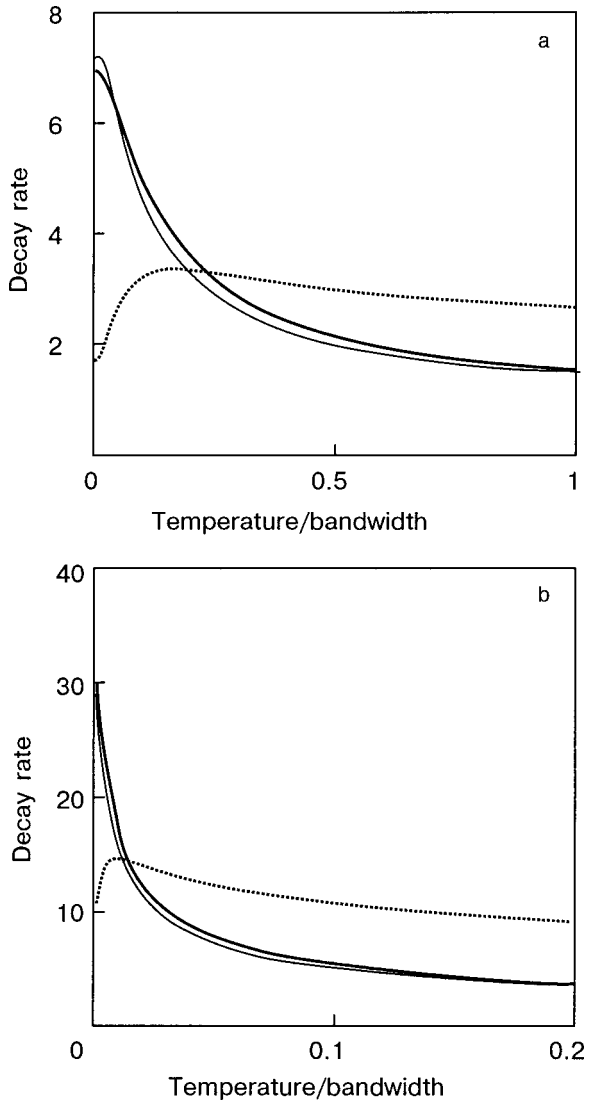

FIG. 3. Temperature dependence of the radiative decay rate $\overline{\Gamma}$ for a chain with off-diagonal disorder in units of that of the monomer. The thick solid line is for an infinitely long disordered chain with $\sigma_{\text{off}}=0.1$ (a) and 0.01 (b). The thin solid line is for a regular chain of length $N=8$ (a) and $N=35$ (b) that best simulates a disordered chain. The dotted line shows the standard deviation of $\overline{\Gamma}$ for random realizations of a disordered chain.

sponding equivalent length with no restrictions on the temperature range. Figures 2 and 3 show examples of such an approximation.

Figures 2 and 3 show the decay rate averaged over a large number of random realizations of a disordered chain. Such averaging occurs in a single excitation pulse, if the pulse is strong enough to excite a large number of chains. If every pulse excites only one molecule (single-molecule spectroscopy), the observed value of $\overline{\Gamma}$ exhibits significant straggling, whose standard deviation is shown in Figs. 2 and 3 (dotted lines).

An infinitely long, irregular chain can be simulated by a regular chain of finite length. However, this correspondence is restricted to the superradiance rate and cannot be extended to the absorption spectrum (which consists of discrete lines for a regular chain and a band for a disordered chain).

The author is grateful to Yu. V. Malyukin and A. M. Ratner for helpful discussions. This work was performed as part of the project INTAS 2001-240.

*E-mail: ratner@isc.kharkov.com

[1] E. E. Jelley, Nature (London) **139**, 631 (1937).
[2] E. W. Knapp, Chem. Phys. **85**, 73 (1984).
[3] H. Fidder and D. A. Wiersma, Phys. Rev. Lett. **66**, 1501 (1991).
[4] H. Fidder, J. Knoester, and D. A. Wiersma, J. Chem. Phys. **95**, 7880 (1991).
[5] J. Knoester, J. Chem. Phys. **99**, 7846 (1993).
[6] M. Wubs and J. Knoester, Chem. Phys. Lett. **284**, 63 (1998).
[7] H. Fidder, J. Knoester, and D. A. Wiersma, J. Chem. Phys. **98**, 6564 (1993).
[8] J. R. Durant, J. Knoester, and D. A. Wiersma, Chem. Phys. Lett. **222**, 450 (1994).
[9] J. Knoester, J. Lumin. **58**, 107 (1994).
[10] J. Klafter and J. Jortner, J. Chem. Phys. **68**, 1513 (1978).
[11] M. Schreiber and Y. Toyozawa, J. Phys. Soc. Jpn. **51**, 1528 (1981).
[12] Th. Renger and V. May, Phys. Rev. Lett. **78**, 3406 (1997).
[13] Th. Renger and V. May, J. Phys. Chem. B **101**, 7211 (1997).
[14] M. Reers, T. W. Smith, and L. B. Chen, Biochemistry **30**, 4480 (1991).
[15] S. Boer and D. A. Wiersma, J. Lumin. **45**, 241 (1990).
[16] V. Sundstrom, T. Gillbro, R. A. Gadonas, and A. Piskarskas, J. Chem. Phys. **89**, 2754 (1988).

This article was published in English in the original Russian journal. Reproduced here with stylistic changes by AIP.

Influence of electron–electron scattering on spin-polarized current states in magnetically wrapped nanowires*

R. N. Gurzhi,** A. N. Kalinenko, A. I. Kopeliovich, and A. V. Yanovsky

B. Verkin Institute for Low Temperature Physics and Engineering of the National Academy of Science of Ukraine, 47 Lenin Ave., Kharkov 61103, Ukraine

E. N. Bogachek and Uzi Landman

School of Physics, Georgia Institute of Technology, Atlanta, Georgia 30332-0430, USA
(Submitted November 29, 2002)
Fiz. Nizk. Temp. **29**, 809–811 (2003)

The role of electron–electron collisions in the formation of spin-polarized current states in a spin guide—a system consisting of a nonmagnetic conducting channel wrapped in a grounded nanoscale magnetic shell—is studied. It is shown that under certain conditions the spin guide can generate and transport nonequilibrium electron density with high spin polarization over long distances even though frequent electron–electron scattering causes drifting of the nonequilibrium electrons as a whole. Ways to convert the spin-polarized electron density into a spin-polarized electric current are proposed. © *2003 American Institute of Physics.*
[DOI: 10.1063/1.1596594]

1. THE SPIN-GUIDE IDEA

Spintronic devices based on a spin degree of freedom in addition to charge may lead to new possibilities in information processing and storage. Efficient spin injection into a semiconductor and long-distance propagation of a spin signal are the main requirements for the development of spintronic devices. Most methods for producing stationary spin polarization are based on spin injection through a ''magnetic conductor (M)—nonmagnetic matter (N)'' interface; we shall refer to it as a spin-filter scheme (see, for example, Refs. 1–3). Recently, we have proposed a new method for generating and transporting currents with high spin polarization—a spin guide scheme.[4] This scheme was proposed as a nonmagnetic conducting channel which is wrapped in a magnetic shell whose external boundaries are grounded; see Fig. 1. (Note that there is no need to wrap a magnetic shell around the nonmagnetic conductor; a contact between it and the grounded magnetic material is sufficient.) Here, unlike the spin-filter scheme, current flows along the M–N interface. The spin-guide scheme is based on the removal of one spin polarization; this contrasts with the spin-filter scheme where spin polarization is produced in a nonmagnetic conductor by electrons injected from the magnetic material. In the spin-guide scheme nonequilibrium electrons with one type of polarization (spin down, for example) which penetrate to M more easily than electrons with the other type of polarization do not return into the channel because the external boundaries of the magnetic shell are grounded. So, as the distance from the channel entrance increases, the polarization of the electric current increases because of spin-down carrier depletion. Note that the spin-guide scheme exploits the removal of one spin component. Therefore to increase the spin polarization the thickness of the magnetic region must be decreased (in contrast to the spin-filter scheme). That is why nanoscale shells are preferable for the spin-guide scheme. As we have shown elsewhere,[4,5] the spin-guide scheme removes some intrinsic limitations of the spin-filter schemes: 1) the spin polarization of the current in a spin guide can be much greater than the spin polarization in the magnetic material; this is never possible in the spin-filter scheme; ii) the spin polarization of the current can be transported over arbitrarily long distances, in contrast to the spin-filter scheme where the transport length is of the order of the diffusion spin-flip length. In the spin-guide scheme the negative role of spin-flip processes is smaller than in the spin-filter scheme in a magnetic shell[5] and in a nonmagnetic channel;[4] iii) spin guides allow easy detection and control of the spin polarization which do not require magnetization inversion of the magnetic material; iv) one-dimensional wires can be used as a nonmagnetic channel for the spin-guide; it is well known that a no-backscattering 1D spin-filter is impossible if the magnetic material is not completely polarized; v) finally, there are a number of spin-guide-specific effects, some of which enable the spin polarization of the current flowing in a spin guide to be observed directly.

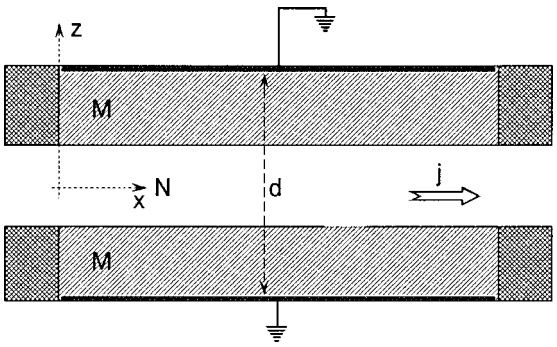

FIG. 1. Spin-guide scheme. d is the distance between the grounded conductors.

In this paper we show that the advantages of spin guides over spin filters remain largely valid even though normal

electron–electron ($e-e$) collisions are the most frequent scattering processes.

2. THE ROLE OF ELECTRON–ELECTRON SCATTERING IN SPIN GUIDES

Normal electron–electron collisions play an essential role in spin-guide schemes. This is because the $e-e$ interaction leads to momentum exchange between the spin-up and spin-down electron subsystems, thereby establishing a drift of the current carriers as a whole in the nonmagnetic channel. As a result, $e-e$ collisions depolarize the current in a spin guide. (In compensated conductors there is no effect because no electric charge is transferred when the carriers drift as a whole.) However, $e-e$ scattering does not affect the spin polarization of the nonequilibrium carrier density because the total spin is conserved in these collisions. So, together with the drift of the nonequilibrium carriers as a whole there is spin polarization of the density in a spin guide. Accordingly, the aforementioned advantages of the spin-guide scheme are substantially preserved. We shall show below that spin-polarized density can be converted into spin-polarized current. Therefore the spin-guide scheme could become quite effective as temperature increases. Note that under certain conditions normal $e-e$ scattering predominates in a two-dimensional degenerate electron gas in high-mobility heterostructures; see, e.g., Ref. 6.

We use the macroscopic transport equations derived by Flensberg *et al.*[7] taking account of $e-e$ scattering. We consider the case of infrequent spin-flip scattering, i.e. $\tau_{sf} > \tau_{ee}$ (τ_{sf} is the spin-flip scattering time and τ_{ee} is the electron–electron scattering time). We rewrite Eqs. (1a) and (1b) of Ref. 7 in the form

$$\operatorname{div} \mathbf{j}_{\uparrow\downarrow} = -\left(\frac{e\Pi_0}{\tau_{sf}}\right)(\mu_{\uparrow\downarrow} - \mu_{\downarrow\uparrow}), \tag{1}$$

$$-e^{-1}\nabla \mu_{\uparrow\downarrow} = \rho_{i\uparrow\downarrow}\mathbf{j}_{\uparrow\downarrow} + An_{\uparrow\downarrow}^{-1}(n_{\uparrow\downarrow}^{-1}\mathbf{j}_{\uparrow\downarrow} - n_{\downarrow\uparrow}^{-1}\mathbf{j}_{\downarrow\uparrow}). \tag{2}$$

Here $\mathbf{j}_{\uparrow\downarrow}$ are the current densities of the spin-up and spin-down electrons, respectively; $\mu_{\uparrow\downarrow}$ are the electrochemical potentials of the spin-up and spin-down electrons; $\rho_{i\uparrow\downarrow}$ are the resistivities; e is the electron charge; $n_{\uparrow\downarrow}$ are the electron densities; $A \approx e^{-2} m \nu_{ee} n_m$ is the $e-e$ spin drag coefficient;[7] $\nu_{ee} = \tau_{ee}^{-1} \propto T^2$ is the $e-e$ collisions frequency; n_m is the lower of the electron densities with the two spin components $\Pi_0^{-1} = \Pi_\uparrow^{-1} + \Pi_\downarrow^{-1}$, where $\Pi_{\uparrow\downarrow}$ are the densities of states at the Fermi surface. The second term on the right-hand side of Eq. (2) describes the mutual friction of the two spin subsystems, which leads to drift of the electron system as a whole. To simplify the problem we ignore the small term related to anisotropic spin-flip scattering.[7]

We consider a simple spin-guide model, i.e. a two-dimensional geometry where the interface is a nonmagnetic plate surrounded by magnetic layers with grounded external boundaries; see Fig. 1. Since we are concerned primarily with the role of $e-e$ scattering, we neglect spin-flip scattering and consider completely polarized magnetic layers only (for example, dilute magnetic semiconductors with giant Zeeman splitting or completely polarized semimetals; see Refs. 3 and 8). Let the x axis be directed along and lie in the middle of the channel and the z axis perpendicular to the interfaces, and let the origin of the coordinate system be located at the center of the entrance into the channel (Fig. 1). Grounding the external boundaries is equivalent to the condition $\mu_{\uparrow\downarrow}\,(z = \pm d/2) = 0$. For definiteness, we shall assume that the magnetic shell is transparent to spin-down electrons. For distances from the entrance such that $x \gg d$, the steady-state solutions of Eqs. (1) and (2) are

$$\mu_\uparrow = a + bx, \quad \mu_\downarrow = 0, \tag{3}$$

where a and b are arbitrary constants (the relation between a and b is determined by the boundary conditions at the channel entrance). Writing the corresponding currents from Eq. (2) shows that $e-e$ collisions radically suppress the spin polarization of the current:

$$\alpha \equiv \frac{j_\uparrow - j_\downarrow}{j_\uparrow + j_\downarrow} = \left(1 + \frac{A}{\rho_i n^2}\right)^{-1} \approx \left(1 + \frac{\nu_{E-E}}{\nu_i}\right)^{-1}, \tag{4}$$

where ν_i is the electron–impurity collision frequency. Thus, as mentioned above, the spin polarization of the electric current tends to 1 when electron–impurity scattering predominates over electron–electron scattering, i.e. $\nu_{ee}/\nu_i \to 0$, and vice versa α tends to 0 (the spin currents will tend to be equalized) as the spin drag coefficient, which is proportional to the $e-e$ collision frequency, increases. On the other hand the relative spin polarization of the electron density is completely dependent on the $e-e$ collision frequency:

$$\beta \equiv \frac{\delta n_\uparrow - \delta n_\downarrow}{eU\Pi} = \frac{\mu_\uparrow - \mu_\downarrow}{eU}. \tag{5}$$

Here $eU\Pi$ is the maximum possible change of the electron density in the potential between the ends of the spin guide U and Π is the electron density of states at the Fermi level in a nonmagnetic conductor.

We note that the spin polarization of the electron density may be converted into essentially 100% spin polarization of the electric current. This can be done in different ways. First, extra local impurity concentration near the exit from the spin guide can be used. Then electron–impurity scattering predominates over electron–electron scattering in this region. A comparatively short dirty region whose width is of the order of d will be adequate for this purpose. Another method is to use electrostatic constrictions or atomic wires at the exits of the nomagnetic channel; the transport mean free path in the constriction must be less than the electron–electron mean free path. For atomic wires (one-dimensional quantum point contacts) the spin polarization of the current at the exit of the spin guide is determined by the ratio between the electrochemical potentials $\mu_{\uparrow\downarrow}$ before the constriction and the electrochemical potential μ_∞ outside the channel. If $\mu_\downarrow \leqslant \mu_\infty$, then the spin polarization of the current will be 100%.

Note that if the resistance of the constriction at the end of a spin guide is much higher than the channel resistance, then the spin polarization β of the density in the channel will be constant, reaching its maximum value $\beta \approx 1$, i.e. the nonequilibrium density is completely polarized.

The research described in this paper was made possible in part by Award No. UP2-2430-KH-02 from the U.S. Civilian Research and Development Foundation for the Independent States of the Former Soviet Union (CRDF). The re-

search performed by E.N.B. and U.L. was also funded by the U.S. Department of Energy, Grant No. FG05-86ER-45234.

*Reported at the 3rd International Workshop on Low Temperature Microgravity Physics (CWS-2002).

**E-mail: gurzhi@ilt.kharkov.ua

[1] A. G. Aronov, JETP Lett. **24**, 32 (1976).
[2] J. C. Egues, Phys. Rev. B **80**, 4578 (1998).
[3] R. Fiederling, M. Kein, G. Reusher, W. Ossau, G. Schmidt, A. Waag, and L. W. Molenkamp, Nature (London) **402**, 787 (1999).
[4] R. N. Gurzhi, A. N. Kalinenko, A. I. Kopeliovich, and A. V. Yanovsky, LANL cond-mat/0109041 (2001); Fiz. Nizk. Temp. **27**, 1332 (2001) [Low Temp. Phys. **27**, 985 (2001)].
[5] R. N. Gurzhi, A. N. Kalinenko, A. I. Kopeliovich, A. V. Yanovsky, E. N. Bogachek, and Uzi Landman, LANL cond-mat/0301142 (2003).
[6] M. J. M. de Jong and L. W. Molenkamp, Phys. Rev. B **51**, 13389 (1995).
[7] K. Flensberg, T. S. Jensen, and N. A. Mortensen, LANL cond-met/0107149.
[8] R. A. de Groot, F. M. Mueller, P. G. V. Engen, and K. H. J. Buschow, Phys. Rev. Lett. **50**, 2024 (1983).

This article was published in English in the original Russian journal. Reproduced here with stylistic changes by AIP.

On the propagation of acoustic waves in quasi-two-dimensional conductors in a quantizing magnetic field

O. V. Kirichenko* and V. G. Peschansky

B. Verkin Institute for Low Temperature Physics and Engineering, National Academy of Sciences of Ukraine, pr. Lenina 47, 61103 Kharkov, Ukraine

O. Galbova, G. Ivanovski, and D. Krstovska

Faculty of Natural Sciences and Mathematics, Physical Institute, P.O. Box 162, 10000 Skopje, Republic of Macedonia

(Submitted December 11, 2002)
Fiz. Nizk. Temp. **29**, 812–816 (July 2003)

The damping of acoustic waves propagating perpendicular to the layers of a quasi-two-dimensional conductor is analyzed for the case of low temperatures, at which the energy quantization of the conduction electrons leads to an oscillatory dependence of the acoustic damping coefficient on the inverse magnetic field. The acoustic damping decrement is found for different orientations of the magnetic field with respect to the layers. It is shown that that a layered conductor is most transparent for an acoustic wave in the case when the magnetic field is perpendicular to the layers. © *2003 American Institute of Physics.* [DOI: 10.1063/1.1596595]

Acoustoelectronic effects in degenerate conductors placed in a sufficiently high magnetic field **H** are extremely sensitive to the form of the energy spectrum of the charge carriers.[1–3] The experimental study of these effects in metals in the case when the gyration frequency Ω of the electrons in the magnetic field is much higher than their collision frequency $1/\tau$ has permitted the complete recovery of the shape of the Fermi surface, the main characteristic of the electron energy spectrum.

At sufficiently low temperatures T, when the distance between electron quantum energy levels $\Delta\varepsilon=\hbar\Omega$ is significantly greater than the temperature smearing of the Fermi distribution function of the charge carriers, $f_0(\varepsilon)$, the acoustic damping decrement Γ undergoes resonance oscillations with variation of the inverse value of the high magnetic field $(\Omega\tau\gg 1)$.

In degenerate conductors having a layered structure the electron energy spectrum is substantially anisotropic and, as a rule, is quasi-two-dimensional. The energy ε of the charge carriers in quasi-two-dimensional conductors depends weakly on the momentum projection p_z onto the normal **n** to the layers.

The specifics of the quasi-two-dimensional electron energy spectrum of layered conductors are manifested in an enhancement of quantum oscillation effects in comparison with ordinary metals, since a rather large number of charge carriers with the Fermi energy ε_F are involved in their formation. At the same time, the low electronic conductivity of layered conductors along the normal to the layers leads to acoustic transparency for waves propagating perpendicular to the layers.[4,5] In this connection let us consider the propagation of an acoustic wave in the easiest direction for it, i.e., along the normal to the layers of a quasi-two-dimensional conductor placed in a magnetic field $\mathbf{H}=(0, H\sin\theta, H\cos\theta)$ inclined at an angle θ to the wave vector **k** and the normal **n**.

At low temperatures the absorption of energy from sound waves in a degenerate conductor is mainly due to the interaction of the charge carriers with the wave and is determined by the dissipative function of the electrons,

$$Q=T\frac{dS}{dt}, \tag{1}$$

where S is the entropy density of the conduction electrons, which is related to the nonequilibrium density matrix $\hat{f}$ by the relation[6,7]

$$S=\mathrm{tr}\{\hat{f}\ln\hat{f}+(1-\hat{f})\ln(1-\hat{f})\}. \tag{2}$$

The summation in (2) is over all variables specifying the state of the conduction electrons except for the spin variables.

The density matrix $\hat{f}$ must be determined with the aid of the kinetic equation

$$\frac{\partial\hat{f}}{\partial t}+\hat{\mathbf{v}}\frac{\partial\hat{f}}{\partial\mathbf{r}}+[\hat{H}_0+\hat{H}_1,\hat{f}]=\hat{W}_{\mathrm{coll}}\{\hat{f}\}, \tag{3}$$

where $\hat{W}_{\mathrm{coll}}(\hat{f})$ is the collision operator of the charge carriers, which describes their scattering by impurity atoms and vibrations of the crystal lattice, i.e., phonons; $\hat{H}_0$ is the Hamiltonian of the conduction electrons in the magnetic field, and $\hat{\mathbf{v}}$ is their velocity operator, and $\hat{H}_1$ is a correction to the unperturbed Hamiltonian $\hat{H}_0$ to take into account the perturbation of the electron system by the acoustic wave.

In a vibrating lattice the electron energy spectrum is sensitive to the strain of the crystal, and in the linear approximation in the small displacement **u** of the lattice ions the energy of the conduction electrons acquires an additional amount $\delta\varepsilon=\lambda_{ik}(\mathbf{p})u_{ik}$, where $u_{ik}=(1/2)(\partial u_i/\partial x_k+\partial u_k/\partial x_i)$ is the strain tensor, and λ_{ik} is the deformation potential tensor.[8] It is natural to assume that the energy spectrum of the charge carriers remains highly anisotropic after renormalization by the sound wave. The components of the deformation potential tensor in the plane of the layers is of the same order of magnitude as the Fermi energy of the

electrons, while the components for which one or both of the indices is z are significantly smaller. It follows from conservation of the number of charge carriers that each of the tensor components λ_{ik} averaged over all states of the conduction electrons is equal to zero.

In addition to renormalization of the energy of the charge carriers a sound wave generates an accompanying electromagnetic wave. The electric field of this wave in a reference frame moving with the vibrating crystal lattice with a velocity $\dot{\mathbf{u}}$ has the form

$$\tilde{\mathbf{E}}=\mathbf{E}+\frac{1}{c}(\dot{\mathbf{u}}\times\mathbf{H})-\frac{m\hat{\mathbf{u}}}{e}, \tag{5}$$

where $\mathbf{E}$ is the electric field in the nonmoving laboratory reference frame, which must be determined from Maxwell's equations

$$\text{curl curl } \mathbf{E}=-\frac{4\pi}{c^2}\frac{\partial\mathbf{j}}{\partial t}-\frac{1}{c^2}\frac{\partial^2\mathbf{E}}{\partial t^2}, \quad \text{div}\,\mathbf{E}=4\pi\rho',$$

supplemented by the constitutive relations linking the current $\mathbf{j}$ to the electric field of the wave. Here c is the speed of light in vacuum, and ρ' is the uncompensated charge density, which is asymptotically vanishing in the expansion in powers of $1/N_e$ in conductors with a high density of conduction electrons N_e. To the same accuracy the charge conservation law has the form

$$\text{div}\,\mathbf{j}=0. \tag{6}$$

The damping of a low-amplitude sound wave can be analyzed with the aid of the solution of the kinetic equation (3), linearized with respect to the deviation of the density matrix from the equilibrium $\hat{f}_0$, and the entropy production

$$\frac{dS}{dt}=\text{tr}\,\hat{W}_{\text{coll}}(\hat{f})\ln\frac{1-\hat{f}}{\hat{f}} \tag{7}$$

is a quadratic function of $\hat{f}_1=\hat{f}-\hat{f}_0$ and can be represented in the form

$$\frac{dS}{dt}=-\text{tr}\,\hat{W}_{\text{coll}}(\hat{f}_1)\frac{\hat{f}_1}{\hat{f}_0(1-\hat{f}_0)}. \tag{8}$$

The diagonal matrix elements of the equilibrium density matrix $\hat{f}_0$ are equal to the Fermi distribution function of the charge carriers $f_{0nn}=f_0(\varepsilon_n(p_H))$, where $\varepsilon_n(p_H)$ are the eigenvalues of the Hamiltonian $\hat{H}_0$, and $p_H=\mathbf{p}\cdot\mathbf{H}/H$.

In a magnetic field the kinematic momentum $\mathbf{p}$ in the expression for the energy $\varepsilon(\mathbf{p})$ should be replaced by $\hat{\mathbf{P}}-(e/c)\mathbf{A}$, where $\hat{\mathbf{P}}=-(i/\hbar)(\partial/\partial\mathbf{r})$ is the generalized momentum of the electron and $\mathbf{A}$ is the vector potential. If the latter is chosen in the Landau gauge, $\mathbf{A}=(0, Hx\cos\theta, -Hx\sin\theta)$, then the Hamiltonian

$$\hat{H}_0=\varepsilon\left(\hat{P}_x,\hat{P}_y-\frac{e}{c}Hx\cos\theta,\hat{P}_z+\frac{e}{c}Hx\sin\theta\right) \tag{9}$$

will depend on only one coordinate, x. In this gauge for the vector potential the solution of the Schrödinger equation

$$\hat{H}_0\Psi=\varepsilon\Psi, \tag{10}$$

which essentially contains only one differential operator, $\hat{P}_x=-i\hbar(\partial/\partial x)$, should be sought in the form

$$\Psi(x,y,z)=\exp(iP_y y/\hbar+iP_z z/\hbar)\psi(x). \tag{11}$$

The energy of the electrons on closed orbits in the magnetic field will depend on the generalized momenta P_y and P_z, which are "good" quantum numbers, and on the discrete quantum number $n=0,1,2,3,\ldots$.

In the summation in (2) over all the electron states, which are specified by the quantum number n and the generalized momenta P_y and P_z, it is more convenient to use combinations of P_y and P_z in the form an integral of the motion: $p_H=P_y\sin\theta+P_z\cos\theta$. Here is is necessary to specify an additional quantum number, e.g., P_y, which in the quasi-classical approximation determines the position of the center of the electron orbit in the magnetic field. For $T\gg\hbar\Omega$ one usually uses the time of motion of the charge in the magnetic field, t_H, instead of P_y as the additional variable along with ε and p_H, in accordance with the equation

$$\frac{\partial p_x}{\partial t_H}=\frac{eH}{c}(v_y\cos\theta-v_z\sin\theta),\ \frac{\partial p_y}{\partial t_H}=-\frac{eH}{c}v_x\cos\theta,$$

$$\frac{\partial p_z}{\partial t_H}=\frac{eH}{c}v_x\sin\theta. \tag{12}$$

In the quasi-classical approximation, when the main role in the electronic absorption of sound waves is played by the charge carriers at energy levels with large values of n, the wave function of the electrons can be found under the most general assumptions about the form of the Hamiltonian. However, in certain particular cases one can find the energy spectrum and the wave function of the conduction electrons for arbitrary values of the high magnetic field, including the ultraquantum limit. As an example of such a case we consider the simplest quasi-two-dimensional electron energy spectrum:

$$\varepsilon(\mathbf{p})=\frac{p_x^2+p_y^2}{2m}-\eta v_0\frac{\hbar}{a}\cos\frac{ap_z}{h}. \tag{13}$$

Here a is the distance between layers, $v_0=(2\varepsilon_F/m)^{1/2}$ is the characteristic velocity along the layers for the electrons with the Fermi energy ε_F, m is the mass of an electron, and $\eta\ll1$ is the quasi-two-dimensionality parameter of the charge-carrier spectrum.

Substituting (11) into Eq. (10), we easily find that for angles θ that are not too large, specifically for $\eta\tan\theta<1$, in the leading approximation in the small parameter aeH/cmv_0 the electron energy levels have the form

$$\varepsilon_n=\left(n+\frac{1}{2}\right)\hbar\Omega\sqrt{1+\eta\frac{v_0am}{\hbar}\tan^2\theta\cos\zeta}$$
$$-\eta\frac{v_0\hbar}{a}\cos\zeta-\eta^2\frac{mv_0^2\tan^2\theta\sin^2\zeta}{2[1+\eta(v_0am/\hbar)\tan^2\theta\cos\zeta]}, \tag{14}$$

where $\zeta=ap_H/(\hbar\cos\theta)$ and $\Omega=eH/(mc\cos\theta)$. If the spin splitting is not taken into account, ε_n depends only on two variables: the continuously varying ζ, and the discrete quantum number n, which enumerates the electron energy levels in the magnetic field.

The kinetic equation linearized with respect to the weak perturbation of the charge carriers by the acoustic wave has the form

$$\left[-i\omega+\frac{i}{\hbar}(\varepsilon_n-\varepsilon_m)\right]f_{1nm}+i\mathbf{k}\cdot\mathbf{v}_{nl}f_{1lm}-\{\hat{W}_{\rm coll}(\hat{f}_1)\}_{nm}$$
$$=\frac{f_0(\varepsilon_m)-f_0(\varepsilon_n)}{\varepsilon_m-\varepsilon_n}(e\tilde{\mathbf{E}}\cdot\mathbf{v}+\omega\lambda_{ij}u_ik_j)_{nm}, \quad (15)$$

where $\mathbf{k}$ is the wave vector of the acoustic wave.

Using the solution of the kinetic equation, one can calculate the dissipative function and, dividing it by the acoustic energy flux density, obtain the damping coefficient for the sound wave:

$$\Gamma=\frac{T}{\rho u^2\omega^2 s/2}\frac{dS}{dt}. \quad (16)$$

Here ρ is the density of the crystal, and s is the sound velocity.

We consider the propagation of a linearly polarized longitudinal wave $\mathbf{u}=(0,0,u)$ along the normal to the layers of the conductor in the case when the following inequality holds:

$$T\ll\hbar\Omega\ll\eta\mu, \quad (17)$$

where μ is the chemical potential.

In the quasi-classical approximation the entropy production in the electron system can be written in the form

$$\frac{dS}{dt}=-\frac{2eH}{c(2\pi\hbar)^2}\sum_{n,m}\int dp_H\hat{W}_{\rm coll}(\hat{f}_1)^{nm}$$
$$\times\frac{f_1^{nm}}{f_0(\varepsilon_n)[1-f_0(\varepsilon_m)]}. \quad (18)$$

The diagonal matrix elements of the operators $\hat{f}_1$ and $\hat{W}_{\rm coll}(\hat{f}_1)$ are quantities averaged over the different phases of the quasi-classical electron trajectory $\varphi=\Omega t_H$. In the case of closed electron orbits the off-diagonal matrix elements v_i^{nm} of the electron velocity operator are proportional to periodic functions of the form $\cos(n-m)\varphi$.

If collisions of electrons with phonons are extremely rare, and the conduction electrons are scattered mainly by impurity atoms, then the dissipative processes in the system of charge carriers can be taken into account with the aid of the relaxation-time (τ) approximation for the collision integral. Applying the Poisson equation to expression (18) and changing from integration over n to integration over ε, we can write the oscillatory (in the magnetic field) part of the acoustic absorption coefficient in the form

$$\Gamma^{\rm osc}=\frac{4\pi}{\rho u^2\omega^2 s}\frac{2eH}{c(2\pi\hbar)^3}2\,{\rm Re}\sum_{N=1}^{\infty}\int d\varepsilon\left(-\frac{\partial f_0(\varepsilon)}{\partial\varepsilon}\right)$$
$$\times\int dp_H\exp[2\pi iNn(\varepsilon,p_H)]\frac{1}{2\pi\Omega\tau}$$
$$\times\int_0^{2\pi}d\varphi\left|\frac{1}{\Omega}\int_{-\infty}^{\varphi}d\varphi' g(\varphi')\right.$$
$$\left.\times\exp\left\{2ikz(\varphi')-i\frac{\omega}{\Omega}\varphi'+\frac{\varphi'}{\Omega\tau}\right\}\right|^2. \quad (19)$$

Here $g(\varphi)=e\tilde{\mathbf{E}}\cdot\mathbf{v}+\lambda_{zz}u\omega k$. The component of the deformation potential can be described by the expression

$$\lambda_{zz}=\eta\lambda\cos\frac{ap_z}{\hbar},\quad \lambda=\frac{mv_0^2}{2}. \quad (20)$$

With the aid of Maxwell's equations (5) and formulas (4) one is readily convinced that in the case of a strong external magnetic field ($\Omega\tau\gg1$) and for $kv_0\tau\eta\ll1$ and $\omega\tau\ll1$ the components of the field of the electromagnetic wave generated by the sound wave have the form

$$\tilde{E}_x=\frac{i\omega}{c}uH\sin\theta\frac{1-i\beta\gamma^2}{1-(\beta\gamma)^2-2i\beta\gamma^2},$$
$$\tilde{E}_y=-\frac{i\omega}{c}uH\sin\theta\frac{i\beta\gamma^2}{1-(\beta\gamma)^2-2i\beta\gamma^2}. \quad (21)$$

Here $\gamma=1/(\Omega\tau)\ll1$, and the parameter $\beta=(s\omega_p/c\omega)^2\omega\tau$ can be quite large if the plasma frequency ω_p has a value comparable to the typical value for an ordinary metal. This assumption is based on the fact that the conductivity in the plane of the layers of organic conductors is of the same order as that of good metals. The formulas given for the electromagnetic field of the wave do not take into account the Shubnikov–de Haas oscillations of the conductivity, the amplitudes of which are a factor of $(\eta\mu/\hbar\Omega)^{1/2}$ smaller than the part of the conductivity that varies monotonically with the magnetic field.

Substituting expressions (20) and (21) into formula (19), we obtain

$$\Gamma^{\rm osc}=\frac{2m^3v_0^2}{\rho s\tau a(2\pi\hbar)^2}{\rm Re}\sum_{N=1}^{\infty}\int d\varepsilon\left(-\frac{\partial f_0(\varepsilon)}{\partial\varepsilon}\right)$$
$$\times\int_0^{2\pi}d\zeta\exp[2\pi iNn(\varepsilon,\zeta)]$$
$$\times\left\{\frac{(kv_0\tau\eta)^2}{2}J_0^2\left(\frac{amv_0}{\hbar}\tan\theta\right)\cos^2\zeta+F(\gamma)\tan^2\theta\right\}. \quad (22)$$

Here J_0 is the Bessel function, and

$$F(\gamma)=\frac{1+\beta^2\gamma^2+\beta^2\gamma^4}{[1-(\beta\gamma)^2]^2+\beta^2\gamma^4}.$$

The second term in curly brackets in formula (22) determines the Joule losses due to the electromagnetic fields excited by the sound wave. The function $F(\gamma)$ is of the order of unity over a wide range of magnetic fields, and only under conditions of resonance coupling of the acoustic and electromagnetic waves, when the wavelength of the helicoidal wave excited by the sound is comparable to the wavelength of the acoustic wave, i.e., $\beta\gamma=1$, does the function $F(\gamma)$ become of the order of $\gamma^{-2}\gg1$. In the case considered here, the Joule losses are much greater than the absorption due to the renormalization of the electron energy directly on account of the deformation of the crystal, when the external magnetic field deviates from the normal to the layers by an angle $\theta\gg kl\eta$.

Performing the integration over ζ and ε in (22), we obtain

$$\Gamma^{\rm osc}=\frac{\Gamma_0}{kl}\sum_{N=1}(-1)^N\Phi(N\Lambda)\cos\left(\frac{2\pi N\mu}{\hbar\Omega}\right)\times\left\{\left(\frac{k/\eta}{2}\right)^2 J_0^2\left(\frac{amv_0}{\hbar}\tan\theta\right)[J_0(2\pi N\chi)-J_2(2\pi N\chi)]+F(\gamma)J_0(2\pi N\chi)\tan^2\theta\right\},\qquad(23)$$

where $\Gamma_0=mN_cv_0\omega/4\pi\rho s^2$, N_c is the density of charge carriers in the conductor, $l=v_0\tau$, μ is the chemical potential, $\Phi(z)=z/\sinh z$, $\Lambda=2\pi^2T/\hbar\Omega$, and $\chi=(\eta v_0/\hbar\Omega)[(\hbar/a)+(ma/2\hbar)\tan\theta]$ is equal in order of magnitude to $\eta\mu/\hbar\Omega$.

At temperatures that are not too low, when $\Lambda\simeq 1$, the amplitude $\Gamma^{\rm osc}$ is smaller by a factor of $(\eta\mu/\hbar\Omega)^{1/2}$ than the part of the acoustic damping coefficients that varies smoothly with magnetic field,

$$\Gamma^{\rm mon}\simeq\frac{\Gamma_0}{kl}\left[\left(\frac{k/\eta}{2}\right)^2 J_0^2\left(\frac{amv_0}{\hbar}\tan\theta\right)+F(\gamma)\tan^2\theta\right].\qquad(24)$$

In the quasi-classical approximation, when $\eta\mu\gg\hbar\Omega$, the following asymptotic expression is valid for $\Gamma^{\rm osc}$:

$$\Gamma^{\rm osc}\simeq\frac{\Gamma_0}{kl}\sum_{N=1}\frac{(-1)^N\Phi(N\Lambda)}{(N\chi)^{1/2}}\cos\left(\frac{2\pi N\mu}{\hbar\Omega}\right)\times\cos\left(2\pi N\chi-\frac{\pi}{4}\right)\left[\left(\frac{kl\eta}{2}\right)^2 J_0^2\left(\frac{amv_0}{\hbar}\tan\theta\right)+F(\gamma)\tan^2\theta\right].\qquad(25)$$

The use of the rather simple model (13) of the dispersion relation for conduction electrons in the calculation permits a correct description of the character of the propagation of sound waves in a quantizing magnetic field (Fig. 1).

In the quasi-classical approximation it is not difficult to generalize the results obtained to the case of a quasi-two-dimensional electron energy spectrum of arbitrary form. As in the case of the dispersion relation (13), a longitudinal sound wave propagates a considerable distance into the interior of the sample along the normal to the layers if the magnetic field deviates from the normal by a small angle $\theta<kl\eta$.[9]

If the Fermi surface for such an orientation of the magnetic field has only two different extremal values of its cross section on a plane $p_H=\text{const}$, viz., $S_{\min}$ and $S_{\max}$, then the ratio $\Gamma_{\rm osc}/\Gamma_{\rm mon}$ can be written in the form

$$\frac{\Gamma_{\rm osc}}{\Gamma_{\rm mon}}\simeq\sqrt{\frac{\hbar\Omega}{\eta\mu}}\sum_{N=1}\frac{(-1)^N}{\sqrt{N}}\Psi(N\Lambda)\times\cos\left(\frac{Nc(S_{\max}+S_{\min})}{2eH\hbar}-\pi N\right)\times\cos\left[\frac{Nc(S_{\max}-S_{\min})}{2eH\hbar}-\frac{\pi}{4}\right].\qquad(26)$$

This case of anomalous acoustic transparency does not take place for transverse polarization of the sound wave, $\mathbf{u}\perp\mathbf{k}$, the damping of which is determined mainly by the Joule losses for any orientation of the magnetic field.

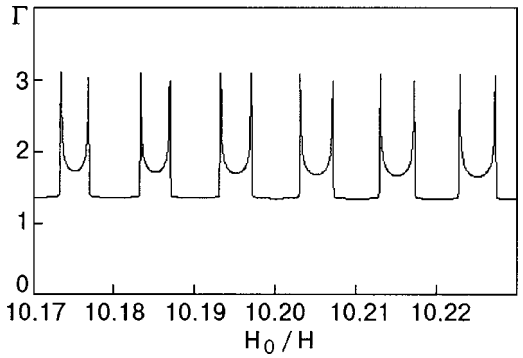

FIG. 1. Acoustic absorption coefficient in a layered conductor as a function of H_0/H ($H_0=\eta\mu mc/e\hbar$) in relative units for $\eta=0.01$, $T/\eta\mu=5\times10^{-3}$, $\theta=0$.

*E-mail: kirichenko@ilt.kharkov.ua

[1] A. B. Pippard, Philos. Mag. **2**, 1147 (1957).
[2] É. F. Kaner, V. G. Peschanskiĭ, and I. A. Privorotskiĭ, Zh. Éksp. Teor. Fiz. **40**, 214 (1961) [Sov. Phys. JETP **13**, 147 (1961)].
[3] V. L. Gurevich, V. G. Skobov, and Yu. D. Firsov, Zh. Éksp. Teor. Fiz. **40**, 786 (1961) [Sov. Phys. JETP **13**, 552 (1961)].
[4] I. V. Kirichenko and V. G. Peschansky, JETP Lett. **64**, 903 (1996).
[5] O. Galbova, G. Ivanovski, O. V. Kirichenko, and V. G. Peschansky, Fiz. Nizk. Temp. **23**, 173 (1997) [Low Temp. Phys. **23**, 127 (1997)].
[6] E. M. Lifshitz and L. P. Pitaevskiĭ, *Statistical Physics*, Part. 2, Nauka, Moscow (1965).
[7] D. N. Zubarev, *Nonequilibrium Statistical Thermodynamics*, Consultants Bureau, New York (1974), Nauka, Moscow (1971).
[8] A. I. Akhiezer, Zh. Éksp. Teor. Fiz. **8**, 1338 (1938).
[9] O. V. Kirichenko and V. G. Peschanskiĭ, Fiz. Nizk. Temp. **27**, 1323 (2002) [Low Temp. Phys. **27**, 978 (2002)].

Translated by Steve Torstveit

Propagation of heat pulses in disordered media*

E. I. Salamatov**

Physicotechnical Institute of the Urals Division of the Russian Academy of Sciences, ul. Kirova 132, 426001 Izhevsk, Russia

(Submitted December 19, 2002)
Fiz. Nizk. Temp. **29**, 817–820 (July 2003)

Processes of heat pulse propagation in nonconducting disordered systems containing thermal-phonon trapping centers (two-level systems) are investigated at low temperatures. The main parameters of the model studied, containing two different two-level systems, are the heat capacity of each of the subsystems and the relaxation time for the inelastic scattering of phonons on the two-level systems. The influence of the interaction of phonons with the two-level centers on the time of arrival of the heat pulse at the bolometer is calculated for different densities of centers. The theoretical calculations are compared with the experimental data on the propagation of slightly nonequilibrium phonons in solid solutions of rare-earth yttrium–aluminum garnets and in two-phase ceramics at helium temperatures. © *2003 American Institute of Physics.* [DOI: 10.1063/1.1596596]

INTRODUCTION

The ''heat pulse'' method, based on analysis of the diffusive propagation of slightly nonequilibrium phonons injected into a sample by a ''heat'' generator ($S/T \ll 1$, S is the amount by which the temperature of the generator exceeds the thermostat temperature T), is an effective way of studying the defect structure of crystalline, amorphous, and ceramic samples.[1–3] The main characteristics analyzed in such studies are the time of arrival of the maximum and the shape of the heat pulse registered by the bolometer. In Ref. 4 a rather simple model was proposed for describing the processes of heat pulse propagation in YErAlO solid solutions, according to which the trapping centers for nonequilibrium phonons are paramagnetic erbium atoms. In these systems the propagation time of the heat pulses is anomalously large—two orders of magnitude larger than in analogous systems with impurities of other rare-earth elements. It was shown in Ref. 4 that this effect is due to the greater difference between the heat capacities of the phonons and impurity two-level subsystems of a paramagnetic nature, since the inelastic scattering of phonons on two-level systems (TLSs) leads to a change in shape of the pulse propagating through the sample and to an increase in the time of arrival of the maximum of the pulse, t_m, which is proportional to the increase of the heat capacity C of the sample upon introduction of the impurity: $1/C = c_{\rm ph}/(c_t + c_{\rm pt})$, where $c_{\rm ph}$ and c_t are the heat capacities of the phonons and of the subsystems of the TLSs. The number of such phonons increases with increasing time of the diffusive propagation of the signal in the absence of phonon trapping centers, $t_0 = L^2/2D_0$ (L is the length of the sample, and D_0 is the phonon diffusion coefficient associated with elastic scattering only). For example, the assumption of elastic Rayleigh scattering of phonons on defects gives $t_0 \propto NL^2T^4$, where N is the density of TLSs. Taking inelastic scattering into account leads to a complex temperature dependence of the time of arrival t_m of the maximum of the phonon nonequilibrium signal at the bolometer in samples containing TLSs (trapping centers for nonequilibrium phonons). The model proposed in Ref. 4 made it possible to describe the main anomalies in the temperature dependence and density dependence of T_m. In the present paper this approach is developed further toward greater complexity of the systems with allowance for phonon–phonon scattering and phonon decomposition processes.

GENERAL FORMALISM

The propagation of a short heat pulse in a sample is a substantially nonsteady process. The presence of trapping centers can lead to spatial inhomogeneity of the system due to the position-dependent temperature dependence of the state of the trapping centers, i.e., it can lead to spatial dispersion of the effective diffusion coefficients. Using the approximations adopted in Ref. 4 for describing the processes of pulse propagation in a sample containing two different TLSs, we can write the shape of the pulse in the Fourier representation as

$$S(t,k) = A_1(k)\exp(-D_1(k)k^2t) + A_2(k) \times \exp(-D_2(k)k^2t) + A_3(k)\exp(-D_3(k)k^2t). \tag{1}$$

The diffusion coefficients $D_i(k)$ and the weight factors $A_i(k)$ in Eq. (1) are solutions of a secular equation of the following form [the system of kinetic equations is analogous to system (1), (2) in Ref. 4]:

$$\begin{aligned} &(p + N_1\Gamma_1 + N_2\Gamma_2 + k^2D_0 + \Gamma_a)S_q(p,k) - N_1\Gamma_1 S_{1t}(p,k) \\ &\quad - N_2\Gamma_2 S_{2t}(p,k) = S(0), \qquad (2) \\ &[p + (c_{\rm ph}/c_{1t})\Gamma_1]S_{1t}(p,k) - (c_{\rm ph}/c_{1t})\Gamma_1 S_q(p,k) = 0, \\ &[p + (c_{\rm ph}/c_{2t})\Gamma_2]S_{2t}(p,k) - (c_{\rm ph}/c_{2t})\Gamma_2 S_q(p,k) = 0. \end{aligned}$$

Here S_i is the deviation of the temperature of a subsystem ($i = q, 1t, 2t$) from the thermostat temperature, N_i is the density of TLSs of type i, Γ_i is the rate of scattering of phonons per defect of type i,

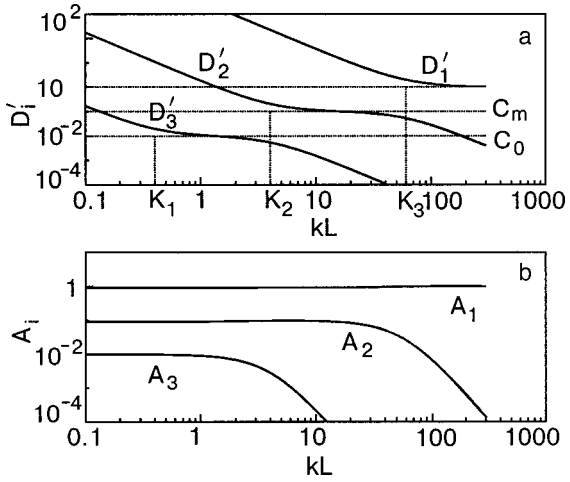

FIG. 1. Spatial dispersion relation of the effective diffusion coefficients $D_i'=D_i/D_0$ (a) and of the weight factors A_i (b).

$$c_{i,t}=(\Delta_i/T)^2\exp(-\Delta_i/T)/(1+\exp(-\Delta_i/T))^2$$

and

$$c_{\rm ph}=4\pi^4(T/T_D)^3/5$$

are the heat capacities of the TLSs and phonons, respectively, Δ_i is a parameter of the TLS, and T_D is the Debye temperature. To describe effects of anharmonicity in the framework of the simple model adopted in Ref. 4, it is necessary to make two main approximations. The first is to take into account only processes of decomposition of thermal phonons. This is justified by the fact that in the experiments discussed below, the condition $n(\omega)\ll 1$ always holds, where $n(\omega)$ is the occupation number of the injected phonons. The second is to assume that the long-wavelength phonons formed in the decomposition of thermal phonons propagate ballistically and do not contribute to the shape of the diffusive signal registered by the bolometer. The corresponding term Γ_a in Eqs. (2) describes only the loss of phonons.

The spatial dispersion of the effective diffusion coefficients obtained from a numerical solution of the characteristic equation (2) of the system is shown in Fig. 1. In the general case the parameters $A_i(k)$ and the dimensionless diffusion coefficients $D_i'=D_i/D_0$ depend on five parameters analogous to those introduced in Ref. 4: $(k_iL)^2=(L/L_0)^2=2t_0/\tau_i$, where τ_i is the relaxation time of the phonons with respect to decomposition $(i=a)$ and to trapping by the subsystems of the TLS $(i=1,2)$; $1/C_i=c_{\rm ph}/(c_{\rm ph}+c_{it}N_i)$. The special points indicated in Fig. 1 are expressed in terms of these parameters as follows:

$$K_1=k_aL,\quad K_2=\sqrt{(k_aL)^2+(k_2L)^2},$$

$$K_3=\sqrt{(k_aL)^2+(k_1L)^2+(k_2L)^2},$$

$$C_m=C_1k_1^2/(k_a^2+k_1^2+k_2^2),$$

$$C_0=c_{\rm ph}/(c_{\rm ph}+c_{1t}N_1+c_{2t}N_2)$$
$$=C_1C_2/(C_1+C_2-C_1C_2).$$

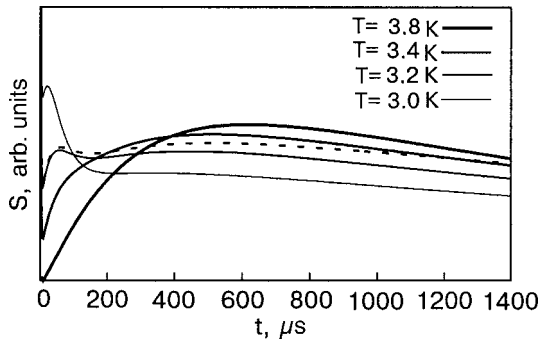

FIG. 2. Shape of the heat pulse (the phonon nonequilibrium signal) calculated with allowance for elastic scattering of phonons on two two-level subsystems and for decomposition processes in the phonon system at different temperatures. The dashed curve was calculated for $A=0$ and $T=3.2$ K.

RESULTS AND DISCUSSION

Figure 2 shows the results of a numerical calculation of the shape of the heat pulse (1) at different temperatures. It was assumed in the calculations that the diffusion coefficient is determined by Rayleigh scattering: $D_0=v^2/3BT^4$, $\Gamma_i=\Gamma_{0i}\exp(-\Delta_i/T)$, and the expression $\Gamma_a=AT^5$ was used for the phonon decomposition rate. The calculations were done for the following values of the parameters: $B=1200\ \mathrm{s^{-1}\cdot K^{-4}}$, $A=10^{-2}\ \mathrm{s^{-1}\cdot K^{-5}}$, $\Delta_1=4.5$ K, $x_1=0.06$, $\Delta_2=29$ K, $x_2=0.6$, $T_D=630$ K, $v=7\times10^5$ cm $\cdot\,\mathrm{s^{-1}}$, and $L=0.5$ cm, where x is the concentration of TLSs expressed in formula units for $Y_{3-x}Er_xAl_5O_{12}$. The fact that the calculated curves are in completely satisfactory agreement with the experimental curves observed for $Y_{3-x}Er_xAl_5O_{12}$ solid solutions (see, e.g., Fig. 5 of Ref. 3) is an indication of the suitability of the model used.

In the following discussion we restrict the analysis to only slow processes, which are dominant in the ''phonon bottleneck'' regime. As was shown in Ref. 4, this regime arises when the time for energy exchange between the phonons and the TLSs becomes much shorter than the diffusion time t_0. In that case the phonon propagation time is determined solely by the effective diffusion coefficient $D_{\rm eff}=C_0D_0$ (the plateau on the lower curve of Fig. 1) and does not depend on τ_1 and τ_2:

$$t_m(T)\simeq\frac{\sqrt{1+4k_a^2(T)}-1}{2k_a^2(T)}t_0(T)/C_0. \qquad (3)$$

For analysis of the decomposition processes we consider a crystal without trapping centers, assuming $C_0=1$. It follows from Eq. (3) that the decomposition processes lead to nonmonotonicity of $t_m(T)$. At low temperatures the arrival time of the maximum increases as T^4, while at high temperatures it falls off by a $T^{-1/2}$ law. Such behavior of t_m, which has been observed[5] in the system $Al_{1-x}Lu_xAlO_3$, can be explained by a high rate of decomposition of the phonons.

Taking the phonon decomposition processes into account makes it possible to explain the strong temperature dependence of the negative derivative $dt_m(T)/dT$—temperature dependence which is characteristic for systems with a large $(x>1.5)$ concentration of erbium atoms.[3] As is shown in Ref. 4, the $t_m(T)$ dependence calculated without taking de-

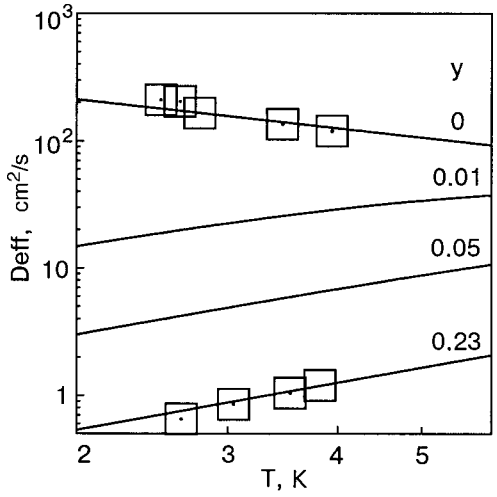

FIG. 3. Temperature dependence of the effective diffusion coefficient for several values of the metallic phase concentration y; the squares indicate the experimental points for the ''base'' sample (upper) and for sample 1 (lower).[6]

composition processes into account for a single TLS has a nonmonotonic character: initially (for $T \leqslant \Delta$) the time increases exponentially, while at higher temperatures $t_m(T)$ falls off by a law close to $1/T$ ($\Delta \ll T_D$). The decomposition processes can lead to a stronger power-law dependence on the high-temperature part of the $t_m(T)$ curve, so that $t_m(T) \propto 1/T^{5.5}$ at large values of the anharmonicity constant.

The fact that the phonon propagation time in the ''phonon bottleneck'' regime is independent of the values of τ_1 and τ_2 allows one to apply the results found to a wider class of systems. Among such systems, it appears, are two-phase ceramics consisting of an insulating matrix with a small concentration of metallic inclusions (cermets). Indeed, the high electronic heat capacity of the metallic particles allows one to assume in a first approximation that they are point centers for the trapping of phonon energy, and the electronic heat capacity of the particles at the temperatures of the experiment (2–4 K) can be much larger than the phonon heat capacity of the matrix. This should lead to small values of the parameter C_0, which, according to the proposed model, is responsible for the delay of the propagation time of the heat pulse in such systems in comparison with systems without phonon trapping centers. Because of the different temperature dependence of the heat capacity of the electron and phonon subsystems, the contribution of the metallic phase to the formation of the phonon nonequilibrium signal can be observed experimentally.

The time of passage of a heat pulse through single-phase corundum (Al_2O_3) ceramics and corundum-based cermets containing up to 20% steel was studied in Ref. 6. Let us estimate the value of the parameter $C_0(T)=(1-y)c_{\rm ph}/[(1-y)c_{\rm ph}+yc_{Me}]$, where $c_{Me}=\gamma T$ is the heat capacity of the electron system. The Debye temperature of corundum is 1042 K. Assuming that the value of γ for iron is 4.9×10^{-3} J/(mole·K^2),[7] we obtain $D_{\rm eff}=C_0D_0=0.01D_0$ for a metallic phase concentration $y=0.2$ and a temperature $T=3.8$ K. This estimate is in good agreement with experiment[6] if it is assumed that D_0 can be taken equal to the diffusion coefficient of the ''base'' sample. Since the diffusion coefficient in single-phase ceramics depends in a complicated way on the method of preparation and heat treatment of the samples,[8] the latter is valid only for sample 1, which was annealed at the same temperature as the ''base'' sample (see Ref. 6).

Under the condition $(1-y)c_{\rm ph} \gg yc_{Me}$ the temperature dependence of the effective diffusion coefficient takes the form $D_{\rm eff}(T)=D_0(T)/T^2$. For a weak dependence of D_0 on temperature this can lead to a change in sign of the derivative dD/dT upon going from the ''base'' sample to the cermets, as has been observed experimentally.[6] Figure 3 shows $D_{\rm eff}(T)$ for $\gamma=4.9\times10^{-3}$ J/(mole·K^2) and for several values of y on the assumption that $D_0 \propto T^{-0.75}$. Unpublished experimental results made available to us by the authors of Ref. 6 are shown by the squares. It is seen that the calculated curves are in good correspondence with the experimental data. However, additional experiments are required in order to reach definitive conclusions.

CONCLUSION

A refinement of the model proposed in Ref. 4 has made it possible to describe a large number of experimental results on the propagation of phonons in samples containing impurity two-level systems. The fact that the parameter introduced is of a general character has made it possible to compare our results with experimental data obtained both for solid solutions of yttrium–erbium garnets, where the trapping centers are paramagnetic erbium atoms, and for insulating ceramics containing metallic inclusions as trapping centers.

The author is grateful to S. N. Ivanov and E. N. Khazanov for fruitful discussions and for providing the opportunity to use their experimental data prior to publication. This study was supported by the Russian Foundation for Basic Research (Grants Nos. 03-02-16233 and 01-02-96462).

*Presented at the Third International Workshop on Low Temperature Physics in Microgravity Environment (CWS-2002)
**E-mail: salam@otf.pti.udm.ru

[1] R. J. van Gutfeld and A. H. Nethercot Jr., Phys. Rev. Lett. **12**, 641 (1964).
[2] S. N. Ivanov and E. N. Khazanov, Zh. Éksp. Teor. Fiz. **88**, 294 (1985) [Sov. Phys. JETP **61**, 172 (1985)].
[3] S. N. Ivanov, A. G. Kozorezov, A. V. Taranov, and E. N. Khazanov, Zh. Éksp. Teor. Fiz. **100**, 1591 (1991) [Sov. Phys. JETP **73**, 880 (1991)].
[4] E. I. Salamatov, Phys. Solid State **44**, 978 (2002).
[5] B. A. Danil'chenko, D. V. Poplavskiĭ, S. N. Ivanov, A. V. Taranov, and E. N. Khazanov, Zh. Éksp. Teor. Fiz. **112**, 326 (1997) [JETP **85**, 179 (1997)].
[6] S. N. Ivanov, E. N. Khazanov, A. V. Taranov *et al.*, Phys. Solid State **43**, 665 (2001).
[7] I. S. Grigor'ev and E. Z. Meĭlikhov, *Physical Constants* [in Russian], Nauka, Moscow (1991).
[8] S. N. Ivanov, A. G. Kozorezov, A. V. Taranov, and E. N. Khazanov, Zh. Éksp. Teor. Fiz. **102**, 600 (1992) [Sov. Phys. JETP **75**, 319 (1992)].

Translated by Steve Torstveit

PERSONALIA

Igor' Mikhaĭlovich Dmitrenko (on his 75th birthday)

[DOI: 10.1063/1.1596597]

July 24, 2003 is the 75th birthday of Igor' Mikhaĭlovich Dmitrenko, a prominent member of the National Academy of Sciences of Ukraine. I. M. Dmitenko's scientific activity has focused exclusively on fundamental and high-priority research in the field of superconductivity and superconducting electronics. Studies published in the 1960s on a new class of quantum coherence effects, the brilliant experiments on the world's first observation of the ac Josephson effect, brought him wide renown and international recognition. His pioneering studies on quantum interference, magnetic flux quantization, the observation of macroscopic quantum tunneling effects, and dynamical chaos in SQUIDs have become classic.

I. M. Dmitrenko has initiated and headed many studies in the field of applied science, directed toward the utilization of the achievements of the physics of superconductivity in modern electronics. He founded a school of experimental physicists and engineers, many of whom have become leaders in new scientific fields.

On I. M. Dmitrenko's initiative a Physicotechnical School was founded at Kharkov Polytechnical Institute in 1972, and later a Department of Technical Cryophysics was set up, where I. M. Dmitrenko for many years pursued pedagogical and methodological activity.

The scientific activity of I. M. Dmitrenko has been reflected in numerous articles, reports, and monographs. In recent years two books of his recollections about his life choices, on the founding and growth of the B. Verkin Institute for Low Temperature Physics and Engineering of the National Academy of Sciences of Ukraine, with which he has been continuously affiliated throughout his life, and about the people he has known, about events and curiosities, and about his favorite animals, which that have been his companions since childhood.

I. M. Dmitrenko has been awarded the Order of Merit of Ukraine in Science, the State Prize of Ukraine, and the Medal of Honor.

We warmly congratulate I. M. Dmitrenko on his birthday. We wish him robust health and well-being, fruitful scientific activity, and bright new reflections of his talented, creative nature.

TheEditorialStaff

Arnol'd Markovich Kosevich (on his 75th birthday)

[DOI: 10.1063/1.1596598]

July 7, 2003 is the 75th birthday of the prominent theoretical physicist Arnol'd Markovich Kosevich, a Correspondent Member of the National Academy of Sciences of Ukraine, the Head of the Theoretical Department of the B. Verkin Institute for Low Temperature Physics and Engineering, National Academy of Sciences of Ukraine, and a Professor at Kharkov National University.

The name of A. M. Kosevich is linked with a number of fundamental problems of solid-state theory. Together with I. M. Lifshits, he constructed a complete theory of quantum oscillation effects in metals. The Lifshits–Kosevich formula, obtained in 1954, made it possible to compare the results of experimental research on quantum oscillations of the magnetic susceptibility of metals with the shape of the Fermi surface. This result has gained international recognition, and it is included in all monographs, textbooks, and review articles on the electronic theory of metals and is still cited in original papers.

Another important area of scientific activity for A. M. Kosevich is the theoretical study of the mechanics of real crystals. He proposed a field approach to the theory of dislocations, which is of fundamental importance and has been the most fruitful approach in the theory of plasticity, and he also did research on dynamic and kinetic phenomena in crystals containing defects. An indication of the authority of Prof. Kosevich in this area was his participation in writing the ''Dislocations'' section of the *Theory of Elasticity* volume of the Course of Theoretical Physics series by L. D. Landau and E. M. Lifshitz. A. M. Kosevich wrote the monograph *Dislocations in the Theory of Elasticity* (1978) and a monographic review of the same title in F. Nabarro's encyclopedic series *Dislocations in Solids* (1979). The theoretical study of elastic twinning of crystals played a large role in experimental research on this phenomenon and served as the basis for the monograph *Reversible Crystal Plasticity* (V. S. Boyko, R. I. Garber, and A. M. Kosevich, Moscow, 1991; New York, 1994). A. M. Kosevich's monographs *Principles of Mechanics of the Crystal Lattice* (1972) and *Theory of the Crystal-Lattice* (1988) have become reference works for investigators doing research on the physics of crystals. In recent years A. M. Kosevich has continued to work in this field, concentrating on the topical problems of the dynamics of layered crystals and superlattices.

In the 1970s A. M. Kosevich and his group of coworkers began their studies in the field of nonlinear dynamics of solids on the basis of modern soliton theory. They obtained a number of important results in the study of nonlinear dynamics of magnetically ordered media and, in particular, in the description of magnetic solitons of various nature, including magnetic vortices and magnetic skyrmions in two-dimensional magnets. A. M. Kosevich formulated the concept of dynamical solitons in nonlinear media as bound states of a large number of elementary excitations. This research was reflected in the monograph *Nonlinear Magnetization Waves. Dynamical and Topological Solitons* (A. M. Kosevich, B. I. Ivanov, and A. S. Kovalev, 1983). An important role in popularizing the ideas of nonlinear physics was played by the monograph *Introduction to Nonlinear Physical Mechanics* (A. M. Kosevich and A. S. Kovalev, 1989).

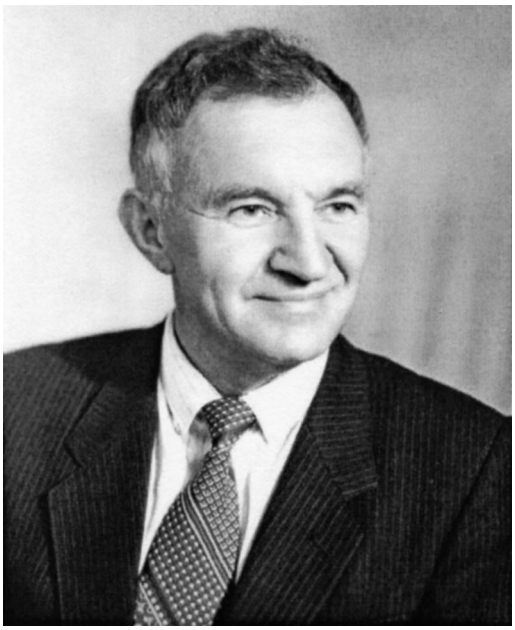

A. M. Kosevich is one of the most prominent representatives of the Kharkov school of theoretical physics, founded by L. D. Landau, A. I. Akhiezer, and I. M. Lifshits, and he is the author of more than 230 scientific papers and review articles and 8 monographs. In recognition of his scientific achievements he has been awarded the Order of Merit of Ukraine in Science and Technology and has won several State and academic prizes of Ukraine.

A. M. Kosevich has played a significant role in the establishment and operation of our journal, serving as a member of the Editorial Board for all of the years of its existence, for 15 of which he served successfully as the Assistant Editor in Chief.

Prof. Kosevich arrives at his 75th year in the flower of his creativity and scientific activity.

We warmly congratulate Prof. Kosevich on his birthday and wish him good health and well-being, creativity, and fruitful scientific activity for many more years to come.

The Editorial Staff